UAB
Universitat Autònoma de Barcelona

CHASING THE SPINAL CIRCUIT FOR REACHING AND GRASPING CONTROL IN RATS

Diego López Santos

UAB
Universitat Autònoma de Barcelona

CHASING THE SPINAL CIRCUIT FOR REACHING AND GRASPING CONTROL IN RATS

ACADEMIC DISSERTATION

To obtain the degree of PhD in Neuroscience by the

Universitat Autònoma de Barcelona

February 2025

PhD Candidate

Diego López Santos

Thesis supervisors

Dr. Guillermo García Alías

Dr. África Flores de los Heros

Academic tutor

Dr. Xavier Navarro Acebes

Group of Neuroplasticity and Regeneration

NeuroPlasticity & Regeneration

BCFI

INc Institut de Neurociències UAB

Fundació La Marató

AGAUR Agència de Gestió d'Ajuts Universitaris i de Recerca

This study was supported by:

- The project TV3-2017-171330 "Regain of arm and hand movements in cervical spinal cord injury patients by means of spinal electric neuromodulation assisted with an arm exoskeleton" from Fundació La Marató de 3Cat to Dr. Guillermo García Alías.
- The National Institute of Health (NIH) / National Institute of Neurological Disorders and Stroke (NINDS) Grant R01 NS112304 to Dr. David S.K. Magnuson and Dr. Scott R. Whittemore, and the Kentucky Spinal Cord and Head Injury Research Trust.
- The grant 2020 FISDU 00149 from Agència de Gestió d'Ajuts Universitaris i de Recerca (AGAUR) affiliated with Secretaria d'Universitats i Recerca del Departament de Recerca i Universitats de la Generalitat de Catalunya to Diego López Santos, co-funded by the European Social Funds.
- The European Molecular Biology Organization (EMBO) Scientific Exchange Grant (10038) to Diego López Santos to perform an international internship at the Kentucky Spinal Cord Injury Research Center, at the University of Louisville

To experimental animals

Acknowledgements

La tesis es mucho más que ese documento escrito, como toda persona que haya pasado por el proceso sabrá. Es un viaje de crecimiento personal y profesional, de alegrías y tristezas, de una pandemia mundial inédita, de un ataque informático y, sobre todo, una época inolvidable de la vida que nunca volverá. Lo bueno, si breve, dos veces bueno, o eso dicen, aunque llamar "breve" a la tesis lo considero una exageración.

Pido perdón por adelantado si me dejo de mencionar a alguien o si alguien considera que no le dedico sufientes palabras, pero también confío que se entienda que el ejercicio de resumir en pocas páginas lo mucho que agradezco y que significan para mi las personas que citaré a continuación es una tarea imposible, me daría para escribir otra tesis, cosa que todos los doctores saben que no va a suceder. Una y no más.

Mi viaje comenzó en 2019 y con las casualidades jugando un papel fundamental, como siempre. Estudiando el máster en París, viajé a Barcelona para cursar una de las asignaturas. Y ahí conocí a Xavi, que explicó algunas de las fascinantes líneas de investigación de su laboratorio. Después de una videollamada desastrosa en la que no funcionaba el sonido y acabamos hablando por Whatsapp, decidí que quería hacer la tesis en el grupo. Y el me abrió las puertas del laboratorio que ha construido durante toda una vida. Pero no tenía hueco en ese momento para mi. Y busqué otro laboratorio, que encontré. Cuando lo tenía apalabrado, recibí un mensaje de alguien del grupo. Y así conocí a Guillermo y a África, que me hicieron una oferta que no pude rechazar. Valoro mucho el haber confiado en mi para este proyecto, y el haber podido ver y aprender de dos puntos de vista a la hora de hacer ciencia, tan diferentes en unos aspectos y tan similares en otros, y como han convergido en esta tesis.

Y en el grupo de Guillermo conocí a Olaia, la que me acompañó por primera vez a que viera lo que era entrenar animales. Y a Lucía, una estudiante de máster fantástica.

Y en el grupo grande conocí Jesús, el dinamizador de los doctorandos. Y a Alba y a su Corpus Curiosum. Ojalá haber coincidido más tiempo en el laboratorio juntos. Su aparición en la casa rural 2.0 fue una de las sorpresas más bonitas que he dado. I la Maria P, la primera doctora que vaig veure defensar a NFIS. Segur que serà una gran docent, ho sé perquè ho he vist amb els meus propis ulls i va ser fantàstic, meravellós. Y a Sara M, casi la primera persona que se fue del laboratorio, aunque por suerte nunca llegó a hacerlo. La creadora de la bonita tradición del "perreo rural", con ella empezó todo. Quien diría que entre personas tan diferentes nos entenderíamos tan bien. I l'Aina, amb qui espero que aviat tornem a ballar el "no rompas más", ara que ja em sé

la coreografia. I la Núria, potser la primera persona que em ve al cap quan penso en NFIS, la que es preocupa per tots nosaltres. Sempre és un plaer parlar amb ella sobre qualsevol cosa. Algun dia anirem junts a donar sang.

Y a Judith y a Sara B, a Sara B y a Judith, ese tándem inseparable que compartió hasta su último día en el laboratorio, como no podría ser de otra manera. Judith, la persona que me marca el camino. Si tengo que seguir los pasos de alguien, ¿de quién mejor? De mayor quiero ser como ella. Sara B, durante mucho tiempo fue el pegamento que mantuvo al grupo unido. Gracias a su regalo del enemigo invisible, estuve durante semanas despertándome cada día a las 2 de la madrugada. Y a Estefanía, que estaba siempre para resolver mis dudas veterinarias. Usaré su truco para descansar la noche previa a la defensa. Y a Vera, la persona que menos soportaba al principio y con la que tuve conversaciones más profundas después. Le deseo lo mejor en su aventura americana. P.D.: La puerta del maletero de mi coche sigue sin funcionar bien. Y a Bruno, mi fiel compañero de habitación y de bromas de los Simpson. Prácticamente en todos los momentos memorables de esta etapa, el estaba allí. Para sorpresa de nadie, nunca más le retaré a hacer flexiones con triple palmada. I el Sergi, una gran persona per tenir al costat, val un milió. Vaig aprendre molt d'ell fent el seu vídeo de tesi. Sempre ens quedaran les nostres experiències en l'Amèrica profunda. I la Georgina, que gràcies a ella dec ser la persona que m'he enregistrat al Turnitin amb més antelació de la història. Disfrutaré del temps que em quedi.

Y a Andrea D, mi vecina de Badako, ¿cómo le explico que soy de Montgat? Aunque haya hecho la tesis exiliada en un despacho donde hace más frío que en la comunión de Pingu, no hay que olvidar que ella tuvo la idea del enemigo invisible. I la Carla, que alguna vegada s'han pensat que érem parella degut a coincidències de noms. Tots els dàtils que aconsegueixi seran per ella. I la Joana, tan intel·ligent com noble i humil. És evident que és molt estimada, amb tot mereixement. A més, m'ha estat animant i resolent dubtes perquè la tesi eixís bé. En tres paraules: és la millor.

Y a Raku, la que más ganas tenía de que acabase y me fuese. En realidad, la voy a echar de menos. Pasas que cosan. Espero que por lo menos espere un par de días antes de quitarme la silla. Siempre podemos quedar para hacer esnórquel en Gili Meno. Y a Néstor, el rey de los chistes malos y de los juegos de la hora de comer en el laboratorio. El más elegante de las cenas de navidad. Es difícil dejar un mayor (y mejor) legado que el suyo. Después de Indonesia ha aprendido a valorar el manjar que es el pan. Y a Bea,

quizá la persona con el corazón más puro que he conocido. La mejor profesora de yoga que he tenido, aunque probablemente yo haya sido de sus peores alumnos, namasté. La clase de pole y el *body painting* nos quedan pendientes. Y a Sònia, una chica nada holgazán con la que compartimos incontables horas con la bata holgada y pintada, colgando registros de *walking track* en la pared. Todo el mundo debería tener una Sònia en su vida, para mi hay un antes y un después de su llegada al laboratorio. Conseguirá todo lo que se proponga y nada ni nadie podrá detenerla, no me cabe duda. I el Marc, el meu *gym bro* durant un mes. Va introduir-se al grup poc a poc, perquè quan va arribar era petit encara, però ara ja ha agafat "esbranzida". Això sí, compta amb despertar-lo de les migdiades, que pot tenir un curtcircuit. Y a Hose, que entró en el laboratorio con muchísima fuerza porque es luz, así de sencillo. Con el descubrí que siempre hay sitio para un nasi goreng más y que hay que tener cuidado con las gaviotas, cosorro. I el Joan, deixeble de Biomed UB, amb els famosos apunts del meu amic Llorca. Tant et fa de paramèdic per monitoritzar el pols i la respiració al taxi com es baixa (pressumptament) a 100 pingüins. Y a Rubén Jr, un personaje único, el fichaje estrella de CCIH. Desde la inundación del laboratorio a la torreznada, seguro que dejará una huella imborrable. Espero que nunca más nos encarguen a los dos la imposible tarea de encender unas velas de cumpleaños.

Y a Judith Sauleda, Genís, María R, Andrea V, Ayesha y Huahua, la nueva generación. Siento nostalgia al veros dar vuestros primeros pasos en el laboratorio, pero a la vez qué bonito es ver que con vosotros continuará esta familia. Prueba de ello es nuestro himno, "La playa", que no queda nadie de las personas que lo convirtieron en la canción del laboratorio, pero que trasciende las generaciones de doctorandos y sigue conectando y emocionando a la actual.

Y además de ellos, también han pertenecido a este grupo, y por ende a esta tesis, doctorandos que han venido de estancia y estudiantes de máster y de grado. Como ya habrá quedado claro, en este laboratorio se conoce a mucha gente, pero no todos son estudiantes. También estaba Mayte, la que más nos ha cuidado, nuestra madre de otra sangre. Su seminario de cómo hacer tiramisú es mi favorito de todos los seminarios NFIS a los que he asistido estos años. Y Neus, la alegría del laboratorio. Cómo se notó su ausencia los meses que no estuvo. Ojalá todo el mundo tuviera la misma actitud que ella para afrontar la vida. Y Quino, Jessica, Eva, Marina, Mónica, Clara, Mireia, Esther, Rubèn, Natalia e Ignacio. Todos ellos hacen que NFIS sea lo que es.

And I went to Louisville, Kentucky. And I met Dr. Magnuson, Brandon, McKenna, Trevor, Morgan, Alice, Christine, Carlos, Savannah, Michael, Neha, Russ and Mary Ellen. Thank you for having me there and introducing me to the midwest.

Aparte de NFIS, no puedo dejarme a NeuroDocs, la asociación de estudiantes del INc-UAB. Es increíble y me hace sentir muy orgulloso ver lo que hemos construido juntos en tan poco tiempo. Es un grupo humano genial y confío que sigan subiendo el listón como ya lo están haciendo y, sobre todo, que valoren (y se valore) lo excepcionales que son. I relacionat amb això em ve a la ment la Roser, que ja va detectar des del principi que a mi era fàcil liar-me. Quina sort té l'INc-UAB de poder comptar amb ella durant tot aquest temps.

Y fuera de la UAB he tenido a los Biomeds, algunos de los cuales ya han pasado por esto. Me encanta que sigamos juntos después de casi 8 años de haber acabado la carrera, y por muchos más. Y también han estado los del pueblo, los de toda la vida, que me han ayudado a desconectar cuando lo he necesitado.

Obviamente, también tengo que acordarme de mi familia. Sin saber del todo lo que hago, me han apoyado lo mejor que han podido. Lo que soy se lo debo en parte a ellos.

Por último, a Carla, la persona que ha vivido más de cerca la tesis después de mi. Esta tesis es en parte suya también, las escuelas de doctorado tendrían que empezar a dar el título de doctor/a consorte. Le doy las gracias por estar ahí siempre y en especial durante los últimos meses, en los que su aliento ha sido fundamental y me ha demostrado muchas cosas.

Y decidí que este apartado sería el primero que empezaría a escribir, aunque no sea lo habitual. El motivo es simple. Este apartado de la tesis para mi es, sin duda, el más importante de todos, porque sin el no existirían los demás.

Index

I. Abstract

Motion is the basis of life. It is coordinated by a highly complex network known as the motor system, which constantly adjusts to a permanent changing environment to produce meaningful movements. We centred this thesis in one of the most representative forms of fine motor control – reaching and grasping (R&G). The role of the spinal cord in its mediation has been traditionally underestimated, despite the presence of spinal networks, called central pattern generators (CPGs), governing behaviours such as locomotion. Thus, we aimed to elucidate the involvement of the spinal cord in forelimb skilled function.

For this purpose, we inflicted excitotoxic injuries by injecting kainic acid into the grey matter of the cervical spinal cord of rats. Hence, we exclusively affected spinal networks while preserving the axons of passage. Motor deficits were evaluated in a variety of behavioural tests of forelimb function that presumably require different neuronal networks. We found that damaging spinal segment sC3 provoked deficits in R&G and other related movements. Subsequently, we showed that sectioning the dorsal and ventral roots of that spinal segment did not impair R&G ability, refuting the intervention of sC3 motoneurons and/or sensory neurons in their control, thus implying the participation of networks of interneurons. Moreover, it suggested the possibility of a R&G CPG at sC3.

Next, we inquired into this hypothetical sC3 network. First, we aimed to identify the spinal cord neuronal populations preferentially activated while R&G, based on the expression of immediate early genes (IEGs) in intact animals. The results showed a trend of a higher number of activated neurons in animals trained for R&G, especially at rostral spinal segments sC2-C5. Finally, to elucidate the role of sC3 interneurons in manual dexterity control, we anatomically targeted and silenced sC3-to-C7 projecting neurons. Nonetheless, inactivation of sC3-to-C7 interneurons did not perturb forelimb function, cancelling the sC3 CPG hypothesis.

On the whole, our findings support the existence of neuronal network necessary for controlling forelimb skilled function at spinal segment sC3. This network is not a CPG, but it could be integrating feedback information and projecting it to supraspinal structures so that the movement is properly executed. Advancing our comprehension of fine motor control will be crucial for developing improved therapeutic strategies, ultimately enhancing the quality of life for patients with associated disorders.

II. Abbreviations

A

AAV: Adeno-associated virus

ACh: Acetylcholine

ALS: Amyotrophic lateral sclerosis

AMPA: alfa-Amino-3-hydroxy-5-methyl-4-isoxazolepropionic acid

ANOVA: Analysis of variance

AP-1: Activating protein complex 1

C

C (as in C3): Cervical segment

CaMK: Calcium/calmodulin-dependent protein kinase

chABC: Chondroitinase ABC

ChAT: Choline acetyltransferase

ChR2: Channelrhodopsin-2

CMV: Cytomegalovirus

CNO: Clozapine N-oxide

CNS: Central nervous system

Col: Coccygeal spinal segment

CPG: Central pattern generator

CSF: Cerebrospinal fluid

CSPG: Chondroitin sulphate proteoglycan

CTb: Cholera toxin subunit B

D

DAB: 3, 3'-diaminobenzidine

DAPI: 4',6-diamidino-2-phenylindole

DCML: Dorsal column-medial lemniscal

DNA: Deoxyribonucleic acid

Dox: Doxycycline hydrochloride

DPI: Days post-intervention

DPX: Dibutylphthalate polystyrene xylene

DREADD: Designer receptor exclusively activated by designer drug

DRG: Dorsal root ganglion

E

EGFP: Enhanced green fluorescent protein

Egr1: Early growth response protein 1

EPSP: Excitatory postsynaptic potential

eTeNT: Enhanced tetanus neurotoxin light chain

F

fps: Frames per second

G

GFAP: Glial fibrillary acidic protein

GFP: Green fluorescent protein

GPCR: G-protein coupled receptor

H

HRP: Horseradish peroxidase

I

Iba1: Ionized calcium-binding adapter molecule 1

IBB: Irvine, Beattie and Bresnahan

IEG: Immediate early gene

i.m.: intramuscular

i.p.: intraperitoneal

K

KA (as in KA1): Kainic acid receptor subunit

L

L (as in L2): Lumbar seegment

L-VSCC: L-type voltage-sensitive calcium channel

M

M1: Primary motor cortex

MAPK: Mitogen-activated protein kinase

MdV: Medullary reticular formation ventral part

MS: Multiple sclerosis

N

NMDA: N-methyl-D-aspartate

Npas4: Neuronal PAS domain protein 4

Ns (as in p = ns): not significant

O

O.C.T.: Optimal cutting temperature

P

PAG: Periaqueductal grey

PB: Phosphate buffer

PHA-L: Phaseolus vulgaris-leucoagglutinin

PMA: Premotor area

PNS: Peripheral nervous system

R

R&G: Reaching and grasping

RNA: Ribonucleic acid

ROS: Reactive oxygen species

rtTAV: Reverse tetracycline transactivator

RVM: Rostral ventromedial medulla

S

s (as in sC3): Spinal segment

S (as in S2): Sacral segment

S1: Primary somatosensory cortex

s.c.: subcutaneous

SCI: Spinal cord injury

SEM: Standard error of mean

SMA: Supplementary motor area

SOD1: Superoxide dismutase 1

T

T (as in T2): Thoracic segment

TRE: Tetracycline-responsive element

V

v (as in vC4): Vertebral segment

VAMP2: Vesicle-associated membrane protein 2

VL: Thalamic ventral lateral nucleus

III. Introduction

1. Sensorimotor control

"To move things is all that mankind can do... for such the sole executant is muscle, whether in whispering a syllable or in felling a forest." (Sherrington, 1924). The motor system forms the foundation of movement and behaviour, encompassing all muscles and the neural circuits that regulate them. This intricate network coordinates nearly 700 muscles within a dynamic and frequently unpredictable environment, enabling a wide range of actions essential to everyday life, from grasping a cup to maintaining balance on uneven terrain.

All mammals possess a nervous system divided into two parts: the central nervous system (CNS) and the peripheral nervous system (PNS). The CNS includes the components protected by bone, such as the brain and spinal cord. The brain, entirely enclosed within the skull, is composed of three primary sections common to all mammals: the cerebrum, the cerebellum, and the brainstem (Figure 1). The PNS encompasses all parts of the nervous system outside the brain and spinal cord and is divided into two subdivisions. The somatic PNS comprises all spinal nerves that govern voluntary movements, such as those controlling the skin, joints, and muscles, as well as sensory nerves that transmit information like touch, proprioception, and pain from the periphery to the CNS. The autonomic PNS, in contrast, consists of neurons that regulate internal organs, blood vessels, and glands, ensuring the seamless functioning of vital physiological processes.

Muscular tissue, too, is categorized into two types: striated and smooth. Smooth muscle, found in structures such as the digestive tract and arteries, is under the control of the autonomic nervous system. Striated muscle is further subdivided into cardiac and skeletal muscle. Cardiac muscle, which makes up the heart, contracts rhythmically even without direct neural input, though its rate is modulated by autonomic influences. Skeletal muscle constitutes the majority of muscle mass in the body and is responsible for moving bones at the joints, controlling eye movements, facilitating respiration, producing facial expressions, and enabling speech. Each skeletal muscle is encased in a connective tissue sheath that typically converges into tendons at one or both ends, anchoring the muscle to bones. Within each muscle lie hundreds of muscle fibres, the individual cells of skeletal muscle, each innervated by a single axon branch from the CNS. Collectively, skeletal muscles and their

controlling nervous system components form the somatic motor system (Bear *et al.*, 2007).

Understanding the anatomical and functional organization of the motor control system, including cortical, subcortical, and brainstem structures, is essential to contextualize the pivotal role of the spinal cord in motor function. These higher-order structures are integral to planning, initiating, and modulating voluntary movements, creating the broader framework within which spinal circuits operate. However, the spinal cord is far from being a mere subordinate in this hierarchy. Instead, it plays a central role in executing motor commands and integrating sensory feedback, forming the final common pathway for motor output while independently mediating reflexes, rhythmical patterns, and sensorimotor integration. This thesis focuses on the spinal cord, particularly its intrinsic circuits, not only as an executor of descending commands but as an active participant in motor control, capable of generating and modulating complex behaviours. By first exploring the broader motor system, this introduction provides the necessary context to highlight the spinal cord's unique contributions and to understand how its circuits function within the larger sensorimotor framework.

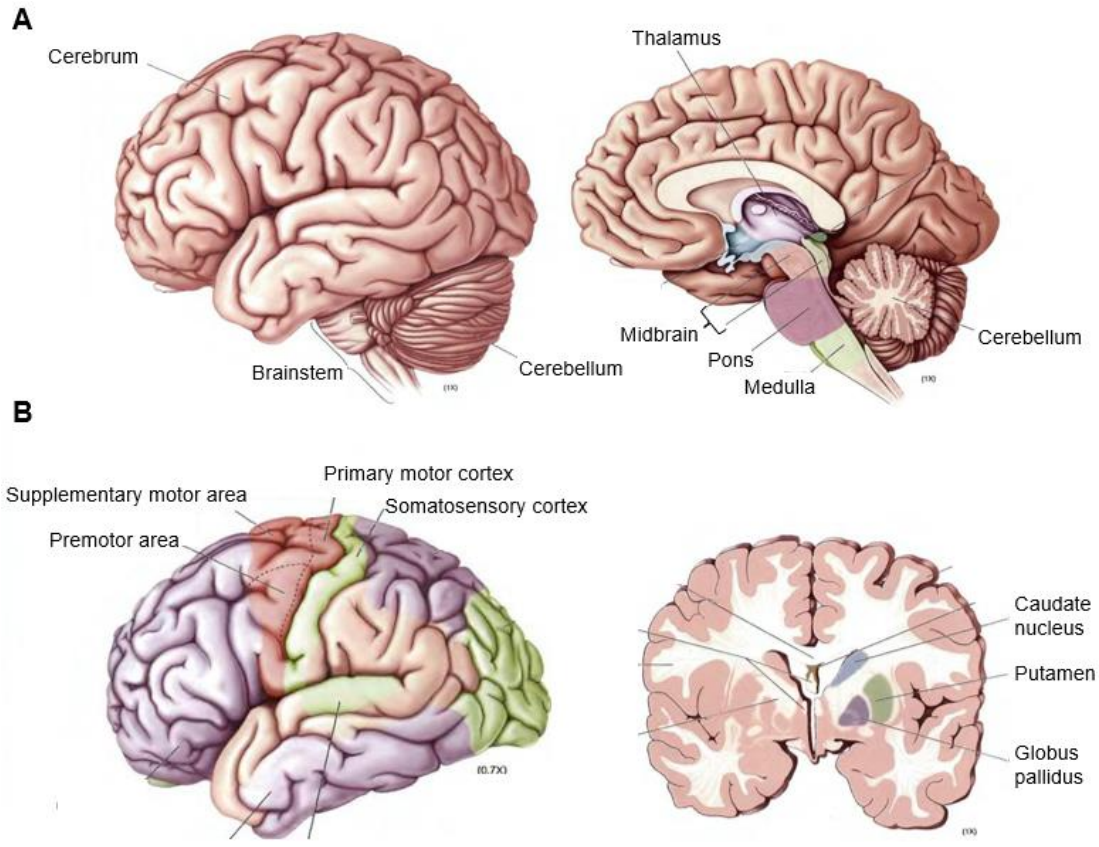

Figure 1. Schematic representation of the main functional and anatomical structures in the brain related to motor control. Adapted from Bear *et al.*, 2007.

1.1. Motor cortex, basal ganglia, cerebellum, brainstem

1.1.1. Brain control of movement

The brain initiates voluntary movement through a hierarchical motor system, with the forebrain at the top and spinal cord at the bottom. The highest level, including the neocortex (especially the motor and prefrontal cortices) and basal ganglia, sets the movement strategy, determining goals and optimal approaches. The middle level, involving also the motor cortex, cerebellum and portions of the brainstem, devises tactical muscle sequences for smooth execution, while the lowest level, comprising the brainstem and spinal cord, activates neurons to perform the movement and stabilize posture. Motor control relies heavily on sensory information from vision, hearing and proprioception, suggesting that the brain's motor system functions as a sensorimotor system. The most advanced levels of processing for somatosensory information take place in the cerebral cortex, particularly in the primary somatosensory cortex (S1) and other related sensory areas (Bear *et al.*, 2007).

1.1.2. Motor cortex

As mentioned, the motor cortex plays a dual role in voluntary movement, interacting with associative and integrative regions to plan and strategize movements, but also translating those plans into precise motor commands for execution. This dual functionality is supported by the distinct subregions of the motor cortex— the primary motor cortex (M1) for generating motor commands, and the premotor area (PMA) and supplementary motor area (SMA) for planning and coordinating movements in conjunction with other associative regions (Figure 1B) (Bear *et al.*, 2007). The human M1 follows a somatotopic organization (i.e., each area is dedicated to a particular muscle/muscle group). The resulting somatotopic representation is sometimes referred to as the Penfield's homunculus. These somatotopic maps do not maintain a proportional scale to the human body. The amount of cortical area dedicated to each body part is proportional to the density of motor output required for its control. Therefore, larger populations of neurons are dedicated to hand and

facial muscles in comparison to other muscles, reflecting the intricate precision needed for hand movements and facial expressions (Penfield & Rasmussen, 1950).

The activation of lower motor neurons (located in brainstem motor nuclei or in the spinal cord) by the motor cortex begins with pyramidal neurons in cortical layer V. These pyramidal neurons project axons via the corticospinal tract to synapse directly on lower motor neurons in the spinal cord or indirectly through interneurons. In addition, layer V pyramidal cells also send axon collaterals to various subcortical regions involved in sensorimotor processing, such as the brainstem reticular formation, red nucleus, and basal ganglia, enabling coordination and modulation of movement. Individual pyramidal cells can influence multiple motor neuron pools, activating muscles across different joints to achieve a coordinated movement toward a specific goal. However, a large portion of the motor cortex is activated for each movement, and movement direction is encoded by the combined activity of a population of neurons (Georgopoulos *et al.*, 1982).

1.1.3. Basal ganglia

The primary subcortical input to the PMA and SMA originates from the ventral lateral (VL) nucleus of the dorsal thalamus, specifically a subdivision known as VLo (*pars oralis*). This input is derived from the basal ganglia, located deep within the telencephalon. The basal ganglia receive signals from the cerebral cortex, particularly from the frontal, prefrontal, and parietal areas. This arrangement creates a loop in which information flows from the cortex through the basal ganglia and thalamus and returns mainly to the SMA, with a key function of selecting and initiating voluntary movements.

The basal ganglia comprise the caudate nucleus, putamen, globus pallidus, and subthalamic nucleus, along with the substantia nigra, which is reciprocally connected to them in the forebrain (Figure 1B). The caudate and putamen, collectively called the striatum, serve as the primary input structures by receiving excitatory cortical signals. The globus pallidus acts as the main output structure, projecting inhibitory signals to the thalamus (specifically VLo). Additional structures, such as the subthalamic nucleus and substantia nigra, contribute modulatory loops that fine-tune the activity of the direct pathway.

In the motor loop, excitatory input from the cortex activates the putamen, which in turn inhibits neurons in the globus pallidus. This inhibition reduces the tonic inhibitory output to VLo, allowing VLo cells to become disinhibited and to activate the SMA via excitatory projections. This sequence forms a positive feedback loop that channels cortical activation toward the SMA and likely serves as a "go" signal for movement once SMA activity reaches a threshold (Bear *et al.*, 2007).

In summary, the basal ganglia facilitate movement by concentrating activity from diverse cortical regions onto the SMA while also filtering out inappropriate movements.

1.1.4. Cerebellum

Located behind the cerebrum, the cerebellum comprises about 10% of the brain's total volume yet contains a number of neurons comparable to the cerebrum (Figure 1A). It plays a critical role in motor control by integrating sensory inputs and motor commands to coordinate movement, maintain posture, and ensure balance. Connected extensively with the cerebrum, brainstem, and spinal cord, it forms a key hub in the sensorimotor system. Unlike the cerebrum, the cerebellum exhibits ipsilateral control, meaning each side controls movements on the same side of the body.

The cerebellum is not sharply divided at the midline; its folia extend uninterrupted across a central bump called the vermis. The vermis separates the two lateral hemispheres and is essential for specific functions. It sends outputs to brainstem structures that influence ventromedial descending spinal pathways managing axial musculature, while the lateral hemispheres primarily regulate limb movements via connections with cortical areas associated with lateral descending pathways.

The cerebellum also participates in multiple loops that integrate cortical signals with sensory feedback to fine-tune movement. Axons from layer V pyramidal cells in the sensorimotor cortex project to clusters in the pontine nuclei, which relay signals to the cerebellum. This corticopontine-cerebellar pathway contains about 20 million axons, roughly 20 times more than the pyramidal tract. The lateral cerebellum then projects back to the motor cortex via a relay in the ventral lateral nucleus of the thalamus. This pathway plays a critical role in executing planned, voluntary multijoint movements. Once the cerebellum receives a signal of movement intent, it

instructs the primary motor cortex on the direction, timing, and force of movement, making compensatory adjustments when discrepancies arise.

In summary, the cerebellum orchestrates the precise sequence of muscle contractions needed for complex movements, ensuring that motor programs for skilled actions are executed accurately and modified as necessary (Bear *et al.*, 2007).

1.1.5. Brainstem

The brainstem connects the cerebrum and cerebellum to the spinal cord and is composed of the midbrain, the pons, and the medulla oblongata (Figure 1A). It serves as a crucial conduit for both voluntary and involuntary motor control by integrating signals from higher brain centres with spinal circuits. Anatomically, the brainstem houses numerous nuclei and fibre tracts. For instance, the reticular formation plays a key role in regulating consciousness and arousal, while the midbrain contains structures such as the substantia nigra, which modulates voluntary movement through dopaminergic signalling. The pons, besides relaying signals between the cerebrum and cerebellum, contains cranial nerve nuclei that contribute to motor functions like facial expression and eye movements. Meanwhile, the medulla oblongata is central to autonomic functions, regulating breathing, heart rate, and temperature control, and governs reflex actions such as swallowing, coughing, sneezing, and vomiting. This combination of roles makes the brainstem one of the most primitive yet vital parts of the brain; damage to it is typically fatal because it disrupts both sensory input and the brain's control over the body (Bear *et al.*, 2007; Dharani, 2015).

1.2. Spinal cord anatomy

The spinal cord is the primary connection between the brain and the body, transmitting motor, sensory, and autonomic information bidirectionally. Far from being a mere relay station, the spinal cord actively integrates and processes these signals. It carries commands from the brain and brainstem to stimulate muscles and simultaneously processes sensory input from the body before relaying it to higher centers (Bear *et al.*, 2007; Watson *et al.*, 2009). In the sections that follow, we will detail its intrinsic circuits and elaborate on its crucial role in shaping complex motor control.

1.2.1. Spinal cord organisation and morphology

The human spinal cord extends from the medulla oblongata of the brainstem to the lower back, ending at the conus medullaris around the second lumbar vertebra. It is protected by the vertebral column and enveloped by three layers of membranes known as the meninges: the dura mater, arachnoid mater, and pia mater (Murray, 2015). The cerebrospinal fluid (CSF) circulates between the arachnoid mater and the pia mater (Bear *et al.*, 2007), providing cushioning to absorb mechanical shocks, maintaining a stable environment for neural tissue, and facilitating the removal of metabolic waste.

When viewed transversely, the spinal cord reveals two distinct regions: centrally located grey matter, shaped like a butterfly, surrounded by white matter on both sides. Additionally, spinal nerves emerge from each side of the cord, innervating specific areas of the body (Watson *et al.*, 2009; Silva *et al.*, 2014).

1.2.1.1. Spinal nerves

Communication between the spinal cord and the body occurs through spinal nerves, part of the peripheral nervous system, which exit through notches between the vertebrae of the spinal column. Each spinal nerve has two roots: the ventral root, which sends efferent motor signals from CNS motoneurons to muscles, and the dorsal root, which transmits afferent sensory information from the periphery to the spinal cord (Figure 2) (Bear *et al.*, 2007). The cell bodies of these sensory neurons are grouped in a structure called the dorsal root ganglion (DRG) along each dorsal root (Silva *et al.*, 2014).

Shortly after exiting the spinal cord, the dorsal and ventral roots combine to form the spinal nerve. Since these spinal nerves contain both sensory and motor fibres, they are classified as mixed nerves. The names of the 31 human spinal nerves correspond to the spinal segment from which they originate: cervical (C1-C8), thoracic (T1-T12), lumbar (L1-L5), sacral (S1-S5), and coccygeal (Co1) (Watson *et al.*, 2009; Silva *et al.*, 2014). Interestingly, there is not a direct correspondence between spinal cord segments (s) and vertebrae (v). For instance, there are 8 cervical spinal cord segments but only 7 cervical vertebrae, and the lumbar spinal segments are protected by the caudal thoracic vertebrae (Figure 2) (Watson *et al.*, 2009).

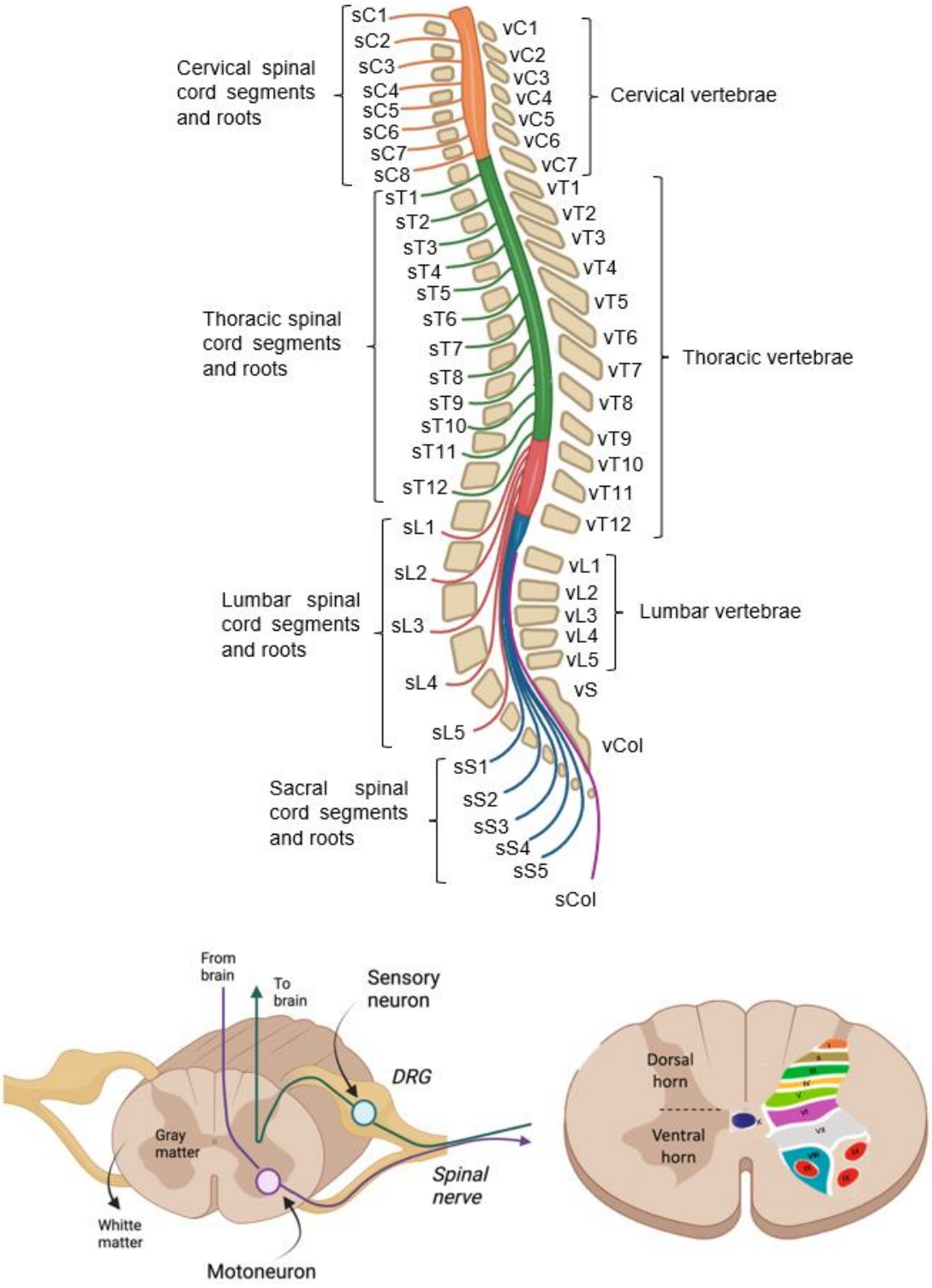

Figure 2. Schematic representation of the basic spinal cord anatomy. Bottom illustrations obtained from the doctoral thesis of Sánchez-Ventura J (2023).

1.2.1.2. Grey matter

The grey matter of the spinal cord contains the cell bodies of interneurons, motoneurons, and glial cells. At the macroscopic level, it is divided into a dorsal section, an intermediate zone and a ventral section (Figure 2). The dorsal region, or dorsal horn, serves as the sensory area, housing nuclei responsible for processing pain, temperature, and proprioception. The ventral sections, known as the ventral horns, make up the motor area, where somatic motor neurons are located. Between these two regions lies the intermediate grey matter (Watson *et al.*, 2009; Silva *et al.*, 2014; Murray, 2015).

On a microscopic level, the grey matter is organized into ten distinct cell layers, known as the Laminae of Rexed, with each lamina containing different types of neurons based on their structure and function (Figure 2) (Rexed, 1952).

1.2.1.2.1. Spinal interneurons

Spinal interneurons serve to connect sensory neurons with motoneurons. They are distributed extensively throughout the grey matter of the spinal cord. These interneurons can be either excitatory or inhibitory, giving them a wide range of properties and functions (Zholudeva *et al.*, 2021). In fact, most input to alpha motor neurons comes from spinal interneurons. These interneurons receive synaptic inputs from primary sensory axons, descending axons from the brain, and collaterals from lower motor neuron axons. The interneurons are interconnected, allowing them to generate coordinated motor programs in response to various inputs (Bear *et al.*, 2007). Spinal interneurons can be classified into two main types: propriospinal neurons, which have ascending and descending projections, and local interneurons, which have either ipsilateral projections or projections that cross the midline (commissural) of the spinal cord (Lane, 2011; Zholudeva *et al.*, 2018).

1.2.1.2.1. Spinal motoneurons

Although spinal motoneurons can be categorized into visceral and somatic types, this doctoral thesis focuses specifically on somatic motoneurons. Somatic motoneurons are cholinergic neurons located in the ventral horn of the spinal cord, particularly within the lamina IX, and they project their axons to skeletal muscles (Watson *et al.*, 2009). Often referred to as lower motor neurons, they differ from upper motor neurons

in the brain that provide input to the spinal cord. It is important to note that only lower motor neurons directly initiate muscle contractions. The distribution of motoneurons throughout the spinal cord is heterogeneous and correlates with the number of skeletal muscles innervated in a given segment. Accordingly, most spinal motoneurons are concentrated in two enlargements: the cervical enlargement, which innervates the forelimbs, and the lumbosacral enlargement, which innervates the hindlimbs (Bear *et al.*, 2007).

Somatic motoneurons can be further divided into alpha (α) and gamma (γ) motoneurons, which differ in morphology and connectivity. Morphologically, α-motoneurons are the most prevalent; they possess larger cell bodies and thicker axons, resulting in faster conduction velocities compared to γ-motoneurons. α-Motoneurons innervate extrafusal muscle fibres responsible for generating force and producing muscle contractions. In contrast, γ-motoneurons innervate intrafusal fibres (muscle spindles), which serve as sensory receptors detecting changes in muscle length (Figure 3). Their primary role is to maintain tension in the muscle spindles so that Ia afferent fibres remain active and transmit accurate sensory information (Bear *et al.*, 2007). In terms of input, α-motoneurons receive c-boutons and proprioceptive sensory inputs derived from Ia fibres, whereas γ-MNs do not (Witts *et al.*, 2014).

Each α-motoneuron, along with the muscle fibres it innervates, constitutes the basic unit of motor control known as the motor unit, a term coined by Sherrington (Liddell & Sherrington, 1925). Muscle contraction results from both the individual and collective actions of these motor units. The group of α-motoneurons that innervates a single muscle is referred to as a motor neuron pool (Bear *et al.*, 2007).

α-Motoneurons receive inputs mainly from spinal interneurons, which can be excitatory or inhibitory. Also, they receive sensory feedback of muscle length from dorsal root ganglion neurons, and from upper motoneurons in the brain and brainstem to initiate and regulate voluntary movement (Bear *et al.*, 2007).

Muscle contraction begins with the release of acetylcholine (ACh) from the terminals of α-motoneurons. This neurotransmitter generates a significant excitatory postsynaptic potential (EPSP) in the muscle cell membrane by activating nicotinic ACh receptors. The presence of voltage-gated sodium channels in the muscle cell membrane allows this EPSP to generate an action potential in the muscle fibre.

Through a process known as excitation-contraction coupling, this action potential triggers the release of calcium ions (Ca^{2+}) from the sarcoplasmic reticulum within the muscle fibre, leading to contraction. Relaxation occurs when the levels of Ca^{2+} decrease due to reuptake into the organelle (Bear *et al.*, 2007).

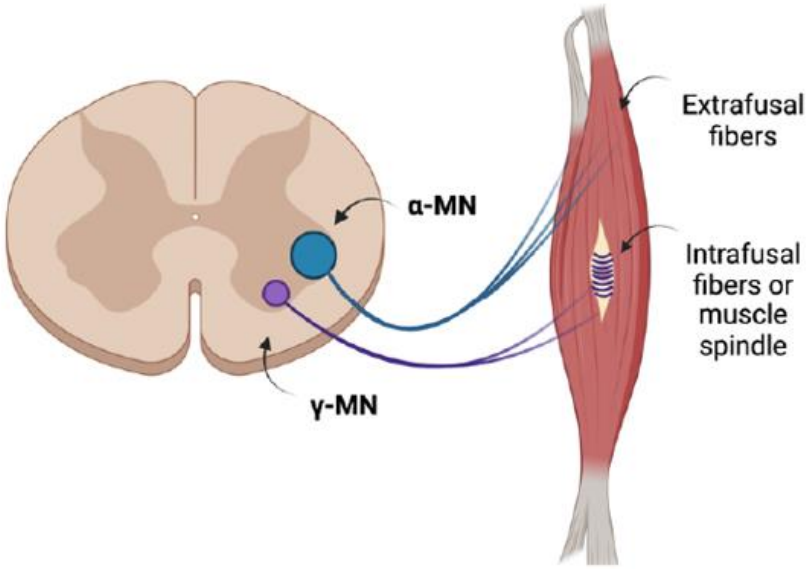

Figure 3. Schematic representation of the muscle innervation by spinal motoneurons. MN: motoneuron. Illustrations obtained from the doctoral thesis of Sánchez-Ventura J (2023).

1.2.1.3. White matter

The white matter consists of axonal projections along with their associated glial cells. These axons run longitudinally through the spinal cord and are organized into specific groups based on their origin, termination, and the type of information they transmit, collectively forming what are known as spinal tracts (Murray, 2015). Spinal tracts can be classified as ascending or descending depending on the direction of information flow. Ascending tracts originate from sensory neurons in the DRG and carry sensory information upward, while descending tracts typically relay motor information from the cortex and subcortical structures downward. Additionally, there are sensory descending pathways, such as those involved in pain modulation (Watson *et al.*, 2009). In the following section, the relevant characteristics of these pathways will be explained in greater detail.

1.3. Spinal pathways and physiology

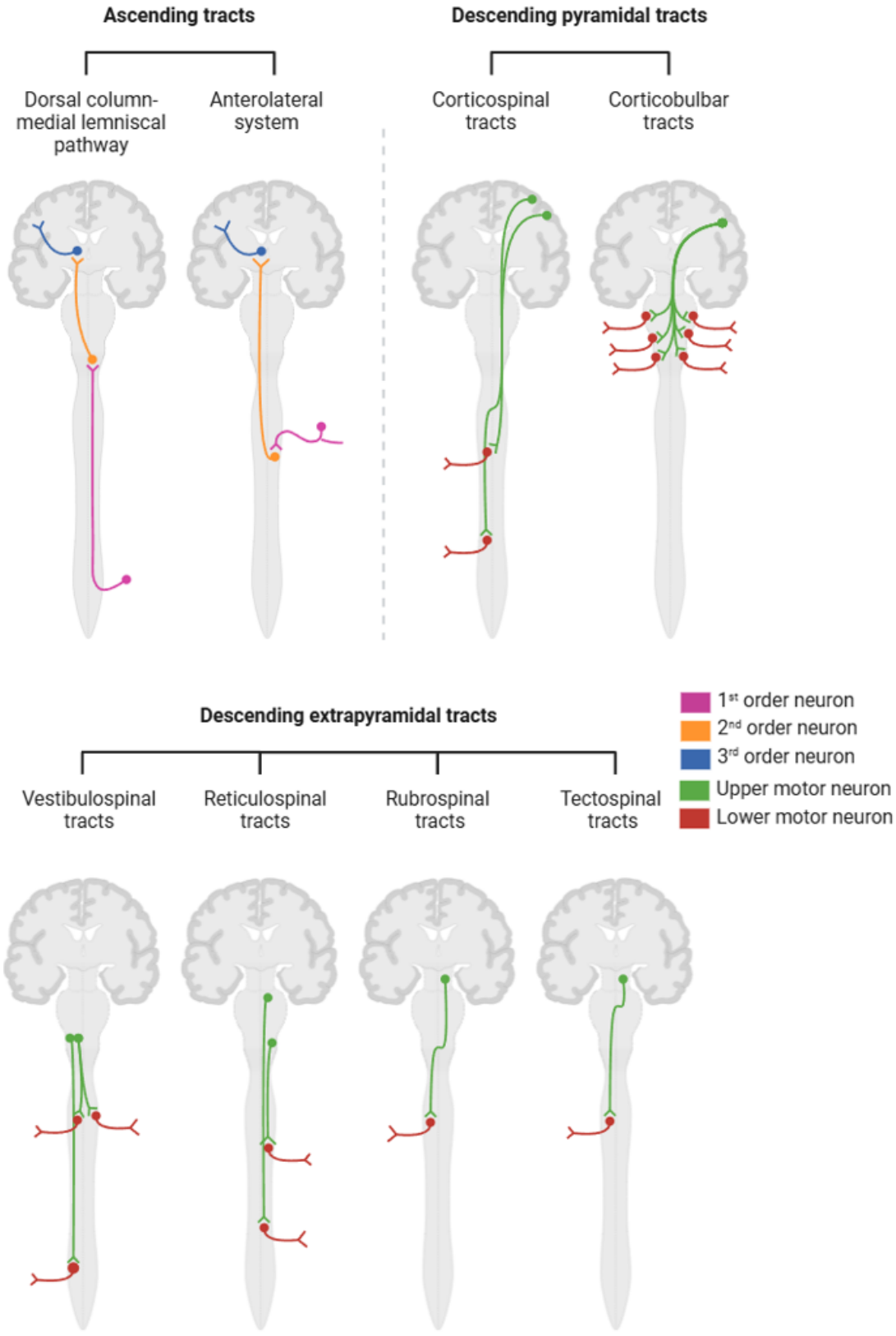

Figure 4. Schematic representation of the spinal cord ascending and descending tracts. Images obtained from BioRender.

1.3.1. Ascending spinal tracts

Ascending tracts transmit two types of afferent information: exteroceptive and proprioceptive. Exteroceptive information originates from the environment outside the body and includes touch, nociception and temperature. In contrast, proprioceptive information comes from within the body, providing information about the state of muscles and joints (Watson *et al.*, 2009).

All ascending pathways consist of at least three distinct types of neurons. The first is the primary afferent, or first-order neuron, whose cell body is located in the DRG and that transmits sensory information from the periphery to the dorsal horn of the spinal cord. The second is the intermediate, or second-order neuron, which relays this information. Finally, the third is the third-order neuron, whose cell body is situated in subcortical areas and sends its axon to either the cerebellar or cerebral cortex (Bear *et al.*, 2007).

There are three types of ascending pathways:

- **Spinocerebellar:** This pathway transmits unconscious proprioceptive signals from muscles and joints. It involves receptors such as muscle spindles and Golgi tendon organs located in the muscles. Muscle spindles are stretch receptors specialized in detecting changes in muscle length. They are innervated by Ia axons, the thickest and fastest myelinated axons in the body, which branch extensively within the spinal cord, forming synapses with both interneurons and alpha motor neurons. In fact, a single Ia axon contacts nearly every alpha motor neuron in the pool that innervates the muscle containing that spindle (Mendell & Henneman, 1971). Golgi tendon organs, located at the junction between muscle and tendon, monitor muscle tension. They are innervated by Ib sensory axons, which are slightly smaller than Ia axons, and they synapse onto interneurons in the ventral horn. Additionally, this proprioceptive information is integrated with input from joint receptors, a process that is particularly vital for executing fine motor tasks (Bear *et al.*, 2007).
- **Spinothalamic:** This pathway processes sensations of touch, pressure, pain, and temperature. The receptors involved are typically non-specialized free nerve endings, including low-threshold mechanoreceptors (which detect

gross touch), nociceptors (which detect pain), and thermoreceptors (which detect temperature). Second-order neurons decussate immediately within the spinal cord and project directly to the thalamus (Figure 4).

- **Dorsal column-medial lemniscal (DCML):** This pathway carries information about vibration, fine touch, and proprioception. The receptors for touch and vibration are mechanoreceptors located in the skin, while proprioceptive signals are provided by muscle spindles and Golgi tendon organs. The axons of first-order neurons ascend ipsilaterally through the dorsal column and relay their signals in the medulla. There, second-order neurons decussate and project to third-order neurons in the thalamus, which then relay the information to the primary somatosensory cortex (Figure 4) (Bear *et al.*, 2007).

1.3.2. Descending spinal tracts

Most descending tracts transmit motor commands generated in the brain or brainstem to α-motoneurons. Traditionally, these motor tracts are described as a two-neuron system, at least in humans and non-human primates, consisting of an upper motor neuron located in the brain or brainstem and a lower motor neuron located in the ventral horn of the spinal cord (or, in some cases, in the brainstem for cranial nerves). The upper motor neuron sends its axon to the spinal cord to synapse with the lower motor neuron (Watson *et al.*, 2009). However, it is now recognized that upper motor neurons often relay information to lower motor neurons via spinal interneurons, not only in non-human animals but also in humans (Witts *et al.*, 2014). Ultimately, the lower motor neuron innervates the skeletal muscle.

There are two main descending pathways:

- **Lateral descending pathway.** This pathway comprises the corticospinal and rubrospinal tracts and is the primary route for controlling voluntary movements of distal muscles (e.g., independent hand and finger movements) (Lawrence & Kuypers, 1968).
    - The corticospinal or pyramidal tract is one of the largest in the CNS and the key component of the lateral pathway. Approximately two-thirds of its axons come from the motor cortex, while the rest primarily originate from the somatosensory cortex, helping to regulate the flow

of sensory information to the brain. In non-human primates and humans, these axons converge to form the medullary pyramid, cross at the pyramidal decussation (situated at the junction of the medulla and spinal cord), and then form the lateral corticospinal tract in the lateral column of the spinal cord. In these species, the axons primarily terminate in the dorsolateral area of the ventral horns and the intermediate grey matter, where they modulate the activity of motor neurons and interneurons controlling distal muscles, especially the flexors. In rodents and other non-primate species, while many corticospinal fibres also cross at the pyramidal decussation, the organization is somewhat different. In these species, a significant proportion of fibres may descend in the dorsal or ventral funiculi rather than forming a distinct lateral tract. Consequently, the terminal distribution of corticospinal axons tends to be more diffuse, reflecting a motor system that is less specialized for the fine, independent control of distal muscles compared to primates (Figure 4).

- The rubrospinal tract is the smaller component of the descending lateral pathway and originates from the red nucleus in the midbrain. Axons from the red nucleus decussate in the pons and join those of the corticospinal tract within the lateral column of the spinal cord. Given that a significant input to the red nucleus comes from the same motor cortical areas that contribute to the corticospinal tract, the corticorubrospinal pathway is considered an indirect route for conveying motor commands (Figure 4) (Bear *et al.*, 2007). Importantly, although the decussation in the pons and integration with corticospinal fibres is conserved across species, the functional emphasis and extent of the rubrospinal tract vary according to the motor demands and evolutionary adaptations of each species. In primates, the rubrospinal tract is relatively small and primarily involved in controlling proximal limb movements, with the corticospinal tract largely dominating fine, distal motor control. In contrast, in species such as rodents and cats, the rubrospinal tract is more prominent and plays a crucial role in coordinating limb movements and overall motor control.

- **Ventromedial descending pathway.** This pathway consists of four tracts that originate in the brainstem and terminate among spinal interneurons controlling proximal and axial muscles (Figure 4). These tracts, namely the vestibulospinal, tectospinal, pontine reticulospinal, and medullary reticulospinal, play key roles in maintaining balance and posture.
    - The vestibulospinal tract, which originates in the vestibular nuclei of the medulla (receiving sensory input from the inner ear's vestibular labyrinth), has two main branches. One projects bilaterally to neck muscles to control head movements, while the other projects ipsilaterally to lumbar segments to support posture by activating leg extensor muscles. In many non-primate species, this tract is particularly robust, reflecting the greater reliance on vestibular inputs for balance in quadrupedal locomotion. In primates, however, the vestibulospinal influence is relatively diminished, as the evolution of fine motor skills has shifted some balance functions to other systems.
    - The tectospinal tract, originating in the superior colliculus of the midbrain, integrates visual, auditory, and somatosensory inputs to form a spatial map of the environment, thereby directing head and eye movements toward salient stimuli. While this pathway is well developed in many mammals for rapid orienting responses, its relative contribution may vary among species, with primates often relying more heavily on direct cortical control for such tasks.
    - The reticulospinal tracts arise from the reticular formation, a complex network of neurons that receives diverse inputs and influences numerous functions. They can be divided into two distinct tracts: the pontine (medial) reticulospinal tract and the medullary (lateral) reticulospinal tract. The pontine reticulospinal tract facilitates antigravity reflexes by enhancing the activity of lower limb extensors, a function crucial for maintaining upright posture. In contrast, the medullary reticulospinal tract reduces reflex control over these muscles. In many non-primate species, these reticulospinal pathways are especially important for coordinating locomotion and posture, whereas in primates, their role is complemented by more advanced cortical control systems. Both tracts are modulated by descending

cortical signals, and the balance between them is essential for proper motor regulation (Bear *et al.*, 2007).

Differences between humans and rats in the location of the ascending and descending tracts within the spinal white matter can be found in Figure 5.

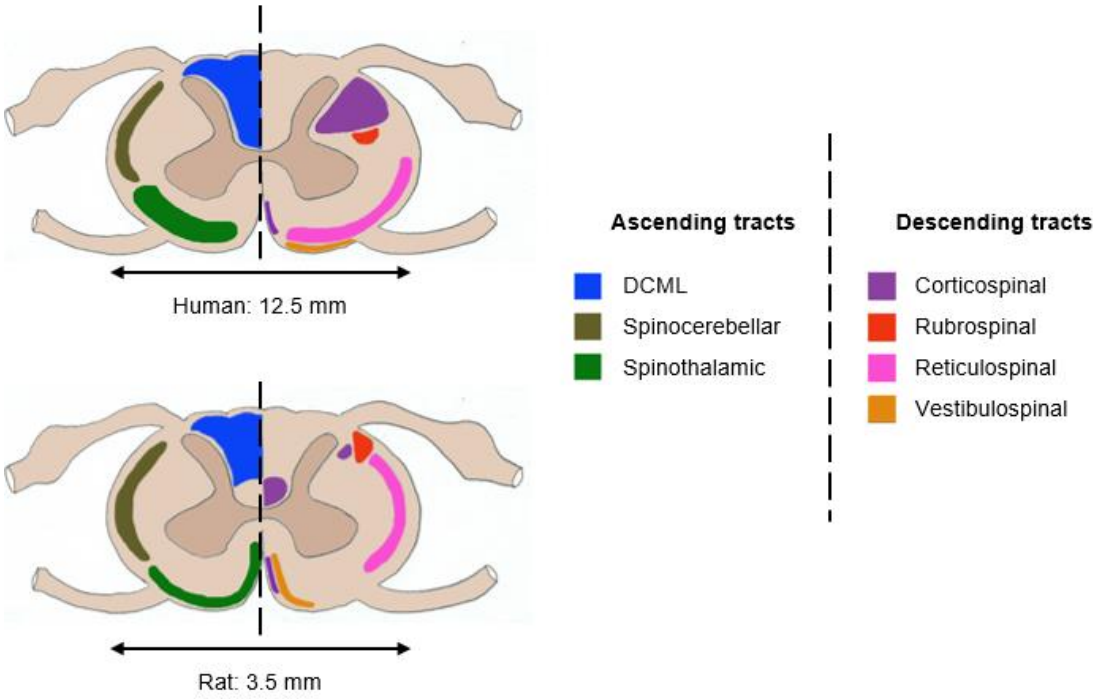

Figure 5. Schematic representation of the spinal cord ascending and descending tracts in humans and rats. Adapted from the doctoral thesis of Baylo-Marín O (2022).

There are also descending pathways that do not directly control motor functions but instead modulate pain perception. These descending modulatory pathways originate in higher centres, such as the periaqueductal grey (PAG) and the rostral ventromedial medulla (RVM), among others. These brain areas regulate pain perception by either inhibiting or facilitating the transmission of nociceptive signals at the level of the dorsal horn. The modulatory effects are primarily mediated by monoaminergic pathways, including serotonin, norepinephrine, and dopamine (Kwon *et al.*, 2014).

2. Spinal networks and sensorimotor behaviour

Although the spinal cord is often regarded as a communication highway because of its well-defined tracts, its functions extend far beyond merely relaying signals between the brain and the body. Indeed, the spinal cord is not merely a conduit for information

but a dynamic hub of interconnected networks that generate and modulate motor output. Basic spinal circuits, such as reflex pathways, central pattern generators (CPGs), propriospinal networks, and presynaptic inhibition mechanisms, form the foundation for sensorimotor integration. For instance, while simple reflexes rapidly maintain posture and protect the body, CPGs generate rhythmic patterns essential for activities like locomotion and breathing. Propriospinal circuits coordinate signals across multiple spinal segments, and presynaptic inhibition finely tunes sensory input to adjust motor commands. In this section, we will first review these fundamental networks and their roles in basic motor control. We will then examine how their integration, along with inputs from higher brain centres, gives rise to complex sensorimotor behaviours such as coordinated locomotion and precise manual dexterity.

2.1. Basic spinal networks

2.1.1. Spinal reflexes

Spinal reflexes are among the most extensively studied spinal circuits because of their significance in maintaining posture and facilitating locomotion. Each spinal reflex consists of at least four components: a somatic receptor, a sensory (afferent) neuron, a motor neuron (efferent neuron), and the skeletal muscle. More complex reflexes include an interneuron in the circuit, allowing for greater flexibility in response. Reflexes can be categorized based on their complexity into monosynaptic and polysynaptic reflexes.

Monosynaptic reflexes involve just two neurons, the sensory neuron and the motor neuron, connected by a single synapse. A classic example is the stretch (myotatic) reflex (Figure 6). Here, muscle spindles detect changes in muscle length and send signals via Ia afferents from the DRG into the spinal cord. These axons synapse directly with α-motoneurons, which then cause contraction of the corresponding extrafusal muscle fibres. Concurrently, reciprocal inhibition, mediated by collaterals that activate inhibitory interneurons, relaxes the antagonist muscle (Bear *et al.*, 2007).

Polysynaptic reflexes involve one or more interneurons, allowing the sensory and motor neurons to communicate indirectly. For example, during muscle contraction, the Golgi tendon organ detects tension and activates its afferents. These, in turn,

stimulate an inhibitory interneuron that reduces the activity of the same α-motor neuron, leading to muscle relaxation (the inverse stretch or Golgi tendon reflex; Figure 6). Another example is the withdrawal reflex, triggered by a painful stimulus. Nociceptors activate interneurons that not only stimulate ipsilateral flexor muscles while inhibiting extensor muscles, but also send collateral signals to the contralateral side, activating extensor and inhibiting flexor muscles, to stabilize posture in the crossed-extensor reflex (Clarke & Harris, 2004).

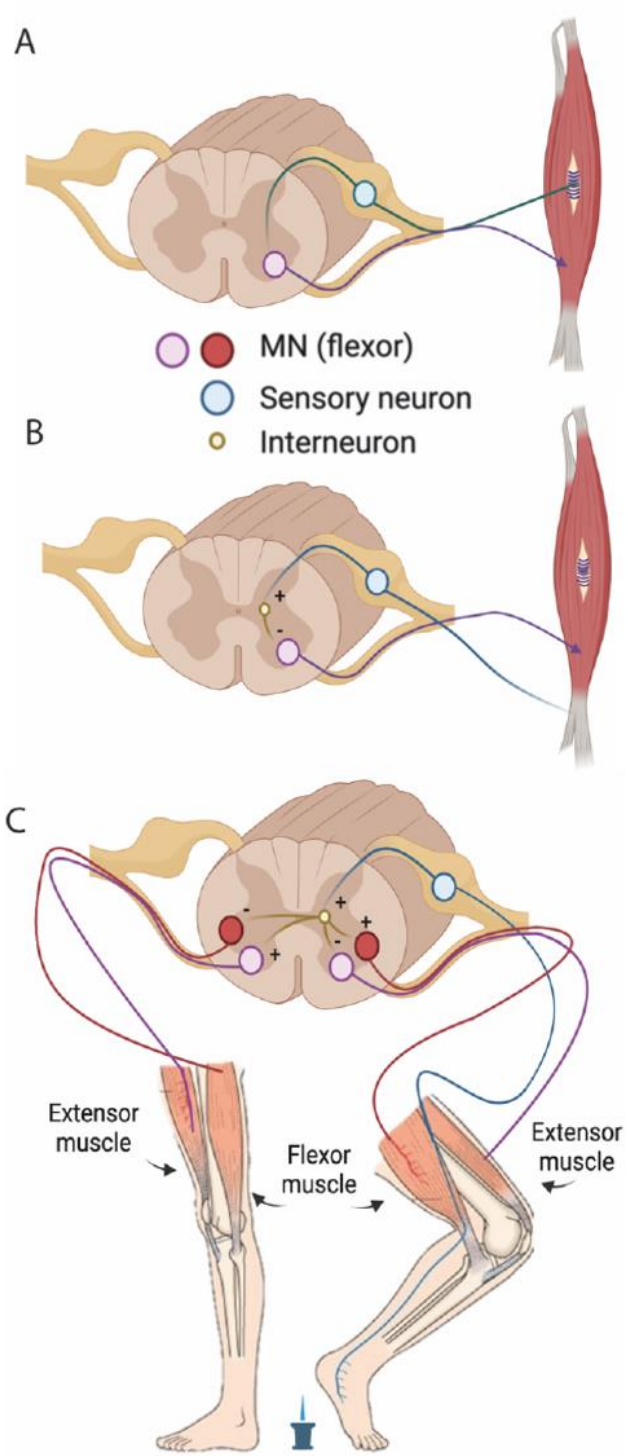

Figure 6. Schematic representation of spinal reflexes. (A) Stretch reflex. **(B)** Inverse stretch reflex. **(C)** Withdrawal reflex. MN: motoneuron. Illustrations obtained from the doctoral thesis of Sánchez-Ventura J (2023).

2.1.2. Presynaptic inhibition circuits

Presynaptic inhibition is a fundamental mechanism that modulates the strength of sensory input before it reaches motoneurons, thereby fine-tuning motor output. This process is mediated by specialized GABAergic interneurons that form axo-axonic synapses on the terminals of sensory afferents. When activated, these interneurons reduce neurotransmitter release from the sensory axon, effectively dampening the signal and preventing excessive or inappropriate reflex responses (Faist *et al.*, 1994). Presynaptic inhibition regulates both reflex pathways and voluntary movement, ensuring that the level of sensory feedback is appropriately scaled during various motor tasks, contributing to smooth and coordinated actions. The level of presynaptic inhibition is dynamically controlled by both local spinal circuits and descending pathways (e.g., corticospinal and reticulospinal tracts).

2.1.3. CPGs

CPGs are intrinsic spinal circuits that generate rhythmic motor patterns required for activities such as walking, swimming, and breathing, without requiring rhythmic input from higher brain centres. Composed of networks of excitatory and inhibitory interneurons, CPGs coordinate alternating phases of muscle activity, for example, flexor and extensor bursts during locomotion. For example, during locomotion, one group drives flexor muscle activity while inhibiting extensor muscles, and vice versa, creating a coordinated gait pattern. Intrinsic membrane properties (e.g., plateau potentials, persistent sodium currents) and synaptic interactions contribute to their rhythmic output. CPGs are not isolated circuits; they are continuously modulated by sensory feedback (e.g., proprioceptive signals from muscle spindles and Golgi tendon organs) and descending commands from supraspinal centres, allowing for adaptation to changing conditions (Grillner, 2006; Kiehn, 2016).

2.1.4. Propriospinal Networks

Propriospinal neurons are interneurons with axons that extend across multiple spinal segments, interconnecting motor circuits at different levels of the spinal cord. These

networks play a critical role in coordinating movements that span several joints or limbs. By integrating descending motor commands with local sensory inputs, propriospinal networks ensure that motor outputs are synchronized across different regions, for example, linking the cervical and lumbar enlargements during coordinated limb movements in locomotion. These neurons come in various types, both excitatory and inhibitory, each contributing to the fine-tuning of motor actions (Jankowska, 1992). In addition, propriospinal pathways are crucial for functional recovery after spinal cord injuries, as they can help reroute motor signals when primary pathways are damaged.

2.2. Complex sensorimotor behaviours

2.2.1. Neural control of locomotion

Locomotion is a complex, rhythmic activity that relies on the seamless coordination of extensor and flexor muscles. This intricate process emerges from the dynamic interplay between motoneurons, CPGs, and various feedback mechanisms (Côté *et al.*, 2018). At the lumbar level, the locomotor CPG generates a basic rhythmic pattern—a motor output based on the crossed-extensor reflex, where one leg extends as the other flexes. Remarkably, this rhythm can be produced even without descending or afferent inputs (Sherrington, 1910). Yet, in everyday movement, descending pathways and sensory feedback are essential for adapting this basic rhythm to real-world conditions, enabling rapid postural adjustments and corrective movements (Rossignol *et al.*, 2006; Jordan & Sławińska, 2014). In this finely tuned system, motoneurons integrate diverse inputs and transform them into precise, coordinated muscle activation.

Descending pathways, both excitatory and inhibitory, further refine this process. Excitatory tracts activate the spinal locomotor network to initiate, halt, and direct locomotion. For instance, the reticulospinal tract is crucial for initiating locomotion, while the vestibulospinal tract contributes to postural control. Voluntary and goal-directed movements are primarily mediated by the corticospinal and rubrospinal tracts, which help guide and adjust the locomotor response (Rossignol & Frigon, 2011). Other descending pathways also regulate presynaptic inhibition of Ia sensory afferents, thereby adjusting spinal circuits such as the stretch reflex (Faist et al., 1994).

Moreover, sensory inputs play a pivotal role in shaping locomotion. Proprioceptors in skeletal muscles (such as muscle spindles, which monitor muscle length, and Golgi tendon organs, which gauge tension in ligaments and tendons) provide critical feedback that is relayed to the CNS. This sensory information, together with signals from skin nociceptors, is integrated within the spinal cord, ensuring that ongoing movements are continuously adjusted and refined (Pearson, 2004).

It is important to note that locomotor strategies differ markedly between quadrupeds and bipeds. Quadrupeds, benefiting from the stability of four-legged gaits, often exhibit more rhythmic and automatic locomotion, with robust spinal circuits coordinating both forelimbs and hindlimbs. In contrast, bipedal locomotion, as seen in humans, demands constant adjustment of the centre of mass and relies more heavily on supraspinal inputs from cortical and cerebellar centres to maintain balance. This increased reliance on higher-level control renders bipedal gait more adaptable yet also more susceptible to perturbations.

2.2.2. Manual dexterity; the physiology and neural connectivity underlaying reaching and grasping

Skilled forelimb movements stand among the most remarkable achievements of the mammalian motor system (Azim *et al.*, 2014). Reaching and grasping (R&G) objects, for instance, involve a precise sequence of events: a swift flexion of the elbow, followed by the simultaneous extension of both the shoulder and elbow. As the forelimb lifts and reaches forward, the forepaw is dorsiflexed and the fingers are drawn together; then, the digits spread and flex to secure the target object or morsel. After grasping, the forepaw undergoes supination as it retracts toward the mouth (Alstermark *et al.*, 1981).

Historically, these skilled movements were thought to rely primarily on the motor cortex through a direct corticomotoneuronal pathway. This direct connection is largely absent in lower species and becomes more pronounced in primates, a pattern that correlates with increased manual dexterity (Bernhard & Bohm, 1954). In primates, finely controlled finger movements are mainly mediated by monosynaptic connections from the motor cortex to spinal motoneurons (Lawrence & Kuypers, 1968). Although rodents exhibit transient monosynaptic corticomotoneuronal

connections during early postnatal development, these are largely pruned as maturation proceeds (Gu et al., 2017).

More recent research has revealed that skilled R&G depend not only on direct cortical projections but also on indirect pathways that traverse propriospinal neurons and segmental interneurons within the spinal cord (Alstermark & Isa, 2012). In this context, propriospinal neurons located in the sC3–C4 segments (rostral to the forelimb segments) play a key role. Disynaptic corticomotoneuronal pathways involving sC3-C4 propriospinal neurons have been identified in cats (Illert *et al.*, 1977), macaque monkeys (Alstermark *et al.*, 1999) and humans (Malmgren & Pierrot-Deseilligny, 1988), but they are absent in rodents (Alstermark & Ogawa, 2004; Alstermark *et al.*, 2004). In cats, such pathways are critical for reaching(Illert *et al.*, 1977), whereas in humans and non-human primates they are essential for both reaching and for grasping (Kinoshita *et al.*, 2012). Moreover, in cats the grasping component appears to depend more on segmental interneurons located in the same segments as the motoneurons (Alstermark & Sasaki, 1985).

The sC3–C4 propriospinal neurons represent a specialized subset of V2a interneurons, predominantly characterized by their expression of Chx10 (Azim *et al.*, 2014; Ueno *et al.*, 2018). They receive convergent excitatory inputs from descending pathways—including the cortico-, rubro-, reticulo-, and tectospinal tracts—and inhibitory feedback from forelimb afferents. These neurons project directly to motoneurons and send ascending collaterals to the lateral reticular nucleus, which relays an efferent copy of motor commands to the cerebellum (Figure 7). This connection is critical for updating cortical commands to a moving target during reaching, as the cerebellum uses visual information via bulbospinal pathways to correct the trajectory (Azim *et al.*, 2014). The cerebellum corrects the ongoing moving trajectory through the bulbospinal pathway based on visual information (Werner, 1993). In addition to visual control, feedback inhibition of the sC3-C4 propriospinal neurons sent from the cutaneous receptors in the forelimb is critical for correct deceleration and accurate termination of reaching at the target location, and a subsequent successful grasp. These inhibitory interneurons have ascending collaterals to the lateral reticular nucleus (Alstermark *et al.*, 1984). Also, Gad2^{+} inhibitory interneurons play a critical role in reaching control through the smoothing of sensory inputs (Fink *et al.*, 2014). In addition, it has been shown that Vglut3^{+} interneurons

control the grasping phase independently from the corticospinal pathway (Ueno *et al.*, 2018).

Recent studies have also underscored the role of brainstem circuits in skilled forelimb function. The lateral rostral medulla, for instance, has been implicated in executing reaching movements (Ruder *et al.*, 2021), whereas the ventral part of the medullary reticular formation (MdV) appears to be crucial for grasping (Figure 7) (Esposito *et al.*, 2014). These findings highlight that the control of skilled forelimb movements is distributed across multiple levels of the nervous system.

Finally, while the motor cortex and corticospinal tract have traditionally been considered the primary structures for skilled movements (Lemon, 2008), studies on rodents (Alstermark & Pettersson, 2014) and non-human primates (Isa, 2019) have shown that skilled hand function can be preserved despite damage to the corticospinal tract. This indicates that the corticospinal pathway may serve more of a processing role rather than directly executing movements (Flores *et al.*, 2021).

Collectively, these studies illustrate the complex, multi-level organization of neural circuits underlying skilled forelimb function. They emphasize the importance of both direct and indirect pathways (from cortical, propriospinal, and brainstem networks) to the precise coordination of R&G movements, providing a robust framework that supports manual dexterity in species where it is most highly developed.

(Figure on the next page)

Figure 7. Schematic comparison of reaching and grasping circuit between different species. AIP: anterior intraparietal area; CFA: caudal forelimb area; Gi: gigantocellular reticular nucleus; LRN: lateral reticular nucleus; M1: primary motor area; M2: secondary motor area; Mc: magnocellular reticular nucleus; MdV: medullary reticular nucleus ventral part; Med: medial cerebellar nucleus; MN: motoneuron; PCRt: parvicellular reticular nucleus; PMd: dorsal premotor area; PMv: ventral premotor area; Pn: pontine reticular nucleus; PrS: propriospinal; PPR: parietal reach region; R: red nucleus; RFA: rostral forelimb area; S1: primary sensory area; SC: superior colliculus; sIN: segmental interneuron; Sp5: spinal trigeminal nucleus; SpVe: spinal vestibular nucleus; Ve: vestibular nucleus. Images from Isa, 2019.

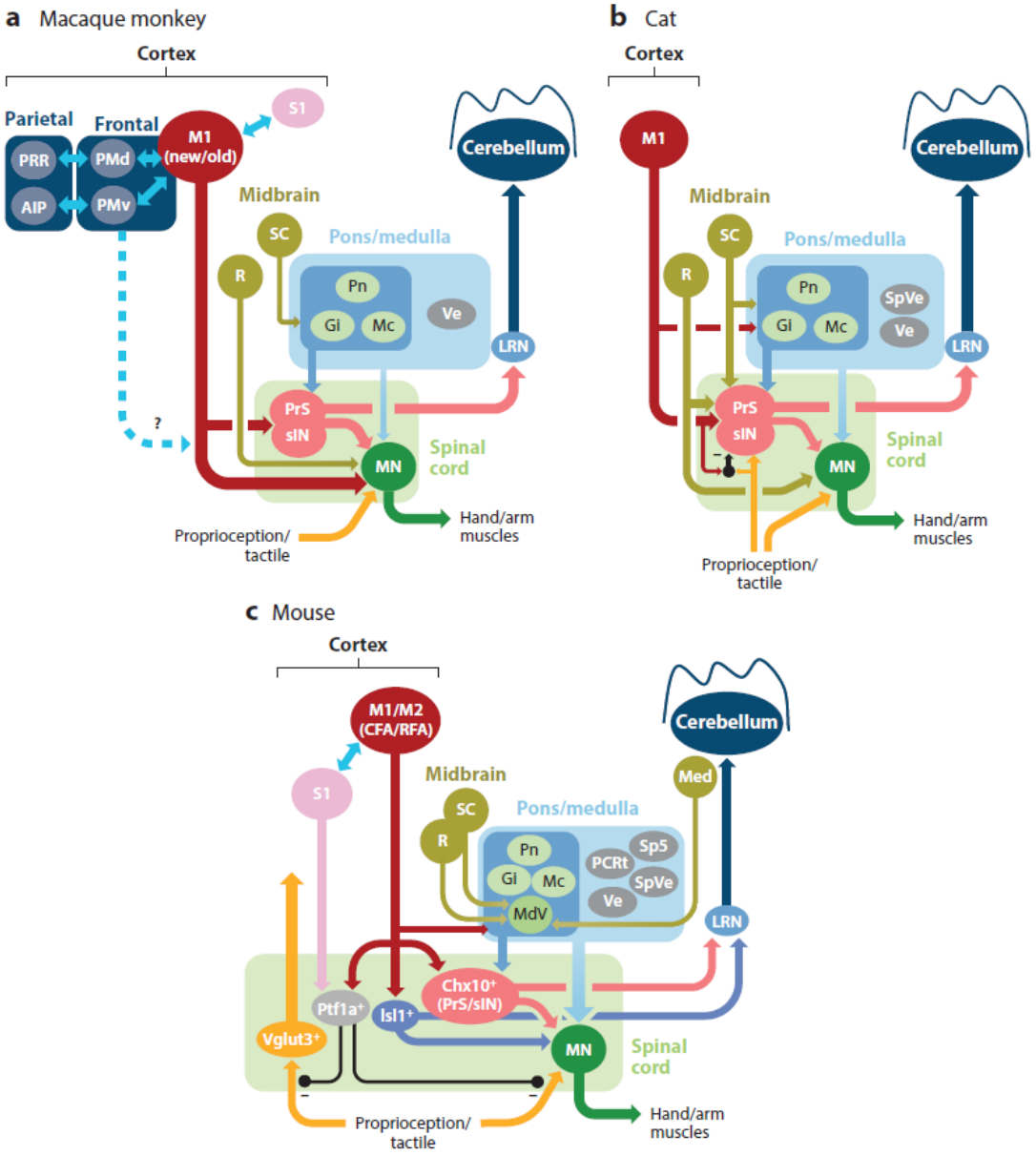

2.3. Translational considerations

Forelimb motor control is critical for everyday functions such as self-care, feeding, and communication, making its impairment particularly debilitating compared to locomotion. While walking and balance are undeniably important, the loss of fine motor skills in the hands can severely compromise an individual's independence and quality of life. Tasks that require precision—like grasping a utensil, writing, or buttoning a shirt—depend on the sophisticated coordination of the forelimb, and deficits in these areas can lead to profound disability. Consequently, understanding the neural mechanisms underlying forelimb motor control is essential for developing targeted rehabilitation strategies for conditions such as stroke, spinal cord injury, and

neurodegenerative diseases. In addition, although locomotion is a fundamental motor function, its impairment can sometimes be compensated by assistive devices or alternative movement strategies. In contrast, the complex, high-resolution control needed for skilled hand movements places a unique burden on neural circuits. This complexity necessitates a deep investigation into the spinal and supraspinal networks that govern forelimb dexterity. Research in this domain has revealed that, despite species-specific variations, many aspects of forelimb motor control are conserved across mammals(Whishaw *et al.*, 1992; Sacrey *et al.*, 2009).

Despite anatomical and physiological differences, the mammalian spinal cord is highly conserved across species, facilitating translational studies between animal models and humans (Flores *et al.*, 2021). Historically, cats were the preferred subjects for experimental spinal cord research, given that their spinal cord has a similar diameter and length to that of humans. Although cats are generally thought to have limited finger dexterity, they do use skilled forelimb and paw movements when hunting prey (Krisa *et al.*, 2018).

Multiple mammal species use their hands to grasp and manipulate food (Iwaniuk & Whishaw, 2000). Rodents and primates present many morphological similarities, including skeletal and muscular structures (Ettema *et al.*, 2006), neural pathways in the spinal cord (Kuypers, 1981), and central motor regions (Donoghue & Wise, 1982; Neafsey *et al.*, 1986). Evidence suggests that skilled reaching behaviour is homologous across species (i.e., it was inherited from a common ancestor) (Whishaw *et al.*, 1992; Sacrey *et al.*, 2009). In both orders, most movements related to transporting and retracting the limb involve similar proximal movements. They also share similarities in hand shaping movements during skilled reaching, including the release, collection, transport, and manipulation phases. In all these species, digit flexion, extension, opening, and closing occur in coordination with hand supination and pronation at comparable temporal sequences and spatial points, demonstrating a consistent pattern throughout the transport and grasp phases of reaching (Figure 8) (Sacrey *et al.*, 2009).

Despite these similarities, there are some differences: humans use a ball-and-socket shoulder joint and can rotate the radius and ulna, enabling greater flexibility in proximal movements. In contrast, rats rely on flexible muscular tethering at the

shoulder for similar actions (Karl & Whishaw, 2011). Additionally, the grasping style varies across species—rats use a whole-hand grasp, humans use a pincer grasp, and titis utilized a modified pincer grasp (using the knuckle of the thumb and second digit), for example. However, the hand-shaping movements that accompany these different grasps remain consistent. For instance, even though humans use a pincer grasp, digits 3-5, which are not involved in the grasp, open with pronation and then close during grasping, similar to the digit behaviour seen in rats. Thus, the digit shaping observed across all species is distinct yet recognizably similar (Figure 8) (Sacrey *et al.*, 2009). This difference in digit shaping arises from the extensive direct corticospinal connections found in humans, and in a reduced manner in other primates, while they are absent in rodents. It allows fractionated digit movement. Since all species exhibit similar hand shaping movements, it is likely that these movements during limb transport are linked to more conserved spinal cord circuits and multisynaptic pathways from the brain (Lemon, 2008).

One potential explanation for the similarities in hand shaping movements across species in skilled reaching is that these movements arise from a set of movement primitives. For instance, in rats, the digits flex and close, then extend and open with each step of a walking cycle, and part of this pattern may be retained during limb transport for reaching. Additionally, the limbs are raised to manipulate objects in front of the animal, and this movement could also be adapted for reaching (Sacrey *et al.*, 2009). This phenomenon where pre-existing movements related to other behaviours are adapted for a new one is known as exaptation (Gould, 1991).

Finally, this homology is significant because it implies a common neural and biomechanical basis of skilled reaching, and because the shared features of their reaching movements reinforce the idea that rodents provide valid experimental models for studying human neurological function and disease (Sacrey *et al.*, 2009). As a matter of fact, rodents are the most commonly used species in experimental spinal cord studies today, due to their availability, ease of care, and financial and ethical reasons (Krisa *et al.*, 2018). These considerations set the stage for the experimental approaches discussed in the following sections, which explore tools and techniques employed to study forelimb motor function in rodent models.

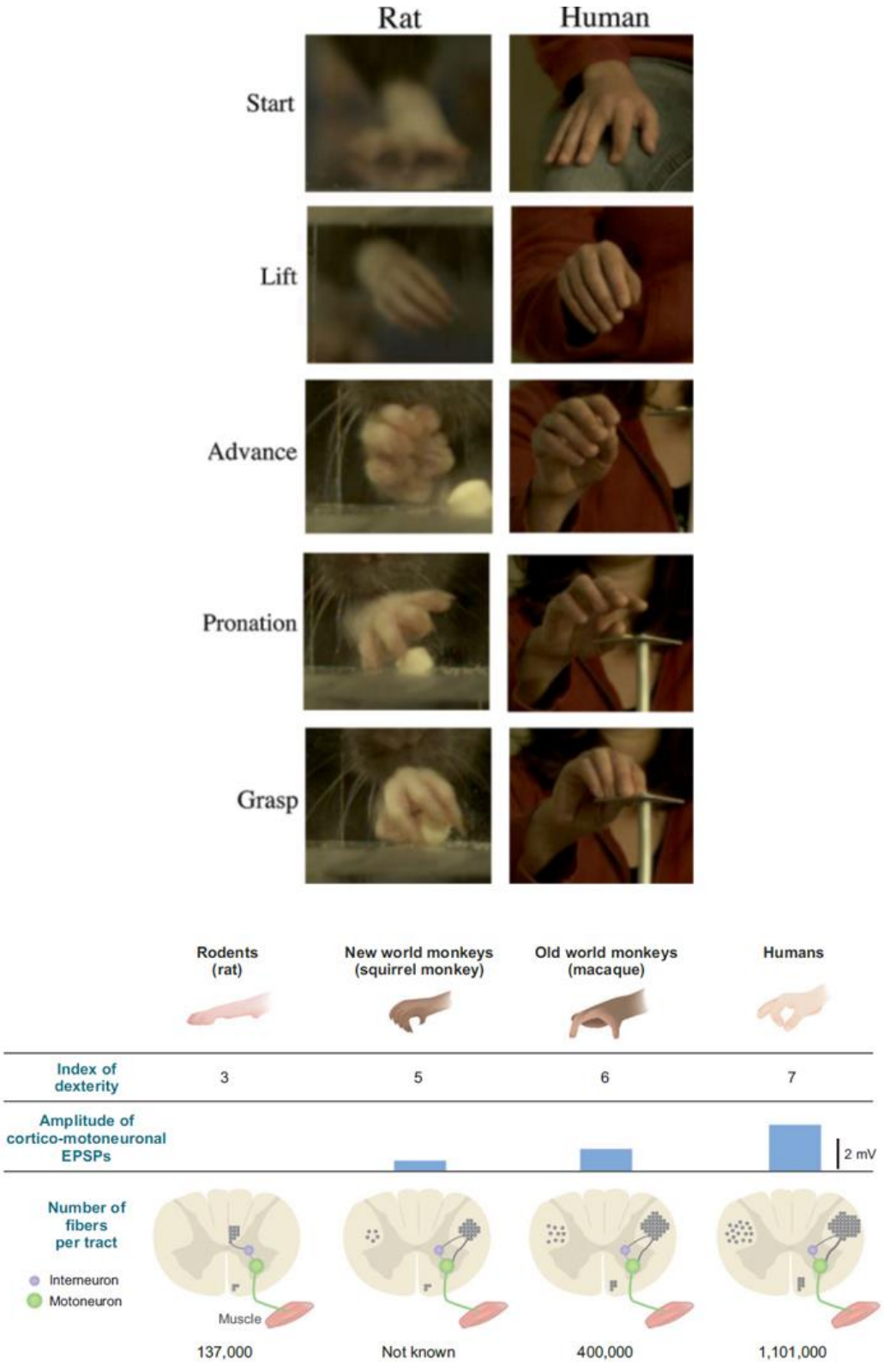

Figure 8. Schematic comparison of R&G movement between different species. Images from Lemon, 2008; Sacrey *et al.*, 2009.

3. Experimental strategies in rodent forelimb motor control research

Understanding the neural circuits and mechanisms underlying forelimb motor control is essential for deciphering normal function and devising therapeutic strategies for recovery after injury. In rodent models, a diverse array of experimental approaches has been developed to probe these complex systems. This section provides an overview of the methodologies commonly employed in this field. We begin by discussing behavioural assessments, which quantitatively measure forelimb function using tasks such as R&G, locomotor evaluations, and grip strength tests (see Table 1). Next, we explore the use of activity-dependent markers, including immediate early genes (IEGs), to map patterns of neural activation during motor tasks. We then review selective injury and manipulation techniques—such as excitotoxic lesions and viral silencing—that allow for precise disruption of specific spinal cord circuits. Finally, we cover additional strategies, including neural tracing, tract sectioning, kinematic analyses, and electrophysiological recordings, which collectively provide a comprehensive understanding of the circuitry and dynamics of forelimb motor control. Together, these approaches form a robust framework for advancing research in this critical area of neurobiology.

3.1. Behavioural assessments

There are numerous functional tests available for assessing forelimb use in experimental animals, particularly in rodents (see Table 1). These tests target different aspects of motor control, ranging from fine dexterity to gross motor strength and coordination, making them invaluable tools in forelimb motor control research.

For example, R&G tasks, such as the single-pellet R&G test (Whishaw *et al.*, 1986), the staircase pellet retrieval task (Montoya *et al.*, 1991), and grid floor-based seed or pellet retrieval (García-Alías *et al.*, 2009), are specifically designed to evaluate fine motor control and manual dexterity (Figure 9) (Flores *et al.*, 2021). These tasks require precise coordination of shoulder, elbow, and digit movements, and they are particularly sensitive to subtle deficits that might arise following cortical or spinal injuries. The single-pellet reaching task emphasizes the

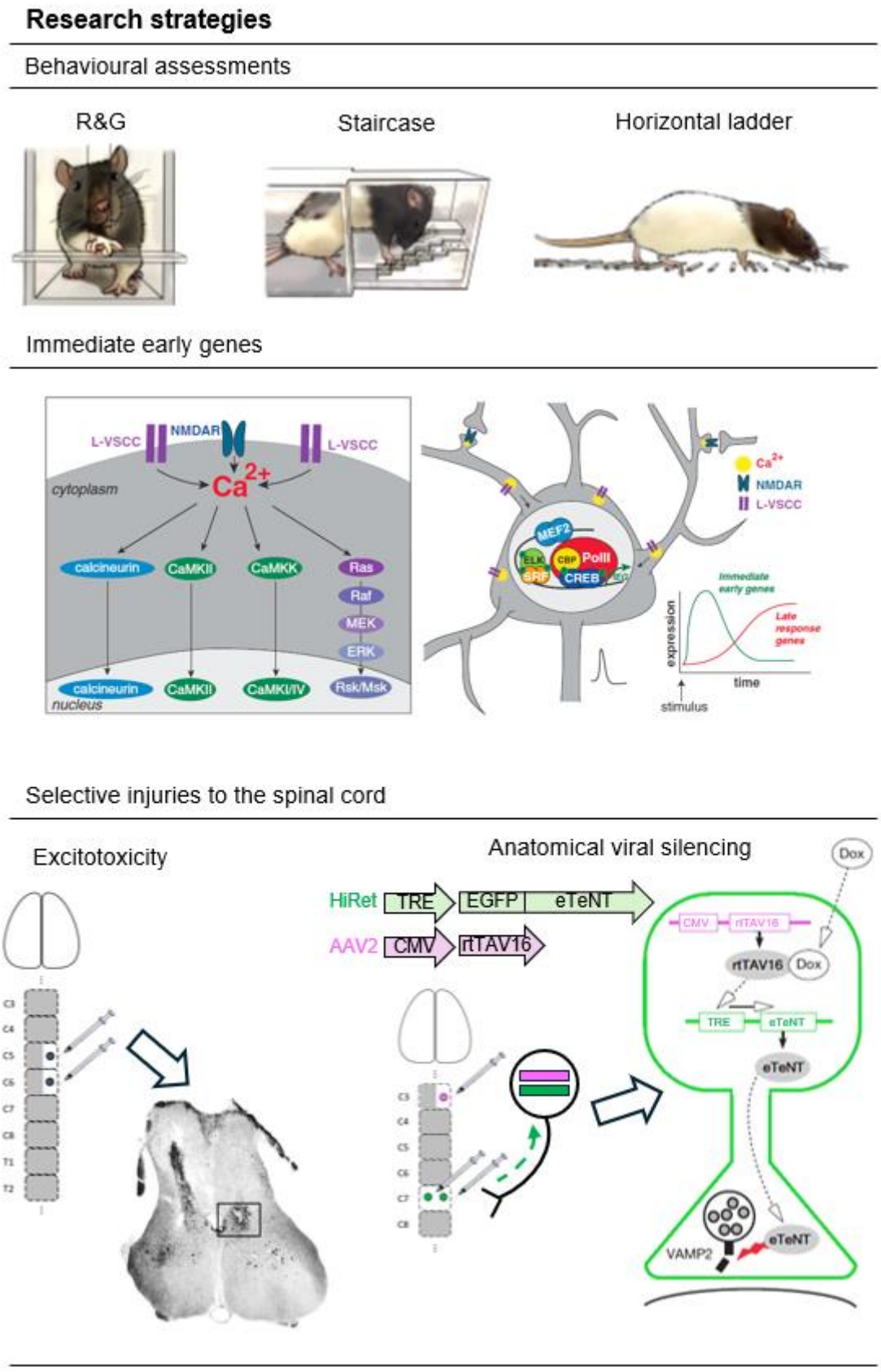

Figure 9. Schematic representation of research strategies for spinal cord forelimb motor control. Images from Magnuson *et al.*, 1999; Yap & Greenberg, 2018.

rapid flexion and extension of the forelimb and precise digit manipulation, while the staircase task challenges spatial coordination by requiring the animal to retrieve pellets from progressively lower steps.

Other tests assess complementary aspects of forelimb function. Overground locomotion evaluations (Anderson *et al.*, 2009; Martinez *et al.*, 2009) and systems like CatWalk (Metz & Whishaw, 2000; Hamers *et al.*, 2001) focus on the integration of forelimb movements during walking. These tests measure parameters such as paw placement, stride length, and gait symmetry, which are critical for understanding overall motor coordination and balance.

Grip strength tests (Soblosky *et al.*, 1997; Metz & Whishaw, 2002) provide quantitative measures of the force that animals can exert with their forelimbs, serving as a direct indicator of neuromuscular integrity and recovery following injury. Similarly, tasks such as tape removal (Bertelli & Mira, 1993; Gensel *et al.*, 2006) assess both sensory-motor integration and fine motor responsiveness by evaluating how quickly an animal detects and removes an adhesive stimulus from its forepaw.

Additional tests, like cereal or pasta manipulation (Schallert *et al.*, 1982; Allred *et al.*, 2008; Bouet *et al.*, 2009), grooming behaviour (Blackwell *et al.*, 2018), and string-pulling tasks, provide insight into natural, spontaneous forelimb use. These tasks can reveal deficits in dexterity or compensatory strategies that animals develop following injury or disease.

It is also important to consider species differences in these assessments. While rodent models are widely used due to their reproducibility and cost-effectiveness, adaptations are often necessary when comparing results across species. For instance, fine digit movements required in single-pellet reaching tasks are more challenging to assess in rodents than in primates, whose forelimb morphology is more conducive to precision grip. Conversely, tasks assessing overground locomotion or grip strength can often be more directly compared across species.

Ultimately, the selection of a specific test (or a battery of tests) depends on the particular aspects of forelimb function under investigation. Researchers choose these tests based on their relevance to the desired outcomes, whether that be evaluating fine motor control, measuring force generation, assessing coordination during locomotion, or understanding compensatory behaviour following neural injury. These

comprehensive assessments allow for a detailed analysis of forelimb motor control and provide critical insights into both normal function and recovery mechanisms in experimental models.

Table 1. Main behavioural assessments of forelimb function.

References	Species	Test	Description
(Anderson *et al.*, 2009; Martinez *et al.*, 2009)	Rat	Overground locomotion	Proper forelimb movements during overground locomotion
(Hamers *et al.*, 2001)	Rat, mouse	CatWalk	Paw placement when walking on a CatWalk
(Whishaw *et al.*, 1986; Metz & Whishaw, 2000)	Rat, mouse	Single pellet retrieval	R&G a food pellet from a platform through a narrow window
(Montoya *et al.*, 1991)	Rat	Staircase pellet retrieval	R&G food pellets from different steps of a staircase
(Schallert *et al.*, 2000)	Rat	Paw use preference	Preferent paw used to lean on cylinder walls
(Hays *et al.*, 2013; Sharp *et al.*, 2016)	Rat	Grip strength	Pull from a device with a resistance to obtain a food reward
(Soblosky *et al.*, 1997; Metz & Whishaw, 2002)	Rat, mouse	Horizontal ladder	Walk on a horizontal ladder with irregularly spaced rungs
(Irvine *et al.*, 2010, 2014)	Rat	Cereal manipulation	Manipulation of a doughnut shaped cereal for eating
(Allred *et al.*, 2008)	Rat	Pasta manipulation	Manipulation of vermicelli for eating
(Schallert *et al.*, 1982; Bouet *et al.*, 2009)	Rat	Tape removal	Adhesive tape is placed on the forepaw's palm
(Bertelli & Mira, 1993; Gensel *et al.*, 2006)	Rat	Grooming	Water is applied to the animal's head and back to induce grooming
(Blackwell *et al.*, 2018)	Rat, mouse	String-pulling	A string with a cereal tied at the end is given to the animal to pull

3.2. Activity dependent markers; IEGs

IEGs provide a powerful tool for mapping neuronal activity because they are rapidly and transiently expressed in response to synaptic activation, offering a snapshot of which neural circuits are engaged during specific behaviours. Synaptic activity is closely linked to rapid gene transcription, a process fundamental to synaptic plasticity and behavioural adaptation (Yap & Greenberg, 2018). This mechanism involves IEGs, a group of genes that are swiftly and temporarily activated by extracellular signals without requiring new protein synthesis. Many IEGs encode transcription factors that drive a subsequent wave of late-response gene expression (Sheng & Greenberg, 1990). These late-response genes typically produce effector proteins involved in cellular processes such as dendritic growth, spine maturation, synapse elimination, and maintaining excitatory/inhibitory balance (West & Greenberg, 2011).

The induction of IEGs by neurotransmitters depends on the influx of extracellular calcium into neurons, primarily through L-type voltage-sensitive calcium channels (L-VSCCs) and also via ligand-gated ion channels like N-methyl-D-aspartate (NMDA) glutamate receptors (West *et al.*, 2001). This rise in cytoplasmic calcium triggers a cascade of signalling pathways, including the Ras-mitogen-activated protein kinase (MAPK), calcium/calmodulin-dependent protein kinase (CaMK), and calcineurin-mediated pathways (Sheng *et al.*, 1991; Bito *et al.*, 1996; Xing *et al.*, 1996). These pathways not only regulate local synaptic changes—such as the surface expression or internalization of glutamate receptors, local messenger ribonucleic acid (mRNA) translation, and protein post-translational modifications—but also stimulate IEG transcription (Figure 9) (Thomas & Huganir, 2004; Wayman *et al.*, 2008; Holt & Schuman, 2013).

The prototypical IEG is the transcription factor *Fos*, which provided the first evidence that mammalian cells could respond to external stimuli within minutes through rapid gene transcription (Greenberg & Ziff, 1984). Once inside the nucleus, *Fos* pairs with its partner *Jun* to form the primary heterodimer of the activating protein complex 1 (AP-1) (Sheng & Greenberg, 1990). Other members of the AP-1 family, such as *Fosb* and *Junb*, can substitute for *Fos* or *Jun*, reflecting significant redundancy within this system. Interestingly, ΔFosB isoform is very stable, and its accumulation is indicative of recurrent activation (Hiroi *et al.*, 1998; Nestler, 2015). Beyond AP-1 family members,

other IEGs activated in neurons in response to activity include early growth response protein 1 (*Egr1*), *Arc*, and neuronal PAS domain protein 4 (*Npas4*) (Christy & Nathans, 1989; Lyford *et al.*, 1995; Lin *et al.*, 2008).

In rodents, researchers have used IEG expression to delineate the spinal networks and supraspinal circuits that support skilled movements, such as R&G. Studies in rats, for example, have correlated IEG patterns with performance on forelimb tasks, revealing the engagement of specific interneuron populations and motoneurons during movement (Jasmin *et al.*, 1994; Ahn *et al.*, 2006; Man'kovskaya *et al.*, 2014). Beyond the spinal cord, IEG-based approaches have also illuminated how cortical and subcortical inputs integrate with spinal circuits to coordinate complex motor functions. By linking IEG expression patterns with behavioural outcomes, researchers can identify and characterize the neural substrates that underlie both normal motor control and adaptive responses following injury.

3.3. Selective inactivation of spinal cord regions

Another approach to investigating motor control involves inducing a loss of function in specific spinal regions or neuronal populations. By selectively ablating, inactivating, or otherwise impairing targeted elements of the motor circuitry, researchers can observe the resulting deficits and thereby gain insight into the roles these components play in motor control. Importantly, this strategy is employed not to model clinically relevant lesions but as a tool to dissect and understand the underlying neural circuitry.

3.3.1. Excitotoxicity

In spinal cord injuries (SCIs), the functional impairments caused by grey matter damage are often overshadowed by the severe deficits associated with white matter damage (Magnuson *et al.*, 1999). To specifically investigate grey matter-related deficits, models involving injection of excitotoxic compounds directly into the spinal cord or intrathecally have been developed. These excitotoxic amino acids are glutamate (Liu *et al.*, 1999) and its analogues, such as alfa-Amino-3-hydroxy-5-methyl-4-isoxazolepropionic acid (AMPA) (Corona & Tapia, 2004), quisqualic acid (Yezierski *et al.*, 1998) and kainic acid (Olney *et al.*, 1974), in which we focused on in this thesis.

Kainic acid is a cyclic analogue of the neurotransmitter glutamate that interacts with neuronal receptors to produce excitotoxic effects, leading to neuronal death in various regions of the CNS. Kainic acid induces an intracellular calcium (Ca^{+2}) influx, which generates free radicals, hyperactivates intracellular enzymes such as poly(ADP-ribose) polymerase-1 and ATPase, and triggers energy depletion, deoxyribonucleic acid (DNA) damage, and ultimately neuronal death (Kuzhandaivel *et al.*, 2010).

Intrathecal kainic acid injection induces transient excitotoxicity through the activation of kainate and AMPA receptors (Sun *et al.*, 2006). These receptors are composed of subunits (GluR5, GluR6, GluR7, KA1, and KA2), whose composition influences their sensitivity to kainic acid (Lerma, 1997). In the rat spinal cord, kainate receptors are predominantly located in the superficial laminae of the dorsal horn and ventral horn (Mazzone *et al.*, 2010). It has been proposed that the excitotoxic effects observed in kainate-treated rats may result from the presence of AMPA receptor subunits in these regions (Tölle *et al.*, 1993), facilitating the release of endogenous glutamate to act on multiple receptor subtypes (Ben-Ari & Cossart, 2000). Additionally, kainate shows preference for interneurons over motoneurons, at least when administered intrathecally (Urca & Urca, 1990). Moreover, the neuronal sensitivity to kainic acid excitotoxicity varies regionally (Magnuson *et al.*, 1999) due to variable numbers of calcium-permeable kainate receptors (Regan, 1996).

Therefore, kainic acid leads to neuronal loss, cavity formation, astrogliosis, and significant inflammation in the spinal cord (Figure 9) (Nakae *et al.*, 2011). One key advantage of this model is its ability to directly link specific tissue damage to behavioural changes, offering a valuable tool for studying grey matter-specific deficits with relative sparing of axons of passage, i.e., white matter (Magnuson *et al.*, 1999). This method has proven useful, for instance, to locate primary neurons of the hindlimb CPG for locomotion in the rostral lumbar enlargement (Magnuson *et al.*, 1999). However, systematic studies on excitotoxic lesions in the spinal cord remain relatively rare (Magnuson *et al.*, 1999).

3.3.2. Pharmacological inactivation with muscimol

Muscimol, a potent $GABA_A$ receptor agonist, acts by hyperpolarizing neurons, thereby rapidly and reversibly silencing local neural activity. By infusing muscimol directly into specific regions of the spinal cord, researchers can transiently disrupt

neural circuits to assess their roles in forelimb motor control. The rapid onset, reversibility, and dose-dependent effects of muscimol make it a useful tool for loss-of-function experiments aimed at understanding the dynamic organization of motor circuits. Nevertheless, its application in evaluating forelimb motor function entails some challenges, since muscimol's effects are transient, typically lasting only a few hours, which restricts the timeframe for behavioural assessments and may require repeated administrations. This entails the local implantation of a cannula. When applied intraparenchymally in the spinal cord, the procedure poses significant technical difficulties and increases the risk of tissue damage and inflammatory responses, but may result feasible when targeting supraspinal regions.

3.3.3. Viral silencing

Viral silencing techniques offer powerful tools to selectively inactivate specific spinal circuits, allowing researchers to dissect the contributions of distinct neuronal populations and pathways to forelimb motor control. Here, we describe three complementary viral silencing approaches each offering unique advantages in terms of temporal precision, targeting specificity, and reversibility.

3.3.3.1. Optogenetics

Optogenetics enables precise manipulation of neural activity with high temporal and spatial resolution, targeting specific cell types (Boyden *et al.*, 2005). This technique relies on the expression of microbial opsins, a group of light-sensitive proteins that, when exposed to light, modulate neuronal electrical activity, either by activation (e.g., channelrhodopsin-2, ChR2) or inhibition (e.g., halorhodopsin) (Yizhar *et al.*, 2011). These excitatory and inhibitory opsins vary in their kinetics, spectral sensitivities, conductance, and mechanisms of action (El-Shamayleh & Horwitz, 2019). While optogenetic targeting is often achieved using cell type–specific promoters, it can also be refined based on neuronal projections, allowing selective modulation of afferent or efferent fibres. In the spinal cord, opsin genes are typically delivered via adeno-associated viral (AAV) vectors (Mondello *et al.*, 2018). Although light penetration can be limited in spinal tissue, recent advancements such as implantable µLED devices (Mondello *et al.*, 2021) have enabled effective optogenetic manipulation in freely moving rats (Mondello *et al.*, 2023).

3.3.3.2. Chemogenetics: DREADDs

Chemogenetic approaches, particularly those employing Designer Receptors Exclusively Activated by Designer Drugs (DREADDs), offer an alternative strategy for modulating neuronal activity. DREADDs are engineered G protein–coupled receptors that respond exclusively to otherwise inert synthetic ligands (e.g., clozapine-N-oxide (CNO) or compound 21) (Armbruster *et al.*, 2007). Once expressed in target neurons via viral vectors, these receptors enable researchers to modulate activity over extended periods without the need for implanted optical hardware. Although DREADDs have a slower temporal resolution compared to optogenetics, they provide the advantage of non-invasive, systemic control and can be targeted to specific neuronal populations or projections using appropriate viral strategies. This approach has proven especially useful for studies requiring sustained modulation of spinal circuits during complex forelimb tasks (Paschon *et al.*, 2020).

3.3.3.3. Projection-specific viral silencing

The projection-specific viral silencing technique exploits connectivity rather than genetic identity to achieve pathway-selective inactivation. This method involves a dual-infection strategy: a retrograde vector (e.g., a HiRet lentivirus) that will infect axon terminals is injected in the target region to deliver an inhibitory molecule, such as the enhanced tetanus neurotoxin light chain (eTeNT) along with a fluorescent reporter (e.g., enhanced green fluorescent protein, EGFP), under the control of a tetracycline-responsive element (TRE) (Figure 9). Simultaneously, an AAV vector carrying a Tet-on system (expressing a reverse tetracycline transactivator (rtTAV) under a ubiquitous promoter like cytomegalovirus, CMV) is delivered to the neuronal cell bodies. Only neurons that are double-infected (those with cell bodies transduced by the AAV and axon terminals reached by the retrograde vector) are affected and rendered inactivatable (Kinoshita *et al.*, 2012). These will express eTeNT only during doxycycline hydrochloride (Dox) exposure, making the process reversible. The expressed eTeNT is transported to the axonal terminals, where it inhibits synaptic vesicle exocytosis by cleaving the vesicle-associated protein 2 (VAMP2), thereby blocking neurotransmission. This reversible, pathway-specific silencing method has been successfully applied in the spinal cords of freely moving rats rats (Pocratsky *et*

al., 2017) and non-human primates (Kinoshita *et al.*, 2012). It offers a robust tool for system-level neuroscience studies aimed at dissecting neural function.

3.4. Other strategies

3.4.1. Tracers

Neuroanatomical tracing methods have been utilized for decades to explore the specific connectivity of functional systems within the nervous system. These methods often involve the uptake and transport of tracers in living neurons. Transport-based tracing is particularly effective for visualizing long-axon projections (Wouterlood, 2015). The techniques which trace from axon terminals back to the cell bodies are named retrograde tracing, including horseradish peroxidase (HRP), cholera toxin subunit B (CTb) and fluorescent hydroxystilbamidine (FluroGold), True Blue, etc; whereas techniques that trace from cell bodies to axon terminals are called anterograde tracing, such as Phaseolus vulgaris-leucoagglutinin (PHA-L) and dextran amines (Saleeba *et al.*, 2019).

More recently, viral tracers have been widely adopted, as they overcome the limitations of conventional tracers: the higher specificity of traced cells and directionality, as well as the possibility of trans-synaptic tracing (Saleeba *et al.*, 2019).

In the context of spinal motor control of limbs, these methodologies have been pivotal for identifying and localizing the columns of motoneurons controlling forelimb muscles within the rat cervical spinal cord (McKenna *et al.*, 2000; Tosolini & Morris, 2012), for example, or for the characterization of the descending pathways that govern these motoneurons (Lemon, 2008). In general, they have been crucial for understanding the link between structure and function in spinal cord circuitry.

3.4.2. Tract sectioning

Once spinal circuits are identified, a straight-forward way of unravelling their function is to interrupt them at the level of interest. This technique has been the predominant tool to characterize the ascending and descending tracts explained earlier. For example, a complete and incomplete corticospinal tract sectioning has revealed the role of direct and indirect corticospinal pathways for hand skilled movements in monkeys (Lawrence & Kuypers, 1968; Sasaki *et al.*, 2004). Indeed, the

contribution of sC3-C4 propriospinal neurons for reaching in the cat and for R&G in the monkey come from sectioning of corticospinal and rubrospinal tracts at sC5 level (Alstermark *et al.*, 1981, 1999). Regarding rats, R&G can be performed in the absence of corticospinal tract connectivity (Alstermark & Pettersson, 2014) or dorsal column hemisection (McKenna & Whishaw, 1999) from sC1-C2 segments, even though the movement is qualitatively affected. In turn, hemisectioning of the rubrospinal tract at sC3-C4 impairs hand rotation in R&G (Morris *et al.*, 2011).

This methodology is additionally used to investigate putative compensation of function between pathways (Maier *et al.*, 2008; Kanagal & Muir, 2009; García-Alías *et al.*, 2015).

3.4.3. Kinematics

When studying movement, the in-depth analysis of the limb trajectories geometry, or kinematics, gives a highly detailed qualitative information that conventional endpoint measures do not (Nica *et al.*, 2017).

Starting with tedious manual scoring of 2D videography (Whishaw & Pellis, 1990; Whishaw *et al.*, 1992), the field has developed in recent years, and now it is possible to automatically track the position of different forelimb (Nica *et al.*, 2017) and hindlimb (Capogrosso *et al.*, 2018) parts during movement based on 2D (Blackwell *et al.*, 2018) and 3D (Capogrosso *et al.*, 2018) videography using machine learning (Mathis *et al.*, 2018).

3.4.4. Electrophysiology

Electrophysiology is an essential technique for exploring the function and connectivity of the nervous system. Over the past several decades, significant progress through various electrophysiological methods (ranging from single-channel recordings to the observation of synchronized activity in intact neuronal networks) has driven remarkable advancements in neuroscience understanding (Hoerbelt & Heifets, 2018).

Electrophysiological research has demonstrated the existence of a CPG for locomotion in the spinal cord, where rhythmic contraction of limb muscles was evoked in decerebrated animals (Grillner, 1981). In forelimb function,

electrophysiology has evidenced that a spinal network at the sC3-C4 level functions as a relay between the brain and motoneurons (Alstermark *et al.*, 2007), and that rats preserve skilled hand function even after damage to the corticospinal tract (Alstermark & Pettersson, 2014), to give a few examples.

4. Spinal cord dysfunction

Although the present thesis is focused on exploring the local spinal circuits that contribute to skilled forelimb movements, it is important to contextualize the relevance of its potential findings within the broader spectrum of spinal cord dysfunction. While traumatic SCI remains one of the most studied conditions, the local spinal circuits uncovered in forelimb motor control research may also hold translational significance for other pathologies, such as spinal cord infarction, neurodegeneration, and demyelinating disorders. A thorough understanding of these circuits is critical, as disruptions in forelimb motor control have profound implications for daily function and quality of life. In this section, we examine various spinal cord pathologies, each of which impacts motor function in distinct ways, and discuss the translational significance of studying these networks.

4.1. Traumatic SCI

SCI is characterized by neurological damage to the spinal cord that leads to motor, sensory, and autonomic dysfunctions, significantly affecting the quality of life for patients (Lima *et al.*, 2022). Traumatic SCI, which accounts for roughly 90 % of SCIs, results from external forces such as traffic accidents or falls and is characterized by immediate mechanical damage to the spinal cord. Other SCI causes include conditions like tumours or infections. Traumatic SCIs most frequently affect the cervical region (59 %), followed by the thoracic (32 %) and lumbosacral (9 %) regions (Ahuja *et al.*, 2017). SCIs are further categorized as complete, where no communication occurs between the brain and spinal cord below the injury, or incomplete, where some transmission remains. Depending on the injury's location, individuals may experience paraplegia, affecting the hindlimbs, or tetraplegia, impacting all four limbs. SCI symptoms commonly include neuropathic pain, spasticity, and loss of bladder, bowel,

respiratory, and sexual functions (Navarro & Udina, 2009; D'Amico *et al.*, 2014; Finnerup, 2017; Nees *et al.*, 2017; Alizadeh *et al.*, 2019).

The physiopathology of SCI involves both primary injury (i.e., direct mechanical disruption resulting in acute haemorrhage, blood-spinal cord barrier breakdown, and immediate cell death) and secondary injury processes (Zhou *et al.*, 2014; Ahuja *et al.*, 2017), which exacerbates neurological damage through a series of vascular, biochemical, and cellular changes, including calcium and glutamate excitotoxicity, vascular injury, ionic imbalances, reactive oxygen species (ROS) production, lipid peroxidation, inflammation, and apoptosis (Oyinbo, 2011; Anjum *et al.*, 2020). These events often culminate in the formation of a cystic cavity and fibro-glial scar (Silver & Miller, 2004; Alizadeh *et al.*, 2019), which inhibit axonal regeneration and contribute to chronic maladaptive changes such as spasticity and neuropathic pain (Fawcett & Asher, 1999; Navarro & Udina, 2009; Sofroniew, 2009; D'Amico *et al.*, 2014; Finnerup, 2017; Nees *et al.*, 2017).

4.2. Spinal cord infarction

Spinal cord infarction is a non-traumatic condition caused by an acute disruption in blood supply to the spinal cord, representing approximately 1 % of all strokes (Romi & Naess, 2016; Gharios *et al.*, 2024; Martin *et al.*, 2024). It is most commonly due to occlusion or severe narrowing of the spinal arteries, particularly the anterior spinal artery, which supplies the anterior two-thirds of the cord. Risk factors include atherosclerosis, embolism, aortic dissection, and complications from aortic surgery, as well as systemic hypotension or vasculitis that may compromise blood flow.

The primary injury in spinal cord infarction is vascular in nature, leading to ischemia and rapid neuronal death in the affected area. The resultant deficits can range from transient sensory disturbances to severe motor impairments, such as paraplegia or tetraplegia, depending on the vascular territory involved. Although the initial insult is different from mechanical trauma, the secondary processes, such as excitotoxicity, inflammation, and maladaptive plasticity, share similarities with traumatic SCI. Understanding the local spinal circuits involved in forelimb control is therefore equally critical for developing interventions aimed at promoting recovery and mitigating long-term disability following spinal cord infarction.

4.3. Neurodegeneration and demyelinating disorders

Amyotrophic lateral sclerosis (ALS) is a fatal progressive neurodegenerative disease affecting the motor system and is the most common type of motor neuron disease. Neurodegeneration primarily impacts the corticospinal and corticobulbar tracts, involving the loss of large pyramidal neurons in the primary motor cortex, as well as damage to the anterior horns of the brainstem and spinal cord. Its pathophysiology is multifactorial, with several mechanisms contributing to motor neuron degeneration. One central feature is glutamate excitotoxicity, where excessive glutamate accumulation overstimulates receptors, leading to calcium influx and neuronal damage. Additionally, protein misfolding and aggregation (such as that of superoxide dismutase 1 (SOD1) in familial cases) play a significant role, as these aggregates disrupt cellular function and trigger apoptotic pathways. Mitochondrial dysfunction, impaired axonal transport, increased oxidative stress, inflammatory processes and microglial activation further contribute to motor neuron death. As spinal motor neurons deteriorate, they exhibit electrical hyperactivity, leading to fasciculations, muscle weakness, and atrophy. This is accompanied by the degeneration of synaptic connections to muscles (Brown & Al-Chalabi, 2017). Most patients succumb to the disease within 2–5 years of diagnosis, primarily due to respiratory failure (Wijesekera & Leigh, 2009).

Additionally, demyelinating disorders like multiple sclerosis (MS) disrupt the integrity of both ascending and descending pathways, compromising the conduction of motor signals and leading to impairments in fine motor control. The disease is driven by an aberrant immune response, in which autoreactive T cells cross the blood-brain barrier and attack the myelin sheath that insulates axons. This immune-mediated demyelination leads to the formation of sclerotic plaques, particularly in the white matter of the brain and spinal cord, although grey matter involvement is increasingly recognized. The loss of myelin disrupts the rapid conduction of electrical impulses along axons, resulting in conduction block and abnormal signal transmission. Over time, these pathological changes lead to permanent neurological deficits and disability, often following a relapsing-remitting or progressive clinical course (Dobson & Giovannoni, 2019).

In both cases, the disruption of spinal circuitry is central to the clinical presentation. Investigating the local spinal networks that underlie skilled forelimb movements can

reveal mechanisms of plasticity, maladaptive reorganization, and potential targets for therapeutic intervention. These insights are particularly important because deficits in forelimb function often have a disproportionately high impact on patients' ability to perform daily tasks and maintain independence.

4.4. Therapeutical interventions and future perspectives

In chronic SCI, the primary goal shifts from acute management to restoring lost motor function. In progressive neurodegenerative or demyelinating disorders, the main objective is to slow disease progression while preserving residual motor function. Hence, therapeutic interventions aim to rebuild and optimize neural circuits to recover or maintain motor skills and improve quality of life. Strategies in this realm include pharmacological treatments that target molecular pathways to promote neuroprotection and plasticity; activity-dependent rehabilitation protocols designed to harness and enhance the inherent adaptability of the nervous system; and neuromodulation techniques, such as electrical or magnetic stimulation, which directly influence neural circuit dynamics. Additionally, emerging approaches like cell-based and gene therapies are under investigation for their potential to further support functional recovery. Together, these interventions work to reactivate dormant pathways, foster new connections, and ultimately restore or maintain motor capabilities across a range of conditions affecting the CNS.

4.4.1. Pharmacological approaches

Pharmacological approaches for managing spinal cord dysfunction employ diverse strategies that target multiple mechanisms to promote neuroprotection, facilitate neural plasticity, and enhance motor function. In the context of SCI, one key strategy involves degrading inhibitory extracellular matrix molecules using agents such as chondroitinase ABC (chABC), which breaks down chondroitin sulphate proteoglycans (CSPGs) and has been shown to improve motor and sensory functions (Barritt *et al.*, 2006; García-Alías *et al.*, 2009). However, its success often depends on the concurrent formation of functional neural networks, a process that can be supported by activity-dependent therapies. Additional treatments focus on counteracting ongoing oxidative stress by using antioxidants like N-acetylcysteine, or reducing excitotoxicity with Riluzole, which dampens glutamate-induced

neuronal damage by inhibiting NMDA receptors and voltage-dependent sodium channels (Doble, 1996). Approaches that promote remyelination and enhance neurotrophic signalling are also being explored, while medications such as baclofen and tizanidine are integrated to alleviate spasticity.

In ALS, therapeutic options are more limited. Riluzole remains the most widely used drug in Europe for mitigating excitotoxicity, although its benefits are modest, extending survival by only 3–4 months (Bensimon *et al.*, 1994). In some regions, edaravone, an antioxidant, has been approved to slow functional decline. Alongside these disease-modifying treatments, symptomatic therapies, such as muscle relaxants, further contribute to improved quality of life.

MS treatments primarily aim to modify the immune response to reduce inflammation, prevent relapses, and slow disease progression. Common disease-modifying therapies include interferon beta, glatiramer acetate, fingolimod, natalizumab, and ocrelizumab, which help reduce demyelination and, in some cases, promote remyelination. Along with these, symptomatic medications are used to manage motor impairments and improve functional outcomes (Dobson & Giovannoni, 2019).

By targeting key pathological processes, whether by promoting regeneration, reducing harmful excitotoxicity and oxidative stress, or modulating immune responses, these pharmacological interventions form an essential component of therapeutic strategies designed to restore or maintain motor function in chronic spinal cord dysfunction.

4.4.2. Activity-dependent therapies

Rehabilitative training, as an activity-dependent therapy, is widely recognized for promoting functional recovery across a range of spinal cord pathologies. In SCI, physical rehabilitation provides repetitive sensory and motor inputs that help reactivate and reorganize damaged spinal circuits, even in the absence of complete descending input (de Leon *et al.*, 1998; Battistuzzo *et al.*, 2017). This activity-dependent plasticity can lead to significant improvements in motor function, as demonstrated in both animal models and clinical studies (Fouad & Tetzlaff, 2012; Torres-Espín *et al.*, 2018). Such training has been shown to be neuroprotective, promote regeneration (Gómez-Pinilla *et al.*, 2002; Molteni *et al.*, 2004), and mitigate secondary complications like neuropathic pain and spasticity (Côté *et al.*, 2014; Nees *et al.*, 2016). Similarly,

rehabilitative training is employed in spinal cord infarction to exploit the residual plasticity of spinal networks. Although recovery in infarction cases tends to be more variable, early and intensive rehabilitation can still improve motor outcomes and functional independence (Romi & Naess, 2016).

In neurodegenerative disorders such as ALS, rehabilitation is used primarily to maintain mobility, reduce spasticity, and improve quality of life, even though the progressive loss of motor neurons limits the potential benefit (Wijesekera & Leigh, 2009). Similarly, in MS, physical therapy plays a crucial role in managing symptoms, reducing fatigue, and enhancing balance and coordination, thereby contributing to better overall function despite the chronic and fluctuating nature of the disease (Dobson & Giovannoni, 2019).

While the mechanisms underlying these activity-dependent improvements are not yet fully understood, and outcomes can vary based on the duration, intensity, and type of training applied (Fouad *et al.*, 2000; van Praag *et al.*, 2000; Nithianantharajah & Hannan, 2006; Manzanares *et al.*, 2018), rehabilitative training remains a cornerstone therapeutic approach across these conditions.

4.4.3. Neuromodulation through electrical or magnetic stimulation

In addition to pharmacological and rehabilitative strategies, neuromodulation through electrical stimulation and related techniques has emerged as a promising avenue for restoring manual dexterity across a range of spinal cord pathologies (Harkema *et al.*, 2022). By delivering targeted stimulation to specific spinal nuclei or supraspinal centres, these approaches aim to reactivate or enhance the function of neural circuits disrupted by injury, infarction, neurodegeneration, or demyelination. For example, epidural electrical stimulation applied to the spinal cord has demonstrated the capacity to improve voluntary motor control in patients with incomplete SCI (Harkema *et al.*, 2011), while techniques such as deep brain stimulation and transcranial magnetic stimulation are under investigation for their potential to modulate cortical networks critical for motor planning and execution (Courtine & Sofroniew, 2019). Identifying and precisely targeting key nuclei, whereas within the spinal cord, brainstem, or cortical areas, could further optimize neuromodulatory interventions, enhancing the recovery of fine motor skills and manual dexterity. This tailored neuromodulation not only holds promise for improving outcomes in

traumatic SCI but may also offer significant benefits in the context of spinal cord infarction, ALS, MS, and other disorders affecting motor function (Zhong *et al.*, 2019).

IV. Hypothesis and objectives

Hypothesis

Forelimb skilled function is essential for our daily activities, ranging from object manipulation to non-verbal communication. Historically, the control of these movements has been attributed primarily to the motor cortex and the "direct" corticospinal pathway. However, other studies have reported the preservation of the R&G capacity after damaging the corticospinal tract, demonstrating the relevance of other nervous system structures in its execution. In this thesis, we hypothesized that a neuronal network within the cervical spinal cord plays a key role in the control of R&G.

Objectives

The general aim of this study is to investigate whether and how the cervical spinal cord participates in forelimb skilled function modulation. To this end, the following specific objectives were:

1. To localise the spinal cord neuronal network controlling the R&G movement via a loss of function study based on excitotoxic injuries.

2. To identify the neuronal populations from the spinal cord that are active while R&G in intact animals, via the analysis of the expression of IEGs.

3. To investigate the downstream projections of the neuronal network required for the correct execution of skilled reaching by reversible neuronal silencing.

V. Materials and methods

Chapter 1. Identifying a spinal neuronal network controlling reaching and grasping

Ethical statement

All experimental procedures were approved by the Animal Experimentation Ethical Committee of Universitat Autònoma de Barcelona and complied with the European Communities Council Directive 2010/63/EU as well as Spanish National Law (RD 53/2013).

Animals

Ninety-six adult female Long Evans rats, aged 10 weeks and weighing between 200-250 g at the start of the experiment, were housed in groups of three under a 12-hour light-dark cycle, with a room temperature maintained at 22±2°C. They had unlimited access to food and water, except during behavioural training and testing periods when they were slightly food-restricted (10-12 g / rat and day) to increase motivation for reward-driven tasks, while maintaining their body weight at ≥ 85 % of the initial value. Upon arrival, the rats were handled for one week. From those animals, thirty-two had to be discarded because of death during the perioperative period (n = 6), or because either during tissue dissection or histological analysis the magnitude of the intervention was shown to be excessive or insufficient (n = 30).

Experimental design

Animals were trained to reach and grasp single pellets in two experimental settings (Whishaw's task and the staircase test) until they reached a performance plateau, and their preferred paw was determined. Subsequently, baseline forelimb motor performance was evaluated using Whishaw's task, the staircase test, the food manipulation task, and overground locomotion, along with a forepaw sensory function assessment using the adhesive removal test. The animals were then divided into four balanced groups and underwent an excitotoxic spinal cord lesion by injecting kainic acid at one of the following vertebral levels: vC3, vC5, vC7 or vT1. Sensorimotor performance was re-evaluated at 7-days post-intervention (DPI) over a 2–3-day period. Later, the animals were perfused, and the spinal cords were processed for histological analysis (Figure 10). Based on these results, that showed no

impairment in any of the groups, the experiment was repeated but injecting kainic acid in two vertebral segments this time: vC2-C3, vC4-C5, vC6-C7, or vT1-T2. One fifth group received vehicle injections at vC2-C3. We performed the behavioural tests at one additional timepoint (14DPI) and added two more behavioural assessments: the R&G on a grid test, and the horizontal ladder walk. In this second experiment, the results showed forelimb skilled function impairment in animals from the vC2-C3 group. Thus, we proceeded to obtain two new groups of rats, in which we injected kainic acid or vehicle at vC2. Finally, in a subsequent experiment, the dorsal and ventral roots of the segments of interest were sectioned to dismiss the possibility of the loss of motoneurons and/or sensory feedback being the cause of the behavioural deficits observed.

Surgeries

For all surgical procedures, the animals were anesthetized via a single intraperitoneal injection of ketamine (90 mg/kg) and xylazine (10 mg/kg). The surgical area was shaved and disinfected with 70% ethanol and betadine. To maintain skin temperature above 32°C, the animals were placed on a heating blanket. At the end of each surgery, the muscle layer and skin were sutured. Postoperative care included analgesia with buprenorphine (0.05 mg/kg, subcutaneously) and amitriptyline (0.09 mg/l in the drinking water), and antibiotic prophylaxis with amoxicillin (0.5 mg/ml in the drinking water).

Cervical spinal cord injections

Excitotoxic lesions were applied to the cervical spinal cord to damage the grey matter while preserving the ascending and descending tracts. A back incision was made near the shoulder, the scapula and paravertebral muscles were retracted, and the vertebral column was exposed. Hemilaminectomy was then performed on one of the following vertebral segments: vC2, vC2-C3, vC3, vC4-C5, vC5, vC6-C7, vC7, vT1 or vT1-T2. The spinal column was stabilized using clamps on the vC2 and vT2 spinous processes. Each animal received two (three in the animals of the two segments groups) unilateral injections of kainic acid (2.5 mM, 0.5 µl per injection, at a rate of 50 nl/min) or vehicle, spaced about 1.5 mm apart along the rostro caudal axis, administered using a 32-gauge Neuros micro syringe (Hamilton GmbH, Germany) attached to a micro-infusion

pump and a stereotaxic system. Injections were made at 0.8 mm lateral to the midline, with the micropipette lowered 1.4 mm to primarily target the dorsal horn and intermediate column of the grey matter (Watson *et al.*, 2009) (Figure 10). The injection side corresponded to the side of the preferent paw of the animal.

Cervical spinal cord roots sectioning

Dorsal and ventral roots of specific cervical spinal cord segments were sectioned to eliminate all their motor output and sensory input while preserving the network's integrity. A back incision was made near the shoulder, the scapula and paravertebral muscles were retracted, and the vertebral column was exposed. Hemilaminectomy was then performed on vC2 or vC2-C3 segments. The laminectomy extended more laterally than for cervical spinal cord injections, in order to clearly expose the dorsal and ventral spinal roots. Once identified, they were both sectioned, from the hemicord corresponding to the preferent paw of the rat (Figure 11).

Importantly, in our experiments, the nomenclature for affected spinal regions is deliberately differentiated based on the method used to induce the lesion. For root sectioning, the impact is confined to the specific spinal segment involved; therefore, we designate these regions with an "s" (for spinal segment), such as sC3, rather than using a "v" designation for vertebrae. This approach accurately reflects the localized nature of the damage in root sectioning. In contrast, lesions induced by kainate injection, although targeted at specific segments, tend to extend both above and below the injection site. Consequently, these are named according to their surgical approach, which better captures the broader distribution of the injury.

Functional outcome measures

R&G training and testing

The standard R&G task (Whishaw *et al.*, 2008) was used as a manual dexterity activity. Rats were acclimated to the Plexiglass box (30 cm × 15 cm × 30 cm) and the banana-flavoured isocaloric pellets (45 mg, Bio-Serv) for one week. Then, each animal was placed individually in the box and trained to reach for and grasp single pellets placed 1 cm away from the front wall on a shelf (3 cm above the surface outside the wall). There was a narrow window (1.5 cm × 3 cm) on the centre of the front wall

(Figure 10A). In each training session, the rats retrieved and consumed pellets until they reached 40-50 attempts, with a maximum time limit of 10 minutes. Each attempt was recorded as either a success or a failure, and the success rate, defined as the number of pellets eaten divided by the number of attempts, was calculated (Whishaw *et al.*, 2008; García-Alías *et al.*, 2015). The rats were trained until they reached their performance plateau, usually after 10-15 sessions and with a success rate of approximately 70 %. The paw preference was identified and taken into consideration for the surgeries.

R&G tests were conducted at baseline prior to surgery, and again at 7DPI and 14DPI. During the testing sessions, each rat was presented with 50 pellets (or maximum 10 min). These sessions were recorded from a frontal view at 120 frames per second (fps) using a GoPro Hero 7 camera. Along with success rate calculations, failed attempts were categorized into six distinct error types to quantify the gesture impairments that occurred while the animal attempted to reach and grasp the pellet (Baylo-Marín *et al.*, 2022):

- **Error type 1**: The paw is lifted and extended towards the platform but does not pass through the window, often hitting the front wall.
- **Error type 2**: The paw crosses the window, but the movement is insufficient to reach the pellet.
- **Error type 3**: The paw crosses the window, but the pellet is out of target in the direction of limb movement.
- **Error type 4**: The paw crosses the window, and the pellet is within reach, but the pellet is displaced during the extension of the fingers.
- **Error type 5**: The paw crosses the window, the pellet is grasped, but it falls during finger flexion or while initiating the paw retraction toward the mouth.
- **Error type 6**: The paw grasps the pellet, but it falls during retraction of the paw toward the mouth.

Staircase training and testing

The staircase test is designed to assess skilled R&G. The setup includes a chamber (28 × 9 × 6 cm) with a central platform (Figure 10B). A removable double staircase is inserted at the end of the box, aligning with the space on either side of the central

platform. Each lateral staircase features six steps where food pellets are placed (Montoya *et al.*, 1991). Steps 1 and 2 contain one pellet each, while the remaining steps contain six pellets each. The top surface of the platform overhangs the sides to prevent rats from simply pushing the food pellets off the platform. The rat is placed on a Plexiglass sheet and must retrieve the food pellets from the steps through a narrow gap between the platform and the top surface. Once accustomed to the setup, the rats are trained to reach for and grasp as many pellets as possible from the 26 pellets distributed across the six steps during 10 min sessions, focusing only on their preferred side. The same conditions are maintained during testing sessions at baseline, 7DPI and 14DPI, all recorded at 60 fps. The measured outcomes include the highest number of pellets eaten with the preferent paw and the lowest step from which a pellet was displaced (whether consumed or not).

Grid R&G testing

The grid R&G test is designed to assess skilled R&G in a setting where the act to reach and grasp the pellet requires less effort to elevate the forelimb, as it is not performed against gravity. Pellets are placed at a level below the resting position of the paw, specifically at the bottom of the grid. The setup includes a Plexiglass box (35 cm × 18.5 cm × 40 cm) with a plastic squared grid (1.2 cm × 1.2 cm × 1.2 cm) attached to the floor (Figure 10C). Several (10-15) food pellets are placed in one of the squares limiting with one of the walls of the box (to facilitate observation). The rat is placed inside the box and must find and eat the pellets on the bottom of that grid square, and the session is recorded at 60 fps. The assessment includes:

- R&G attempt with preferent paw
- Pellet reach (the pellet is touched) with preferent paw
- Success (the pellet is successfully grasped and brought to the rat's mouth) with preferent paw
- R&G attempt with non-preferent paw

Every parameter receives a semiquantitative score of 0 (not occurred), 0.5 (occurred in a non-canonical gesture) or 1 (occurred). The test ends when there are no more pellets in the square, or a maximum time limit of 3 minutes is achieved.

Food Manipulation Task (IBB Scale)

The ability of the animals to manipulate donut-shaped cereal was evaluated using the methods outlined in the Irvine, Beattie, and Bresnahan (IBB) task (Irvine *et al.*, 2014). Prior to testing, the rats were acclimated to the environment as well as the smell and taste of the sweetened cereal. Each animal was placed individually in transparent cases (Figure 10E) or their home cage and provided with donut-shaped cereal pieces ("Froot Loops™", Kellogg's Co.) that were uniform in size and shape. The rats were filmed at 120 fps while consuming at least two complete donut-shaped pieces to ensure accurate assessment. The trials were recorded and scored based on the IBB scale (0-9 score), which evaluates forelimb behaviours such as joint positioning, object support, wrist and digit movements, and the grasping technique used while eating.

Horizontal ladder walk

This task assessed forelimb paw placement on the rungs of a 1 m long horizontal ladder (Figure 10D), serving as a measure of skilled locomotion. The rungs were spaced irregularly, with a minimum distance of 1 cm between them (Whishaw *et al.*, 2010; Verma *et al.*, 2019). Plexiglass sidewalls, 19 cm high, formed an alley tailored to the size of the animal, preventing it from turning around. To minimize distractions and enhance performance, the rats were acclimated to the ladder over 4-5 days. During testing, they were motivated to walk along the ladder by a flavoured pellet placed at the end. Each rat completed 2-3 trials in both directions on the ladder. The analysis of forelimb placement for the preferred paw was conducted using video footage recorded at 60 fps. Successful placements were defined as instances where the palm of the forepaw, positioned between the wrist and digits, contacted the rung during active walking. All other placements were categorized as missed steps, with results expressed as percentage errors.

Overground locomotion

Locomotor paw and limb function was evaluated using a walking track within a confined walkway. This walkway featured a dark shelter at the end of a 10 × 100 cm corridor, with white paper of the same dimensions placed on the bottom (Figure 10F). To clearly distinguish between fore- and hindlimbs, the rats' anterior and posterior

paws were dipped in ink of different colour (blue, pink or black) before they were positioned at the entrance of the walkway to walk across it. Each rat underwent two to three trials, and only footprints made during continuous, uninterrupted walking were selected for measurement. The paired footprint parameters measured included stride length (the distance from one foot strike to the next foot strike of the same foot), base of support (the distance between the limbs perpendicular to the direction of travel), and footprint dimensions. These measurements were taken separately for the left and right sides as well as for the hind- and forelimbs (Lakes & Allen, 2016).

Adhesive removal test

This test is regarded as a sensitive method for evaluating forepaw sensorimotor deficits (Bouet *et al.*, 2009). It involves applying a small piece of adhesive tape (1 × 1 cm) to the forepaws and measuring the time taken for the rats to sense and remove the tape. This procedure helps identify changes in paw sensitivity (time-to-sense) as well as forepaw dexterity in removing the tape (time-to-remove). Following acclimation to the environment and the transparent testing box (Figure 10E), two strips of adhesive tape are applied with equal pressure to each animal's forepaws, covering the thenar and hypothenar pads. The order of application is randomized between the left and right paws. The rat is then placed in the testing box, where sense time (defined as the moment the rat reacts to the presence of the adhesive tape) and removal time are video recorded at 30 fps, with a cut-off at 180 seconds. This procedure is repeated 2-3 times, leaving minimum 1 hour between trials, and the trial with the best performance is selected for quantification.

(Figure on the next page)

Figure 10. Apparatus used for behavioural tests in Chapter 2. Rats were tested for **(A)** R&G, **(B)** staircase, **(C)** grid R&G, **(D)** horizontal ladder walk, **(E)** food manipulation, adhesive removal and **(F)** overground locomotion.

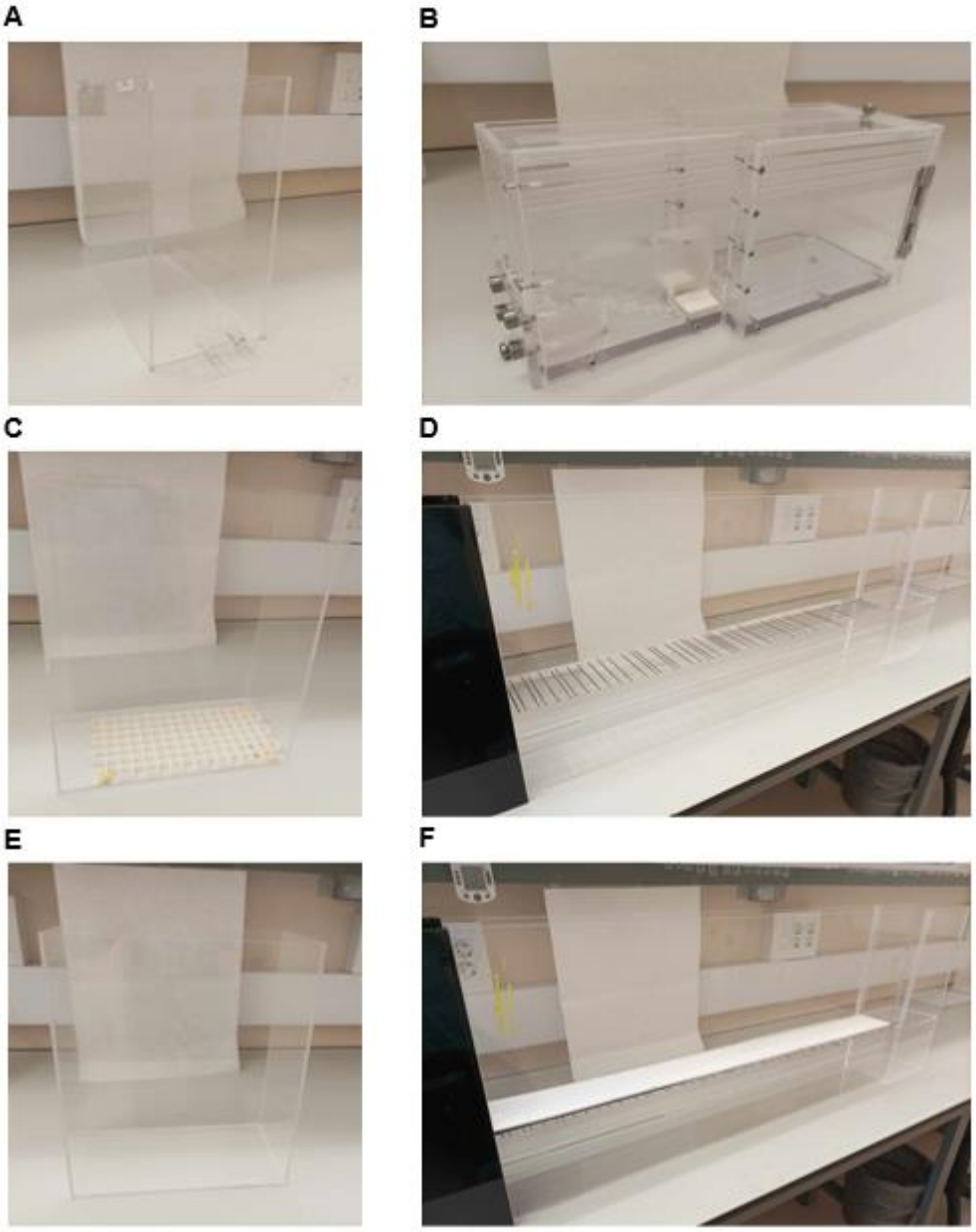

Histological assessment

At the conclusion of the evaluation, the rats were anesthetized with pentobarbital and transcardially perfused with 4 % paraformaldehyde in a 0.1 M phosphate buffer solution. Spinal cord segments from the vC2 to vT2 levels were dissected and post-fixed in the same fixative for 24 hours, followed by cryoprotection in 30% sucrose. The spinal cords were then embedded in optimal cutting temperature (O.C.T.) compound embedding medium (Tissue-Tek) and rapidly frozen. Sample blocks were sectioned serially at 25 µm using a cryostat, collected directly onto gelatine-coated porta-objects, and stored at -20°C. To assess the location and extent of the injury,

serial transverse sections throughout the entire cervical enlargement, spaced 250 µm apart, were stained/immunostained with the following procedures:

- Cresyl violet staining: Used to assess the location and extent of the injury, based on grey matter and motoneuronal preservation.
- Luxol blue: Used to assess white matter preservation.
- NeuN: Used to assess neuronal preservation.
- Glial fibrillary acidic protein (GFAP): Used to assess astrocyte presence in the injection level.
- Ionized calcium-binding adapter molecule 1 (Iba1): Used to assess the presence of gliosis (microglia) at the injection level.

Table 2. List of antibodies used for tissue immunostaining/immunofluorescence in chapter 1.

	Antigen	Dilution	Description	Reference number
Primary antibodies	GFAP	1:400	Rabbit polyclonal	Millipore #AB5804
	Iba1	1:400	Goat polyclonal	Abcam #ab5076
	NeuN	1:200	Mouse monoclonal	Millipore #MAB377
Secondary antibodies	Rabbit A594	1:200	Donkey polyclonal	Life Technologies #A21207
	Goat A594	1:200	Donkey polyclonal	Life Technologies #A11058
	Mouse Biotinylated IgG	1:200	Horse polyclonal	Vector #BA-2000

Image processing

Images were captured using an epifluorescence Olympus BX51 microscope with a DP73 Olympus camera and a DS-Ri2 Nikon camera connected to an epifluorescence Eclipse Ni Nikon microscope. High-resolution images of all stained/immunostained sections were obtained to investigate grey/white matter preservation and possible effects on neurons, motoneurons, astrocytes and microglia. Separate measurements of the preserved grey/white matter areas were processed and analysed using ImageJ software. The boundary between grey and white matter was determined for each section using a custom semi-automated method based on the intensity of cresyl staining and the heterogeneity of the tissue characteristic of grey matter. An equivalent method was used to investigate white matter preservation based on luxol staining. Sections were individually reviewed, and the grey/white matter boundary was manually adjusted if needed. Motoneurons were identified and manually quantified from cresyl-stained sections, based on their location in the lateral ventral horn and specific morphological and size criteria, including a polygonal shape, prominent nucleoli, and a diameter exceeding 30 µm (Ferrucci *et al.*, 2018). All the above analyses were conducted for each hemicord separately. Sections of poor quality were excluded from the analysis.

Statistical analyses

All data sets were analysed using GraphPad Prism 9 (version 9.0.0). For behavioural data of the first batch of animals, Gaussian data was analysed using repeated measures two-way analysis of variance (ANOVA) with timepoint as within-subject factor and group as between-subject factor, followed by Šídák's post hoc comparisons; and non-Gaussian data was compared with Wilcoxon non-parametric test. For the rest of the animal batches, when the data followed a normal distribution and two timepoints were compared, we used a paired t test. If we were comparing three timepoints, data was analysed by repeated measures one-way ANOVA (or mixed-effects analysis model using the restricted maximum likelihood method, if values were missing), followed by Tukey's post hoc analysis to correct for multiple comparisons, if a significant effect had been found. Data were presented as mean ± standard error of mean (SEM). For data that did not conform to a normal distribution (food manipulation and grid R&G tests), two timepoints were compared with Wilcoxon

test, and three timepoints were analysed by Kruskal-Wallis test followed by Dunn's multiple comparisons test. These non-parametric data was shown as median ± interquartile range.

Regarding histological data, the area of preserved grey/white matter and the motoneuronal preservation were calculated as a percentage compared to standard values, determined as follows. A standard curve for absolute grey/white matter area values and motoneuronal counts along the rostrocaudal axis within the cervical enlargement was derived from the intact segments of all the processed spinal cords (approximately 10 mm caudal and rostral to the injection site) and was used as a control for both the ipsilateral and contralateral sides. This was for two reasons: to minimize the number of animals used and to increase the representativity of the standard curve, using animals from the same cohort. An additional normalisation was implemented for each animal individually, where mean percentage of grey matter, white matter or motoneuron preservation of the uninjured segments of both hemicords together was normalised to 100, and the values for the injured segments corrected accordingly. The rationale for this second standardisation is to correct for the fact that the size of the spinal cord of different animals may vary because of the size of the animal, or due to subtle variability while tissue processing, that could mask a potential change in the assessed parameters. The statistical analyses consisted of repeated measures two-way ANOVA (or mixed-effects analysis model using the restricted maximum likelihood method, when values were missing), with Group as the between-subject factor and Distance as the within-subject factor, when comparing the injection epicentre and in the real rostrocaudal position when there was a vehicle group. Tukey's multiple comparisons test was subsequently applied when corresponding. When there was not a vehicle/control group for the real rostrocaudal position graphs, the data was compared by one sample t test vs a hypothetical mean of 100, followed by Benjamini-Horchberg correction for multiple comparisons.

(Figure on the next page)

Figure 11. Schematic representation of the methods used in Chapter 1. Rats were trained for the behavioural tests, and their performance assessed before and after the surgery. After their last testing session, spinal cords were harvested for histological analyses. LE: Long Evans.

Chapter 1

Experimental design

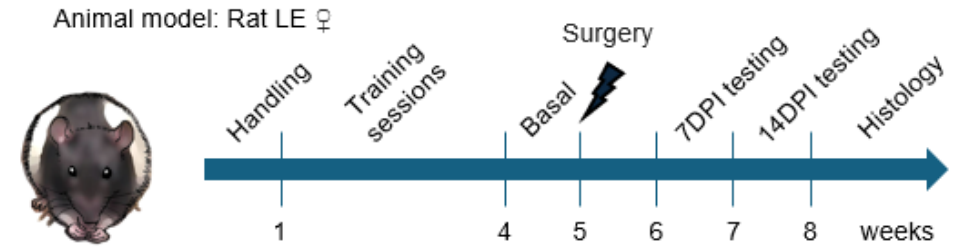

Experimental groups

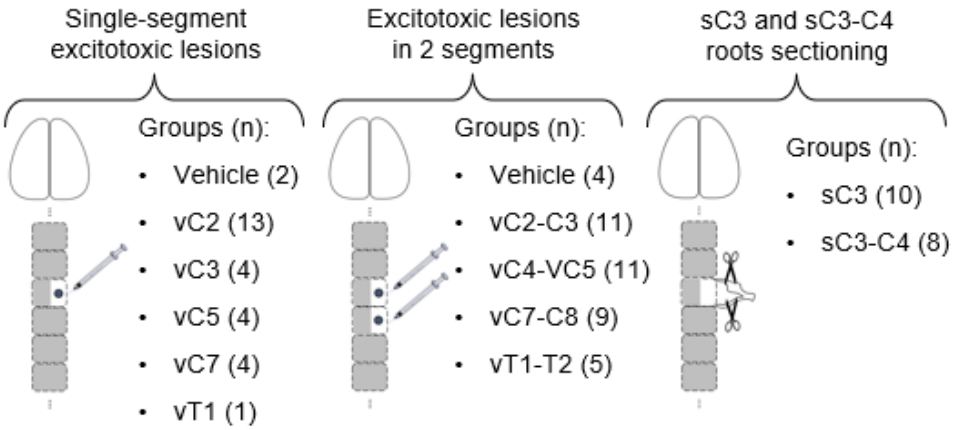

Functional assessments

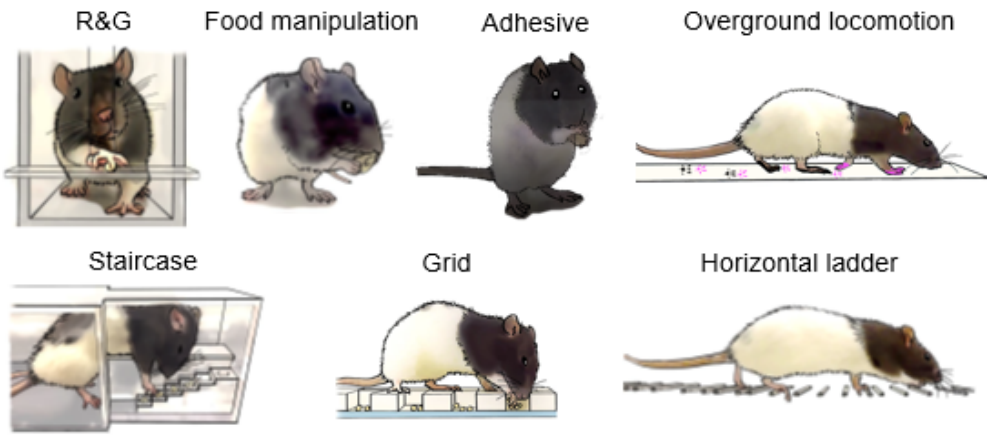

Histological analysis

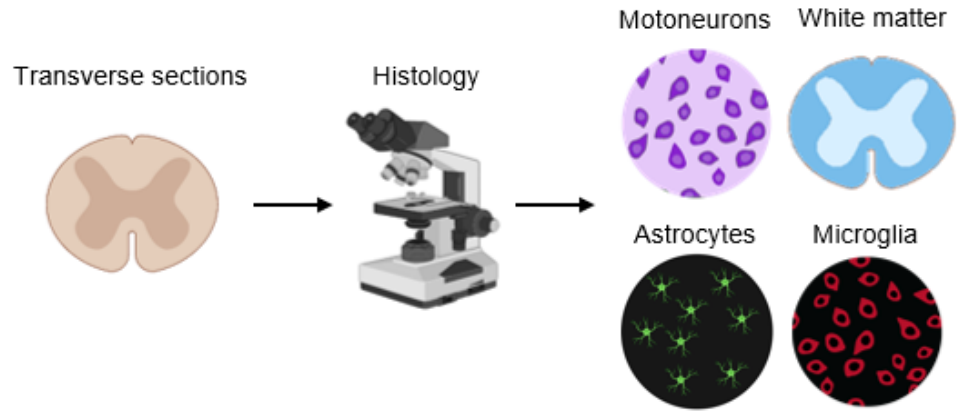

Chapter 2. Characterising the identified spinal neuronal network controlling reaching and grasping

Chapter 2.1. Spinal neuronal activation after reaching and grasping

Ethical statement

All experimental procedures were approved by the Animal Experimentation Ethical Committee of Universitat Autònoma de Barcelona and complied with the European Communities Council Directive 2010/63/EU as well as Spanish National Law (RD 53/2013).

Animals

Forty adult female Long Evans rats, aged 10 weeks and weighing between 200-250 g at the start of the experiment, were kept in groups of three under a 12-hour light-dark cycle, with a room temperature maintained at 22 ± 2°C. Upon arrival, the rats were handled for two weeks. They had unlimited access to food and water until the start of the behavioural sessions period, when they were slightly food-restricted (10-12 g / rat and day) to increase motivation for the task, while always maintaining their body weight at ≥ 90 % of the initial value. From those rats, twenty-two had to be discarded due to substandard tissue preservation. One last animal was discarded because it was identified as an outlier based on its c-Fos and FosB data.

Experimental design

The goal of this experiment was to identify the neuronal populations from the spinal cord that are active while R&G in intact animals, via analysis of the expression of IEGs.

Rats were divided into six experimental groups:

- **"Early R&G training"**: These animals were trained to reach and grasp until they showed a marked progression in the learning curve. This positive shift in performance was defined as the first day that the rat consumed ≥ 60 pellets with a success rate of ≥ 40 % and that the total number of attempts was ≥ 150. Animals were perfused after this training session.

- **"Late R&G training"**: These rats were trained to reach and grasp until they reached their performance plateau, usually after 10-15 sessions and with a success rate of approximately 70%, when they were perfused.
- **"No reaching"**: Rats were not trained for R&G. Instead, they were placed in a similar Plexiglass box with the same food pellets on the floor, so they could eat them without R&G, for 30 minutes per session, both during training period and on the perfusion day.
- **"Treadmill training"**: Animals were trained for an alternative behavioural task that involved continuous, cyclic use of the forelimbs, i.e., treadmill walking. Training consisted of 10 sessions, with each session involving 20 min of walking on a treadmill at a speed of 12 cm / s. This pace corresponds to regular walking and is not considered to require significant effort.

This design allowed us to differentiate IEG expression induced by the training process from that induced by performing the task itself, as well as to distinguish between IEG expression triggered by R&G and by other forelimb motor tasks. Additionally, the inclusion of "early R&G training" and "late R&G training" groups enabled us to detect changes in IEG expression across different phases of the learning process (Figure 12).

R&G

The standard R&G task (Whishaw *et al.*, 2008) was used as a manual dexterity activity. Rats were acclimated to the Plexiglass box (30 cm × 15 cm × 30 cm) and the isocaloric pellets (20 mg, Bio-Serv) for one week. They were given pellets from three different flavours (chocolate, banana and unflavoured) and their preference was assessed. Then, each animal was placed individually in the box and trained to reach for and grasp single pellets placed 1 cm away from the front wall on a shelf (3 cm above the surface outside the wall). There was a narrow window (1 cm × 3 cm) on the centre of the front wall. In each session, the rats were encouraged to make as many pellet reach and grasp attempts as possible, until the rat stopped making attempts, but always with a minimum duration of 30 min (Figure 12). These sessions were recorded and the performance evaluated in the same terms as in Chapter 1).

Treadmill

For the locomotor task, animals were acclimated to the treadmill apparatus (40 cm × 10.3 cm × 14.7 cm, LE 8706, LSI Letica Scientific Instruments) and trained to walk on it for 20-30 min per session at a speed of 12 cm/s. Notably, motivation was enhanced by placing stuck isocaloric food pellets (20 mg, Bio-Serv) at the end of the treadmill, and no negative stimulus (i.e. electric shock) was given. These rats received treadmill training instead of R&G training. Several parameters were annotated to evaluate the performance, such as number of turns, stops, and time walking forward.

Histological assessment

After their last behavioural session, the rats were anesthetized with pentobarbital and transcardially perfused with 4% paraformaldehyde in a 0.1 M phosphate buffer solution 90-120 min after the session had ended, the timing where the expression of IEGs should be higher (Wiedmann *et al.*, 2021). Spinal cord segments from the sC2 to sT2 levels were dissected and post-fixed in the same fixative for 24 hours, followed by cryoprotection in 30% sucrose. The spinal cords were then embedded in O.C.T. compound embedding medium (Tissue-Tek) and rapidly frozen with isopentane. Sample blocks were sectioned serially at 25 µm using a cryostat (Leica CM190), collected in free-floating in cryoprotective solution (40 % phosphate buffer (PB) 0.1 M, 30 % ethylene glycol, 30 % glycerol), and stored at -20°C. A small hole was made on the left ventromedial white matter of the spinal cord using a 30G needle, to be able to identify the left and the right hemicords afterwards. For the analysis of tissue preservation quality, transverse sections from all spinal segments of all the animals were blocked with normal donkey serum and immunostained overnight at 4ºC with antibodies against NeuN. The following day, they were incubated with biotinylated secondary antibodies for 2 hours at room temperature, transferred to glass slides, then stained with 3, 3'-diaminobenzidine (DAB, Merck), dehydrated with ethanol, cleared with xylene, mounted with dibutylphthalate polystyrene xylene (DPX, Merck) and coverslipped. To assess the location and number of cells expressing IEGs serial transverse sections from all the rats were blocked with normal donkey serum and immunostained overnight at 4ºC with antibodies against IEGs throughout the entire cervical enlargement. Then, they were incubated with secondary antibodies for 2

hours at room temperature. Finally, sections were mounted on slide with 4',6-diamidino-2-phenylindole (DAPI) Fluoromount (SouthernBiotech) and coverslipped.

Table 3. List of antibodies used for tissue immunofluorescence in chapter 2.1.

	Antigen	Dilution	Host, type	Reference number
Primary antibodies	c-Fos	1:1000	Rabbit monoclonal	Cell Signaling #2250
	FosB	1:500	Mouse monoclonal	Abcam #ab11959
	Arc	1:500	Rabbit polyclonal	Synaptic Systems #156003
	Egr1	1:100 1:1000 1:5000	Mouse monoclonal	Santa Cruz Biotechnology #sc-515830
	NeuN	1:200	Mouse monoclonal	Millipore #MAB377
Secondary antibodies	Rabbit A594	1:200	Donkey polyclonal	Life Technologies #A21207
	Mouse A594	1:200	Donkey polyclonal	Life Technologies #A21203
	Mouse A488	1:200	Donkey polyclonal	Life Technologies #A21202
	Mouse Biotinylated IgG	1:200	Horse polyclonal	Vector #BA-2000

Image processing

Images were captured using a DS-Ri2 Nikon camera connected to an epifluorescence Eclipse Ni Nikon microscope at 10x magnification. High-resolution images of 2-4 immunostained sections per segment for each animal were obtained to identify the presence, number and distribution (both dorsoventrally and rostrocaudally) of IEG expressing cells, or the quality of the tissue preservation on bright field mode for NeuN immunostaining. Images were processed and analysed using ImageJ software. Each section was individually reviewed, and the number of positive cells in each Rexed lamina of each hemicord was manually quantified by an experimenter blinded to the experimental group the rat whose section was being analysed belonged to (Figure 12), using rat templates of spinal cord Rexed laminae (Watson *et al.*, 2009). Sections of poor quality were excluded from the analysis.

Statistical analyses

All data sets were analysed using GraphPad Prism 9 (version 9.0.0). The percentage of positively immunostained cells in one hemicord relative to the total number of positive cells was tested by one sample t test vs a theoretical mean of 50 (corresponding to an equitable distribution), using Benjamini-Hochberg correction for multiple comparisons. The rest of the data was compared with mixed-effects model using the restricted maximum likelihood method, with Group as between-subject factor and Segment/Session as within-subject factor, followed by Tukey's multiple comparisons test when a significant difference had been found. In addition, correlation analyses of behavioural and histological (or histological vs histological) results were performed. Data was presented as mean ± SEM, and the significance level was set at $p < 0.05$ in all analyses.

(Figure on the next page)

Figure 12. Schematic representation of the methods used in Chapter 2.1. Rats were trained for R&G or treadmill, or were not trained. After their last session, animals were perfused and the IEG expression in the spinal cord was assessed. LE: Long Evans.

Chapter 2.1

Experimental design

Animal model: Rat LE ♀

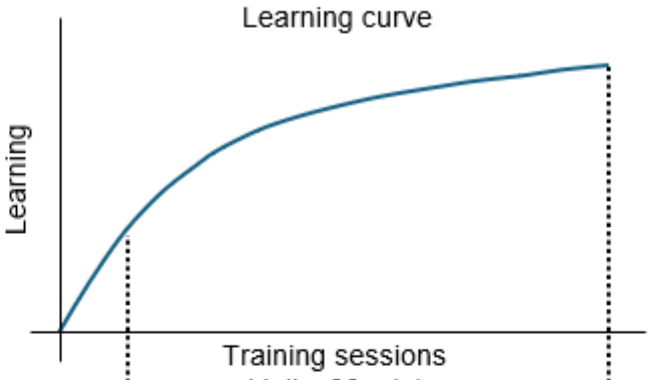

Experimental groups

- R&G early (n = 9)
- R&G late (n = 15)
- No training (n = 9)
- Treadmill (n = 7)

Conditions:
- successful attempts ≥ 60
- success rate ≥ 40%
- total attempts ≥ 150

Behavioural trainings

Reaching and grasping

Treadmill locomotion

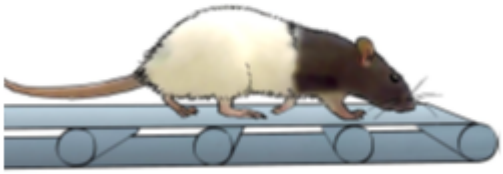

Histological analysis

Transverse sections

Immunostaining

All neurons

Activated neurons

Chapter 2.2. Reversible silencing of sC3-to-C7 projecting neurons

Ethical statement

All experimental procedures were carried out following the Public Health Service Policy on the Humane Care and Use of Laboratory Animals, along with the guidelines set by the University of Louisville's Institutional Animal Care and Use Committee and Institutional Biosafety Committees.

Animals

Twenty-two Adult female Sprague Dawley rats, aged 10 weeks and weighing between 200-250 g at the start of the experiment, were kept in groups of three under a 12-hour light-dark cycle, with a room temperature maintained at 22±2°C. They had unlimited access to food and water, except during behavioural training and testing periods when they were food-restricted to maintain their body weight at ≥ 95 % of the initial value. Upon arrival, the rats were handled for one week. From those animals, two had to be discarded because of death during perioperative period. The reason behind using a different rat strain with respect to the other experiments was that the viral targeting technique used has been developed and proven to work in Sprague Dawley strain, not yet in Long Evans.

Experimental design

First, we investigated the descending projections of sC3 interneurons to sC7 interneurons or motoneurons required for distal forelimb muscles' movement with an anatomical approach. Specifically, we quantified the number of neurons from the sC3 segment that projected ipsilaterally and contralaterally to the sC7 segment. This experiment also laid the foundation for subsequent functional studies of these interneurons. Ten animals received unilateral surgical injections of AAV2-CAG-FLEx-GFP at C3 and HiRet-Lenti-Cre at sC7 to uniquely label sC3-to-C7 projecting neurons. The FLEx (flip-excision) system incorporated into the AAV2 vector is designed so that the GFP gene is initially in an inverted, non-expressing orientation. Only in the presence of Cre recombinase—delivered by the HiRet-Lenti-Cre injection at sC7—does the FLEx system mediate the inversion of the GFP gene into the correct orientation, allowing its expression. Thus, only those sC3 neurons that project to sC7,

and thereby receive Cre, will express GFP. Half of the animals received the injections on the same side (ipsilaterally), and the other half received them on opposite sides (contralaterally) (Figure 13). The vectors were allowed four weeks to reach the cell soma (in the case of the lentiviral vector) and to achieve maximal expression, at which time the rats were perfused for histological analysis of the spinal cords.

A second cohort of 12 rats was used for the reversible silencing experiment. These animals were gently acclimated and trained for both R&G and high-speed locomotion, with high-quality video recordings obtained to assess their forelimb skilled function and locomotion. After baseline testing, they underwent similar injection surgeries as the first cohort. However, in this experiment, the viral constructs injected were AAV2-CMV-rtTAV16 at sC3 (unilaterally, on the side of the animal's preferred paw) and HiRet-Lenti-EGFP.eTeNT at sC7 bilaterally (Figure 13). In the presence of Dox, this approach allowed us to silence all sC3-to-C7 projecting neurons from the preferred hemicord. Three weeks post-surgery, Dox (20 mg/ml; Fisher Scientific BP2653-5, Pittsburgh, PA) dissolved in a 3% sucrose solution was provided ad libitum for 8 days, with daily recordings of approximate consumption. Functional testing was conducted prior to injections (Baseline), before Dox treatment (Pre-Dox), and during Dox treatment on days 5 and 8 (Dox^{ON}-D5 and Dox^{ON}-D8). Individual and group comparisons were made between control time points (Baseline, Pre-Dox) and experimental time points (Dox^{ON}-D5, Dox^{ON}-D8). At the conclusion of the experiment, the rats were perfused for histological analysis of the spinal cords.

Surgeries

The animals were anesthetized using a combination of ketamine, xylazine, and acepromazine (50, 4, and 0.5 mg/kg, i.p.), with supplemental 1-2.5 % isoflurane in 98 % oxygen at a flow rate of 1 L/min as required. Before surgery, they received 5 mL of saline (s.c.), meloxicam (5 mg/kg, s.c.), atropine (0.05 mg/kg, i.m.), sustained-release buprenorphine (0.8 mg/kg, s.c.), and an eye lubricant was applied. Incisions were sutured in layers and closed with surgical staples. Liposomal bupivacaine (5.3 mg/kg, s.c.) was administered once directly at the incision site immediately after wound closure. Following surgery, animals were housed individually for 7 days, given saline (5 ml) twice daily for 3-5 days, meloxicam (5 mg/kg) once daily for 3 days, and gentamicin (20 mg/kg) once daily for 7 days.

Viral vectors and silencing strategy

Virus production and characterization were conducted as previously described (Pocratsky *et al.*, 2017, 2018, 2020; Shepard *et al.*, 2021). In summary, we employed a dual viral vector technique to target sC3 interneurons through their terminals (sC7-C8) and cell bodies (sC3). HiRet-TRE-EGFP.eTeNT was injected at sC7-C8, while AAV2-CMV-rtTAV16 was injected at sC3, following earlier protocols (Pocratsky *et al.*, 2020; Shepard *et al.*, 2021). In the presence of Dox, only the doubly infected neurons that continuously express the rtTAV16 Tet-On sequence would trigger the expression of eTeNT, which would subsequently be transported anterogradely to the terminals (Figure 13). At the terminals, eTeNT inhibits the release of synaptic vesicles, resulting in 'silenced' neurotransmission that takes 3–5 days to establish after Dox administration. Upon removal of Dox, this silencing is reversed, and functional neurotransmission is restored within a period of 3 to 5 days (Kinoshita *et al.*, 2012).

Functional outcome measures

R&G training and testing

As detailed above, the standard R&G task used to evaluate manual dexterity. Each animal was placed individually in a Plexiglass box (30 cm × 15 cm × 30 cm) with one small window (1 cm × 15 cm) on the centre of the front wall. A shelf was positioned 3 cm above the surface outside the wall to hold food pellets (Figure 13). The rats were trained to reach for and grasp single banana-flavoured isocaloric pellets (45 mg, Bio-Serv) placed 1.6 cm away from the front wall. In each session, the rats made about 40 attempts to retrieve and eat the pellets. Each attempt was recorded as in previous chapters. The rats were trained until they reached their performance plateau, usually after 10-15 sessions and with a success rate of approximately 60 %. The paw preference was identified and taken into consideration for the injection surgeries.

R&G tests were conducted at baseline prior to viral vectors injection surgery, and again Pre-Dox, Dox^{ON}-day 5 and Dox^{ON}-day 8. During the testing sessions, each rat was presented with 40 pellets per slit, and their movements were recorded at 120 fps using two GoPro Hero 8 cameras perpendicularly placed, therefore obtaining both the frontal and lateral view of the animal's movements. Success rate and types of error were quantified as detailed above.

Additionally, the movement strategy in successful attempts was further characterised based on 11 movement components previously described (Karl & Whishaw, 2011):

1. **Orient:** The head is oriented towards the pellet, which is sniffed.
2. **Limb lift:** The body weight is shifted to the back and the hindlimbs are aligned with the body when the forepaw is lifted.
3. **Digits close:** The digits present a biomechanic semiflexion and the palm is partially supinated towards the midline of the body.
4. **Aim:** The elbow moves towards alignment with the body midline, with the hand located just under the mouth.
5. **Advance:** The forelimb advances straight forward and directed to the target.
6. **Digits open:** The digits extend and open with the palm still not fully pronated.
7. **Pronation:** The elbow abducts, pronating the palm over the food pellet in an arpeggio movement.
8. **Grasp:** The digits close to grasp the pellet and the paw is lifted.
9. **Supination I:** The palm is supinated 90° as the paw is withdrawn.
10. **Supination II:** The paw is further supinated so that the palm faces the mouth.
11. **Release:** The food is released into the mouth by opening the digits.

Each component was given a score of "0" (if it appears normal), "1" (if it is slightly abnormal but recognisable) or "2" (if it is absent or completely abnormal). The score of every component for every animal was independently averaged from 5 successful attempts distributed equitably between all successful attempts from that session.

Locomotion assessments

To evaluate locomotion, a long plexiglass tank (305 x 14 cm) with a Sylgard-coated walking surface for improved grip was used (Figure 13). Animals were acclimated to the tank along with their cage mates for five days. During acclimation, treat rewards were sporadically provided at both ends of the tank to discourage stopping mid-pass. All tank passes during this phase and beyond were entirely voluntary. Once acclimation was complete, with animals consistently traversing the tank, a 10-day training period commenced, divided into two five-day segments. Each session

involved placing individual animals in the tank for 10 minutes in a quiet, distraction-free room. Stricter reward criteria were implemented during this phase; treat rewards were only given for "perfect passes"—those that did not involve stopping, sniffing, exploring, or rearing. Observational notes were taken to track the animals' behaviour and progress. By the end of the second training week, all animals displayed a range of speed-dependent gaits, from walking to full bounding. At this stage, treat rewards became intermittent and were no longer necessary to ensure the animals traversed the entire tank length appropriately. At behavioural testing timepoints, performance was assessed by recording the animals in the tank. Recordings were captured using six high-speed (200 Hz) Basler cameras: two positioned below the tank to capture ventral views and four facing the tank sides (two on each side) to capture sagittal views. This camera setup allowed for detailed analysis of interlimb and intralimb coordination, with parameters such as swing time or instantaneous speed (Pocratsky *et al.*, 2017, 2020; Shepard *et al.*, 2021).

Histological assessment

At the conclusion of the evaluation, rats were administered an overdose of sodium pentobarbital and perfused with a 4% paraformaldehyde solution in 0.1 M phosphate buffer. Spinal cord segments from levels sC2 to sT2 were dissected and post-fixed, followed by cryoprotection in 30 % sucrose, embedding in tissue freezing medium, and sectioning at 30 µm using a cryostat. The expression of EGFP.eTeNT in cervical spinal cord transverse sections spaced 300 µm apart was confirmed immunohistochemically using primary antibodies against GFP (Table 4), following the immunofluorescence protocol detailed in chapter 1. Images were acquired using an Eclipse Ni Nikon microscope and processed as previously described.

Statistical analyses

Statistical analyses were conducted using GraphPad Prism 9 (version 9.0.0). The comparison between ipsilateral and contralateral sC3-C7 projections was performed by repeated measures two-way ANOVA, with Side as between-subjects factor and Distance as within-subjects factor, followed by Šídák's multiple comparisons test. Behavioural data fitting a Gaussian distribution was analysed by repeated measures one-way ANOVA followed by Tukey's multiple comparisons test. Otherwise, data

was tested by Friedman's nonparametric test followed by Dunn's multiple comparisons test. Gaussian data is shown as mean ± SEM, whereas nonparametric data is presented as median ± interquartile range. Differences between groups were deemed statistically significant for p-values ‹ 0.05.

Table 4. List of antibodies used for tissue immunofluorescence in chapter 2.2.

	Antigen	Dilution	Description	Reference number
Primary antibodies	NeuN	1:200	Mouse monoclonal	Millipore #MAB377
	GFP	1:200	Rabbit polyclonal	Invitrogen #A6455
	NeuN	1:1000	Mouse	*Abcam #ab5076*
	GFP	1:5000	Rabbit polyclonal	Abcam #ab290
Secondary antibodies	Mouse A594	1:200	Donkey polyclonal	Life Technologies #A21203
	Rabbit A488	1:200	Donkey polyclonal	Life Technologies #A21206
	Mouse A647	1:200	Donkey polyclonal	Jackson Immunoresearch #715-605-151
	Rabbit A Plus 488	1:400	Donkey polyclonal	Invitrogen #A32790

(Figure on the next page)

Figure 13. Schematic representation of the methods used in Chapter 2.2. Rats were injected either the tracing or silencing vectors. The performance of "silenced" rats was assessed before and upon Dox administration. Spinal cords were ultimately harvested for histological analyses. SD: Sprague Dawley.

Chapter 2.2

Experimental design

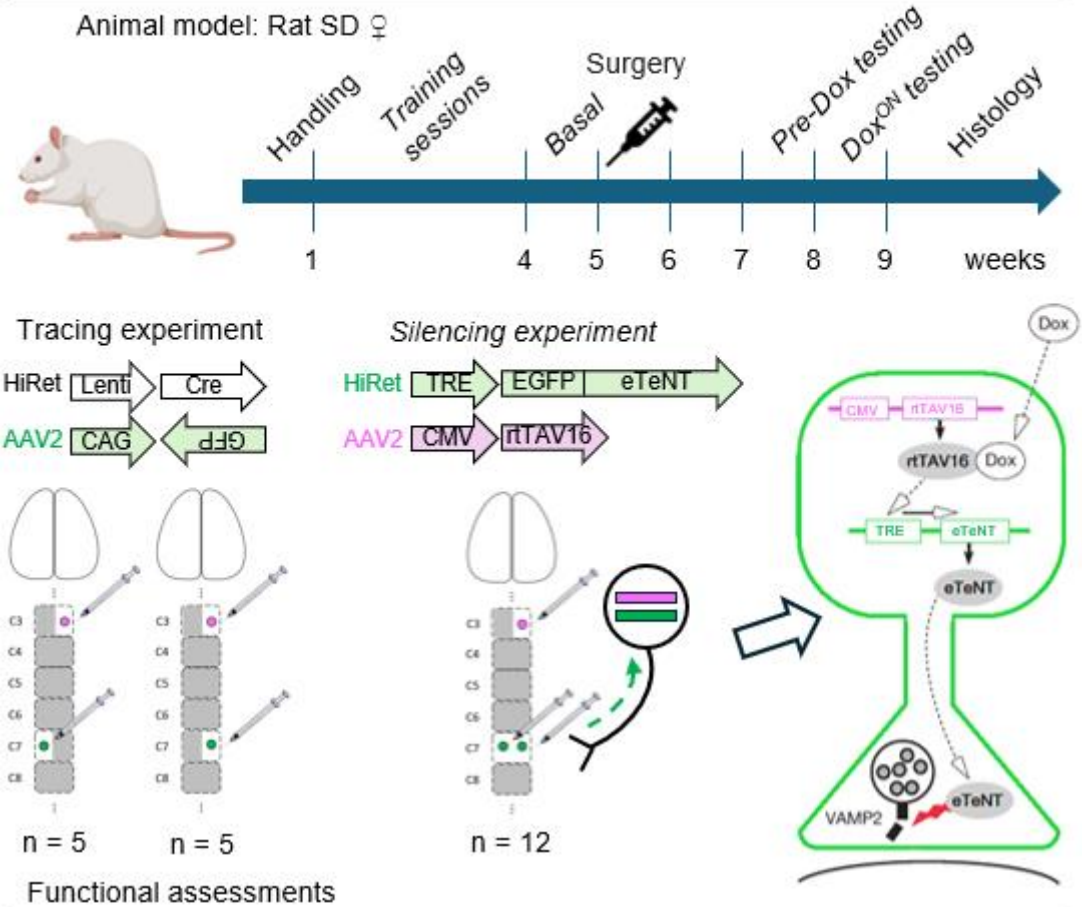

Functional assessments

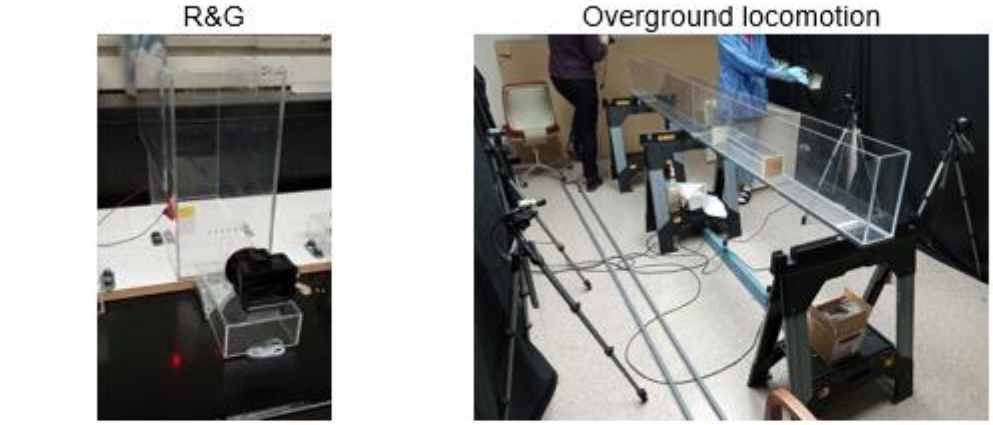

Histological analysis

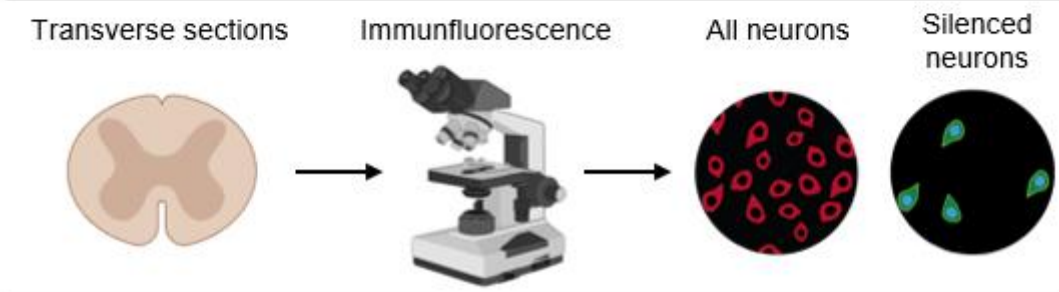

VI. Results

Chapter 1

Identifying a spinal neuronal network controlling reaching and grasping

Overview

In this project, we aimed to unveil the presence and location of a hypothetic spinal neuronal network necessary for the control of manual dexterity. In the first chapter, we used a functional mapping strategy based on loss of function. We inflicted excitotoxic injuries to rats at different cervical spinal cord levels using kainic acid, for exclusively affecting spinal networks while preserving descending commands. Motor deficits were evaluated by comparing the performance, before versus after the intervention, in multiple behavioural tests of forelimb muscles' function that likely require distinct neuronal networks. In a subsequent experiment, the dorsal and ventral roots of the segments of interest were sectioned to dismiss the possibility of the loss of motoneurons and/or sensory feedback being the cause of the behavioural deficits observed.

Functional and morphological impact of excitotoxic lesions in different cervical spinal segments

Single-segment injection of kainic acid induces localised grey matter damage in the cervical spinal cord

As part of a preliminary screening along the cervical spinal cord, four groups of animals received kainic acid injections at different segments (vC3, vC5, vC7, or vT1). Kainic acid has been shown to selectively damage grey matter, which contains the spinal networks, while sparing the white matter (Magnuson *et al.*, 1999). Using the vertebral (v) nomenclature for these lesions reflects the broader extent of damage induced by kainate, which, although targeted at particular segments, often affects areas both above and below the injection site. This approach allows us to correlate deficits in skilled hand function with the specific spinal levels affected, providing evidence that neurons critical for these movements are localized at those segments.

After behavioural assessments were completed (described in the next section), histological analysis was conducted following the perfusion and collection of the spinal cords in order to characterize the extent of the inflicted injuries. Spinal cord sections were stained with Cresyl violet in order to observe the grey matter preservation. For all groups, ipsilateral shrinkage of the grey matter was appreciated at the level of kainic acid injection, which recovered its normal shape at the rostral and caudal spinal segments (Figure 14A). Grey matter preservation was quantified comparing the areas of grey matter of each hemicord to a standard area for that specific spinal cord segment. The standard curve was derived from the intact segments of the processed spinal cords, approximately 10 mm rostral and caudal to the injection epicentre (for further details, see Materials and methods section).

In all groups receiving kainic acid injection in the cervical spinal cord, the injury extended for approximately 6 mm along the rostrocaudal axis, where a progressive significant reduction of grey matter preservation percentage was observed until reaching around 60 % of ipsilateral grey matter area vs standard curve in the epicentre, being the lowest 59.25 ± 5.68 % ($p < 0.05$) for vC3 group, 56 ± 3.39 % ($p < 0.01$) for vC5 group and 59 ± 3.08 % ($p < 0.01$) for vC7 group (Figure 14B). However, at the contralateral spinal cord, grey matter was preserved in all groups, and only one sporadic statistically significant increase (and not a reduction) in grey matter

percentage in vC5 group ($p < 0.5$) was found (Figure 14C). This single difference is probably a consequence of interindividual variability inside normality and has an unlikely biological relevance.

Then, we proceeded to compare the grey matter preservation curves between groups, after centring the injury epicentre of all animals. For the ipsilateral hemicord, the comparison revealed significant differences for distance ($F_{(2.04, 17.09)} = 13.75$, $p < 0.001$) and group ($F_{(3, 9)} = 5.26$, $p < 0.05$) effects, but not for the interaction ($F_{(99, 277)} = 1.19$, p = ns) (Figure 14D). The only significant difference found post hoc was between vC3 and vC7 groups at 2.5 mm (93.5 ± 4.17 vs 71 ± 4.60 %, respectively; $p = 0.0421$) and 2.75 mm (97.5 ± 4.19 vs 74.75 ± 4.35 %, respectively; $p = 0.0354$) rostral of the epicentre, which suggests a similar impact of kainic acid at the different cervical spinal cord segments injected. In the contralateral side, the effect of distance was significant ($F_{(3.63, 30.50)} = 3.71$, $p < 0.05$), but not that of group ($F_{(3, 9)} = 0.87$, p = ns) or interaction ($F_{(99, 277)} = 1.03$, p = ns) (Figure 14E). Finally, the animal injected at vT1 showed a milder grey matter loss compared to the other groups, achieving a minimum level of 81 %. This could reflect the regional differences in kainic acid effect suggested in literature (Regan, 1996; Magnuson *et al.*, 1999). Nonetheless, being only one animal, the observation must be interpreted with caution.

These results indicate that excitotoxic injury via kainic acid leads to consistent grey matter loss across cervical segments, with some subtle segment-specific variations. On the ipsilateral side, significant differences suggest that the injury's impact may vary slightly depending on the specific spinal segment, possibly due to differences in grey matter shape, neuronal density, or intrinsic vulnerability. In contrast, grey matter is generally well preserved on the contralateral side, with no significant differences among groups. Overall, these data support the idea that localized excitotoxic lesions can be employed to reveal important functional distinctions among spinal segments.

Subsequently, we assessed whether the white matter remained unaffected upon kainic acid injection, as this would permit our conclusions to be attributed entirely to the grey matter harm. The quantification was made using spinal cord sections stained with Luxol blue (Figure 15A), following the same procedure and comparison to a standard curve as explained above for grey matter analysis. Here, we did not find a statistically significant difference in white matter in neither ipsilateral ($F_{(4.47, 32.39)} = 1.29$, p = ns for distance effect and $F_{(3, 9)} = 0.54$, p = ns for group effect) nor contralateral

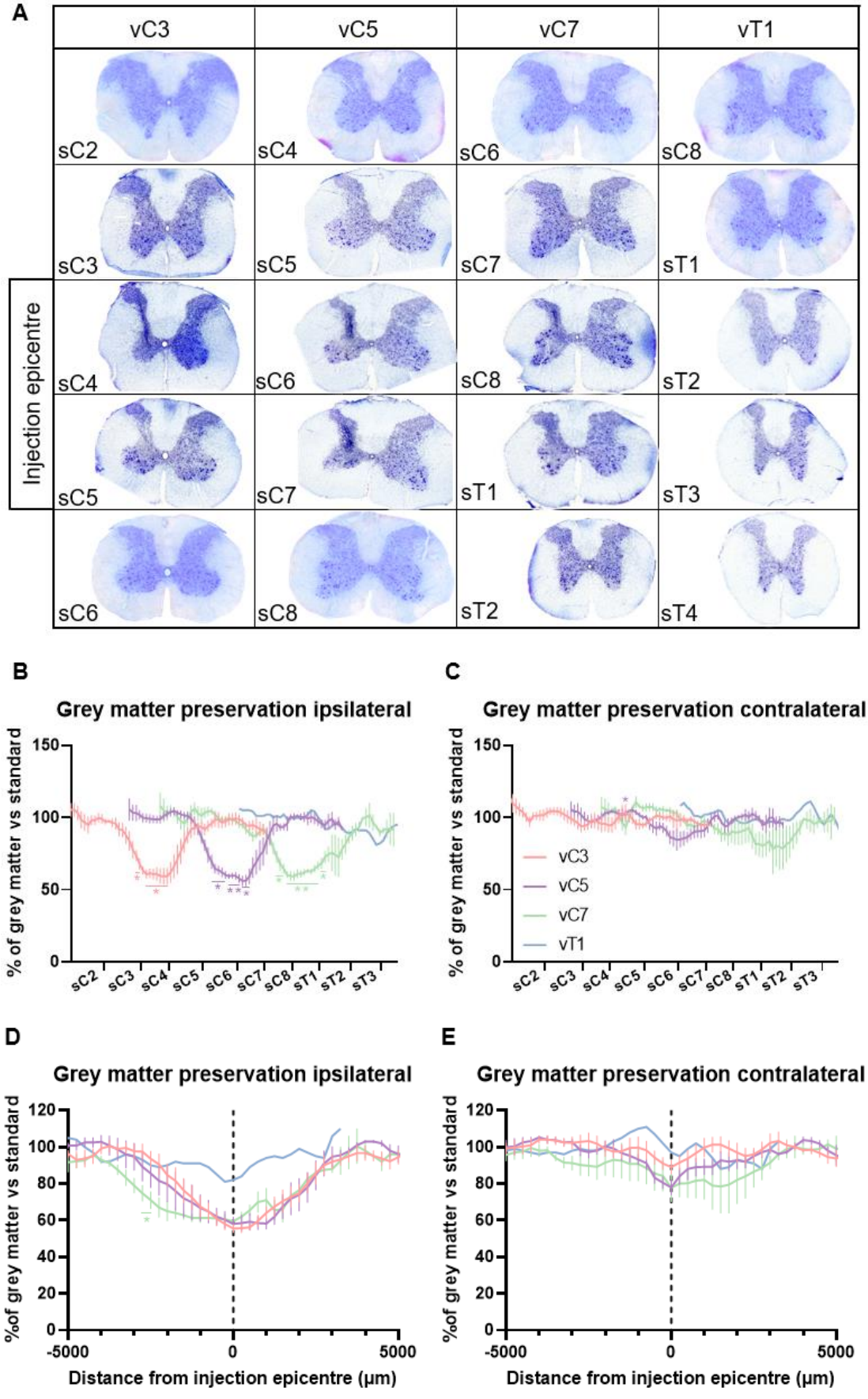
A
vC3
vC5
vC7
vT1
sC2
sC4
sC6
sC8
sC3
sC5
sC7
sT1
sC4
sC6
sC8
sT2
sC5
sC7
sT1
sT3
sC6
sC8
sT2
sT4
Injection epicentre
B
Grey matter preservation ipsilateral
% of grey matter vs standard
150
100
50
0
sC2
sC3
sC4
sC5
sC6
sC7
sC8
sT1
sT2
sT3
C
Grey matter preservation contralateral
% of grey matter vs standard
vC3
vC5
vC7
vT1
D
Grey matter preservation ipsilateral
%of grey matter vs standard
120
100
80
60
40
20
0
-5000
0
5000
Distance from injection epicentre (µm)
E
Grey matter preservation contralateral
%of grey matter vs standard
Distance from injection epicentre (µm)

Figure 14. Excitotoxic injections in different spinal cord segments. (A) Representative Cresyl violet-stained spinal cord images from all experimental groups at relevant segments (i.e. at the segments of kainic acid injection and their surroundings). Grey matter preservation was quantified in the hemicords corresponding to the **(B)** ipsilateral or **(C)** contralateral side. The curve at the injection epicentre was also compared at the **(D)** ipsilateral and **(E)** contralateral hemicords. Groups: vC3 (n = 4), vC5 (n = 4), vC7 (n = 4), vT1 (n = 1). **(B-C) *** $p < 0.05$, ****** $p < 0.01$; as calculated by one sample t test vs a hypothetical mean of 100, followed by Benjamini-Hochberg correction for multiple comparisons. **(D-E) *** $p < 0.05$ vs vC3; as calculated by mixed-effects analysis model using the restricted maximum likelihood method, followed by Tukey's multiple comparisons test. Data presented as mean ± SEM.

($F_{(4.73, 31.97)} = 1.19$, p = ns for distance effect and $F_{(3, 9)} = 0.87$, p = ns for group effect) hemicords (Figures 15B-C). Likewise, the white matter preservation curves at the injection epicentre were similar between all groups, for both the ipsilateral ($F_{(5.11, 54.12)} = 1.30$, p = ns for distance effect and $F_{(3, 9)} = 1.75$, p = ns for group effect) (Figure 15D) and contralateral ($F_{(5.56, 58.91)} = 1.73$, p = ns for distance effect and $F_{(3, 9)} = 2.05$, p = ns for group effect) (Figure 15E) sides. Therefore, the potential functional impairments observed can be attributed solely to the effect of kainic acid on the grey matter.

Single-segment kainic acid injections do not impair forelimb function

Once we had ensured the specificity of kainic acid for grey matter, we proceeded to analyse the forelimb functional impairments in the different groups of animals and link them to the neuronal populations present at the affected segments. Initially, we assessed manual dexterity using the traditional R&G test, in which rats were placed in a transparent box and required to reach and grasp food pellets from an elevated platform situated outside of a narrow window. Animals were trained five days per week until reaching a performance plateau and were then tested both before and after the intervention. R&G performance was evaluated by measuring the percentage of successful attempts and by analysing the types of errors committed when the pellet was not grasped, with errors classified according to the movement phase during which the unsuccessful attempt occurred (for more details, see Materials and methods section).

Surprisingly, there was not a significant change in success percentage ($F_{(3, 9)} = 1.57$, p = ns for group; $F_{(1, 9)} = 0.01$, p = ns for timepoint; and $F_{(3, 9)} = 1.22$, p = ns for interaction

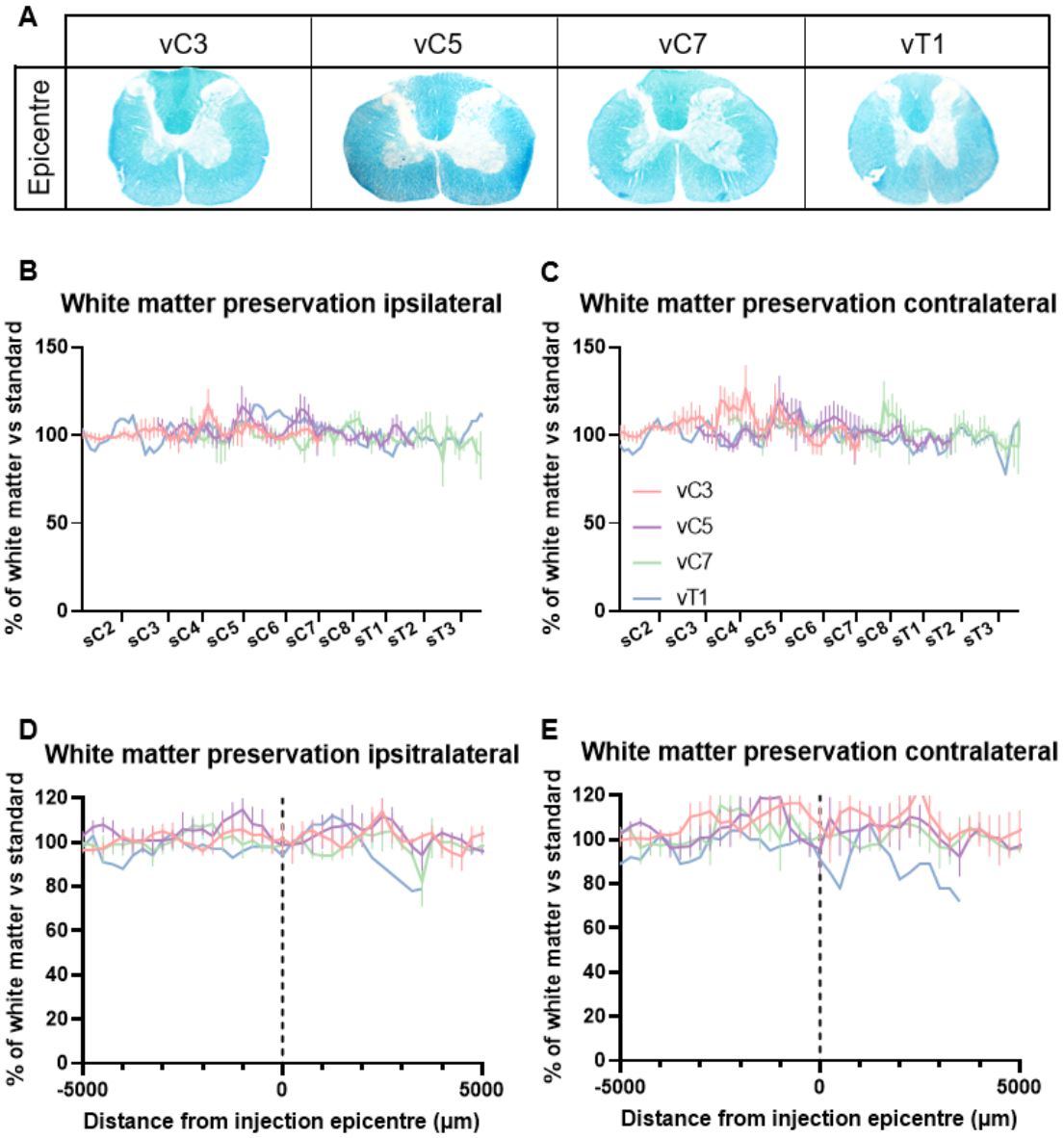

Figure 15. Kainic acid effect on white matter. **(A)** Representative Luxol blue-stained spinal cord images from all experimental groups at the injection epicentre. White matter preservation was quantified in the hemicords corresponding to the **(B)** ipsilateral or **(C)** contralateral side. The curve at the injection epicentre was also compared at the **(D)** ipsilateral and **(E)** contralateral hemicords. Groups: vC3 (n = 4), vC5 (n = 4), vC7 (n = 4), vT1 (n = 1). Analysis performed by mixed-effects analysis model using the restricted maximum likelihood method. Data is presented as mean ± SEM.

effects), as it remained between 60 and 80 % approximately (Figure 16A). Accordingly, the frequency percentage of the six types of error remained grossly unaffected in all groups (Figures 16B-F), with the only exception of a significant variation in the frequency of error type 4, where the pellet is displaced during the

fingers' extension right before grasping ($F_{(3, 9)} = 2.13$, p = ns for group; $F_{(1, 9)} = 6.99$, $p < 0.05$ for timepoint; and $F_{(3, 9)} = 2.42$, p = ns for interaction effects), that post hoc comparisons revealed as a frequency increase for group vC5 ($p < 0.01$) (Figure 16E). A significant timepoint effect ($F_{(1, 9)} = 5.89$, $p < 0.05$) was also observed for error type 2, where the forepaw advance is insufficient to reach the pellet position ($F_{(3, 9)} = 1.60$, p = ns for group; and $F_{(3, 9)} = 0.64$, p = ns for interaction effects), but none of the multiple comparisons achieved statistical significance (lowest p = 0.2708 for group vC3) (Figure 16C). Of note, the animal from injected at vT1 could not be used for statistical analyses but was kept in the graphs as a control of the specificity of kainic acid effect in the cervical spinal cord. In conclusion, the excitotoxic lesion mediated by single-segment kainic acid in vC3, vC5, vC7 or vT1 did not alter the capacity of performing the classical R&G movement task.

To further characterise potential deficits, we evaluated both skilled and unskilled forelimb functions using several additional behavioural tests: R&G food pellets on different steps of a staircase (Montoya *et al.*, 1991) ($F_{(3, 9)} = 0.65$, p = ns for group; $F_{(1, 9)} = 0.05$, p = ns for timepoint; and $F_{(3, 9)} = 0.65$, p = ns for interaction effects) (Figure 17A), the manipulation of a doughnut shaped cereal for eating (Irvine *et al.*, 2010, 2014) (Figure 17B), the removal of adhesive stickers on the palm of the forepaws ($F_{(3, 9)} = 2.13$, p = ns for group; $F_{(1, 9)} = 1.99$, p = ns for timepoint; and $F_{(3, 9)} = 0.64$, p = ns for interaction effects) (Figure 17C) and overground locomotion (Lakes & Allen, 2016) (Stride length: $F_{(3, 9)} = 0.20$, p = ns for group; $F_{(1, 9)} = 0.56$, p = ns for timepoint; and $F_{(3, 9)} = 0.73$, p = ns for interaction effects. Base of support: $F_{(3, 9)} = 2.86$, p = ns for group; $F_{(1, 9)} = 0.85$, p = ns for timepoint; and $F_{(3, 9)} = 0.12$, p = ns for interaction effects. Forepaw width: $F_{(3, 8)} = 1.20$, p = ns for group; $F_{(1, 8)} = 0.41$, p = ns for timepoint; and $F_{(3, 8)} = 1.63$, p = ns for interaction effects) (Figures 17D-F). In line with the previous results, we did not observe a significant detriment in any of the multiple behavioural assessments implemented, even though the tasks evaluated different expressions of forelimb skilled function and forelimb unskilled function. We must mention the tendency of a decrease in adhesive detection time for groups vC5 (basal 3.5 ± 0.96 vs 1 s at 7DPI) and vC7 (basal 2.75 ± 1.18 vs 1.5 ± 0.5 s at 7DPI), that did not reach statistical significance (Figure 17C). In any case, this tendency would indicate an increase, and not a decrease, in forepaw sensory function. Overall, the combined results from Figures 16 and 17 indicate that forelimb function remains intact despite the localized decrease in grey

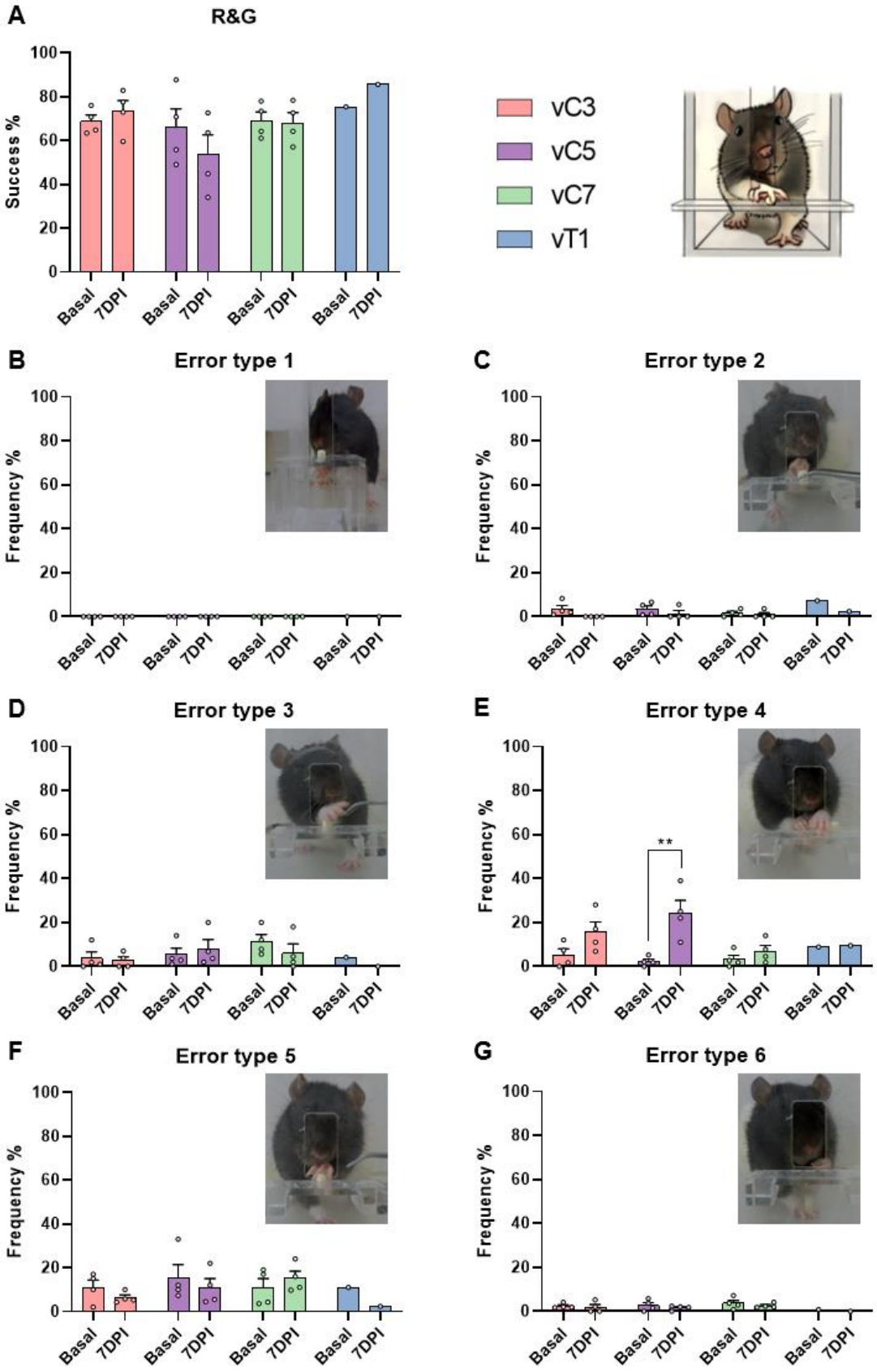
A
R&G
Success %
vC3
vC5
vC7
vT1
B
Error type 1
Frequency %
C
Error type 2
Frequency %
D
Error type 3
Frequency %
E
Error type 4
Frequency %
**
F
Error type 5
Frequency %
G
Error type 6
Frequency %
Basal
7DPI

Figure 16. R&G assessment after kainic acid injection. R&G performance was analysed before and 7 days after the surgery by means of **(A)** success percentage and frequency of errors type **(B)** 1, **(C)** 2, **(D)** 3, **(E)** 4, **(F)** 5 and **(G)** 6. Groups: vC3 (n = 4), vC5 (n = 4), vC7 (n = 4), vT1 (n = 1). ** $p < 0.01$, as calculated by repeated measures two-way ANOVA with timepoint as within-subject factor and group as between-subject factor, followed by Šídák's multiple comparison tests when significant differences were present. Data is shown as mean ± SEM.

matter area elicited by single-segment kainic acid injections in the examined cervical segments.

Functional and morphological impact of excitotoxic lesions in two consecutive cervical spinal segments

Kainic acid injection in two consecutive spinal segments causes a bigger grey matter area reduction, astrogliosis and inflammation, sparing the white matter

In light of the lack of behavioural effects observed with single-segment injections at vC3, vC5, vC7, or vT1, we hypothesized that these focal lesions might have been too restricted to effectively disrupt the putative spinal network controlling manual dexterity, which could extend over multiple segments. As the initial screening did not cover the entire cervical spinal cord, we expanded our approach to target a broader area. Four groups of animals received kainic acid injections spanning two consecutive spinal segments (vC2-C3, vC4-C5, vC6-C7, or vT1-T2) thereby covering almost the entire cervical enlargement. A fifth group received vehicle injections at vC2-C3. This more extensive lesioning strategy increases the likelihood of disrupting the hypothetical network, if it exists, and may help reveal its contribution to forelimb motor control.

As before, grey matter preservation was assessed using sections stained with Cresyl violet. In all groups receiving kainic acid injections, grey matter shrinkage at the level of injection was observed, whereas the vehicle group showed no such change (Figure 18A). In this experiment, however, the extension of the excitotoxic injury was larger, approximately 8 mm along the rostrocaudal axis, with a slight overlap between the caudal lesioned area of one group and the rostral lesioned area of the subsequent group (Figures 18A-B). Another notable difference is that the maximum injury was less severe than in animals injected at a single segment. In the previous experiment, the

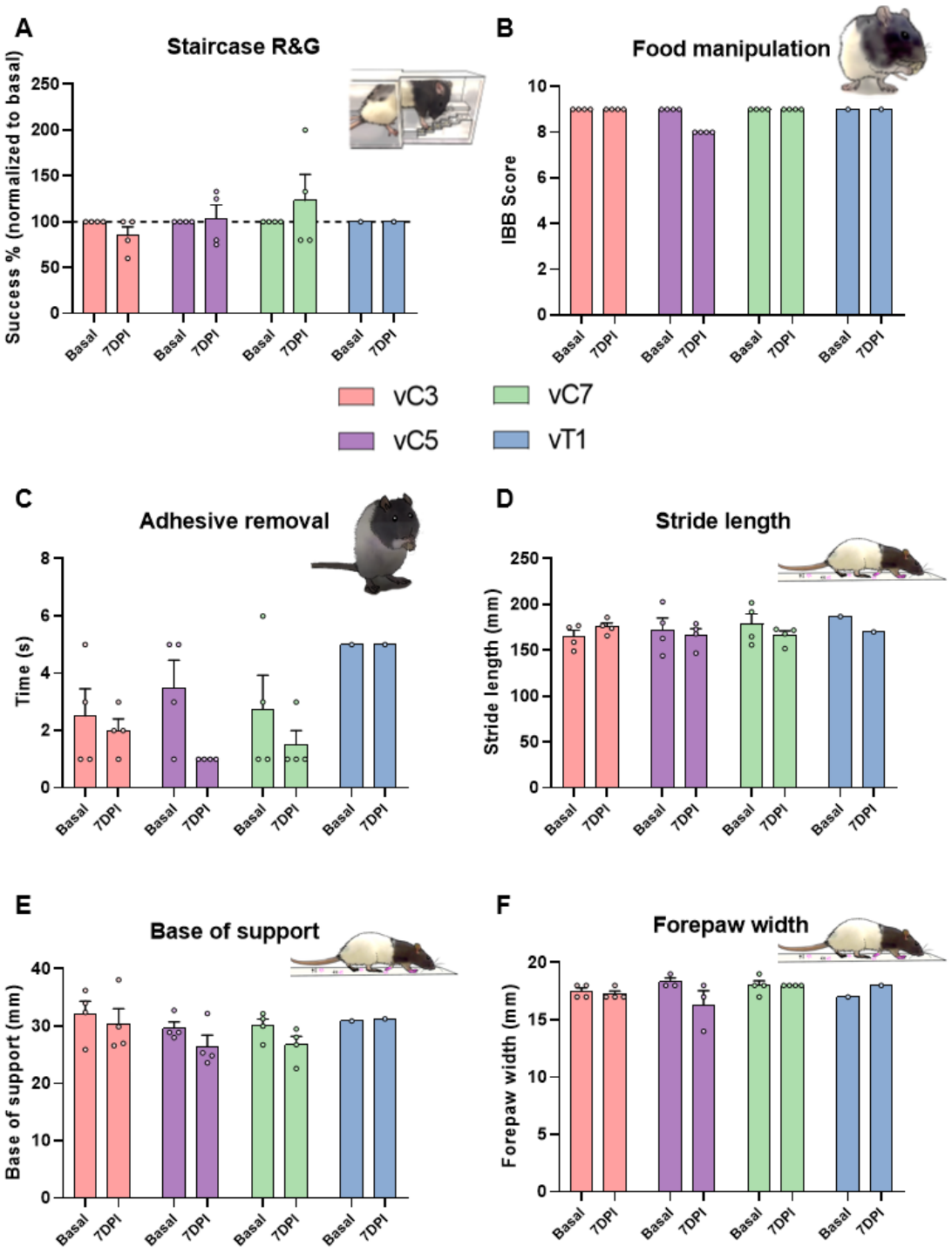

Figure 17. Forelimb function evaluation after kainic acid injection. Forelimb function was assessed with several behavioural tests: **(A)** staircase R&G **(B)** food manipulation, **(C)** adhesive removal and overground locomotion, where **(D)** forelimb stride length, **(E)** base of support and **(F)** pawprint width were measured. Groups: vC3 (n = 4), vC5 (n = 3-4), vC7 (n = 4), vT1 (n = 1). Statistical analyses performed by repeated measures two-way ANOVA with timepoint as within-subject factor and group as between-subject factor. **(B)** Compared by Wilcoxon test in vC5 group (in the other groups, all values were the same at basal and 7DPI,

so no statistical test was needed). Data presented as mean ± SEM except in **(B)**, where data is shown as mean ± interquartile range.

minimum grey matter preservation in the ipsilateral hemicord was around 60%, whereas here it was closer to 70%, ranging from 66.43 ± 4.50% in the vC4-C5 group to 82.8 ± 9.41% in the vT1-T2 group (Figure 18B). Significant effects were found for group ($F_{(4, 29)} = 3.63$, $p < 0.05$) and for the interaction ($F_{(380, 2293)} = 7.43$, $p < 0.001$) effects, while the effect of distance did not reach significance ($F_{(5.60, 135.3)} = 1.172$, p = ns). Post hoc comparisons showed a significant grey matter decrease in vC2-C3 (peak of 72.22 ± 3.61 vs 100.75 ± 2.50 %, $p < 0.001$), vC4-C5 (peak of 71.25 ± 3.82 vs 98.75 ± 1.93 %, $p < 0.001$), and vC6-7 (peak of 76.63 ± 2.49 vs 102.75 ± 2.32 %, $p < 0.001$), groups compared to the vehicle group, but it did not reach statistical significance in vT1-T2 group (peak of 83.8 ± 7.47 vs 99 ± 3.61 %, p = ns), consistent with the milder effect of kainic acid effect in that region. Regarding the contralateral hemicord, no statistically significant differences were observed for distance ($F_{(6.13, 147.0)} = 1.78$, p = ns) and group ($F_{(4, 29)} = 1.35$, p = ns) effects individually, but there was a significant interaction ($F_{(380, 2280)} = 1.34$, $p < 0.001$) (Figure 18C). Post hoc comparisons revealed punctual significant differences at the level of injection for groups vC2-C3 (92.78 ± 2.94 vs 102.5 ± 1.76 %, p = 0.0476) and vC4-C5 (lowest 89.57 ± 2.51 vs 100.5 ± 0.96 %, $p < 0.05$), and a few sporadic significant decreases elsewhere in groups vC2-C3 (lowest 94.88 ± 2.37 vs 104.25 ± 1.70 %, $p < 0.05$, at sT1), vC4-C5 (93 ± 1.53 vs 101 ± 1.68 %, p = 0.0498, at rostral sC2) and vC6-C7 (lowest of 98.33 ± 0.88 vs 104 ± 0.71 %, $p < 0.05$, at caudal sC2). Again, no significant effect was observed in vT1-T2 group (92.5 ± 1.5 vs 101 ± 1.68 %, p = ns, at rostral sC2).

We then compared the grey matter preservation curve aligned at the injection epicentre. For the ipsilateral hemicord, there were statistically significant effects of distance ($F_{(2.73, 72.82)} = 20.38$, $p < 0.001$), group ($F_{(4, 29)} = 3.42$, $p < 0.05$) and interaction ($F_{(160, 1068)} = 2.17$, $p < 0.001$). (Figure 18D). With multiple comparisons, groups vC2-C3 (lowest of 63.33 ± 2.87 vs 93 ± 2.27 %, $p < 0.001$), vC4-C5 (lowest of 64.75 ± 3.32 vs 95 ± 1.29 %, $p < 0.001$), vC6-C7 (lowest of 73.13 ± 2.36 vs 95 ± 1.29 %, $p < 0.001$) and vT1-T2 (lowest of 74.4 ± 4.48 vs 95.25 ± 2.78 %, $p < 0.05$) presented a significant reduction of grey matter preservation percentage in comparison to the vehicle group. Regarding the contralateral hemicord, statistically significant differences were observed for

distance ($F_{(5.78, 153.7)} = 4.78$, $p < 0.001$) and interaction ($F_{(160, 1063)} = 1.44$, $p < 0.001$) effects, with no significant effect of group ($F_{(4, 29)} = 0.32$, p = ns) (Figure 18E). Post hoc, we observed that most of the segments preserved the grey matter in comparison to the vehicle, with the exception of vC2-C3 (lowest of 88 ± 2.05 vs 99.75 ± 0.95 %, $p < 0.01$) and vC4-C5 (lowest of 88.25 ± 3.48 vs 101.5 ± 1.26 %, $p < 0.05$) groups at the injection epicentre, and sporadic differences for groups vC2-C3 (lowest of 96.13 ± 2.24 vs 108 ± 1.29 %, $p < 0.01$), vC4-C5 (lowest of 97.29 ± 1.08 vs 108.5 ± 1.32 %, $p < 0.01$) and vC6-C7 (lowest of 96.75 ± 2.02 vs 105.75 ± 1.75 %, $p < 0.05$) far caudally from the injections. Last, it is important to note that the multiple comparisons for both ipsilateral and contralateral epicentres compared all groups between them, not solely against the vehicle, and no statistically significant differences were found.

Altogether, these results indicate that excitotoxic injuries inflicted over two consecutive segments extended over an average of 8 mm on the rostrocaudal axis. The lesions were predominantly confined to the ipsilateral hemicord, and the extent of the injury was equivalent across the different kainic acid groups. The lesions from the four animal groups effectively covered almost the entire cervical enlargement, allowing us to dissect the functional consequences of damaging nearly every specific cervical segment.

(Figure on the next pages)

Figure 18. Excitotoxic injections in 2 spinal cord segments. (A) Representative Cresyl violet-stained spinal cord images from all experimental groups at segments sC2-T2. Grey matter preservation throughout the cervical and rostral thoracic spinal cords was quantified for the **(B)** ipsilateral and **(C)** contralateral hemicords. The preservation at the injection epicentre was also quantified in the hemicords corresponding to the **(D)** ipsilateral or **(E)** contralateral side. Groups: Vehicle (n = 4), vC2-C3 (n = 9), vC4-C5 (n = 8), vC6-C7 (n = 8), vT1-T2 (n = 5). * $p < 0.05$, ** $p < 0.01$, *** $p < 0.001$; as calculated by mixed-effects analysis model using the restricted maximum likelihood method, followed by Tukey's multiple comparisons test versus the vehicle group **(B-C)** or between all groups **(D-E)**. Data presented as mean ± SEM.

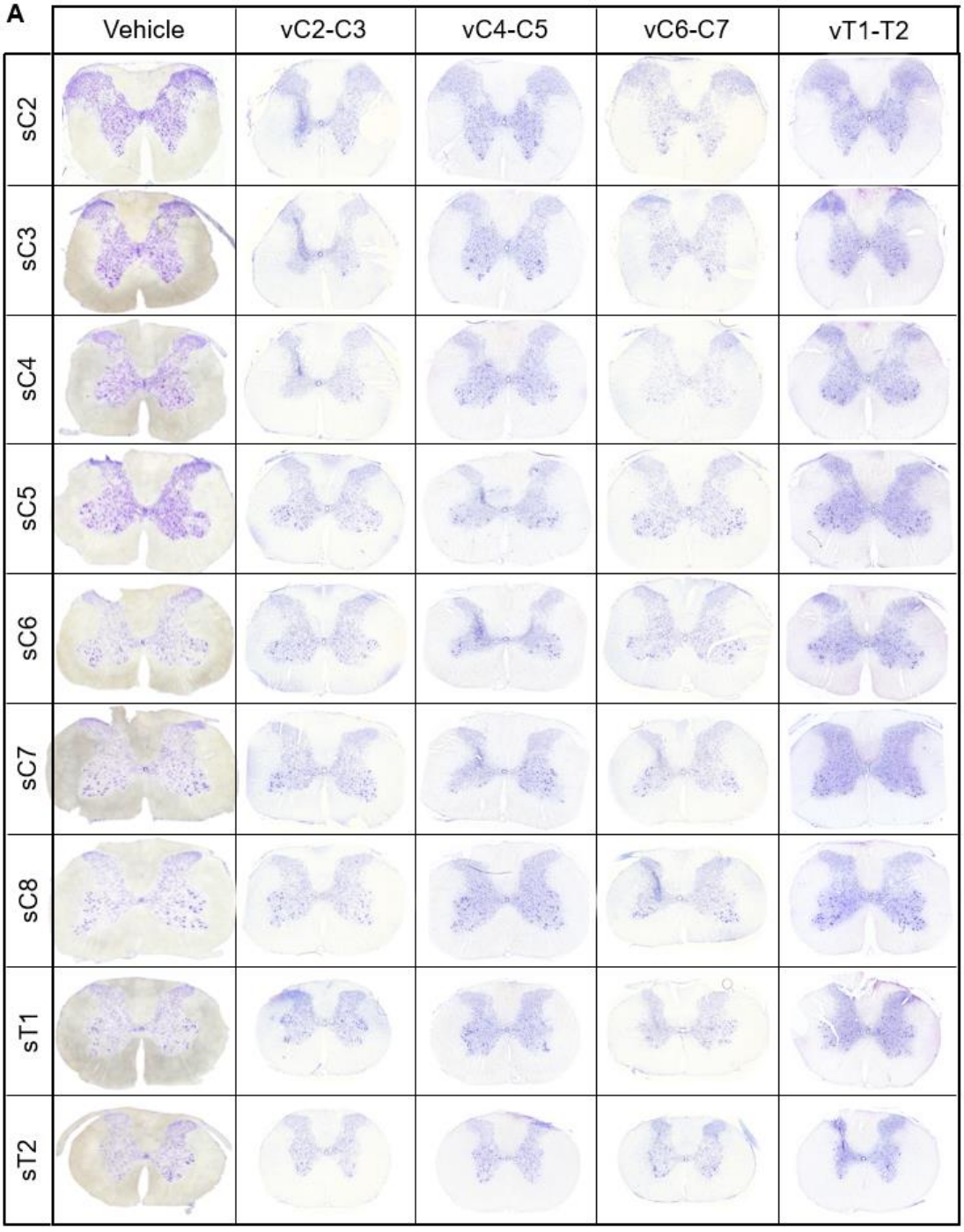
A
Vehicle
vC2-C3
vC4-C5
vC6-C7
vT1-T2
sC2
sC3
sC4
sC5
sC6
sC7
sC8
sT1
sT2
B
Grey matter preservation ipsilateral
% of grey matter vs standard
150
100
50
0
sC2
sC3
sC4
sC5
sC6
sC7
sC8
sT1
sT2
sT3
C
Grey matter preservation contralateral
% of grey matter vs standard
150
100
50
0
Vehicle
vC2-C3
vC4-C5
vC6-C7
vT1-T2
sC2
sC3
sC4
sC5
sC6
sC7
sC8
sT1
sT2
sT3

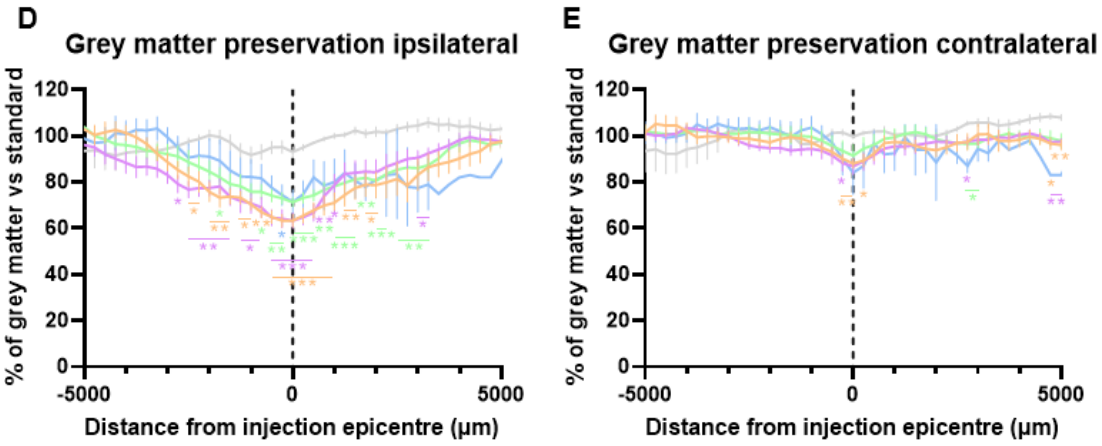

Next, we investigated whether the injection of kainic acid in two consecutive spinal segments selectively affected the grey matter or also damaged the white matter. As before, we quantified the white matter area and calculated the white matter preservation percentage from spinal cord sections stained with Luxol blue (Figure 19A). As in single segment excitotoxic injection animals, we did not find statistically significant differences in the ipsilateral ($F_{(9.84, 230.8)} = 0.94$, p = ns for distance effect and $F_{(4, 29)} = 1.20$, p = ns for group effect) nor contralateral ($F_{(8.21, 190.7)} = 1.16$, p = ns for distance effect and $F_{(4, 29)} = 0.38$, p = ns for group effect) white matter preservation percentages (Figures 19B-C). When we analysed the injection epicentre of the ipsilateral hemicord, we found a significant effect of the interaction ($F_{(160, 1066)} = 1.32$, $p < 0.01$), but not for distance ($F_{(7.13, 190.1)} = 0.87$, p = ns) and group ($F_{(4, 29)} = 1.32$, p = ns) by themselves (Figure 19D). This time, post hoc comparisons revealed significant differences versus the vehicle but also between other kainic acid groups. Compared with the vehicle, vC2-C3 group displayed a significant increase 5 mm rostral to the injection epicentre ($p < 0.05$), whereas vC4-C5 ($p < 0.01$) and vC6-C7 ($p < 0.05$) showed a decrease around 1 mm caudally, and vT1-T2 a decrease 4 mm caudal to the epicentre ($p < 0.01$). Regarding comparison of kainic acid groups, vC4-C5 group displayed lower white matter area versus vC2-C3 group at 5 mm rostral coordinates ($p < 0.05$), and the rest of the significant differences were in relation to vT1-T2 group. At 1 mm rostral to the injury epicentre, vT1-T2 white matter area (116.75 ± 4.13 %) was higher than that of vC4-C5 ($p < 0.05$) and vC6-C7 ($p < 0.05$) groups, and at 4 mm caudal, it was significantly lower (83 ± 1 %) than vC2-C3 ($p < 0.01$) and vC4-C5 ($p < 0.01$) groups. However, no effect was observed for distance ($F_{(5.86, 153.8)} = 0.43$, p = ns), group ($F_{(4, 29)} = 0.40$, p = ns) or interaction ($F_{(160, 1051)} = 0.80$, p = ns) in the contralateral side of the

injections (Figure 19E). Considering that no consistent differences were detected in the white matter of the ipsilateral hemicords across the entire cervical and rostral thoracic regions, nor on the contralateral side (both overall and at the epicentre) and given that the few observed differences did not follow a systematic pattern, it is likely that these variations are due either to chance or to artifacts arising from histological processing, rather than reflecting true biological effects. Therefore, we conclude that the injection of kainic acid into two consecutive spinal cord segments selectively impairs grey matter while sparing white matter.

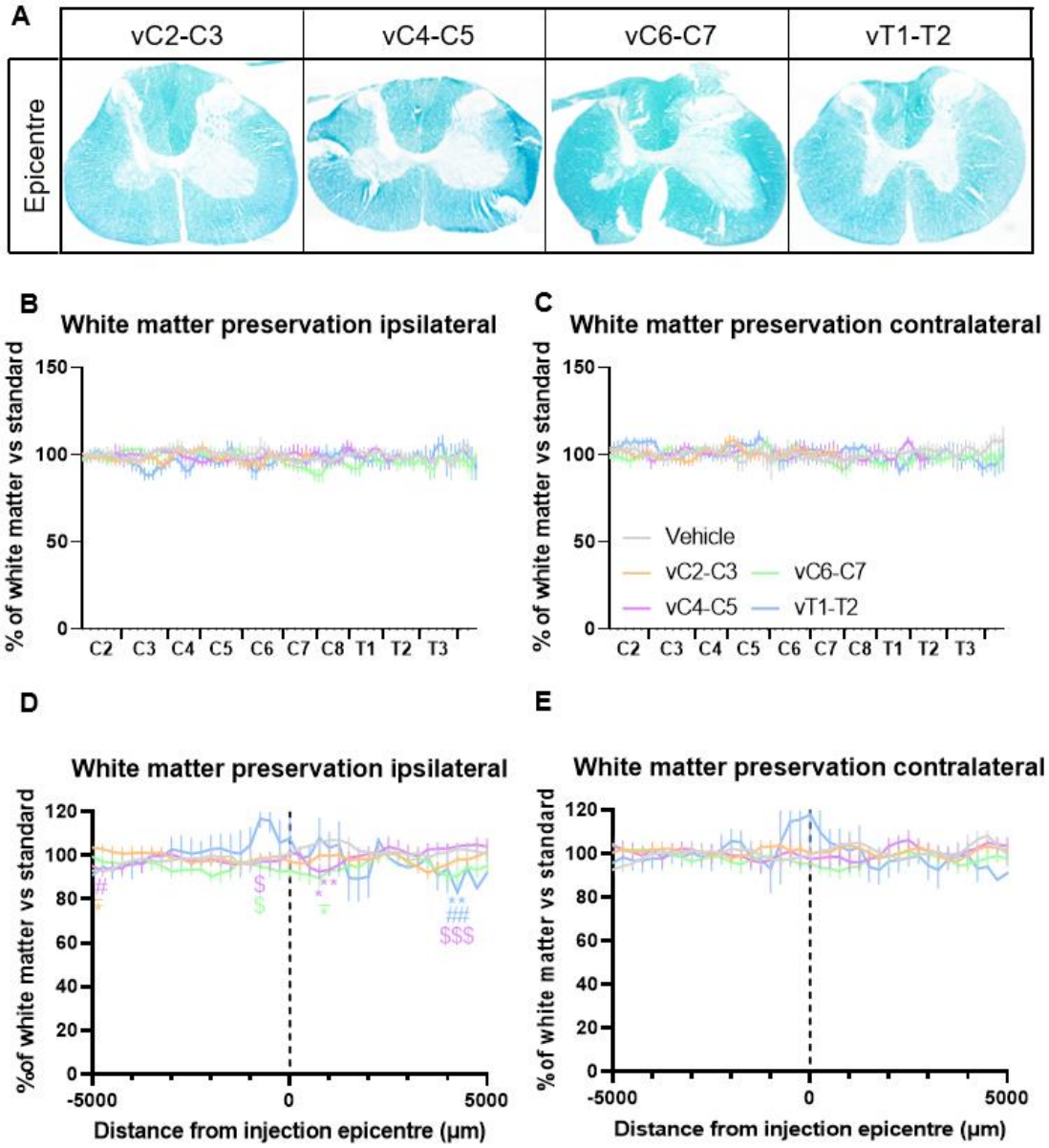

Figure 19. White matter preservation after kainic acid injections in 2 spinal cord segments. (A) Representative Luxol blue-stained spinal cord images at the kainic acid injection epicentre for all injured groups. White matter preservation throughout the cervical

and rostral thoracic spinal cords was quantified for the **(B)** ipsilateral and **(C)** contralateral hemicords. The preservation at the injection epicentre was also quantified in the hemicords corresponding to the **(D)** ipsilateral or **(E)** contralateral side. Groups: Vehicle (n = 4), vC2-C3 (n = 9), vC4-C5 (n = 8), vC6-C7 (n = 8), vT1-T2 (n = 5). * p < 0.05, ** p < 0.01, vs Vehicle; # p < 0.05, ## p < 0.01 vs vC2-C3, $ p < 0.05, $$$ p < 0.001 vs vT1-T2; as calculated by mixed-effects analysis model using the restricted maximum likelihood method, followed by Tukey's multiple comparisons test versus the vehicle group **(B-C)** or between all groups **(D-E)**. Data presented as mean ± SEM.

Following the white matter analysis, we used NeuN immunostaining to observe whether the previously detected grey matter reduction was linked to a decrease in the number of neurons present. As expected, kainic acid excitotoxicity caused neuronal death. It expanded across all laminae, but was especially notable at the intermediate grey matter (where the injection took place). The diminishment in neuronal preservation reached around 60 % at the ipsilateral hemicord at the injury epicentre (Figure 20).

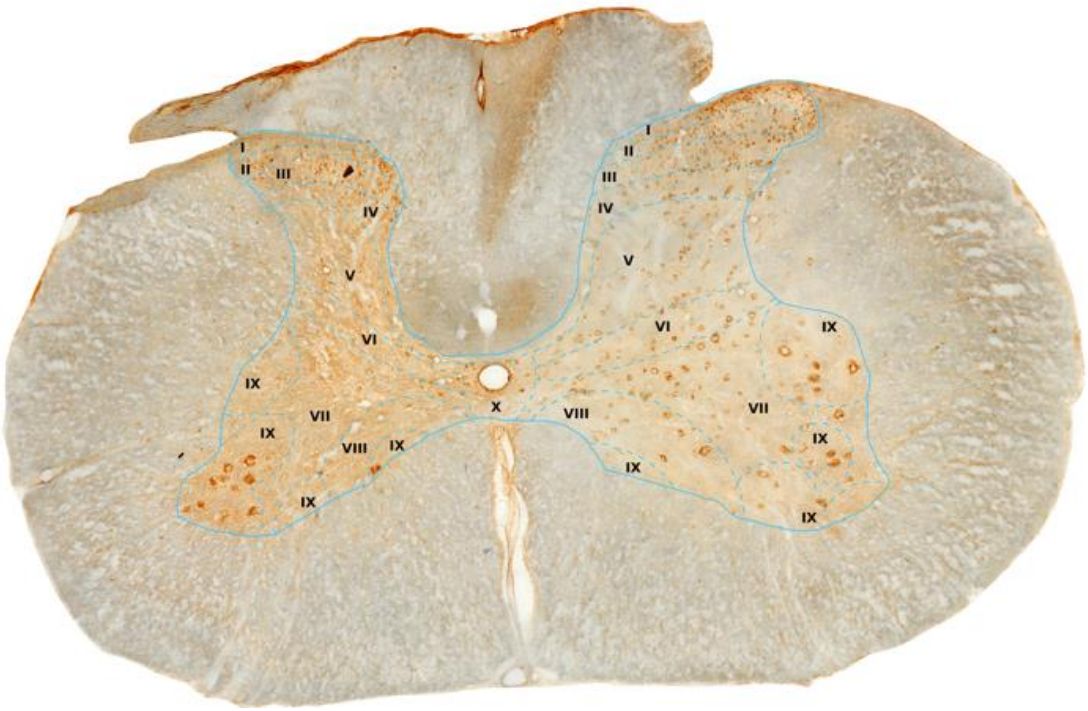

Figure 20. Neuronal death after kainic acid injections. Representative NeuN immunohistochemical image showing that kainic acid injection provokes neuronal death in the ipsilateral hemicord. Rexed laminae overlapped.

Last, we examined the effect of kainic acid in non-neuronal cells, as this compound has been shown to cause astrogliosis and inflammation when injected in the spinal cord (Nakae *et al.*, 2011). Immunostaining against GFAP revealed the characteristic upregulation of the protein and hypertrophy of reactive astrocytes in response to neurotrauma (Figures 21C, G) when compared to an intact spinal cord (Figures 21A, E). This astrogliosis was more prominent in the grey matter around (but not inside) the injected area, and diminished progressively as rostrocaudal distance from the epicentre augmented, inversely to grey matter damage. Similarly, extensive microglial activation and hypertrophy was observed at the kainic acid injection epicentre area with antibodies against Iba1 (Figures 21D, H). However, the location of the reactive microglia within the grey matter differed from that of astrocytes. In this case, Iba1$^+$ cells were present exactly inside the injected area, and not around it distributed along the rest of the grey matter. In contrast, active microglia was almost absent in the grey matter of an intact spinal cord (Figures 21B, F). This excitotoxic effect on non-neuronal cells indicates that the observed results with kainic acid should be interpreted in a wider context than only regarding neurons.

Forelimb R&G is compromised in animals receiving kainic acid injections at vC2-C3

Optimal motor performance requires not only the integrity of the neural circuitry that governs movement but also the proper function of the entire ensemble of executing organs and tissues, including the locomotor system and the skin. In our study, some rats injected with kainic acid in the cervical spinal cord displayed signs of paraesthesia, which generally corresponded to the dermatome pattern associated with the lesion in the injected segments (Figure 22A). Paraesthesia manifested as self-barbering, excessive licking, and even inflammation of the affected skin areas, particularly the digits (Figure 22B). Animals from vC2-C3 group were affected in the ear and nape area, whereas rats from vT1-T2 and vehicle groups did not show this side

(Figure on the next page)

Figure 21. Astrogliosis and inflammation after kainic acid injections. Representative immunohistochemical images showing that kainic acid injection provokes **(C,** zoomed in at **G)** astrogliosis (GFAP$^+$) and **(D,** zoomed in at **H)** microglial activation (Iba1$^+$) compared to intact spinal cords (**A** and **B**, magnified at **E** and **F**, respectively). Scale bars: 200 µm.

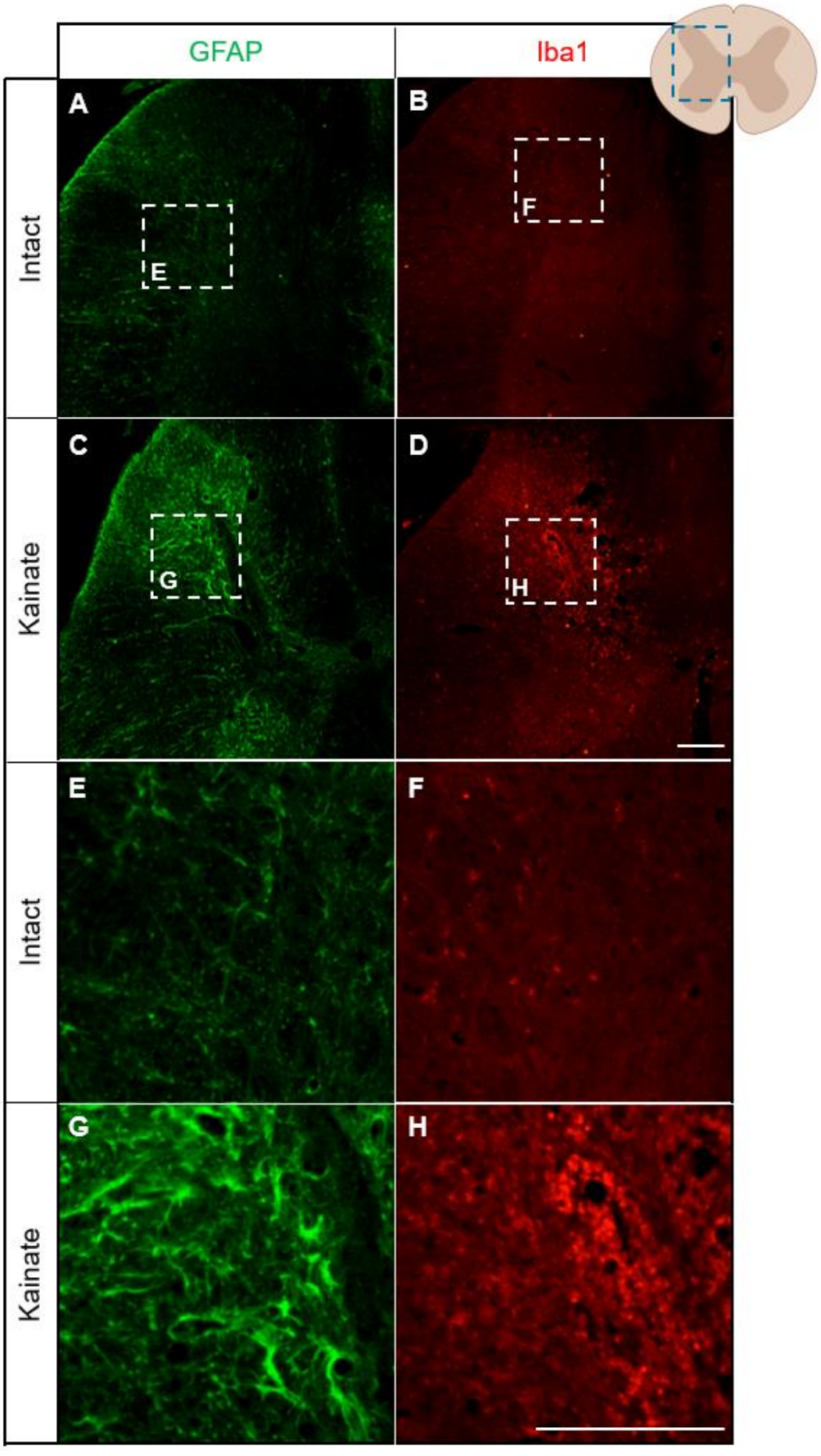
GFAP
Iba1
Intact
Kainate
Intact
Kainate
A
B
C
D
E
F
G
H
E
F
G
H

effect. Remarkably, vC4-C5 and vC6-C7 groups, which were injected precisely at the spinal segments involved in forelimb dermatomes, displayed oedema in fingers 2nd and 5th, respectively. Additionally, vC6-C7 animals were also affected at the back mid-thorax area. Such manifestations compromised the animals' performance in sensorimotor tasks, as their difficulties were not solely attributable to motor control deficits but also to peripheral soft tissue involvement. This underscores the importance of considering both neural and peripheral contributions when assessing sensorimotor function. Therefore, before assessing forelimb motor function, we used the adhesive removal test to investigate the sensory function of the forepaws (Schallert *et al.*, 1982; Bouet *et al.*, 2009) (Figure 22C). Only animals from vC2-C3 showed a significant change after the surgery ($F_{(2, 19)} = 6.79$, $p < 0.01$). In particular, the time to detect the adhesive sticker at 7DPI (1.67 ± 0.44 s, $p < 0.05$) and 14DPI (1 s, $p < 0.05$) was reduced (not increased) in comparison to basal performance (5.11 ± 1.10 s). Of note, the variability in most groups at basal level, which largely disappears at latter timepoints, could be reflecting the animals having learned the task. Overall, these results suggest that tactile sensory function was not diminished by the kainic acid injections. It should be noted, however, that while the adhesive removal test indicates preserved tactile sensitivity, the presence of paraesthesia may still interfere with certain processes, particularly in animals that injure their own peripheral tissues due to excessive licking.

Then, we proceeded by evaluating manual dexterity with the gold standard for it, the R&G test (Whishaw *et al.*, 1986; Metz & Whishaw, 2000). This time, there was a significant effect of group ($F_{(4, 29)} = 7.76$, $p < 0.001$), timepoint ($F_{(1.87, 51.32)} = 17.19$, $p < 0.001$) and interaction ($F_{(8, 55)} = 4.81$, $p < 0.001$) (Figure 23A). Based on post hoc comparisons, the performance of animals injected at vT1-T2 (p = ns), vC6-C7 (84.35 ± 2.87 % at baseline vs 55.31 ± 10.57 % at 7DPI and 62.71 ± 8.99 % at 14DPI, with p = 0.1049 and 0.1351, respectively) or with vehicle (p = ns) did not change before versus after the surgery. Regarding the vC4-C5 group, the success percentage diminished after the intervention (81.06 ± 2.62 % at baseline vs 52.06 ± 6.61 % at 7DPI and 53.03 ± 4.46 % at 14DPI, with $p < 0.05$ and $p < 0.01$, respectively). When we analysed the frequency of each of the six types of error (Figures 23B-G), we found significant differences in error types 1 ($F_{(4, 29)} = 3.16$, $p < 0.05$ for group; $F_{(1.03, 28.43)} = 2.34$, p = ns for timepoint; and $F_{(8, 55)} = 2.86$, $p < 0.01$ for interaction), 2 ($F_{(4, 84)} = 3.90$, $p < 0.01$ for group; $F_{(1.16, 48.66)} = 5.05$, $p < 0.05$ for timepoint; and $F_{(8, 84)} = 3.66$, $p < 0.01$ for interaction), 4 (F

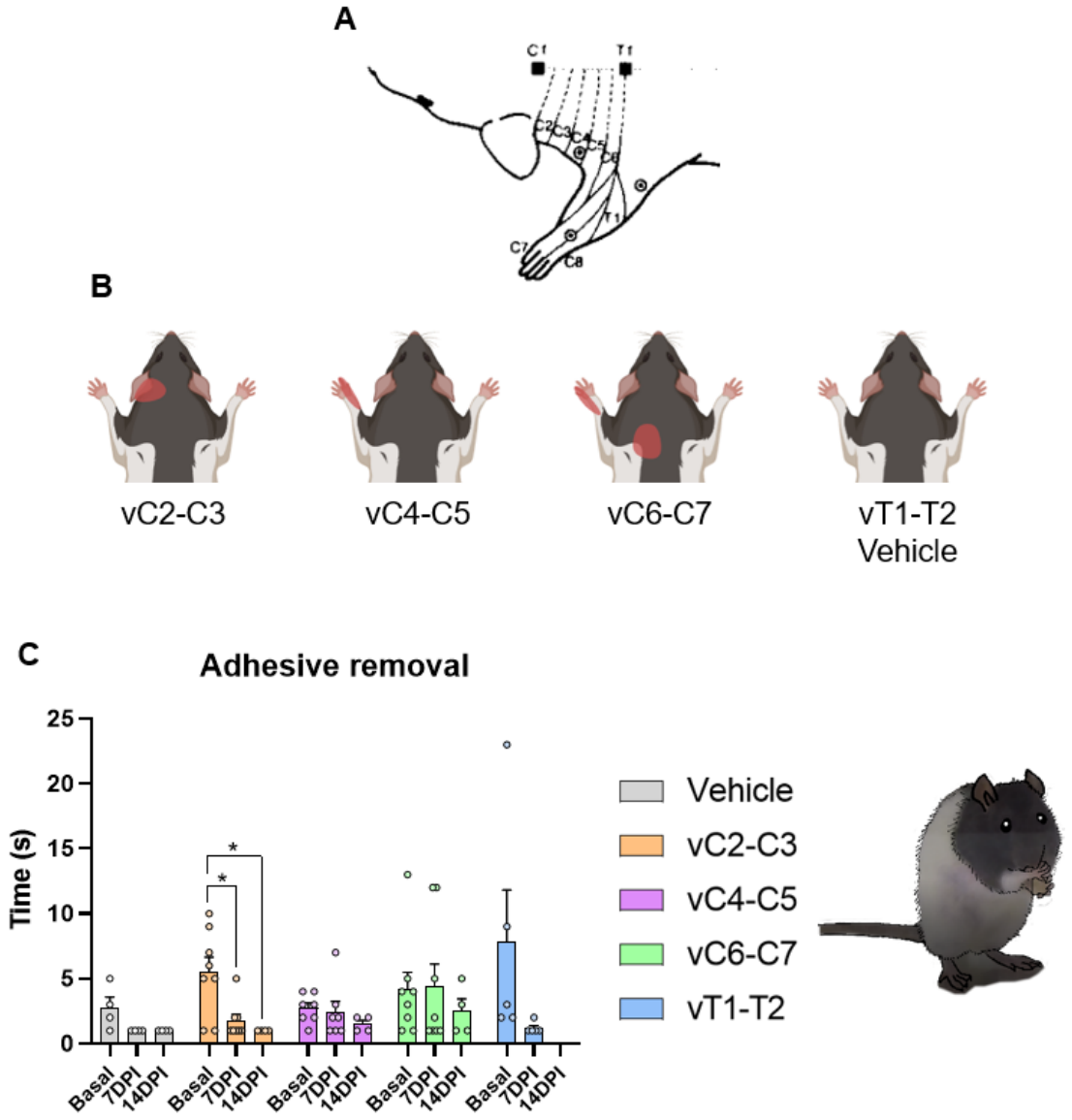

Figure 22. Sensory effect of kainic acid injections in 2 spinal segments. (A) Rat forelimb's dermatomes (Takahashi & Nakajima, 1996). **(B)** Schematic representation of the locations where animals from different experimental groups presented self-barbering evidence. **(C)** Time to contact an adhesive sticker on the palm of the forepaw. Groups: Vehicle (n = 4), vC2-C3 (n = 8), vC4-C5 (n = 7), vC6-C7 (n = 8), vT1-T2 (n = 5). * $p < 0.05$, as calculated by repeated measures one-way ANOVA followed by Tukey's multiple comparisons test. For group vT1-T2, calculated by paired t test. Data is shown as mean ± SEM.

$_{(4, 29)}$ = 1.56, p = ns for group; F $_{(1.50, 41.33)}$ = 1.43, p = ns for timepoint; and F $_{(8, 55)}$ = 2.42, p < 0.05 for interaction) and 5 (F $_{(4, 84)}$ = 1.70, p = ns for group; F $_{(1.22, 51.04)}$ = 11.46, p < 0.001 for timepoint; and F $_{(8, 84)}$ = 0.99, p = ns for interaction). For error type 1, multiple comparisons were not statistically significant (lowest p = 0.1380, comparing basal

versus 7DPI frequencies of vC2-C3 group) (Figure 23B). Regarding error type 2, there was a decrease in its frequency from 7DPI to 14DPI in vC2-C3 group (35.23 ± 11.28 % vs 2.14 ± 1.44 %, respectively, $p < 0.05$), possibly reflecting some level of plasticity or a compensatory mechanism (Figure 23C). Post hoc comparisons revealed changes in vC4-C5 group, specifically a decrease in error type 4 frequency at 14DPI (0.66 ± 0.66 % vs 5.72 ± 1.59 % at baseline, $p < 0.01$) and an increase of the frequency percentage of error type 5 at 14DPI (31.13 ± 6.64 %) compared to basal (7.30 ± 1.84 %, $p < 0.05$) and 7DPI (10.59 ± 2.61 %, $p < 0.05$) values (Figures 23E-F). Last, there was a significant increase of the frequency of error type 5 in the vehicle between the basal and the 14DPI percentages (5.49 ± 1.36 % vs 12.69 ± 2.26 %, respectively, $p < 0.05$) (Figure 23F), but we consider it a result of the inherent task variability. In conclusion, the increase in group vC4-C5 of error type 5, where the animal reaches the pellet correctly but is not able to grasp it properly by flexion of the fingers, accounts for the reduction in success percentage observed. We attribute it to biomechanical deficits due to the oedema in the 2nd finger, instead of a direct effect on the spinal neuronal network controlling R&G. Interestingly, animals from vC2-C3 group also showed R&G movement impairment and, even though they did not present self-barbering evidences on the fingers (as vC4-C5 and vC6-C7 groups), the reduction of R&G success percentage from basal (79.01 ± 2.06 %) to 7DPI (19.77 ± 6.98 %, $p < 0.001$) and 14DPI (37.56 ± 14.70 %, $p < 0.05$) levels was maximal (Figure 23A). Moreover, this reduction in success percentage was a consequence of an increase in the frequency of error type 1 mainly (0.16 ± 0.16 % at baseline vs 29.79 ± 13.80 % at 7DPI and 33.58 ± 21.00 % at 14DPI) (Figure 23B), where the animal's paw is not able to cross the window during protraction to reach for the pellet, even though it did not reach statistical significance. Some of these rats could not successfully retrieve one single pellet after the kainic acid injection.

In summary, R&G was impaired in groups vC2-C3 (~ sC3-C4) and vC4-C5 (~ sC5-C6), and there was a non-statistically significant tendency for vC6-C7 (~ sC7-C8) group. These results could be explained by finger oedema that leads to unsuccessful grasping for groups vC4-C5 and vC6-C7, and by the loss of the ability to lift, protract and target the forepaw in vC2-C3 group. However, it cannot be ruled out that the deficits observed in the oedema groups may also have a neural basis.

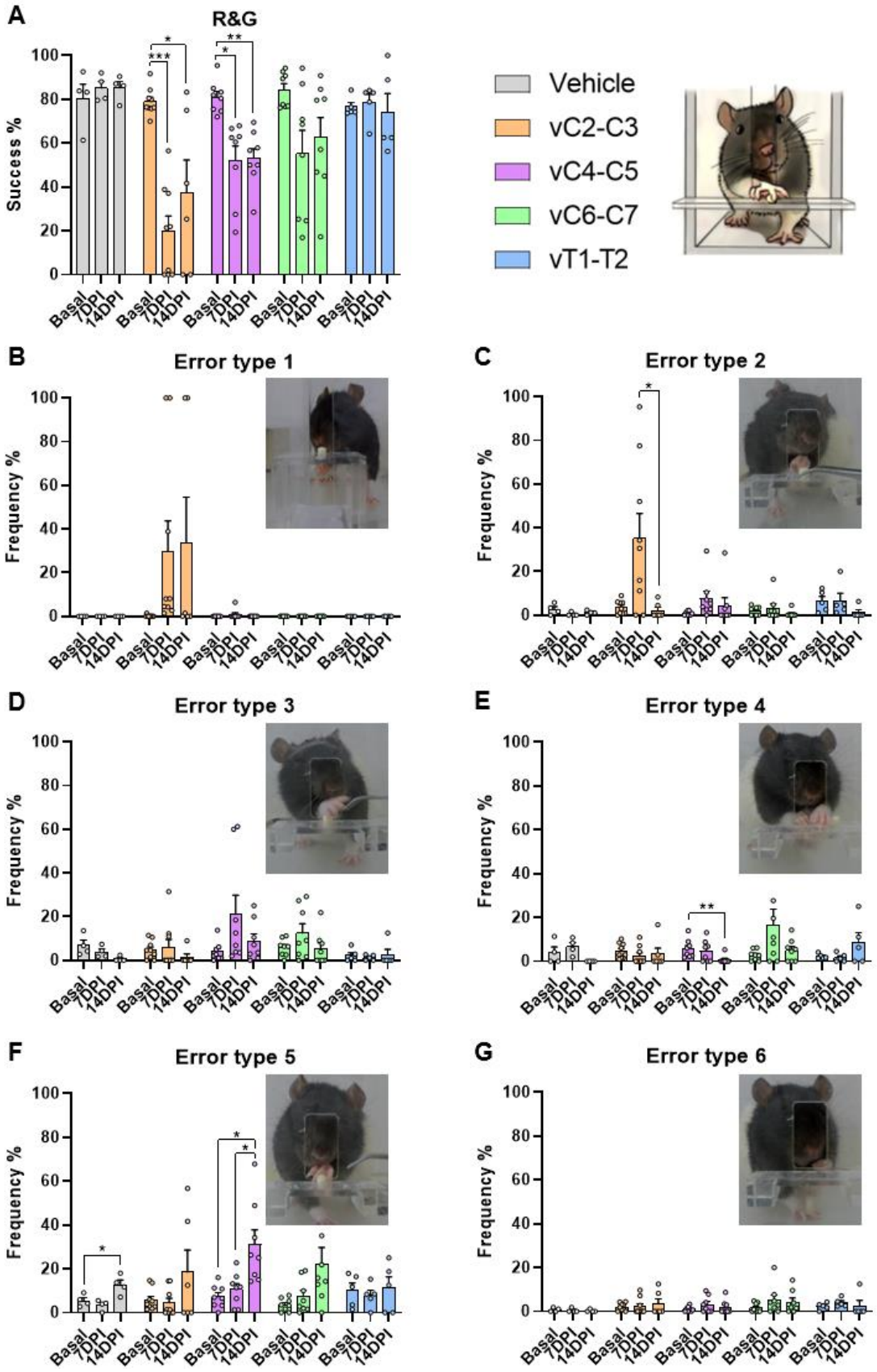

Figure 23. R&G assessment after kainic acid/vehicle injection in 2 spinal segments. (A) R&G success percentage and **(B-G)** frequency of error types 1-6. Groups: Vehicle (n = 4), vC2-C3 (n = 9), vC4-C5 (n = 8), vC6-C7 (n = 8), vT1-T2 (n = 5). * $p < 0.05$, ** $p < 0.01$, *** $p < 0.001$;

by mixed-effects analysis model using the restricted maximum likelihood method with timepoint as within-subject factor and group as between-subject factor, followed by Tukey's multiple comparison tests when significant differences were found. Data presented as mean ± SEM.

Further, we analysed other complementary forelimb skilled function behavioural tests to dig deeper into the effect of this excitotoxic lesion. These tests require movements that recruit the same muscles as R&G and need the musculoskeletal system and the motoneurons that innervate those muscles to be functional, so they would be useful to better delimitate the cause/s of the observed deficits. We used the staircase R&G test (Figure 24A); the food manipulation test (Figure 24B); the grid R&G test, where rats reach and grasp pellets from the bottom of a grid, thus in a setting that the movement does not require going against gravity or forepaw protraction (Figure 24C); skilled locomotion, where the animals walk in a horizontal ladder with irregularly spaced rungs (Soblosky *et al.*, 1997; Metz & Whishaw, 2002), so the animals must quickly calculate the distance to the next rung and target their forelimb, to reach and grasp it with the paw (Figure 24D); and overground locomotion (Figures 24E-G). As expected, vehicle animals did not present a significant change in any of the tests: nor in staircase R&G ($F_{(1.03, 3.09)} = 2.30$, p = ns), food manipulation, grid R&G, or locomotion stride length ($F_{(1.14, 3.41)} = 0.22$, p = ns), base of support ($F_{(1.68, 5.04)} = 0.69$, p = ns) and forepaw width ($F_{(1.42, 4.27)} = 0.27$, p = ns). Likewise, neither the vT1-T2 group was affected in the staircase R&G ($t_{(4)} = 0.30$, p = ns), food manipulation, horizontal ladder ($t_{(4)} = 0.04$, p = ns) or locomotion stride length ($t_{(4)} = 1.96$, p = ns), base of support ($t_{(4)} = 2.46$, p = ns) or forepaw width ($t_{(4)} = 1.5$, p = ns). This indicates a preserved forelimb function in those groups. Rats from vC6-C7 group presented a reduction of forepaw width ($F_{(1.73, 9.52)} = 9.05$, $p < 0.01$), significant between basal and 7DPI values (17.88 ± 0.13 vs 13.63 ± 1.10 mm, respectively, $p < 0.05$) in particular (Figure 24G). This result is to be expected due to the 5th finger oedema that those animals suffered. However, as with R&G, these animals did not show significant changes in staircase R&G ($F_{(2, 18)} = 2.39$, p = ns), grid R&G, food manipulation, horizontal ladder ($t_{(2)} = 0.10$, p = ns), locomotor stride length ($F_{(1.51, 13.63)} = 3.73$, p = ns) or locomotor base of support ($F_{(1.75, 15.78)} = 0.33$, p = ns), even though there was a tendency of a decrease in some of the tests (Figures 24A-F). Regarding vC4-C5 group, we also had the presumed affected forepaw width ($F_{(1.04, 5.19)} = 9.92$, $p < 0.05$), resulting from 2nd finger oedema in this case, that post hoc comparisons revealed different between basal and

7DPI measurements (17.5 ± 0.19 vs 15.25 ± 0.65 mm, respectively, $p < 0.05$) (Figure 24G). Apart from that parameter, the locomotor function remained unaffected in terms of stride length ($F_{(1.63, 8.17)} = 0.10$, p = ns), base of support ($F_{(1.67, 8.35)} = 1.94$, p = ns), and successful paw placement in the horizontal ladder ($t_{(3)} = 0.01$, p = ns) (Figures 24D-F). Nonetheless, R&G from the staircase was impaired ($F_{(2, 15)} = 20.28$, $p < 0.001$) when comparing basal performance to 7DPI (61.75 ± 6.44 %, $p < 0.001$) and 14DPI (48.50 ± 10.63 %, $p < 0.001$) (Figure 24A). Some animals were able to reach, but not successfully grasp, pellets from the bottom of a grid after the injury (Figure 24C), although the score did not reach a significant difference ($H_{(2)} = 5.46$, p = 0.0725). The last behavioural test analysed, food manipulation, also revealed a significant change ($H_{(2)} = 12.78$, $p < 0.001$), with a decrease in the score both at 7DPI ($p < 0.01$) and 14DPI ($p < 0.05$) (Figure 24B). This difference IBB score is caused by the use of a pincer or fist grip type, the non-adaptable forepaw position to the cereal shape and the loss of the predominant volar contact with the doughnut, all of which could potentially be explained by the finger oedema. Finally, food manipulation in vC2-C3 group, which is a substantially different behaviour compared to R&G, was not affected ($H_{(2)} = 3.38$, p = ns) (Figure 24B). The success percentage in the staircase test showed a tendency of a mild decrease (Figure 24A), even though statistical significance was not achieved ($F_{(2, 17)} = 3.24$, p = 0.0641). However, a clear impairment was observed in the grid R&G task ($H_{(2)} = 9$, $p < 0.05$), where the score fell from 1 at basal to 0 at 7DPI in all tested animals ($p < 0.05$), meaning that none of them could even reach any pellet during the assessment (Figure 24C). The significant decrease remained at 14DPI ($p < 0.05$). Regarding locomotion, their ability to walk on the horizontal ladder was impaired after the surgical intervention (45.38 ± 3.63 vs 24.88 ± 4.19 % of successful paw placement; $t_{(4)} = 3.20$, $p < 0.05$) (Figure 24D). This paw misplacement could indicate a proximal forelimb control impairment to target the next rung. Concomitantly, stride length during regular overground locomotion was also significantly reduced in this group ($F_{(1.82, 17.26)} = 10.35$, $p < 0.01$), specifically between basal and 7DPI timepoints (173.63 ± 3.88 vs 148.13 ± 6.23 mm, respectively, $p < 0.05$) (Figure 24E), whereas base of support ($F_{(1.99, 10.95)} = 1.56$, p = ns) and forepaw width ($F_{(0.75, 4.15)} = 1.92$, p = ns) remained unaffected (Figures 24F-G).

In conclusion, injection of kainic acid in two consecutive cervical spinal cord segments was successful in revealing motor disfunction and therefore its requirement for forelimb skilled function. While animals injected with kainic acid at vT1-T2 (~ T1-

T3) or at vC2-C3 (~ sC3-C4) with vehicle did not suffer any detectable impairment in the multiple assessments executed, the same was not true for the remaining groups. Animals from groups vC4-C5 (~ sC5-C6) and vC6-C7 (~ sC7-C8) presented evidence of paraesthesia that affected the fingers. This directly correlates with the reduction in pawprint width in both groups. The fact that the resulting oedema occurred in the 2nd finger for group vC4-C5 and in the 5th finger for group vC6-C7, and the hierarchical superiority of the former versus the latter finger in forepaw function, could explain why the observed impairments in the grasping phase of R&G movement and the fine manipulation of the cereal achieved statistical significance in group vC4-C5 but not in vC6-C7 (although the same tendency was present). However, the biggest deficits belonged to the vC2-C3 group, which did not suffer the previously mentioned finger paraesthesia. These animals failed in targeting the forepaw forward during the reaching phase of R&G, and also during skilled and unskilled locomotion. Meanwhile, fine food manipulation and other locomotor parameters such as base of support and forepaw width were not affected. Taken together, these results suggested a key role for spinal segments vC2-C3 (~ sC3-C4) in the control of R&G movement, particularly in the reaching phase. Thus, we focused on those segments in our following experiment.

(Figure on the next page)

Figure 24. Forelimb skilled function assessment after kainic acid/vehicle injection in 2 spinal segments. Forelimb function evaluated before vs after 7 and 14 DPI in **(A)** ability to reach and grasp pellets from different steps of a staircase and **(B)** from the bottom of a grid, and **(C)** food manipulation based on the IBB scale. Forelimb locomotor function was assessed in **(D)** successful paw placement on a horizontal ladder, and **(E)** stride length, **(F)** base of support and **(G)** forepaw width during locomotion. Groups: Vehicle (n = 4), vC2-C3 (n = 4-9), vC4-C5 (n = 4-8), vC6-C7 (n = 3-8), vT1-T2 (n = 5). * $p < 0.05$, ** $p < 0.001$. *** $p < 0.001$; as calculated **(A, D-G)** by repeated measures one-way ANOVA followed by Tukey's multiple comparisons test when three timepoints were compared or paired t test when there were two timepoints of Gaussian data; or **(B-C)** by Kruskal-Wallis test followed by Dunn's multiple comparisons test when comparing three timepoints of non-Gaussian data, and Wilcoxon test when comparing two paired groups. Data is shown as median ± interquartile range in **(B-C)**, and as mean ± SEM elsewhere.

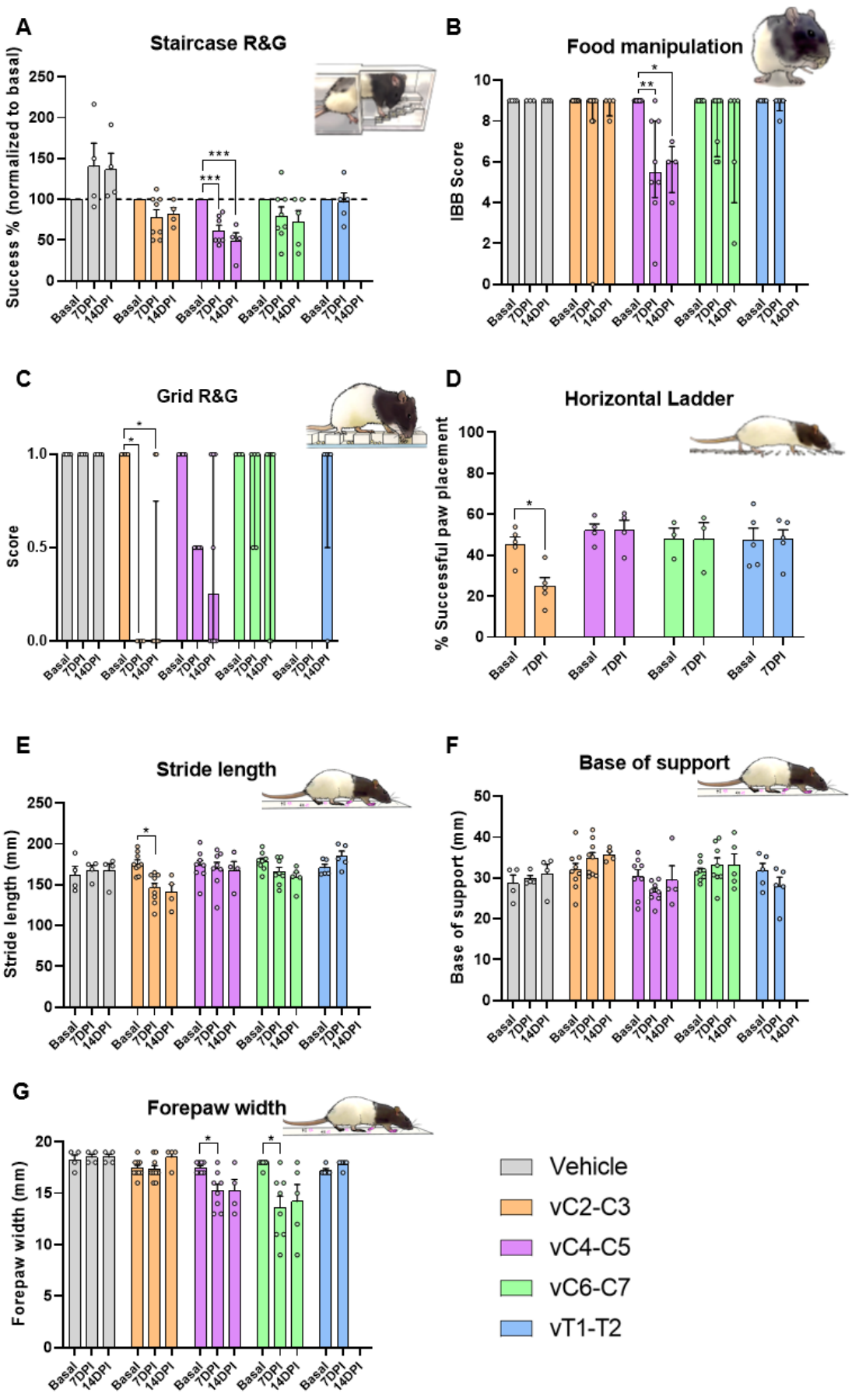
A
Staircase R&G
Success % (normalized to basal)
250
200
150
100
50
0
***
***
B
Food manipulation
IBB Score
10
8
6
4
2
0
*
**
C
Grid R&G
Score
1.0
0.5
0.0
*
*
D
Horizontal Ladder
% Successful paw placement
100
80
60
40
20
0
*
E
Stride length
Stride length (mm)
250
200
150
100
50
0
*
F
Base of support
Base of support (mm)
50
40
30
20
10
0
G
Forepaw width
Forepaw width (mm)
20
15
10
5
0
*
*
Basal
7DPI
14DPI
Vehicle
vC2-C3
vC4-C5
vC6-C7
vT1-T2

Functional and morphological impact of excitotoxic lesions in vC2 and vC3 cervical spinal segments

Forelimb function is impaired in animals injected with kainic acid at vC2 segment only

Once we had identified a candidate region spanning vC2-C3 (~ sC3-C4) as potentially crucial for the proper execution of R&G, we sought to determine whether the deficits observed were due to damage in segments located in both vC2 (~ sC3) and vC3 (~ sC4) or if injuring only the vC2 region would be sufficient to induce impairment. To address this, we employed the same excitotoxic approach, but this time injected kainic acid or vehicle into only one spinal segment (vC2) in order to narrow down the location of the hypothetical R&G network. For comparison, data from animals that had previously received injections solely in vC3 (which were shown to produce no significant effects) were also included in these graphs.

We began our assessment with R&G success percentage and frequency of error types analysis (Figure 25). Animals from the vehicle group did not suffer a detriment in R&G performance ($F_{(1, 1)} = 0.43$, p = ns) (Figure 25A), and there were no significant differences in error types frequency either (Figures 25B-G). Previously, we had already shown that vC3 group preserved the R&G capacity intact (Figures 16, 25). However, the results for animals injected at vC2 only were strikingly different. There was a significant reduction of success percentage ($F_{(1, 5)} = 557.9$, $p < 0.001$), at both 7DPI (1.79 ± 1.79 %, $p < 0.001$) and (0 %, $p < 0.001$) 14DPI compared to baseline (82.04 ± 4.23 %) (Figure 25A). As with vC2-C3 group, the error that increased the most after injury was error type 1 (from 0 % at basal to 18.75 ± 10.03 % at 7DPI) (Figure 25B), even though, like in vC2-C3 analysis, it did not reach statistical significance ($F_{(0.97, 6.31)} = 3.44$, p = 0.1112). Significant differences were observed for error type 3 ($F_{(1.83, 11.91)} = 7.02$, $p < 0.05$), consisting of a forepaw reach out of target of the position of the pellet (Figure 25D), and the frequency increased from basal to 7DPI (0.94 ± 0.30 vs 7.5 ± 1.88 %, respectively, $p < 0.05$). This result correlates with vC2-C3 animals that presented a deficit in the earlier (reaching) phase of the movement.

Fast forward, we evaluated the performance of these animals in other behavioural tests of skilled and unskilled forelimb function. We had already shown that vC3 group did not suffer a significant impairment in any of the assessments (Figures 17, 26). The

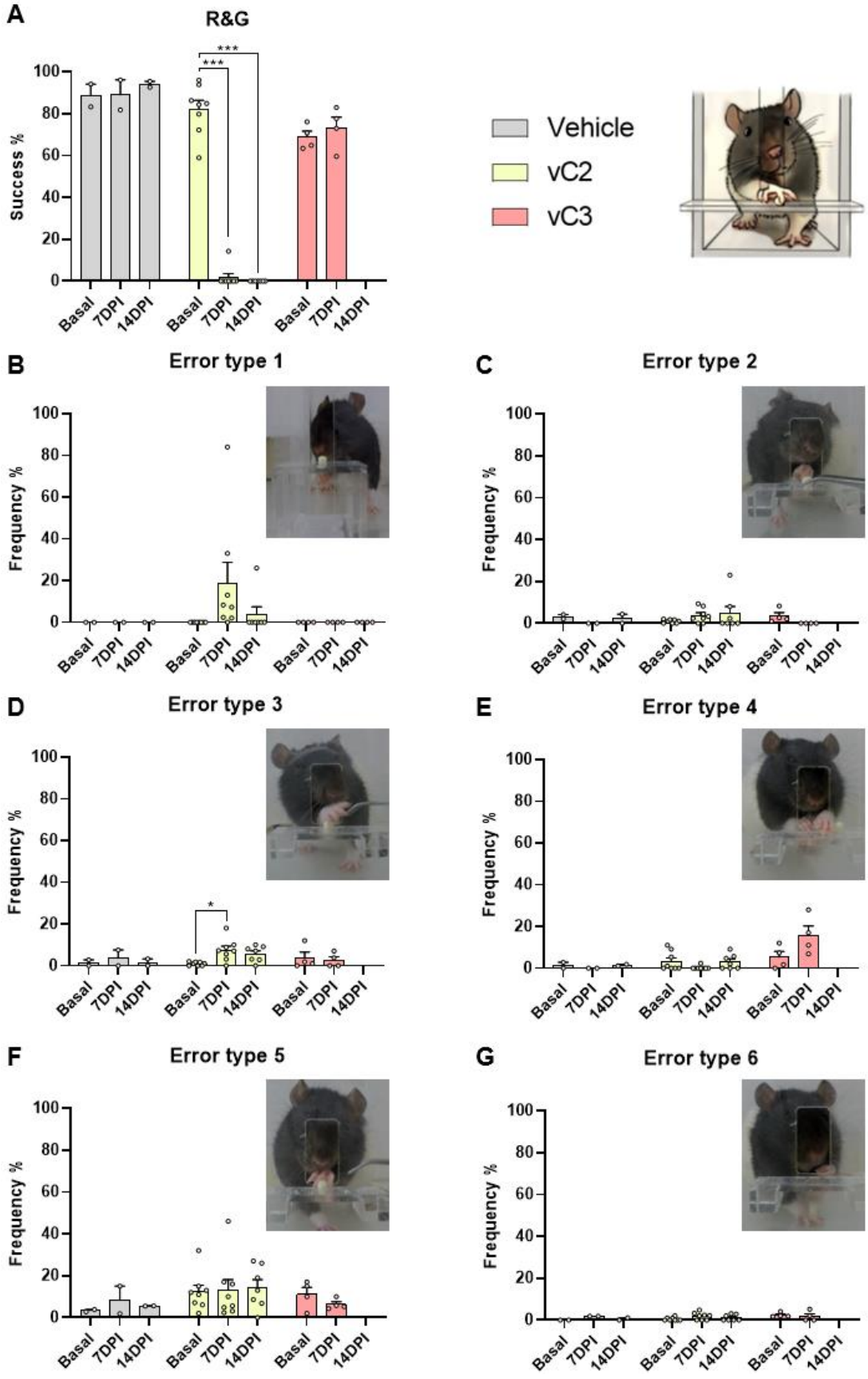

Figure 25. Forelimb R&G assessment after kainic acid/vehicle injection in vC2 or vC3 spinal segments. R&G performance was evaluated before vs after 7 and 14 DPI in **(A)** R&G success percentage and the frequency of error types **(B)** 1, **(C)** 2, **(D)** 3, **(E)** 4, **(F)** 5 and **(G)**

6. Groups: Vehicle (n = 2), vC2 (n = 8), vC3 (n = 4). * p < 0.05, *** p < 0.001; as calculated by repeated measures one-way ANOVA followed by Tukey's multiple comparisons test. For vC3 group, analysis executed by paired t test. Data presented as mean ± SEM.

same was the case for rats injected with vehicle at vC2, where no change between timepoints was appreciated for staircase R&G ($F_{(1,1)} = 1.80$, p = ns) (Figure 26A), food manipulation (Figure 26B), grid R&G (Figure 26C), adhesive removal ($F_{(1,1)} = 0.70$, p = ns) (Figure 26D), locomotion stride length ($F_{(1,1)} = 0.17$, p = ns) (Figure 26E), base of support ($F_{(1,1)} = 2.98$, p = ns) (Figure 26F) or forepaw width ($F_{(1,1)} = 0.33$, p = ns) (Figure 26G). Conversely, vC2 group presented a statistically significant R&G impairment in the staircase ($F_{(1.29, 7.73)} = 20.68$, p < 0.01) (Figure 26A) and grid ($Q_{(2)} = 15.44$, p < 0.001) (Figure 26C) tests, both at 7DPI (staircase 55.84 ± 11.78 % vs basal, p < 0.05; grid p < 0.01) and 14DPI (staircase 45.54 ± 8.17 % vs basal, p < 0.01; grid p < 0.05). Notably, they were not able to reach any pellet from the bottom of the grid at 7DPI, and only one animal was capable of reaching (but not grasping) at least one pellet at 14DPI. In other non-reaching forelimb tasks, i.e. food manipulation ($Q_{(2)} = 2$, p = ns) (Figure 26B) and adhesive removal ($F_{(1.07, 7.47)} = 0.46$, p = ns) (Figure 26D), no differences were observed before and after the surgery. Finally, stride length during locomotion was affected ($F_{(1.52, 9.14)} = 10.27$, p < 0.01) (Figure 26E), at both 7DPI (161.43 ± 4.47 mm, p < 0.05) and 14DPI (156.71 ± 4.02 mm, p < 0.05) compared to baseline (174 ± 2.68 mm). Base of support ($F_{(1.90, 11.41)} = 3.21$, p = 0.0801) (Figure 26F) and forepaw width ($F_{(1.75, 10.47)} = 0.55$, p = ns) (Figure 26G) values remained intact.

These findings indicate that the performance of the vC2 (~ sC3) group closely resembled that of the vC2-C3 (~ sC3-C4) group, suggesting that vC2 (~ sC3), rather than vC3 (~ sC4), may be the critical segment involved in controlling R&G.

(Figure on the next page)

Figure 26. Forelimb function assessment after kainic acid/vehicle injection in vC2 and vC3. Forelimb function evaluated before vs after 7 and 14 DPI in **(A)** ability to reach and grasp pellets from different steps of a staircase or **(C)** from the bottom of a grid, **(B)** food manipulation based on the IBB scale, **(D)** the time to contact an adhesive sticker on the palm of the forepaw, and **(E)** stride length, **(F)** base of support and **(G)** forepaw width during locomotion. Groups: Vehicle (n = 2), vC2 (n = 7-8), vC3 (n = 4). * p < 0.05, ** p < 0.01; as calculated by **(A, D, E, F, G)** repeated measures one-way ANOVA followed by Tukey's multiple comparisons test when three timepoints were compared and paired t test when there were only two timepoints, or **(B-C)** by Friedman test followed by Dunn's multiple comparisons test. No statistical test was performed for the cases were all the values in all the timepoints were the same. Data presented as median ± interquartile range in **(B-C)**, and as mean ± SEM elsewhere.

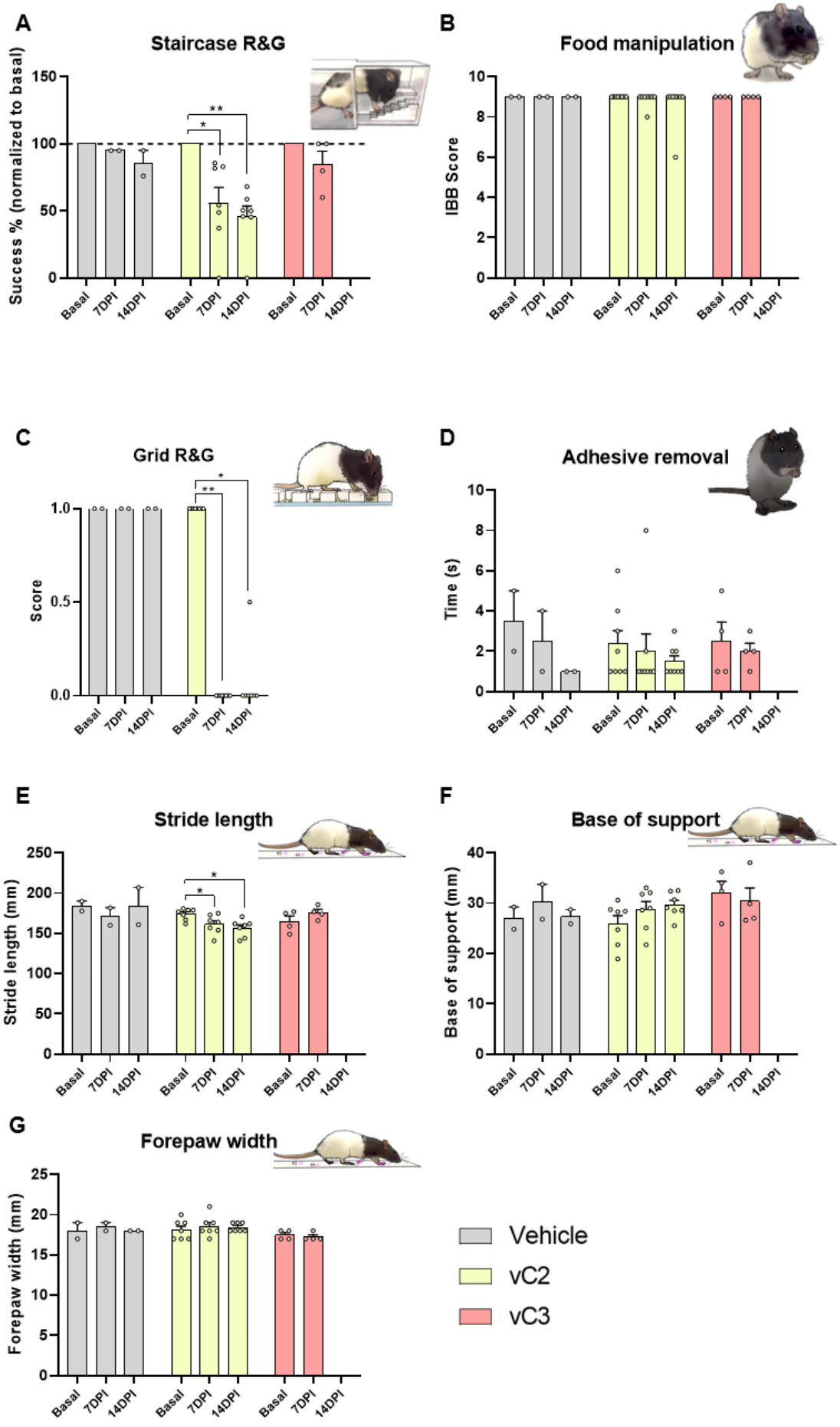
A
Staircase R&G
Success % (normalized to basal)
150
100
50
0
**
*
Basal
7DPI
14DPI
B
Food manipulation
IBB Score
10
8
6
4
2
0
C
Grid R&G
Score
1.0
0.5
0.0
D
Adhesive removal
Time (s)
E
Stride length
Stride length (mm)
250
200
150
100
50
F
Base of support
Base of support (mm)
40
30
20
G
Forepaw width
Forepaw width (mm)
25
20
15
10
5
Vehicle
vC2
vC3

Grey matter damage is accompanied by a reduction in the number of motoneurons upon kainic acid injection

The preservation of motoneurons was investigated based on transverse spinal cord sections stained with Cresyl violet. Motoneurons were identified based on location, size and morphology (Ferrucci *et al.*, 2018). By observation on the microscope, it was clear that, at the level of injection, there was a concomitant reduction of grey matter area and of the number of motoneurons (Figure 27A). In the ipsilateral hemicord (Figure 27B), there was a statistically significant effect of group ($F_{(2, 11)} = 4.41$, $p < 0.05$) and interaction ($F_{(72, 372)} = 4.83$, $p < 0.001$), but not for distance ($F_{(3.45, 35.59)} = 1.90$, p = ns). Post hoc comparisons versus the vehicle group revealed a significant decrease in motoneuron preservation percentage for vC2 (lowest of 39 ± 11.73 vs 102 ± 1 %, $p < 0.01$) and vC3 (lowest of 28.5 ± 7.86 vs 114 ± 11 %, $p < 0.05$) groups, especially at the injection epicentre. The shape and extension of the curve resembled that of the grey matter, with approximately 5-6 mm affected. In the contralateral side (Figure 27C), a significant interaction effect was present ($F_{(72, 373)} = 1.37$, $p < 0.05$), without distance ($F_{(5.21, 53.98)} = 0.55$, p = ns) or group ($F_{(2, 11)} = 2.13$, p = ns) individual effects. With multiple comparisons, we found only one coordinate different for vC2 (106.75 ± 7.10 vs 84 ± 3 %, $p < 0.05$), and a few for vC3 (highest of 135 ± 10.93 vs 82 ± 3 %, $p < 0.05$), but that were always a significant increase (and not decrease) in the motoneuron percentage with respect to vehicles. These differences in the contralateral hemicord were probably due to the low number of vehicle animals and the relatively high variability in motoneuron counts. In any case, these results show a parallel effect of kainic acid on grey matter area and on motoneuron preservation, confined to the ipsilateral side in our experiments.

(Figure on the next page)

Figure 27. Motoneuron preservation after kainic acid/vehicle injections in vC2 or vC3 spinal cord segments. (A) Representative Cresyl violet-stained ventral horns showing the excitotoxic effect of kainic acid on motoneurons. Motoneuron preservation at the injection epicentre was quantified in the hemicords corresponding to the **(B)** ipsilateral or **(C)** contralateral side. Groups: Vehicle (n = 2), vC2 (n = 8), vC3 (n = 4). * $p < 0.05$, ** $p < 0.01$, *** $p < 0.001$; as calculated by mixed-effects analysis model using the restricted maximum likelihood method, followed by Tukey's multiple comparisons test against the vehicle group. Data is presented as mean ± SEM. Scale bar: 200 µm. MN: motoneuron.

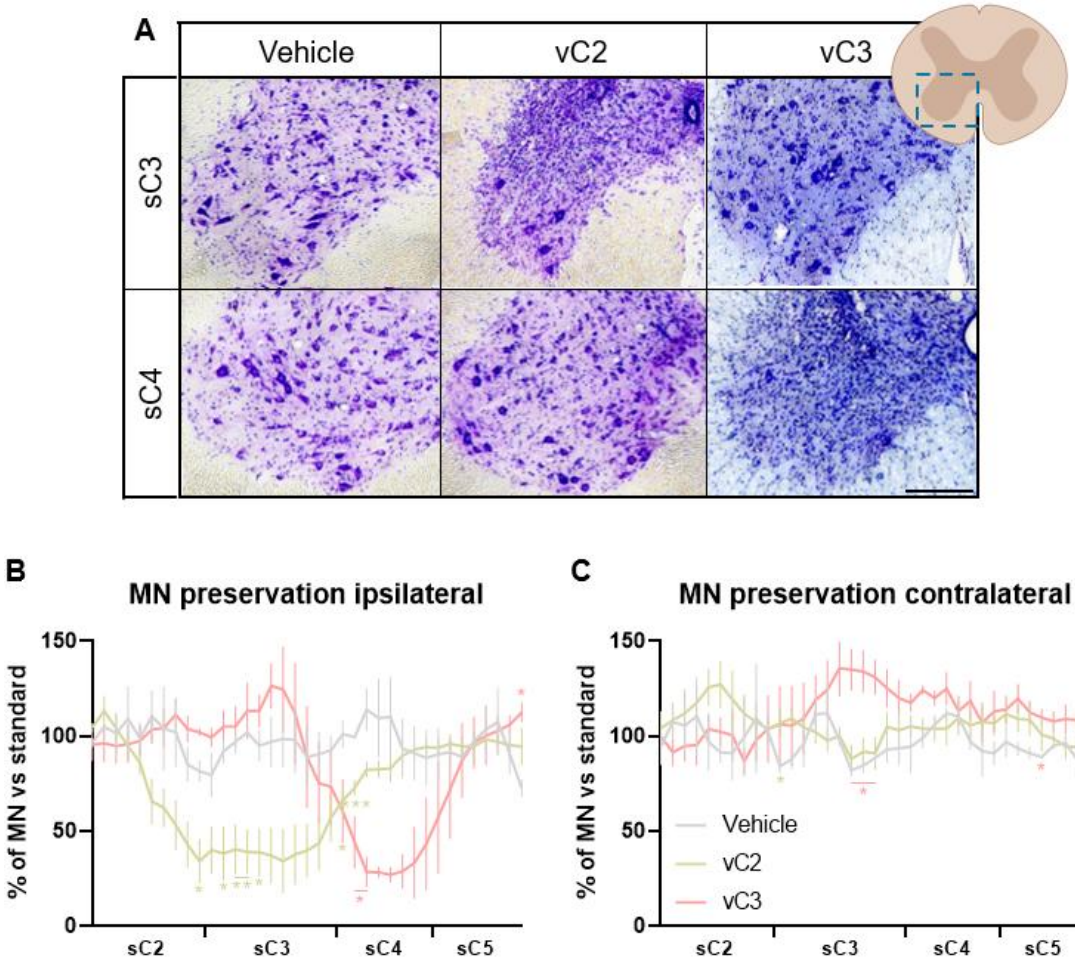

The goal of our study was to investigate the spinal cord neuronal networks involved in R&G control. These hypothetical networks must be upstream of the motoneurons, which are the final effectors of the movements through muscle contraction activation. The motoneurons responsible for the contraction of forelimb muscles are well characterised (McKenna *et al.*, 2000) and they were not the focus of this thesis. That is why we injected kainic acid at the intermediate grey matter, and observed the biggest neuronal death at intermediate Rexed laminae with NeuN immunostaining. Nonetheless, considering the reduction in the number of motoneurons observed, one could rightfully suggest that our results are not due to the presence of a neuronal network necessary for the control of reaching at grasping at vC2 (~ sC3), but merely because there are not enough final effectors (motoneurons) to execute the movement. This remaining question led us to pursue one more experiment.

Sectioning of spinal roots sC3 and sC3-C4

Rats preserve their forelimb function after sC3 and sC3-C4 dorsal and ventral root sectioning

To rule out the possibility that the effects observed in the kainic acid vC2 (~ sC3) and vC2-C3 (~ sC3-C4) groups were caused by excitotoxic damage to motoneurons rather than disruption of interneuronal networks controlling R&G, we conducted an additional experiment. In this experiment, we sectioned both the dorsal and ventral roots of spinal segments sC3 or sC3-C4, thereby eliminating all direct sensory afferents and motor efferents from these segments while preserving the interneuronal networks. Thus, if the animals were still able to execute reaching, grasping, and other skilled forelimb movements properly, it would indicate that the deficits observed with kainic acid injections are not due to the loss of motoneurons and sensory neurons but rather result from effects on the local interneurons, thereby confirming our hypothesis. This experimental design followed the same protocol as previous experiments, with the only difference being the surgical intervention: instead of injecting kainic acid or vehicle into the spinal cord, we performed root sectioning on the designated segments.

First, for R&G success percentage, a significant timepoint effect ($F_{(1.24, 6.21)} = 6.44$, $p < 0.05$) was observed, but not for group ($F_{(1, 5)} = 3.61$, p = ns) or interaction ($F_{(2, 10)} = 1.19$, p = ns) (Figure 28A). Nevertheless, none of the multiple comparisons achieved statistical significance (lowest $p = 0.0806$ when comparing basal versus 14DPI values in group sC3). Moreover, the mean success percentage was, if anything, higher at 7DPI (83.01 ± 3.86 % for sC3 and 64.33 ± 16.80 % for sC3-C4) and 14DPI (86.67 ± 2.88 % for sC3 and 59.33 ± 14.11 % for sC3-C4) compared to baseline levels (76.99 ± 1.95 % for sC3 and 50 ± 15.01 % for sC3-C4). Of note, no differences in the frequency of the other error types were present (Figures 28B-G), except for error type 5 (Figure 28F), corresponding to an incorrect grasping of the pellet by digit flexion ($F_{(1, 5)} = 4.29$, p = ns for group effect; $F_{(1.64, 8.21)} = 23.93$, $p < 0.001$ for timepoint effect; $F_{(2, 10)} = 3.99$, p = ns for interaction effect). Post hoc analysis showed a decrease in error type 5 frequency at 7DPI (6.45 ± 2.33 vs 14.4 ± 2.69 %, $p < 0.05$). In the case of sC3-C4 group, there was an increase in the frequency of that error from 7DPI to 14DPI (21.33 ± 9.26 vs 29.67 ± 9.82 %, respectively, $p < 0.05$). In general, these changes in error type 5 frequency could

correspond to the oscillations in success percentages and to the inherent variability of the task. Thus, no R&G deficits were observed in any of the groups.

Interestingly, sC3 and sC3-C4 animals did not display a statistically significant performance detriment in neither staircase R&G ($F_{(1, 5)} = 0.01$, p = ns for group; $F_{(1.59, 7.96)} = 3.22$, p = ns for timepoint; and $F_{(2, 10)} = 1.83$, p = ns for interaction effects) (Figure 29A), food manipulation (Figure 29B), grid R&G (Figure 29C), adhesive removal ($F_{(1, 5)} = 2.14$, p = ns for group; $F_{(1.44, 7.18)} = 1.37$, p = ns for timepoint; and $F_{(2, 10)} = 1.37$, p = ns for interaction effects) (Figure 29D), locomotion base of support ($F_{(1, 5)} = 1.47$, p = ns for group; $F_{(1.13, 5.66)} = 1.64$, p = ns for timepoint; and $F_{(2, 10)} = 2.64$, p = ns for interaction effects) (Figure 29F), or locomotion forepaw width ($F_{(1, 5)} = 1.15$, p = ns for group; $F_{(1.30, 6.50)} = 0.57$, p = ns for timepoint; and $F_{(2, 10)} = 1.23$, p = ns for interaction effects) (Figure 29G). Significant timepoint ($F_{(1.20, 5.39)} = 7.85$, $p < 0.05$) and group ($F_{(1, 5)} = 7.02$, $p < 0.05$) effects, but no significant interaction ($F_{(2, 9)} = 0.64$, p = ns), were observed for locomotion stride length, although post hoc comparisons were not statistically significant (lowest p = 0.0766 when comparing basal versus 14DPI performance for sC3-C4 group) (Figure 29E). Therefore, as was hypothesized, the animals with spinal roots sectioned at segments sC3 and sC3-C4 conserved their forelimb skilled and unskilled function, demonstrating that the impairments of animals with kainic acid injected at vC2 (~ sC3) and vC2-C3 (~ sC3-C4) were not due to the excitotoxicity on motoneurons and/or sensory neurons.

In summary, these results suggest a relevant role for sC3 segment in the control of R&G and other related forelimb movements. Besides, this network present at sC3 does not require the local motoneurons and/or sensory feedback to function properly. In the next chapter, we will try to elucidate further information on that hypothetical sC3 spinal network.

(Figure on the next page)

Figure 28. Forelimb R&G assessment after spinal roots sectioning. Forelimb R&G was evaluated before vs after 7 and 14 DPI in **(A)** R&G success percentage and the frequency of error types **(B)** 1, **(C)** 2, **(D)** 3, **(E)** 4, **(F)** 5 and **(G)** 6. Groups: Roots sC3 (n = 4), Roots sC3-C4 (n = 3). * $p < 0.05$; as calculated by repeated measures two-way ANOVA with group as between-subject factor and timepoint as within-subject factor, followed by Tukey's multiple comparisons test. Data presented as mean ± SEM.

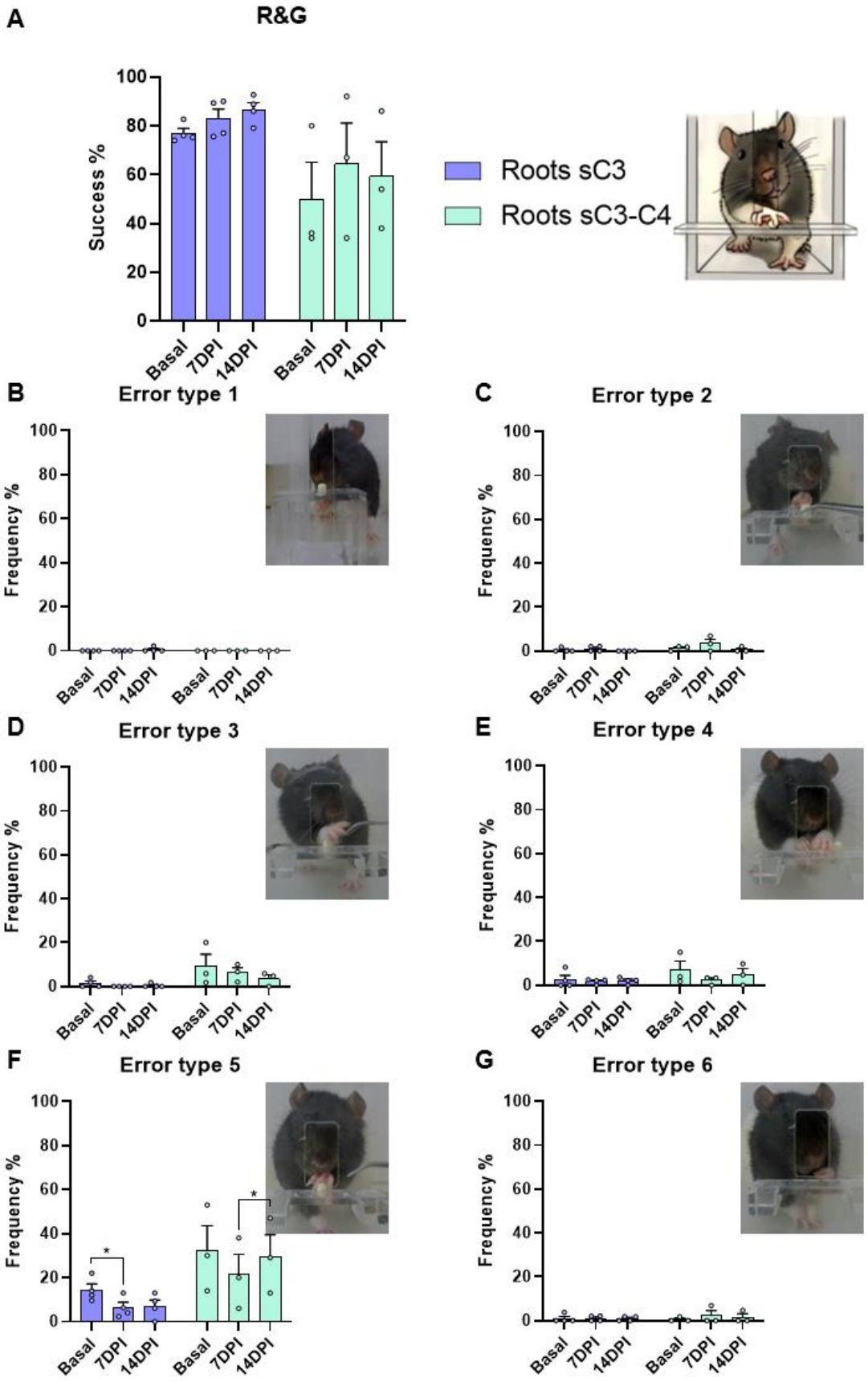
A
R&G
Success %
Roots sC3
Roots sC3-C4
Basal
7DPI
14DPI
B
Error type 1
C
Error type 2
D
Error type 3
E
Error type 4
F
Error type 5
G
Error type 6
Frequency %

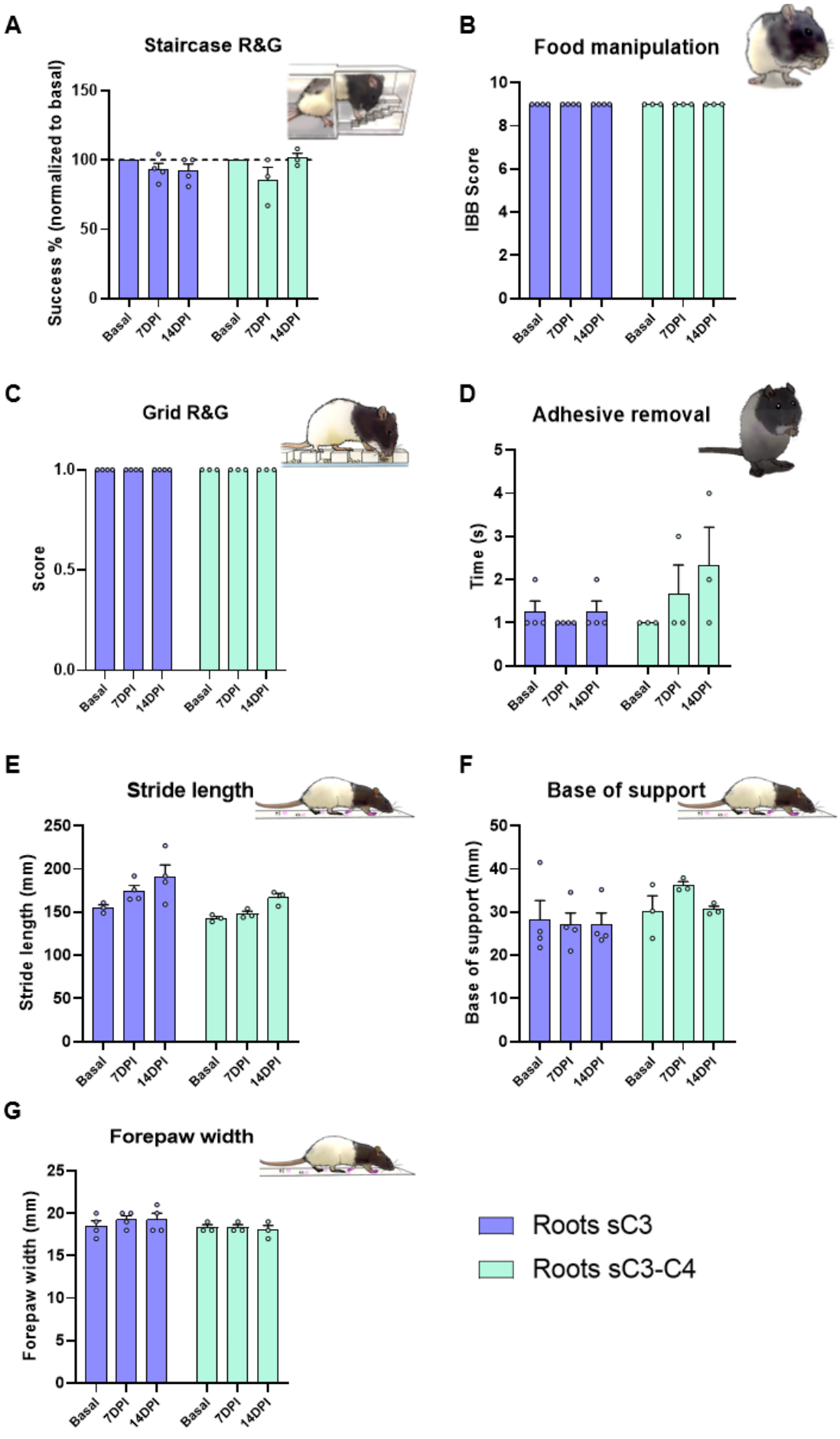
A
Staircase R&G
Success % (normalized to basal)
150
100
50
0
Basal
7DPI
14DPI
Basal
7DPI
14DPI
B
Food manipulation
IBB Score
10
8
6
4
2
0
Basal
7DPI
14DPI
Basal
7DPI
14DPI
C
Grid R&G
Score
1.0
0.5
0.0
Basal
7DPI
14DPI
Basal
7DPI
14DPI
D
Adhesive removal
Time (s)
5
4
3
2
1
0
Basal
7DPI
14DPI
Basal
7DPI
14DPI
E
Stride length
Stride length (mm)
250
200
150
100
50
0
Basal
7DPI
14DPI
Basal
7DPI
14DPI
F
Base of support
Base of support (mm)
50
40
30
20
10
0
Basal
7DPI
14DPI
Basal
7DPI
14DPI
G
Forepaw width
Forepaw width (mm)
25
20
15
10
5
0
Basal
7DPI
14DPI
Basal
7DPI
14DPI
Roots sC3
Roots sC3-C4

Figure 29. Forelimb function assessment after spinal roots sectioning. Forelimb function evaluated before vs after 7 and 14 DPI in **(A)** ability to reach and grasp pellets from different steps of a staircase and **(C)** from the bottom of a grid, **(B)** food manipulation based on the IBB scale, **(D)** the time to contact an adhesive sticker on the palm of the forepaw, and **(E)** stride length, **(F)** base of support and **(G)** forepaw width during locomotion. Groups: Roots sC3 (n = 4), Roots sC4 (n = 3). No significant differences between timepoints were found by **(A, D, E, F, G)** repeated measures two-way ANOVA with group as between-subject factor and timepoint as within-subject factor, followed by Tukey's multiple comparisons test. **(B, C)** No statistical analyses were executed when the all the values in all timepoints were the same. Data presented as **(A, D, E, F, G)** mean ± SEM or as **(B, C)** median ± interquartile range, depending on if the data followed a Gaussian distribution or not, respectively.

Chapter 2

Characterising the identified spinal neuronal network controlling reaching and grasping

Overview

The role of the cervical spinal cord in the control of manual dexterity, and in R&G in particular, is not fully understood. In the previous chapter, we have identified spinal segment sC3 as a key region containing a neuronal network necessary for executing those movements. This chapter focuses on the characterization of this potential sC3 network, exploring both its molecular signature via the expression IEGs during various forelimb motor tasks, and its functional connectivity with downstream targets involved in distal forelimb control.

First, we sought to identify the neuronal populations in the spinal cord that are active during R&G in intact animals by analysing the expression of IEGs. While excitotoxic lesion studies provided a broad map of functionally critical regions, they lacked the resolution to delineate the precise laminae or specific locations of the putative neuronal network. To overcome this limitation, we divided the rats into different groups (those trained for R&G, those trained for treadmill locomotion, and untrained controls) and perfused them after their last behavioural session. This allowed us to compare the expression patterns of various IEGs within the cervical spinal cord as a result of performing different forelimb motor tasks. Moreover, by incorporating both "early R&G training" and "late R&G training" groups, we could observe changes in IEG expression during different stages of the learning process, providing crucial insights into the specific spinal laminae and neuronal populations involved in manual dexterity.

Second, to demonstrate the role of sC3 interneurons in controlling R&G, we investigated their descending projections to sC7 interneurons and motoneurons, which innervate the distal forelimb muscles. We anatomically traced and quantified the proportions of sC3 neurons projecting both ipsilaterally and contralaterally. Subsequently, we reversibly silenced these sC3-to-sC7 projecting neurons. This work was carried out during an internship in Dr. David S. K. Magnuson's laboratory at the Kentucky Spinal Cord Injury Research Center, which has established expertise in inactivating spinal interneurons in Sprague Dawley rats using this technique.

Spinal neuronal activation after R&G

After identifying of a potential neuronal network in the cervical spinal cord key for the correct execution of R&G, we investigated whether distinct neuronal populations in intact animals are preferentially activated by R&G compared to a forelimb-unskilled task (locomotion) or basal (no activity) conditions. The hypothesis underlying this experiment is that the execution of R&G recruits a specific pool of neurons that are necessary for its proper performance. In this activated pool, indicated by the expression of IEGs, we expect to find the neurons belonging to the spinal network that specifically controls R&G. By comparing the neuronal activation patterns after R&G with those observed under basal conditions or following a task that engages the forelimb but is distinct from R&G, we aim to specifically identify the neurons that contribute to this skilled motor function. Additionally, given the uncertainty as to whether the activation pattern related to R&G control will be detectable during the learning phase or only once the behaviour is well established, we opted to analyse IEG expression at two distinct stages: "early R&G training" and "late R&G training."

Defining experimental groups based on their R&G performance

To establish an unbiased basis for defining our experimental groups (namely, "early R&G training" and "late R&G training") animals were allocated according to their performance during the learning phase of the R&G task. All animals were maintained under a mild food deprivation regimen, receiving approximately 5 % of their body weight in food per day to sustain motivation for motor tasks. Notably, the body weight of all animals remained above 90 % of their initial value throughout the experiment (lowest mean body weight: 96.91 ± 0.28 %) (Figure 30A).

Regarding animals trained for R&G, some of them would make a subset of their attempts with their non preferent paw, but after 7-8 training sessions, virtually all R&G attempts were executed with the preferent paw (Figure 30B). They were assigned to two different experimental groups: "early R&G" and "late R&G". The reasoning behind this division is that we hypothesized that the neuronal network is plastic and would be refined during learning. Therefore, we would expect a more widespread, less defined population of neurons active at the peak of the learning curve

("early R&G" group) and a more discretely localized network after the learning curve has reached its plateau ("late R&G" group).

Thus, a key aspect for R&G training was to objectively determine the transition from learning to plateau. We found that the best parameter to assess learning in R&G was the number of successful attempts, as it combines the total attempts with the percentage of success (Figures 30C, E-F). It recapitulates the typical shape of a learning curve, so animals receiving R&G training could be subdivided into two groups based on that curve and perfused when the slope was maximal (group "early R&G") or minimal (group "late R&G"). The "learning peak" was defined as the first day where the animal reached ≥ 60 successful attempts with a success rate of ≥ 40 % and from a total number of ≥ 150 attempts (Figure 30D). Hence, the number of animals in the previous R&G curves progressively decreased from training sessions 1 (n = 9) to 7 (n = 2). The performance of the rats from the "late R&G" group stabilized at ~ 200 successful attempts in 30 minutes sessions, achieving four consecutive days where the average varied from a minimum of 198 ± 25.50 successful attempts to a maximum of 208 ± 34.14 successful reaches. The learning curves from "early R&G" and "late R&G" were equivalent, whether analysed by the number of successful attempts ($F_{(1, 22)} = 0.01$, p = ns for group effect, $F_{(2.39, 43.36)} = 6.73$, $p < 0.01$ for session effect and $F_{(6, 109)} = 0.79$, p = ns for the interaction), the total number of attempts ($F_{(1, 22)} = 0.81$, p = ns for group effect, $F_{(2.29, 41.67)} = 6.26$, $p < 0.01$ for session effect and $F_{(6, 109)} = 1.02$, p = ns for the interaction) or the success percentage ($F_{(1, 22)} = 0.14$, p = ns for group effect, $F_{(2.96, 53.80)} = 6.05$, $p < 0.01$ for session effect and $F_{(6, 109)} = 1.36$, p = ns for the interaction).

Also other groups were run in parallel to those R&G groups, each of them with a specific purpose. Animals from the "no reaching" group were placed inside the R&G box for 30 min, but with food pellets placed on the floor (that can be eaten without the use of the forepaws) instead of on the elevated platform, used for R&G attempts. Animals trained for treadmill locomotion were placed inside the treadmill apparatus for 20 min per session, at a speed of 12 cm/s. Food pellets were stuck at the end of the treadmill to increase motivation, as no negative stimulus were applied. The performance remained relatively stable over time, as monitored by the time walking forward (88.14 ± 4.29 % of the time on the last session), times walking backwards (0.19 ± 0.10 times / minute on the first session vs 0.18 ± 0.06 times / minute on the last one), number of turns (1.04 ± 0.16 turns / minute on the first session vs 1.21 ± 0.28 turns

/ minute on the last one) and number of stops (0.27 ± 0.12 stops / minute on the first session vs 0.23 ± 0.10 stops / minute on the last one). In spite of the food rewards, their body weight remained relatively constant throughout the experiment, with all animals always above 90 % from their initial value (lowest mean body weight 96.91 ± 0.28 %) (Figure 30A).

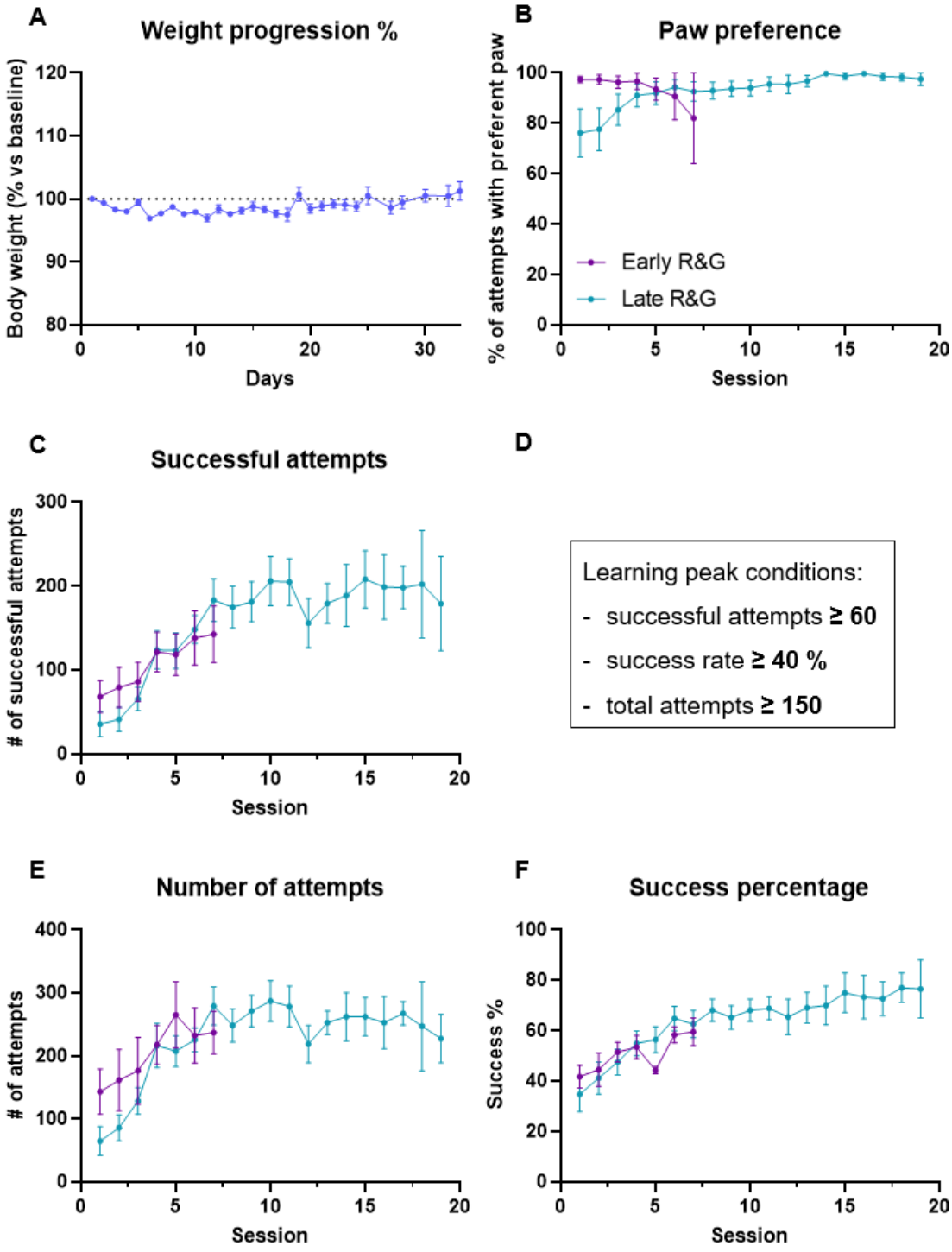

Figure 30. Behavioural training. (A) Despite food deprivation, body weight did not decrease under 90 % in any animal (n = 40). **(B)** Percentage of R&G attempts with the preferent paw

per session. **(C)** R&G learning curve based on the number of successful attempts per session with the preferent paw. **(D)** Definition criteria of learning curve peak. **(E)** Number of R&G attempts and **(F)** success percentage during training sessions with the preferent paw. R&G groups: Early R&G training (n = 9 at session 1,..., n = 2 at session 7), late R&G training (n = 15). Analysis performed with mixed-effects model using the restricted maximum likelihood method. Data presented as mean ± SEM.

Quality checkpoint for ensuring adequate tissue preservation

After perfusion, dissection, post-fixation and further tissue processing for immunohistochemical analysis, we noted that the state of preservation of the spinal cords of several animals was substandard. This was likely due to the use of paraformaldehyde with an acid pH for perfusion, to the inappropriate state of one or some of the buffers used, or to an inadequate freezing process. Therefore, we performed an immunostaining against the common neuronal marker NeuN (Sukhorukova *et al.*, 2015) using DAB as labelling agent. The immunostaining clearly revealed the tissue that was properly preserved (18 / 40 animals, from 2 / 3 batches) (Figures 31A, C, E) and the tissue that was not (22 / 40 animals, from 2 / 3 batches) (Figure 31B, D, F). Only the spinal cords that displayed an appropriate NeuN-DAB labelling were used in the subsequent analyses: n = 4 in "no reaching" group, n = 4 in "early R&G" group, n = 6 in "late R&G" group, and n = 2 in "treadmill" group.

IEG expression in the cervical spinal cord

Once having selected the properly preserved tissue, we proceeded to test antibodies against multiple IEGs, using tissue from animals of the "treadmill" group as a positive control, given that this activity is known to induce IEG expression in the lumbar spinal cord (Ahn *et al.*, 2006). Our initial intention was to assess a panel of four IEGs (namely, c-Fos, FosB, Arc, and Egr1) each of which provides complementary insights into neuronal activation and plasticity. c-Fos serves as an immediate marker of neuronal activation, rapidly induced by synaptic stimulation, while FosB (and its stable isoform ΔFosB) reflects recurrent activation and long-term adaptations. Arc is closely associated with synaptic plasticity and activity-dependent remodeling, and Egr1 plays a key role in regulating gene transcription during learning. However, after several optimization phases of the immunostaining protocol, we obtained clear positive immunostaining for c-Fos and FosB in both the cervical and lumbar spinal

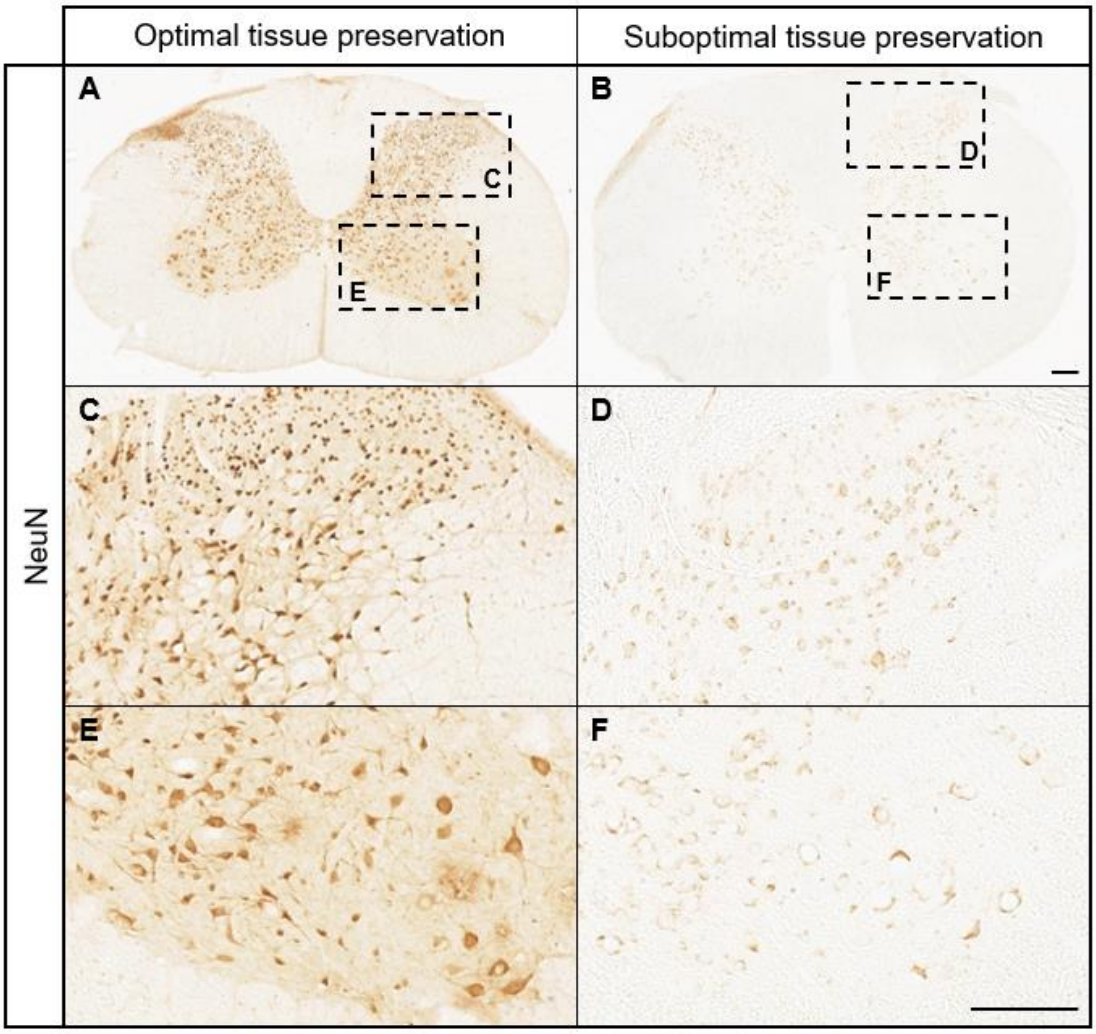

Figure 31. Tissue preservation assay. NeuN-DAB immunostaining was used to distinguish between **(A)** well preserved (n = 18) and **(B)** not well preserved (n = 22) tissue. Insets from **(C-D)** dorsal and **(E-F)** ventral horns. Scale bars: 200 µm.

cords (Figure 32). Unfortunately, we were unable to detect Arc$^+$ or Egr1$^+$ cells under our experimental conditions, and consequently, these markers were excluded from further analysis.

Thus, the neuronal activation within the cervical spinal cord was evaluated from the assessment of c-Fos and FosB expression. First, we compared the expression of c-Fos and FosB in the spinal hemicord corresponding to the preferent paw of the animal versus the non-preferent paw, or left versus right in the case of animals not trained for R&G. Notably, no significant differences between hemicords in the number of c-Fos$^+$ or FosB$^+$ cells were observed in any of the groups (Figures 33A-B). Therefore, the mean of both hemicords was used for the rest of the comparisons.

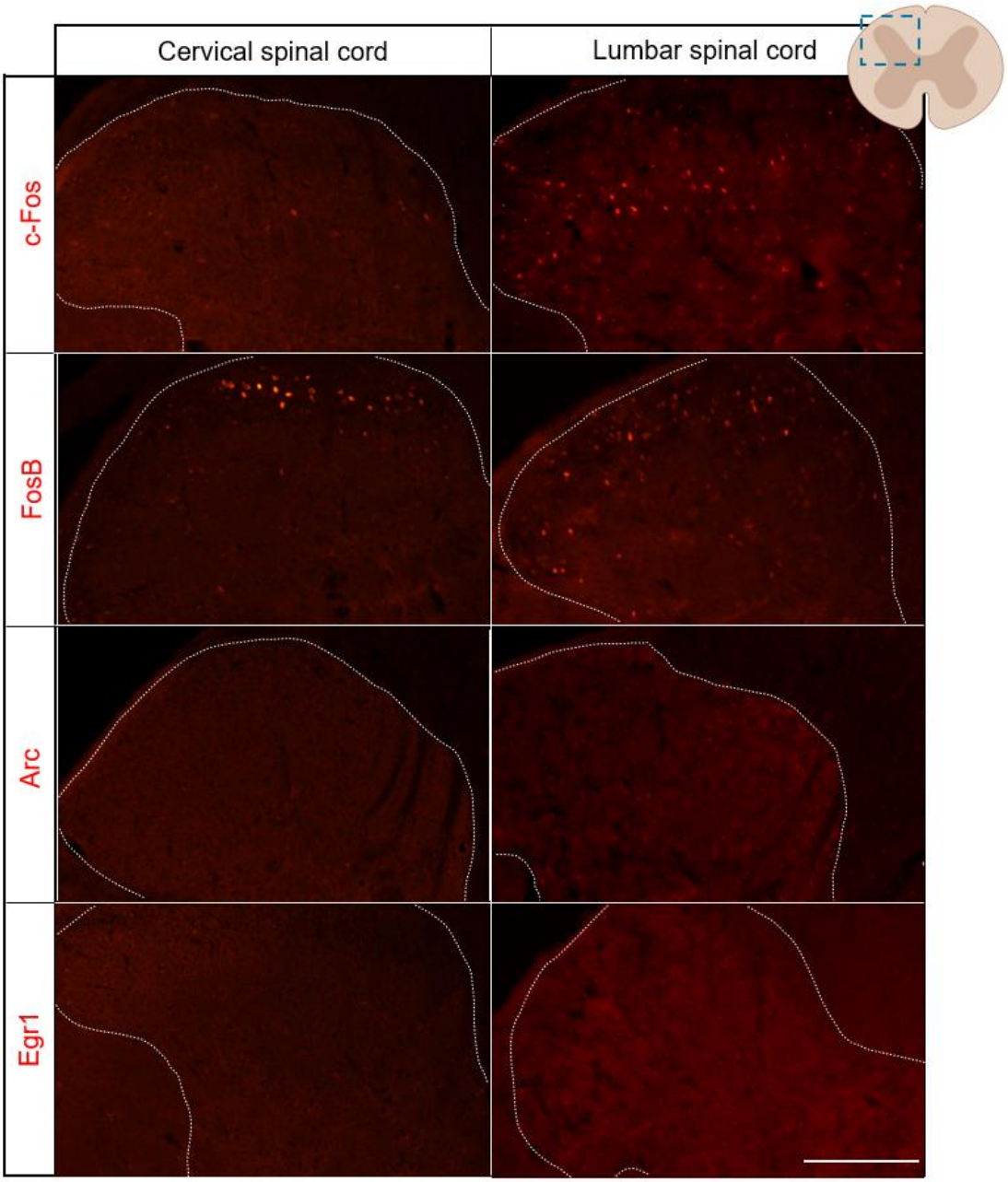

Figure 32. IEGs expression assay in the spinal cord. Representative immunostained dorsal horn images from the cervical and the lumbar spinal cord with antibodies against c-Fos, FosB, Arc and Egr1. Grey and white matter delimitated by white dashed lines. Scale bar: 200 µm.

(Figure on the next page)

Figure 33. Comparison of IEGs expression between hemicords. Expression of **(A)** c-Fos and **(B)** FosB of the preferent hemicord with respect to the total number of immunopositive cells throughout the cervical spinal cord. Groups: "no reaching" (n = 4), "early R&G" (n = 4), "late R&G" (n = 6), "treadmill" (n = 2). Analysis performed by one sample t test vs a theoretical mean of 50 %, correcting for multiple comparisons with Benjamini-Hochberg method. Data presented as mean ± SEM.

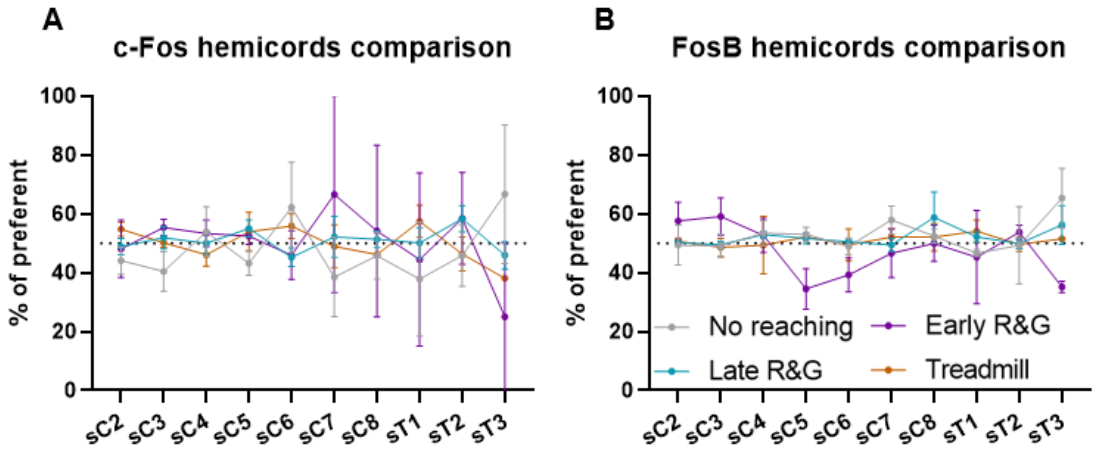

Then, we compared the number of c-Fos⁺ cells present in the different cervical spinal cord segments of the different groups of animals. Representative images from each of these experimental groups can be seen in Figure 34A. To prevent differences between immunostaining batches, the number of immunopositive cells was normalized to the number of immunopositive cells counted from the lumbar spinal cord of a control animal, whose sections were immunostained together with all batches. The values of positive cell counts were corrected accordingly. Significant differences of c-Fos⁺ cell count were found for spinal cord segment ($F_{(2.28, 24.05)} = 6.06$, $p < 0.01$) and experimental group ($F_{(3, 11)} = 7.82$, $p < 0.01$), but not for the interaction ($F_{(27, 95)} = 0.60$, p = ns). Tukey's post hoc comparisons revealed that significant differences between "no reaching" and R&G groups were only present between "no reaching" (0.93 ± 0.35 c-Fos⁺ cells) and "late R&G" (3.25 ± 0.60 c-Fos⁺ cells) groups at T2 level ($p < 0.05$) (Figure 34C). Further, there were fewer c-Fos⁺ cells in the "early R&G" group compared to the "late R&G" group at spinal levels sC6 (1.65 ± 0.40 vs 3.6 ± 0.28 c-Fos⁺ cells; $p < 0.05$), T1 (0.65 ± 0.22 vs 3.2 ± 0.60 c-Fos⁺ cells; $p < 0.05$) and sT2 (0.78 ± 0.10 vs 3.25 ± 0.60 c-Fos⁺ cells; $p < 0.05$). In the latter segment, the number of positive neurons was also significantly lower than in the "treadmill" group (1.65 ± 0.05 c-Fos⁺ cells; $p < 0.01$).

The quantification also took into account the location of the positive cell within the grey matter by overlaying the corresponding rat Rexed laminae templates (Figure 34B). At the dorsal grey matter (Rexed laminae I-IV), significant differences were observed regarding group ($F_{(3, 11)} = 6.76$, $p < 0.01$) and segment ($F_{(2.29, 24.13)} = 4.07$, $p < 0.05$), but not for the interaction ($F_{(27, 95)} = 0.75$, p = ns) (Figure 34D). With multiple comparisons, "late R&G" group presented a significant increase in the number of c-Fos⁺ cells compared to the "no reaching" group at both sC2 (4.57 ± 0.68 vs 1.5 ± 0.25 c-Fos⁺ cells, respectively, $p < 0.05$) and sC3 (4.52 ± 0.71 vs 1.6 ± 0.31 c-Fos⁺ cells,

respectively, $p < 0.05$), and compared to the "early R&G" group at sC2 (4.57 ± 0.68 vs 1.48 ± 0.46 c-Fos⁺ cells, respectively, $p < 0.05$). Finally, when assessing intermediate and ventral Rexed laminae (V-X), statistically significant differences were found between groups ($F_{(3, 11)} = 5.32$, $p < 0.05$ for group effect; $F_{(2.72, 28.71)} = 5.17$, $p < 0.01$ for segment effect; and $F_{(27, 95)} = 0.77$, p = ns for the interaction). Post hoc comparison unveiled significantly increased c-Fos⁺ cells from the "late R&G" group at sC8 (1.3 ± 0.17 c-Fos⁺ cells), sT1 (1.45 ± 0.22 c-Fos⁺ cells) and sT2 (1.33 ± 0.16 c-Fos⁺ cells) segments compared to "early R&G" group (0.4 ± 0.17, 0.15 ± 0.09 and 0.45 ± 0.13 c-Fos⁺ cells, respectively, with p values of < 0.05, < 0.01 and < 0.05), at segment sC8 compared to "no reaching" group (0.6 ± 0.1 c-Fos⁺ cells, $p < 0.05$), and at segment sC5 compared to treadmill group (2.12 ± 0.42 vs 0.55 ± 0.05 c-Fos⁺ cells, respectively, $p < 0.05$) (Figure 34E). Remarkably, the motoneurons that control muscles involved in forelimb skilled function are located approximately in these spinal segments (Figure 34F). In conclusion, there is a tendency for animals repeatedly trained for R&G to present a higher number of (putatively activated) c-Fos⁺ cells throughout the cervical spinal cord compared to animals from "treadmill", "no reaching" and "early R&G" groups. This is especially evident for dorsal laminae in rostral spinal segments and for intermediate and ventral laminae at caudal spinal segments, suggesting that those two regions could be playing a role in the execution of R&G.

Nonetheless, the overall number of immunostained cells was very low, even testimonial in those referred segments, contrary to what we expected.

We complemented these results with immunostaining for FosB. Notably, one of its isoforms, ΔFosB, accumulates and remains stably expressed over time (Hiroi *et al.*, 1998; Nestler, 2015), unlike c-Fos, which declines significantly after 120 minutes (Yap & Greenberg, 2018). Consequently, ΔFosB serves as an effective marker of recurrent neuronal activation, potentially revealing the neuronal populations that are repeatedly engaged during behavioural training sessions.

FosB-positive cells were quantified using the same methodology as for c-Fos-positive cells. A visual inspection clearly indicates that a substantially greater number of FosB-immunostained cells were observed in this case (Figure 35A). There were significant differences in FosB⁺ cell counts regarding group ($F_{(3, 11)} = 10.96$, $p < 0.01$), segment ($F_{(1.44, 14.91)} = 13.98$, $p < 0.001$) and interaction ($F_{(27, 93)} = 3.19$, $p < 0.001$) effects. Animals that had been trained to R&G until reaching their performance plateau ("late R&G"

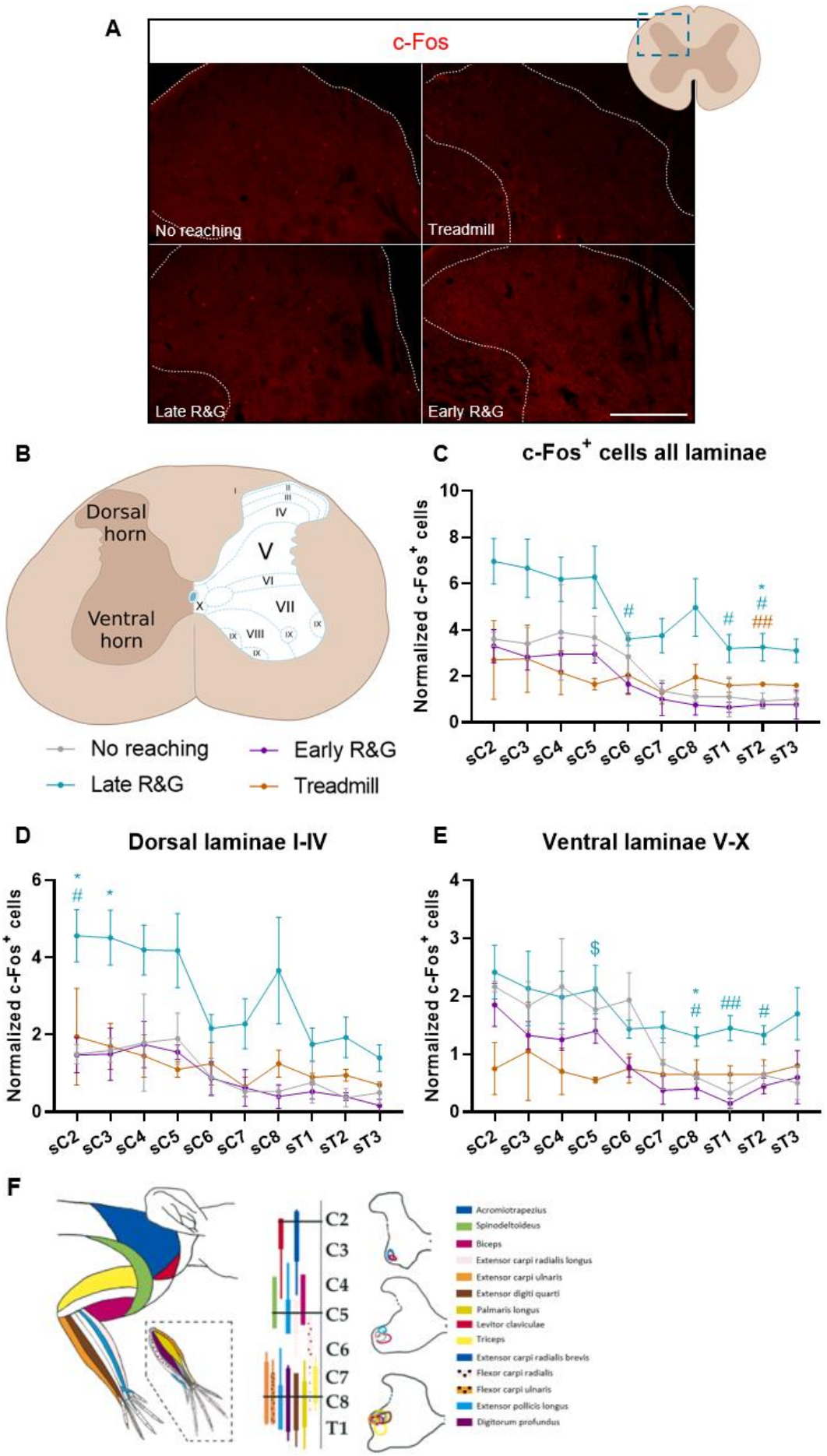
A
c-Fos
No reaching
Treadmill
Late R&G
Early R&G
B
Dorsal horn
Ventral horn
I
II
III
IV
V
VI
VII
VIII
IX
X
No reaching
Late R&G
Early R&G
Treadmill
C
c-Fos+ cells all laminae
Normalized c-Fos+ cells
sC2 sC3 sC4 sC5 sC6 sC7 sC8 sT1 sT2 sT3
D
Dorsal laminae I-IV
Normalized c-Fos+ cells
E
Ventral laminae V-X
Normalized c-Fos+ cells
F
C2
C3
C4
C5
C6
C7
C8
T1
Acromiotrapezius
Spinodeltoideus
Biceps
Extensor carpi radialis longus
Extensor carpi ulnaris
Extensor digiti quarti
Palmaris longus
Levitor claviculae
Triceps
Extensor carpi radialis brevis
Flexor carpi radialis
Flexor carpi ulnaris
Extensor pollicis longus
Digitorum profundus

Figure 34. c-Fos expression in the cervical spinal cord. (A) Representative sC3-C4 c-Fos immunostained dorsal horn images from the different experimental groups, with grey and white matter delimitated by white dashed lines. **(B)** Scheme of Rexed laminae division of the spinal grey matter. Graphs of c-Fos$^+$ cells per hemicord in **(C)** the entire grey matter, in **(D)** dorsal laminae I-IV, and in **(E)** intermediate and ventral laminae V-X. **(F)** Rat cervical motor columns scheme, from Mckenna *et al*., 2000. Groups: "no reaching" (n = 3), "early R&G" (n = 4), "late R&G" (n = 6), "treadmill" (n = 2). * $p < 0.05$ vs "No reaching"; # $p < 0.05$, ## $p < 0.01$ vs "Early R&G", $ $p < 0.05$ vs "Treadmill"; as calculated by mixed-effects analysis model using the restricted maximum likelihood method, followed by Tukey's multiple comparisons test. Data is shown as mean ± SEM. Scale bar: 200 µm.

group) showed significantly higher FosB$^+$ cells than animals trained only for a few days ("early R&G" group) throughout the cervical and rostral thoracic spinal cord (sC2-T2 average 29.26 ± 1.74 vs 6.77 ± 0.57 FosB$^+$ cells, p values ranging from a minimum of $p = 0.0011$ at T1 to a maximum of $p = 0.0470$ at sC3) (Figure 35B). They also showed an increased number of FosB$^+$ cells than the "no reaching" group at segments sC2, sC6, sC7, sT1 and sT2 (highest difference at sC2 with 47.18 ± 4.76 vs 11.7 ± 1.99 FosB$^+$ cells, respectively, $p < 0.01$). Moreover, "early R&G" animals also showed decreased number of FosB$^+$ cells in sC3 (10.35 ± 1.99 FosB$^+$ cells; $p < 0.05$) and sC7 (4.38 ± 1.28 FosB$^+$ cells; $p < 0.01$) segments compared to the "treadmill" group (20.86 ± 0.83 and 16.42 ± 1.04 FosB$^+$ cells, respectively). Last, there was a significant decrease in the FosB$^+$ cell count at sC5 in "early R&G" with respect to the "no reaching" group (7.98 ± 1.28 vs 15.03 ± 0.82 FosB$^+$ cells, respectively, $p < 0.05$).

When studying in more detail where those FosB$^+$ cells were located within the spinal cord, we found a difference compared to c-Fos results. Unlike in c-Fos$^+$ cells, where they were somewhat equitably distributed between dorsal (sC2-T3 laminae I-IV average 1.87 ± 0.15 c-Fos$^+$ cells) and ventral (sC2-T3 laminae V-X average 1.28 ± 0.07 c-Fos$^+$ cells) horns, with an approximate proportion of 60-40 %, for FosB we observed a marked focus. While at intermediate and ventral laminae the number of positive neurons was still low (sC2-T3 laminae V-X average 1.93 ± 0.09 FosB$^+$ cells) and with statistical differences (effect of group $F_{(3, 11)} = 5.78$, $p < 0.05$; segment $F_{(3.90, 40.25)} = 4.91$, $p < 0.01$; and interaction $F_{(27, 93)} = 1.10$, p = ns) found only at sC2 between "treadmill" (3.65 ± 0.04 FosB$^+$ cells) versus "no reaching" (2.53 ± 0.15 FosB$^+$ cells, $p = 0.0303$) and "early R&G" groups (1.95 ± 0.26 FosB$^+$ cells, $p < 0.05$) (Figure 35D), around 90 % (15.53 ± 1.01) of the FosB$^+$ cells were confined to the dorsal laminae I-IV, which accounted for the results explained in relation to the total number of FosB$^+$ cells (Figure 35C). Therefore, significant differences were present in relation to group ($F_{(3, 11)} = 10.85$, $p <$

0.01), segment ($F_{(1.39, 14.66)} = 14.54$, $p < 0.001$) and interaction ($F_{(27, 95)} = 3.43$, $p < 0.001$) effects. Similarly to the analysis of all laminae together, the number of FosB$^+$ cells in dorsal laminae I-IV was higher in "late R&G" compared to "early R&G" group from sC2-T2 (maximum $p = 0.0451$ at C3, minimum $p = 0.0014$ at sC2), and compared to "no reaching" group at segments sC2, sC5, sC6, sC7, sT1 and sT2 (lowest $p = 0.0015$ at sC2). Likewise, there were significantly more FosB$^+$ cells in segments sC4 ($p < 0.05$), sC6 ($p < 0.05$), sC7 ($p < 0.01$) and sT2 ($p < 0.05$) when comparing "treadmill" versus "early R&G" groups, and when comparing "treadmill" versus "no reaching" group at sC7 ($p < 0.05$). Additionally, especially in the "late R&G" group, there are more FosB$^+$ cells in the rostral cervical spinal cord segments (sC2-C5 average 37.14 ± 2.92 FosB$^+$ cells) compared to the caudal cervical spinal cord and rostral thoracic spinal cord segments (sC6-T3 average 22.06 ± 1.21 FosB$^+$ cells). In particular, when comparing the different segments from this group, sC2 showed a significant increase in FosB$^+$ cells compared to sC6-T3 segments (p value ranging from 0.0005 minimum versus sC8 to 0.0279 maximum versus sC7). Segments sC3, sC4 and sC5 all presented significantly more FosB$^+$ cells than sC8 ($p < 0.05$).

Last, we assessed if there was a possible correlation between the number of c-Fos$^+$ and FosB$^+$ cells, and between the number of c-Fos$^+$ and/or FosB$^+$ cells and behavioural parameters observed during R&G training. First, there was a strong positive correlation between the number of c-Fos$^+$ and the number of FosB$^+$ neurons ($r = 0.87$, $p < 0.001$) (Figure 36A). When comparing histology with behaviour, we found a positive correlation between the number of training sessions and the number of c-Fos$^+$ ($r = 0.85$, $p < 0.01$) and FosB$^+$ ($r = 0.94$, $p < 0.001$) cells in the cervical and rostral thoracic spinal cord (Figures 36B-C). In addition, the accumulated number of R&G attempts throughout all training sessions correlated with FosB+ cell counts ($r = 0.64$, $p < 0.05$), but not with c-Fos quantification ($r = 0.56$, $p = 0.0911$) (Figures 36D-E). Interestingly, however, there was neither a correlation between the number of c-Fos$^+$ cells or FosB$^+$ cells and the accumulated success rate from all training sessions ($r = 0.10$, $p =$ ns; and $r = 0.15$, $p =$ ns, respectively) (Figures 36F-G) or the success percentage from the final session prior to perfusion ($r = 0.17$, $p =$ ns; and $r = 0.32$, $p =$ ns, respectively) (Figure 36H-I).

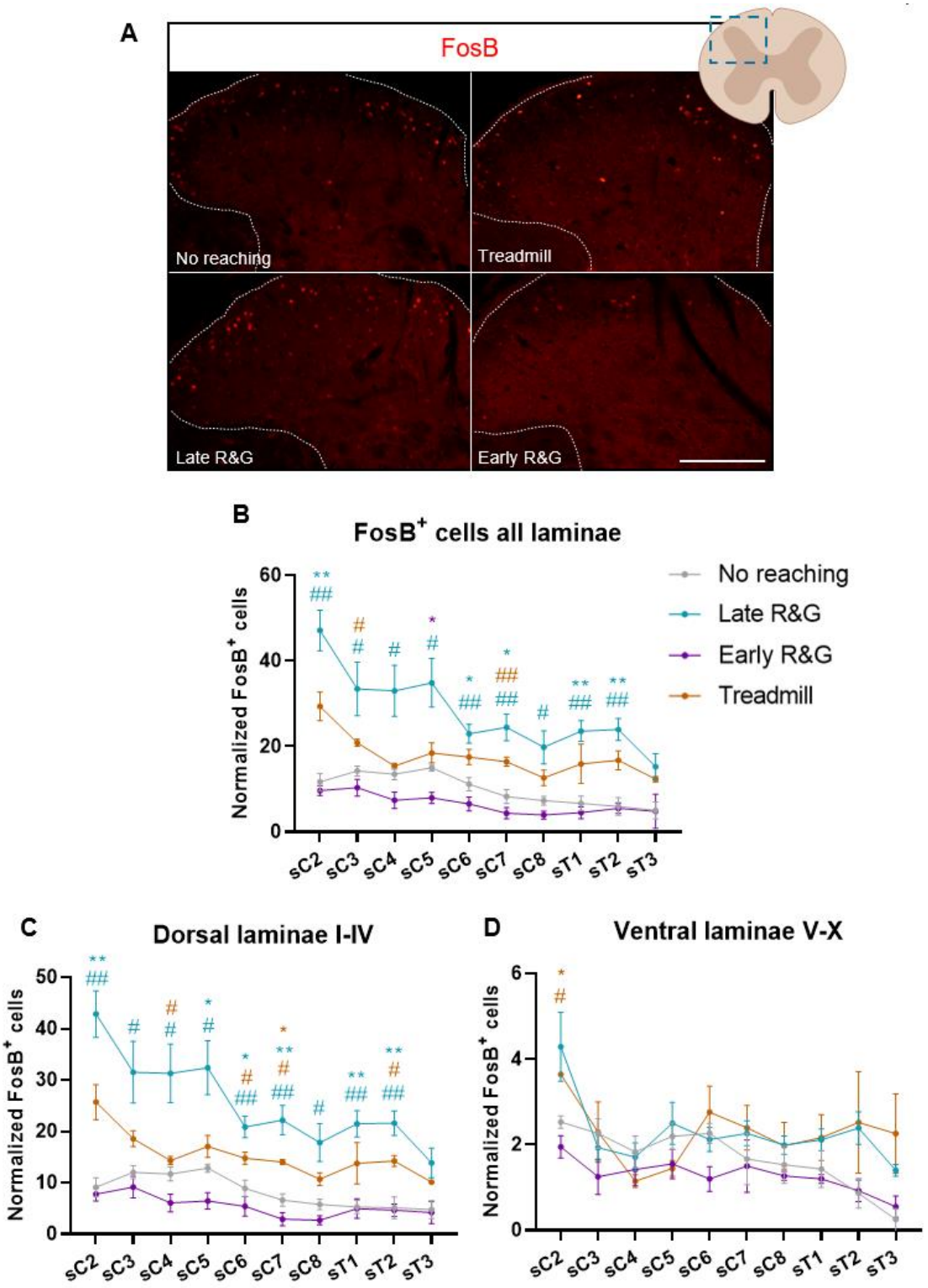

Figure 35. FosB expression in the cervical spinal cord. (A) Representative sC3-C4 FosB immunostained dorsal horn images from the different experimental groups, with grey and white matter delimitated by white dashed lines. Graphs of FosB⁺ cells per hemicord in **(B)** the entire grey matter, in **(C)** dorsal laminae I-IV, and in **(D)** intermediate and ventral laminae V-X. Groups: "no reaching" (n = 3), "early R&G" (n = 4), "late R&G" (n = 6), "treadmill" (n = 2). # $p < 0.05$, ## $p < 0.01$ vs "Early R&G"; as calculated by mixed-effects analysis model using the restricted maximum likelihood method, followed by Tukey's multiple comparisons test. Data presented as mean ± SEM. Scale bar: 200 µm.

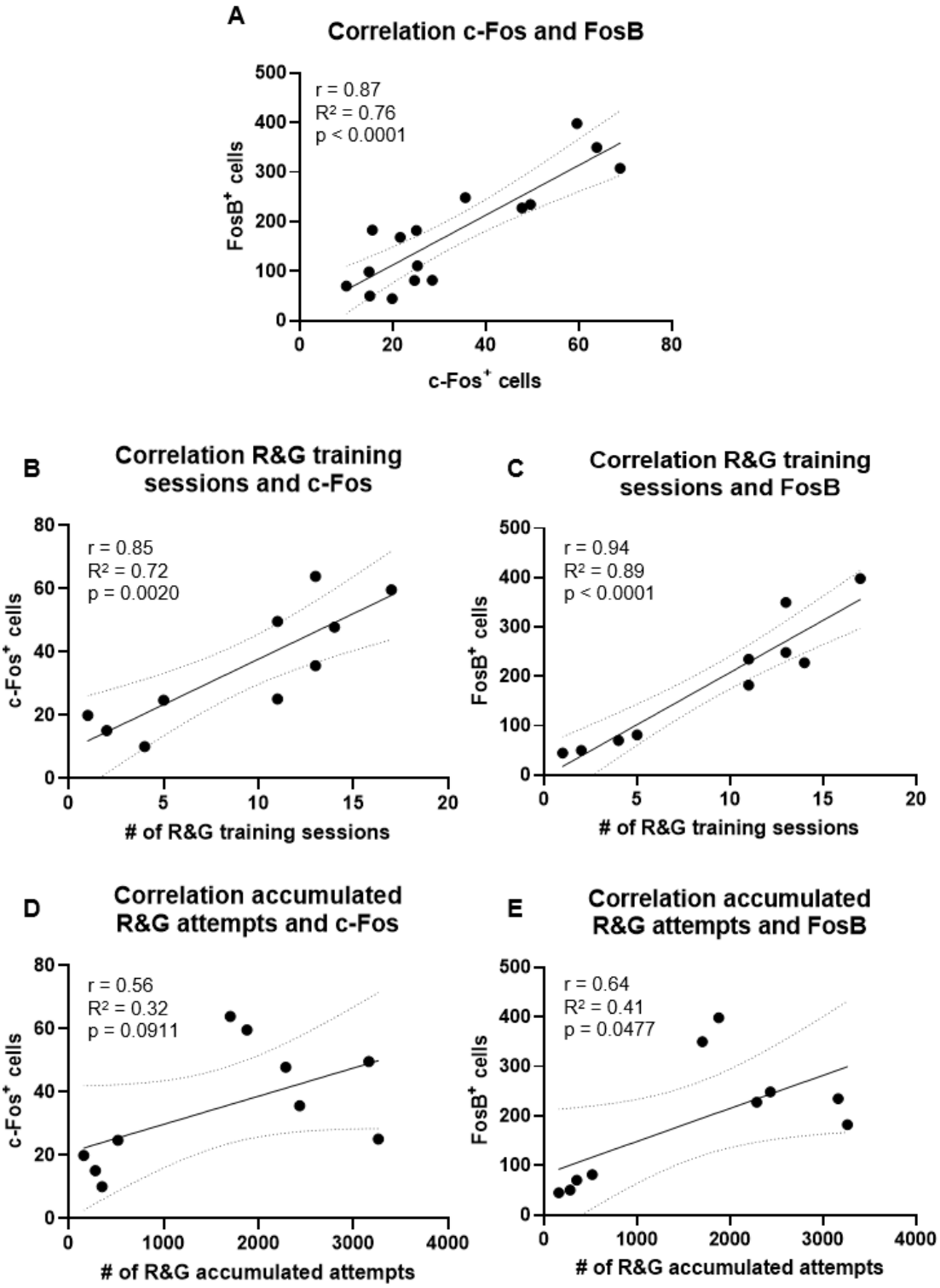
A
Correlation c-Fos and FosB
r = 0.87
R² = 0.76
p < 0.0001
FosB⁺ cells
c-Fos⁺ cells
B
Correlation R&G training sessions and c-Fos
r = 0.85
R² = 0.72
p = 0.0020
c-Fos⁺ cells
# of R&G training sessions
C
Correlation R&G training sessions and FosB
r = 0.94
R² = 0.89
p < 0.0001
FosB⁺ cells
# of R&G training sessions
D
Correlation accumulated R&G attempts and c-Fos
r = 0.56
R² = 0.32
p = 0.0911
c-Fos⁺ cells
# of R&G accumulated attempts
E
Correlation accumulated R&G attempts and FosB
r = 0.64
R² = 0.41
p = 0.0477
FosB⁺ cells
# of R&G accumulated attempts

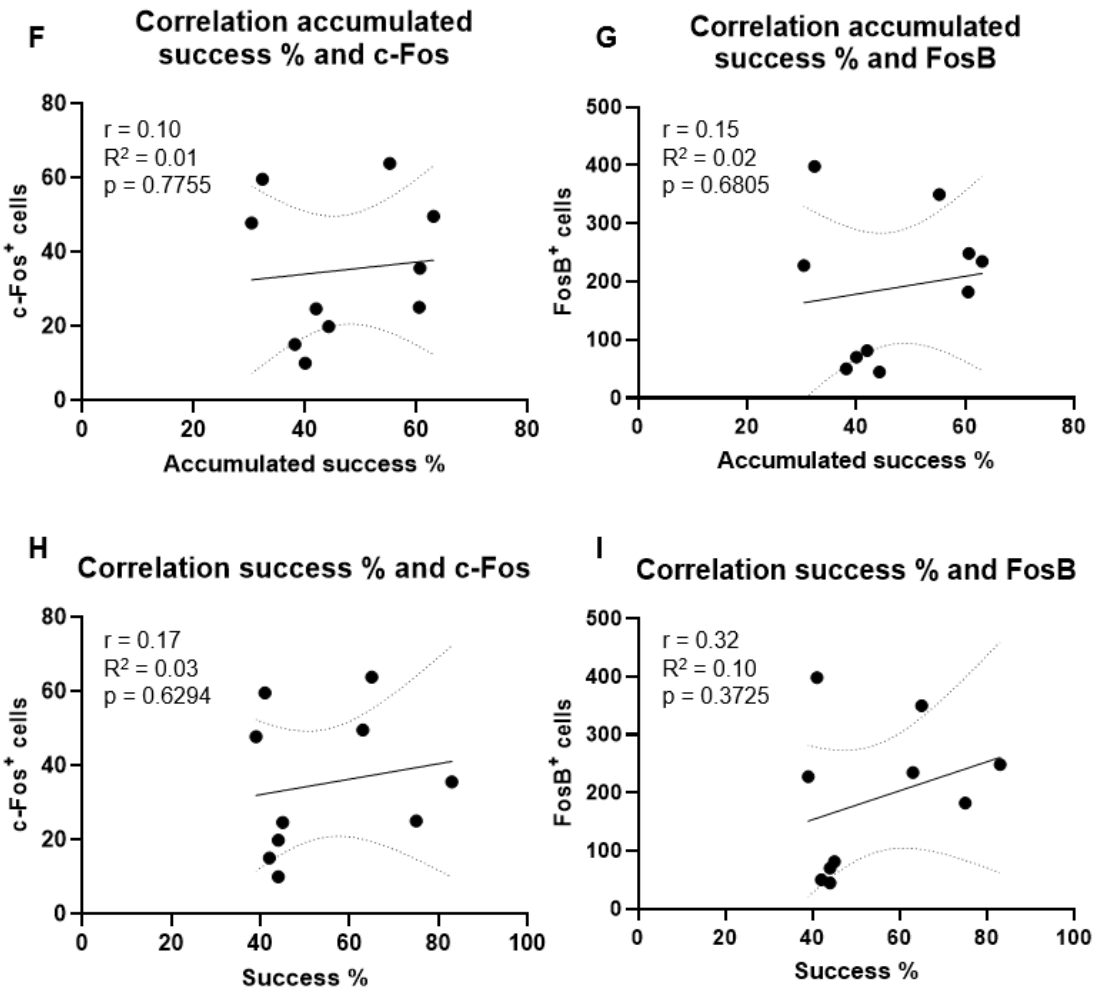

Figure 36. c-Fos and FosB correlations with R&G training. (A) Correlation of c-Fos and FosB in all animals. Correlation between number of R&G training sessions and count of **(B)** c-Fos⁺ and **(C)** FosB⁺ cells. Correlation of **(D)** c-Fos⁺ neurons or **(E)** FosB⁺ neurons with the accumulated R&G attempts throughout all training sessions. Correlation of **(F)** c-Fos⁺ neurons or **(G)** FosB⁺ neurons with the accumulated R&G success percentage throughout all training sessions. Correlation of **(H)** c-Fos⁺ neurons or **(I)** FosB⁺ neurons with the R&G success percentage of the testing session. In (A), n = 16; n = 10 elsewhere. Correlation plots show Pearson's r coefficient and R square fit calculation.

Collectively, these argue that the repetitive execution and perfectioning of R&G is accompanied by an augment in the number of neurons involved in the network, especially in rostral spinal segments sC2-C5, in comparison to animals not performing the movement, executing other forelimb movements that are not R&G, or R&G but for fewer training sessions.

Reversible silencing of sC3-to-C7 projecting neurons

Continuing with the focus on the spinal network mediating R&G, we aimed to investigate the potentiality of sC3 for housing a R&G CPG. If that were the case, sC3 interneurons would be controlling segmental interneurons and/or motoneurons responsible for contracting forelimb muscles required for R&G. Some of those neurons can be found at sC7. Thus, our hypothesis was that, upon inactivation of sC3-to-C7 projecting neurons, manual dexterity would be impaired, and baseline function would be restored once silencing stopped.

Tracing sC3-to-C7 ipsilateral and contralateral projections

First, we investigated the descending projections of sC3 interneurons to sC7 interneurons or motoneurons involved in the control of distal forelimb muscles using an anatomical approach. As previously mentioned, we utilized Sprague Dawley rats rather than Long Evans rats because the method had been optimized for the former strain. Ten animals received unilateral surgical injections of AAV2-CAG-FLEx-GFP at sC3 and HiRet-Lenti-Cre at sC7. Half of the rats received injections at both segments on the same side (ipsilaterally), while the remaining half received injections contralaterally. This dual-injection system ensured that only neurons with cell bodies in one injection site and projections in the other would contain both viral constructs, resulting in fluorescent labelling with GFP (for further details, see the Materials and Methods section). This approach allowed us to quantify the number of sC3-to-C7 projecting neurons and to estimate the proportions projecting ipsilaterally versus contralaterally.

Doubly infected neurons expressing GFP were found both in animals injected ipsilaterally and contralaterally (Figure 37A). GFP^+ cells were manually quantified along the cervical spinal cord, and their dorsoventral location within the grey matter was annotated relative to Rexed laminae (Figure 37B). Coherently to the spinal segments of injection, GFP^+ neurons were located from sC3 to sC5 segments, especially at the intersection between sC3 and sC4 (Figure 37C). Even though there is a tendency of a higher number of labelled neurons at the rostral half of sC4 in the ipsilaterally injected animals (reaching a maximum of 8.5 ± 3.86 vs 5.2 ± 2.24 GFP^+ cells), this difference was not statistically significant (Effect of side $F_{(1,7)} = 3.64$, p = ns;

distance $F_{(1.67, 11.69)} = 7.43$, $p < 0.05$; and interaction $F_{(23, 161)} = 0.67$, $p = ns$). Analysis of the dorsoventral location of these neurons revealed that most sC3-to-C7 projecting neurons were located at the intermediate and ventral regions of the grey matter, whereas their presence at dorsal laminae was practically inexistent (Figures 37D-E). For dorsal laminae (I-IV), the statistical analysis revealed a significant effect for the interaction between side and distance ($F_{(23, 161)} = 1.88$, $p < 0.05$), but not for side ($F_{(1, 7)} = 3.11$, $p = ns$) or distance ($F_{(1.71, 11.99)} = 3.09$, $p = ns$) individually (Figure 37D). However, post hoc comparisons were not significant at any particular distance within the spinal cord (lowest $p = 0.9369$, 1 ± 0.36 vs 0.2 ± 0.13 GFP^+ cells projecting ipsilaterally vs contralaterally, respectively, at caudal sC3). Regarding intermediate and ventral spinal laminae (V-X) (Figure 37E), like in the analysis of all laminae together, a significant effect was found for distance ($F_{(1.61, 11.28)} = 6.95$, $p < 0.05$), but not for projecting side ($F_{(1, 7)} = 2.99$, $p = ns$) or for the interaction ($F_{(23, 161)} = 0.55$, $p = ns$). This pattern of innervation correlates with the one present in sL2-L5 interneurons that are key for locomotion control (Pocratsky *et al.*, 2017).

Targeted silencing of sC3-to-C7 projecting neurons

Sprague Dawley rats show a R&G learning curve comparable to that of the Long Evans strain

With these results, we used a second batch of rats (n = 12) for the reversible silencing experiment. They were gentled, acclimated and trained for both R&G and high-speed locomotion inside a 3 m long tank. To increase motivation for both behavioural training tasks, animals were mildly food deprived (receiving 5 % of their body weight in food per day), always maintaining their body weight over 95 % of the initial value (Figure 38A). As with Long Evans rats in the previous chapters, Sprague Dawley rats were successfully trained for the skilled reaching task and showed a similar learning curve regarding the progression of paw preference (Figure 38B), the number of successful R&G attempts (Figure 38C) and the success percentage (Figure 38D). Animals were assessed for both behavioural tests before the surgery (see below).

sC3-to-C7 projecting neurons were successfully silenced upon Dox administration

The viral injection surgeries for the silencing experiment were very similar to the ones

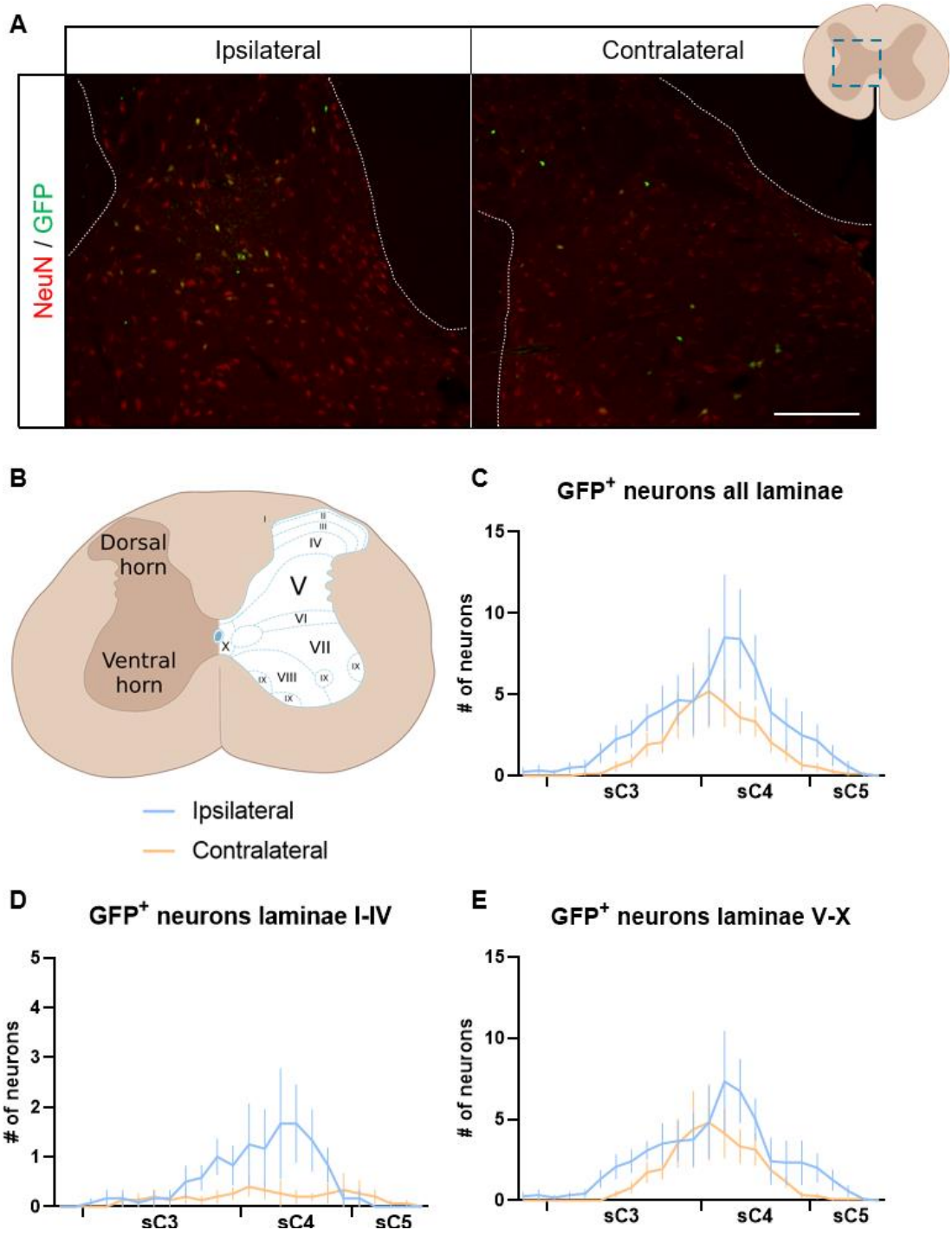

Figure 37. Tracing sC3-to-C7 projecting neurons. (A) Representative images of double-infected (GFP⁺) neurons (NeuN⁺) with viral vectors injected ipsilaterally or contralaterally. **(B)** Scheme of Rexed laminae division of the spinal grey matter. Graphs of c-Fos⁺ cells per hemicord in **(C)** the entire grey matter, in **(D)** dorsal laminae I-IV, and in **(E)** intermediate and ventral laminae V-X. Groups: Ipsilateral (n = 4), contralateral (n = 5). Analysis performed by repeated measures two-way ANOVA followed by Šídák's multiple comparisons test. Data is shown as mean ± SEM. Scale bar: 200 µm.

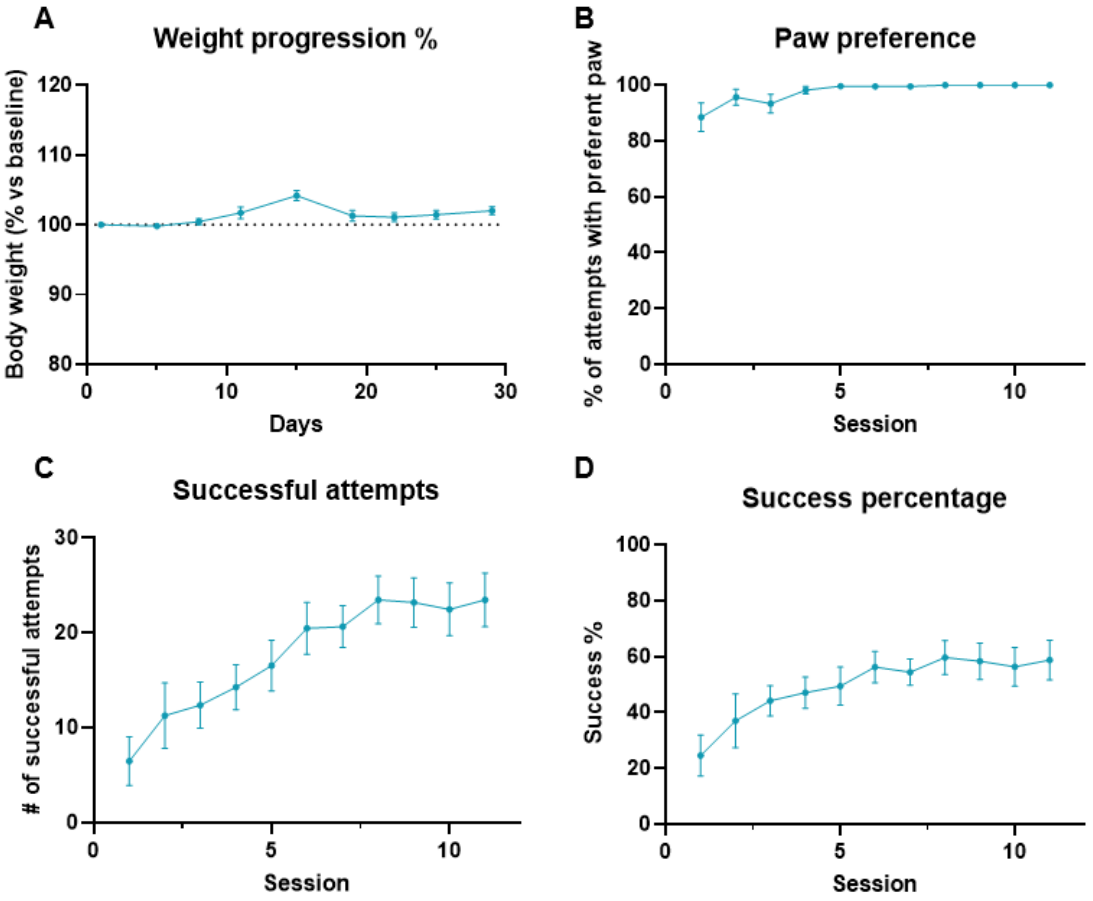

Figure 38. Behavioural training. (A) Despite food deprivation, body weight did not decrease under 95 % in any animal. **(B)** Evolution of percentage of attempts with the preferent paw. R&G learning curves based on **(C)** the number of successful attempts per session and **(D)** the success percentage. Data presented as mean ± SEM.

for the tracing experiment. The difference was that this time, the viral constructs injected were AAV2-CMV-rtTAV16 at spinal segment sC3 unilaterally and HiRet-Lenti-EGFP.eTeNT at segment sC7 bilaterally. This way, we would silence all neurons from the sC3 hemicord corresponding to the preferent paw of the animal that project to sC7 ipsilaterally and contralaterally. These neurons would be the only ones that, in the presence of Dox, would express enhanced tetanus neurotoxin, which would prevent vesicle exocytosis and neurotransmission. After Dox is cleared from the animal's body, the silencing would be reverted. A representative spinal cord section showing GFP$^+$ neurons, which would be potentially inactivated by Dox, can be found in Figure 39.

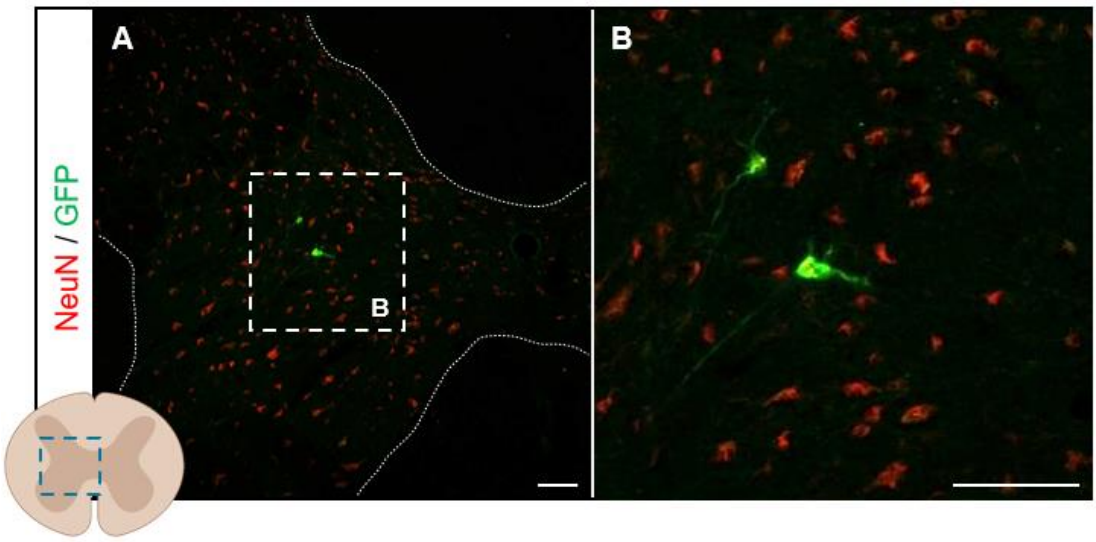

Figure 39. Silencing vectors injection. (A) Representative image of double-infected (GFP^+) neurons ($NeuN^+$) with viral vectors injected at spinal sC3 and at sC7, indicating potential silencing. **(B)** Amplification of region of interest showing two GFP^+ neurons. Scale bars: 100 µm.

Inactivation of sC3-to-C7 projecting neurons did not perturb forelimb R&G or locomotor functions

Forelimb skilled function and locomotor capacity were evaluated before the surgeries (Baseline) and two weeks after the viral injections before Dox administration (Pre-Dox), to rule out the possible functional impairments being a result of the surgical procedure. Then, starting four weeks after the intervention, Dox was administered in the drinking water (20 mg/ml) with 3 % sucrose solution and replenished daily. At days 5 (Dox^{ON}-D5) and 8 (Dox^{ON}-D8), when the doubly infected neurons are inactivated, the animals received behavioural testing (for more details, go to Materials and methods section).

Surprisingly, R&G success percentage was not altered in the different timepoints ($F_{(2.00, 19.96)} = 0.25$, p = ns), and stayed almost invariable in baseline (58.18 ± 6.74 %), Pre-Dox (56.18 ± 6.04 %), Dox^{ON}-D5 (58 ± 5.96 %) and Dox^{ON}-D8 (60.09 ± 7.38 %) assessments (Figure 40A). When analysing the types of error that would lead to misses in R&G attempts (Figure 40B), no statistically significant differences were found between any timepoint for any type of error (respective statistical test results for error types 2-6 of $F_{(1.40, 14.04)} = 1.12$, p = ns; $F_{(2.24, 22.38)} = 2.27$, p = ns; $F_{(2.22, 22.22)} = 0.50$, p = ns; $F_{(2.33, 23.32)} = 0.70$, p = ns; and $F_{(1.83, 18.29)} = 0.56$, p = ns). At baseline, Pre-Dox, Dox^{ON}-D5 and Dox^{ON}-D8, the most common type of error was error 5 (frequencies of

28.45 ± 4.64, 25.73 ± 4.32, 26.36 ± 4.35 and 23.64 ± 4.70 %, respectively), corresponding to the grasping phase of the movement. Further, we decided to investigate the R&G performance with higher detail, so we gave a score to 11 different components/gestures in which the R&G movement can be subdivided (Karl & Whishaw, 2011). A normal gesture is given a score of 0, a slightly abnormal but recognisable gesture is given a score of 1, and an absent or completely abnormal gesture is given a score of 2 (Figure 40C). Most of the gestures did not show a significant impairment between timepoints (orient: $Q_{(3)} = 5.84$, p = ns; limb lift: $Q_{(3)} = 6.03$, p = ns; digits close: $Q_{(3)} = 5.24$, p = ns; aim: $Q_{(3)} = 5.50$, p = ns; digits open: $Q_{(3)} = 0.88$, p = ns; pronation: $Q_{(3)} = 0.61$, p = ns; supination I: $Q_{(3)} = 1.76$, p = ns; release: $Q_{(3)} = 5.39$, p = ns). Interestingly, there was a significant change in the forepaw advance gesture ($Q_{(3)} = 7.99$, $p < 0.05$), but the only difference observed with multiple comparisons was between the Dox^{ON}-D5 and Dox^{ON}-D8 ($p < 0.05$) evaluations, not with the baseline timepoint. Similarly, "supination II" component was altered ($Q_{(3)} = 9.79$, $p < 0.05$), and post hoc comparisons revealed an impairment between Pre-Dox and Dox^{ON}-D5 assessments ($p < 0.05$). Last, there were significant differences regarding the grasping gesture ($Q_{(3)} = 8.68$, $p < 0.05$), specifically and increased score (which correlates with a worse performance) from baseline to Dox^{ON}-D5 ($p < 0.05$). Nonetheless, these differences might be considered circumstantial and do not alter the global observation, which is that the ability to execute the R&G movement was not altered in this experiment, neither by the surgical intervention or by the inactivation of sC3-to-C7 projecting neurons during 8 days of Dox administration.

Last, forelimb locomotor function was evaluated. Starting with the preferent paw, nor stride length (260.01 ± 8.07 mm at baseline vs 261.29 ± 5.70 mm at Dox^{ON}-D5 and 257.51 ± 4.49 mm at Dox^{ON}-D8; $F_{(1.56, 15.51)} = 0.11$, p = ns), swing time (baseline of 0.19 ± 0.01 s vs 0.20 ± 0.01 and 0.19 ± 0.01 s at Dox^{ON}-D5 and Dox^{ON}-D8, respectively; $F_{(1.39, 13.89)} = 0.16$, p = ns) or instantaneous speed (baseline of 139.20 ± 8.02 cm/s vs 135.68 ± 5.84 and 135.21 ± 4.95 cm/s at Dox^{ON}-D5 and Dox^{ON}-D8, respectively; $F_{(1.42, 14.24)} = 0.14$, p = ns) were altered with Dox administration (Figures 41A, C, E). The same results were obtained for the non-preferent paw (stride length: $F_{(1.44, 14.42)} = 0.33$, p = ns; swing time: $F_{(1.81, 18.13)} = 0.04$, p = ns; instantaneous speed: $F_{(1.66, 16.56)} = 0.10$, p = ns) (Figures 41B, D, F). Thus, silencing sC3-to-C7 interneurons did not significantly impair locomotion.

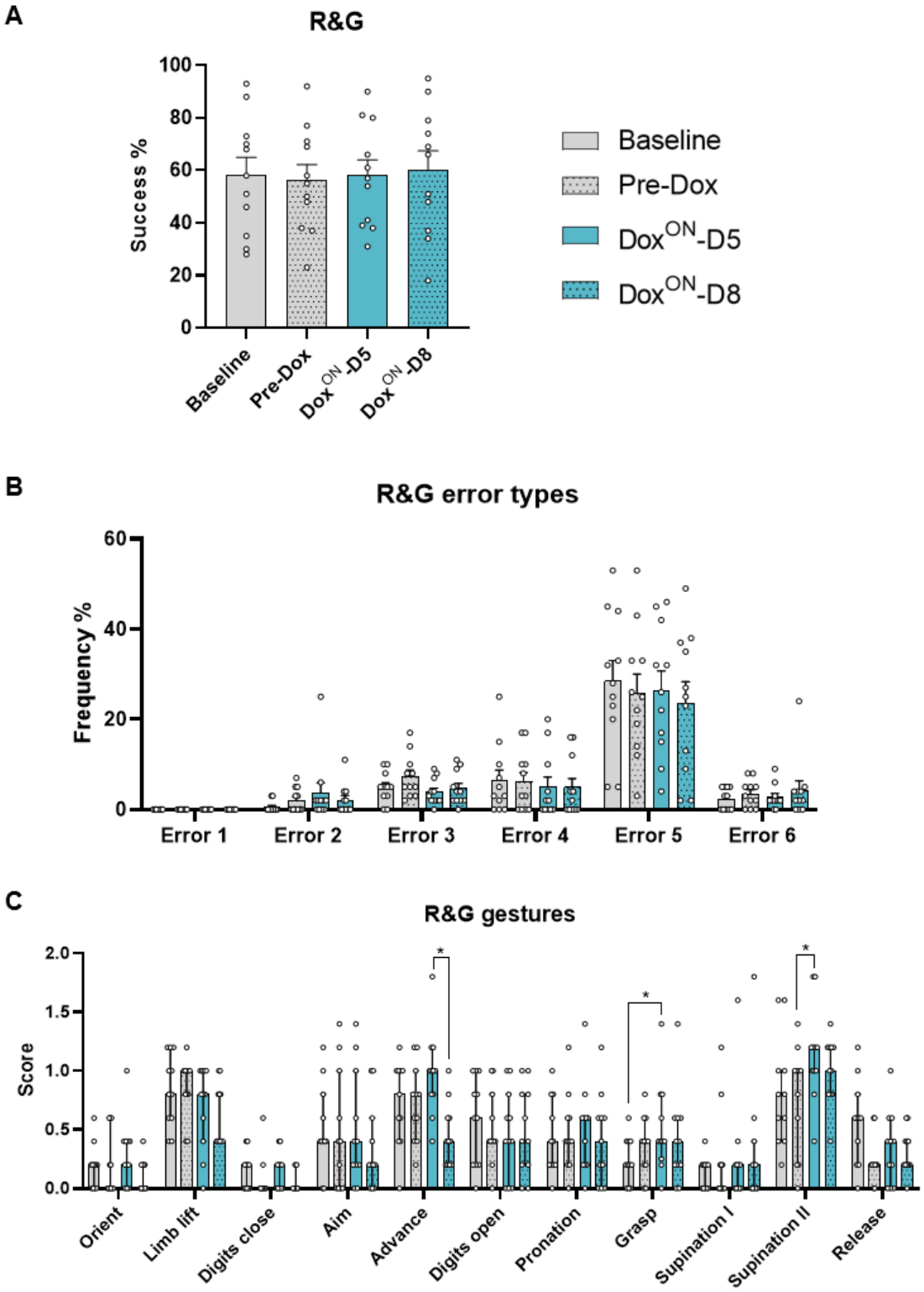

Figure 40. R&G results. R&G ability was assessed in detail, including **(A)** success percentage, **(B)** types of error and **(C)** R&G movement components/gestures. Performance of animals (n = 11) was compared at different timepoints: Baseline, Pre-Dox, Dox^{ON}-D5 and Dox^{ON}-D8. * $p < 0.05$; as calculated by one-way ANOVA followed by Tukey's multiple comparisons test (when a Gaussian distribution of residuals was present), or by Friedman's nonparametric test followed by Dunn's multiple comparisons test (when the data did not follow a normal distribution). Gaussian data is shown as mean ± SEM, and non-Gaussian data is presented as median ± interquartile range.

Altogether, the inactivation of sC3-to-C7 projecting neurons failed to elicit a phenotypic change in terms of forelimb function detriment either on skilled reaching or on unskilled overground locomotion. Notably, the number of neurons projecting to sC7 from sC3 was relatively low. These observations suggest that the results from kainic acid injections at vC2 (~ sC3) and vC2-C3 (~ sC3-C4) were not mediated by the excitotoxicity on these cells. Rather, the sC3 neurons required for R&G execution might be projecting downstream to other spinal segments of the cervical enlargement and/or upstream to supraspinal motor control centres such as the brainstem or the cerebellum. Further investigation will be needed to elucidate the concrete organisation of this network.

(Figure on the next page)

Figure 41. Locomotion results. (A-B) Stride length, **(C-D)** swing time and **(E-F)** instantaneous speed of both **(A, C, E)** preferent and **(B, D, F)** non preferent forepaws were used as the parameters to test locomotor function in rats from silencing experiment. Performance of animals (n = 11) was compared at different timepoints: Baseline, Dox^{ON}-D5 and Dox^{ON}-D8. No significant differences ($p > 0.05$) were found between timepoints with repeated measures one-way ANOVA. Data presented as mean ± SEM.

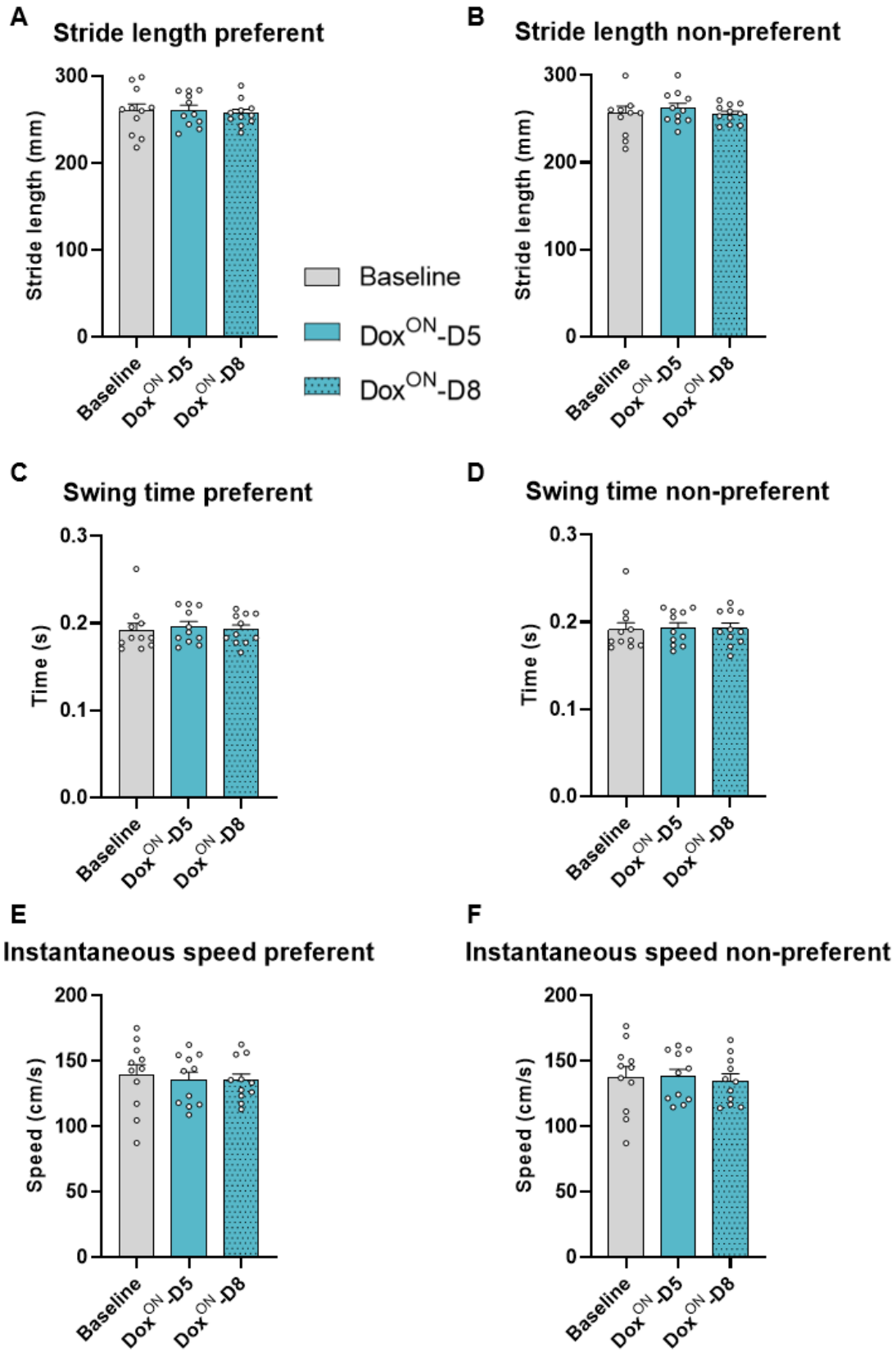
A
Stride length preferent
Stride length (mm)
300
200
100
0
Baseline
Dox ON -D5
Dox ON -D8
B
Stride length non-preferent
Stride length (mm)
300
200
100
0
Baseline
Dox ON -D5
Dox ON -D8
Baseline
Dox ON -D5
Dox ON -D8
C
Swing time preferent
Time (s)
0.3
0.2
0.1
0.0
Baseline
Dox ON -D5
Dox ON -D8
D
Swing time non-preferent
Time (s)
0.3
0.2
0.1
0.0
Baseline
Dox ON -D5
Dox ON -D8
E
Instantaneous speed preferent
Speed (cm/s)
200
150
100
50
0
Baseline
Dox ON -D5
Dox ON -D8
F
Instantaneous speed non-preferent
Speed (cm/s)
200
150
100
50
0
Baseline
Dox ON -D5
Dox ON -D8

VII. Discussion

Manual dexterity is essential to conduct the vast majority of our daily tasks, ranging from object manipulation to nonverbal communication. These movements rely on fine motor control to make precise adjustments. Achieving a high level of dexterity requires the coordinated function of multiple neural systems, including visual areas for eye-paw coordination, motor cortices, the corticospinal tract, and descending pathways originating in the brainstem. These systems converge in the grey matter of the cervical spinal cord segments (Karl & Whishaw, 2013; Isa, 2019).

This thesis explored the contribution of the spinal cord to forelimb skilled function, with a particular focus on R&G movement due to its preservation across species, its high translational relevance and its essential role in daily activities. While traditionally considered a movement controlled primarily by supraspinal structures, we hypothesized that spinal interneurons play a crucial role in coordinating R&G execution. To address this, we employed a multimodal approach combining targeted spinal lesions, neuronal activation mapping, and functional inactivation experiments.

First, we identified a candidate spinal region necessary for R&G by inducing excitotoxic lesions in different cervical segments using kainic acid, a glutamate receptor agonist that selectively damages spinal grey matter while preserving axonal tracts. Rats injected at vC2 and vC2-C3 (corresponding to sC3 and sC3-C4, respectively) exhibited selective impairments in R&G, whereas lesions at other segments did not produce functional deficits. These impairments were specific to R&G and other forelimb movements with a strong reaching component, as tasks requiring fine motor control but lacking a reaching phase (e.g., food manipulation) remained unaffected.

Next, we ruled out the possibility that the observed impairments were due to motoneuron or sensory neuron loss rather than interneuron dysfunction. To do so, we performed dorsal and ventral root sectioning of the identified segments (sC3 and sC3-C4), thus eliminating motor output and sensory input while sparing intrinsic spinal networks. The fact that these animals retained normal R&G function indicates that the deficits observed after kainic acid injections were due to interneuron loss, reinforcing the idea that a spinal network at sC3 contributes to R&G control.

To further explore the role of spinal interneurons in R&G, we assessed neuronal activation in intact animals performing R&G or locomotion by quantifying IEG expression in the cervical spinal cord. We hypothesized that if a dedicated R&G

network existed, it would exhibit localized activation. Instead, we observed a broader, more distributed activation pattern spanning sC2-C5, with a tendency for increased activation in animals subjected to prolonged R&G training. This suggests that instead of refining into a discrete R&G-specific network, the recruitment of spinal interneurons expands with practice, potentially reflecting neuroplasticity mechanisms.

Finally, we investigated whether sC3 interneurons contribute to R&G by transmitting motor commands downstream. We reversibly silenced sC3-to-C7 projecting interneurons, a population hypothesized to mediate direct spinal control over distal forelimb movement. However, this inactivation did not disrupt R&G or locomotor function. While this could indicate that sC3 interneurons do not directly control R&G execution, the interpretation is limited by methodological constraints. Factors such as incomplete silencing, compensatory mechanisms, or functional redundancy may have masked an effect. Thus, rather than refuting the presence of a spinal network involved in R&G, these results highlight the complexity of spinal-supraspinal interactions and suggest that sC3 interneurons may contribute to R&G in a modulatory rather than a strictly executive role.

In summary, our findings indicate that a spinal network located at sC3 is necessary for the proper execution of R&G movements. Furthermore, they demonstrate that the motor cortex and other brain structures are necessary, but not sufficient, to control forelimb skilled function. This challenges the traditional view that the spinal cord merely transmits motor commands from the brain and underscores its role in skilled forelimb function. These insights advance our understanding of fine motor control and hold translational potential for optimizing neuromodulatory strategies aimed at restoring upper limb function in spinal cord dysfunction.

A two-hypotheses scenario

The R&G movement begins with a quick elbow bend, followed by the coordinated extension of both the shoulder and the elbow. As the forepaw lifts and moves forward, it tilts upward, and the fingers come together. Next, the fingers spread apart and curl to capture the object or food, depending on the case. After securing the item, the forepaw rotates outward during the withdrawal phase before being guided to the

mouth (Alstermark *et al.*, 1981). Moreover, stereotypic features of these forelimb movements suggest that some level of control may be exerted from the spinal cord. Traditionally, however, it has been considered that the correct execution of manual dexterity movements primarily depends on the brain, mainly on the motor cortex, and the spinal cord would "merely" be the substrate for the information to be transmitted from the brain to the muscle (Holmes, 2017). As of today, however, the responsibility of the spinal cord for the correct execution of this evolutionary conserved behaviour is still not fully understood. There are two main hypotheses in that regard, which will be detailed below.

First, there could be a specific compartment or region within the spinal cord containing a neuronal network, formed by interneurons, that would be responsible for the coordination of R&G. This would correlate with research that indicates that certain movements correspond to specific spinal cord levels (Takei & Seki, 2010; Alstermark *et al.*, 2011), underscoring the grey matter's role in supporting control exerted by the corticospinal tract and other descending pathways. Remarkably, for locomotion, many studies have described the presence of intrinsic spinal networks that generate the coordinated muscle activity associated with stereotypic limb movements during stepping, which have been named CPGs (Magnuson *et al.*, 2005). In rodents, the hindlimb locomotion CPG is discretely located at spinal cord lumbar segments sL1-L2 (Cazalets *et al.*, 1995; Kiehn, 2006). Injuring these segments typically eliminates or significantly disrupts locomotion (Rossignol & Frigon, 2011). Therefore, the first hypothesis consists of the existence of a CPG-like circuit located in a specific segment/s within the spinal cord for R&G control. The activation of this circuit would initiate the downstream coordinated execution of a full complex action command for R&G.

An alternative possibility is that the interneurons playing a role in the control of R&G are distributed along the spinal cord, following a segmental distribution, as the motoneurons do. The collection of motoneurons that produce the contraction of a specific muscle are named motor columns. Limb motor columns present a rostrocaudal-proximodistal organization in the spinal cord. That is, proximal limb muscles are innervated by motoneurons located at rostral spinal cord segments, whereas caudally situated motoneurons control distal limb muscles (McKenna *et al.*, 2000). It would be coherent that the interneurons that coordinate the action of these

motoneurons would follow the same type of distribution, in a way that the motor column of a given muscle would parallel an overlapping column of interneurons governing it. Thus, R&G would be the result of the sum of multiple related, though considerably independent, small subphases of the movement earlier described (elbow flexion, shoulder extension, digit opening, etc).

The following sections of the discussion will explore whether our results support either of these two hypotheses.

Model validity of R&G in rats

Numerous mammalian species, such as non-human primates, cats, dogs, pigs, mice and rats, have been utilized in experimental research on the spinal cord and SCI. Non-human primates are evolutionarily closer to humans. However, conducting studies with non-human primates is limited to a small number of research facilities due to their high cost and the considerable ethical challenges involved. Thus, cats were historically favoured as subjects for experimental spinal cord research because their spinal cord closely resembles that of humans in both diameter and length. While cats are often considered to have limited finger dexterity, they demonstrate skilled forelimb and paw movements during prey hunting (Krisa *et al.*, 2018).

Fast forward, rodents are now the most widely used species in experimental spinal cord research due to their accessibility, simple care requirements and reduced financial and ethical constraints (Krisa *et al.*, 2018). Moreover, mouse models offer the advantage of genetic engineering, enabling the investigation of molecular and cellular changes after spinal cord interventions (Krisa *et al.*, 2018). Meanwhile, rats share a closer genetic similarity to humans compared to mice and can be trained to carry out behavioural tasks essential for evaluating fine motor skills (Mondello *et al.*, 2018). Thus, rats serve as valuable models for studying fine motor skills that resemble those of humans, including R&G (Krakauer *et al.*, 2012). Despite some species-specific differences between rodents and primates, particularly in the capacity of fractionated finger movements, the hand and arm movements involved in R&G objects are generally conserved, and a variety of functional tests are available to evaluate forelimb use in rodent models (Whishaw *et al.*, 2010).

Of note, a key distinction exists in the corticospinal tract, which plays a dominant role in fine motor control in primates but is less direct in rodents. In primates, the CST establishes monosynaptic connections with forelimb motor neurons, enabling independent finger movements and precision grips (Lawrence & Kuypers, 1968; Lemon, 2008). In contrast, rodents lack direct cortico-motoneuronal projections, relying instead on multi-synaptic circuits via propriospinal and reticulospinal pathways to execute skilled forelimb movements (Alstermark & Isa, 2012; Zaaimi *et al.*, 2012). This alternative motor control architecture suggests that rodents might rely more on spinal circuitries to coordinate forelimb movements, which aligns with our findings pointing to an important spinal segment, sC3, in R&G control. However, this does not necessarily mean that a similar spinal circuit is not crucial for R&G in primates, as it could still play a fundamental role alongside the more dominant corticospinal pathways. Despite the fact that humans are bipedal and rodents are quadrupedal animals, it must be noted that all non-human primate species are exclusively or predominantly quadrupedal as well. Moreover, humans still retain spinal circuits that may contribute to automatic forelimb control, particularly in rhythmic or cyclical movements such as arm swinging during locomotion (Dietz, 2002; Zehr & Duysens, 2004). Studies have shown that under certain experimental conditions, rhythmic arm movements can be evoked in humans without cortical input, indicating that propriospinal circuits in the cervical spinal cord can function independently to generate coordinated arm movements (Jankowska & Edgley, 2006). This raises an intriguing question: could the spinal networks we identified in rodents represent an evolutionary conserved system, potentially serving as a substrate for automatic or subcortically driven components of R&G in humans? This idea aligns with the theory that targeted reaching may have evolved from more ancestral rhythmic behaviours such as scratching or digging, which are known to rely on spinal pattern generators (Kiehn, 2016).

Taken together, these arguments provide strong construct validity for the rat model in investigating spinal contributions to R&G, as it shares core motor mechanisms with primates despite the differences in corticospinal organization. Furthermore, the predictive validity of the model is supported by its potential to inform neuromodulatory and rehabilitative strategies for restoring upper limb function in humans, particularly through targeted stimulation of specific spinal segments (see discussion below). If sC3 in rats plays a crucial role in forelimb control, its functional

equivalent in humans could represent a promising therapeutic target for interventions aimed at improving dexterity after SCIs or other motor impairments.

Identification of a sC3 spinal circuit for R&G through excitotoxic lesions

Understanding the spinal cord's role in mediating or generating upper limb movement patterns necessitates elucidating whether or not there are key segments involved in these motor behaviours and, if so, identifying them. To explore these possibilities, we opted to use a functional mapping approach based on loss of function. The idea was to clarify how injuries at different levels of the cervical spinal cord correlate with specific functional impairments. Most studies investigating forelimb function and cervical injuries use compressive or contusion models that affect both spinal grey and white matter, making it difficult to distinguish functional losses caused by spinal circuit damage from those due to pathway disruption (Kjell & Olson, 2016; Verma *et al.*, 2019). Here, we inflicted unilateral excitotoxic injuries to rats at different spinal cord levels covering from sC2 to sT2 using kainic acid, as this compound has been shown to almost exclusively affect the grey matter (which contains the spinal networks and neuronal somas) while preserving the white matter and therefore the descending commands (Pisharodi & Nauta, 1985; Magnuson *et al.*, 1999). A major benefit of this model is its capacity to directly connect specific tissue damage to behavioural changes. This way, when damage at a specific level results in deficits in hand skilled function, it will be possible to conclude that neurons importantly involved in the movement are located there.

In a first experiment, four groups were established based on the cervical segments targeted by kainic acid injections: vC3, vC5, vC7 and vT1. As expected, histological analyses revealed a grey matter loss that correlated with the segments of injection in terms of location, extent and severity (Figure 14), and which was presumably accompanied by the loss of spinal premotor circuits. Regarding white matter, some authors have reported a possible kainic acid detrimental effect (Matute *et al.*, 2007; Nishida *et al.*, 2015). Conversely, as Magnuson *et al.*, 1999, we did not detect a significant impact on the white matter by these injections (Figure 15). Motor deficits were evaluated by comparing the performance, before versus after the intervention, in

a variety of behavioural tests: R&G (Whishaw *et al.*, 2008), staircase (Montoya *et al.*, 1991), food manipulation (Irvine *et al.*, 2014), and overground locomotion on a walking track (Lakes & Allen, 2016), among others. These tests likely engage distinct neuronal networks despite recruiting the same forelimb muscles. Notably, we have not identified any other study incorporating as many functional assessments as the present one (Figures 16-17). If the hypothesis of a segmental distribution of interneuron columns throughout the spinal cord were correct, we would expect that kainic acid injections at different spinal levels would selectively disrupt specific movement phases while preserving others. Surprisingly, none of the experimental groups exhibited significant forelimb functional deficits. We interpreted this outcome as a consequence of the injections affecting an insufficient number of neurons or grey matter area when restricted to a single spinal segment.

To further investigate the potential involvement of spinal circuits in R&G control, we conducted a second experiment with a new cohort of animals. This time, kainic acid was injected into two consecutive spinal segments to expand the lesion area: vC2-C3, vC4-C5, vC6-C7, and vT1-T2. Additionally, a fifth group received vehicle injections at vC2-C3, serving as a control to account for any effects of the surgical procedure itself and ensure that observed outcomes in the experimental groups were attributable solely to kainic acid. As in the previous experiment, grey matter area was progressively reduced, with the most pronounced decrease occurring at the injection epicentre. Notably, the rostrocaudal extension of the lesion increased from approximately 6 mm (in single-segment injections) to 8 mm in this experiment. Importantly, white matter remained unaffected (Figures 18-19). The grey matter reduction was accompanied by a loss of neurons in all of the dorsoventral Rexed laminae, especially in the intermediate ones (Figure 20).

Immunostaining for GFAP and Iba1 confirmed that kainic acid-induced excitotoxic injury was associated with a pronounced astroglial and microglial response, characterized by astrogliosis and reactive microglia, respectively (Figure 21). This activation is consistent with the fact that both astrocytes and microglia express AMPA receptors (Zanuzzi *et al.*, 2019), making them susceptible to excitotoxic damage. Consequently, while our study primarily aimed to assess the impact of excitotoxic lesions on spinal neuronal networks, it is important to consider the potential contribution of astroglial and microglial reactivity to the observed

functional outcomes. This neuroinflammatory response could modulate synaptic plasticity, affect neuronal survival, or influence recovery processes, thereby playing a role in shaping the effects of the lesion beyond direct neuronal loss.

In this second batch of experiments, a notable drawback was the development of oedema in the 2nd and 5th fingers in some animals from the vC4-C5 and vC6-C7 groups, respectively, as a result of excessive licking and self-grooming behaviours. This phenomenon was likely triggered by excitotoxic damage affecting the forelimb dermatomes (Figure 22). To mitigate this effect, we administered amitriptyline, but it did not prevent the excessive self-grooming observed in affected animals. Given that sensory disturbances could introduce a confounding factor in the interpretation of motor deficits, we assessed forelimb sensory function using the adhesive removal test, which measures the time required to detect and remove an adhesive tape from the palm. Encouragingly, none of the experimental groups exhibited delayed detection times following kainic acid injections, suggesting that forepaw tactile sensitivity remained intact. However, it is important to note that excitotoxic models have been associated with the development of mechanical allodynia (Nakae *et al.*, 2011), raising the possibility that animals experienced altered sensory processing, which may have influenced their behaviour despite normal detection times.

We then proceeded with the forelimb motor function assessments described previously, incorporating two additional tests: grid R&G, which eliminates the need for forepaw protraction and overcoming gravity, and the horizontal ladder test ladder (Whishaw *et al.*, 2010; Verma *et al.*, 2019), which evaluates skilled locomotion by requiring animals to traverse irregularly spaced rungs.

Starting with the vT1-T2 group, no deficits were observed in any of the behavioural tests (Figures 23-24). In contrast, animals from the vC4-C5 and vC6-C7 groups, which exhibited signs of finger paraesthesia, showed a reduction in forepaw width during locomotion, likely due to oedema affecting the digits. Rats from the vC6-C7 group, which developed oedema in the 5th finger, showed a non-significant tendency toward impairment in R&G and food manipulation tests. However, in the vC4-C5 group, where the oedema was located in the 2nd finger, a digit with greater relevance for dexterous movements than the 5th, the tendency for impairment reached statistical significance in R&G from a platform, R&G from a staircase, and cereal manipulation. This could be explained by the biomechanical limitation imposed by

the extensive 2nd finger oedema, as R&G success percentage reduction in those animals correlated with a significant increase in the frequency of error type 5, where the pellet is lost during the flexion phase of the digits, at 14DPI.

Despite these results, animals from the vC2-C3 group were the only ones that consistently exhibited significant impairments in forelimb skilled function at both 7 and 14 DPI, specifically in R&G from a platform, R&G from the bottom of a grid, and the horizontal ladder test, which involves a relevant R&G movement component. The decrease in performance was severe, and R&G capacity was almost completely abolished. This correlated with a significant increase in error types 1 and 2, which correspond to errors in the earliest phases of the movement, where the forepaw is unable to cross the window or does not advance far enough to reach the pellet.

It is important to consider that despite the severity of the deficits observed in vC2-C3 animals, the excitotoxic injury was relatively small and well-localized, affecting only the ipsilateral hemicord across two spinal segments, with a rostrocaudal extension of around 8 mm, and reducing grey matter by a maximum of 40% at the injury epicentre. The contralateral hemicord, white matter, and the supraspinal structures involved in movement control, such as the brain, brainstem, and cerebellum, remained intact. Additionally, forelimb motoneurons are located at sC5-T1, distal and caudal to the affected sC2-C3 segments, yet the most pronounced R&G deficits occurred when the lesion was placed at sC2-C3, further supporting the existence of a spinal network in this region that is crucial for initiating or coordinating these movements. Moreover, while the vC4-C5 and vC6-C7 groups suffered from finger oedema, which could partially explain some of their impairments, vC2-C3 animals did not exhibit such biomechanical constraints, confirming that their deficits were due to the disruption of spinal circuits rather than peripheral alterations. Interestingly, their stride length during locomotion was also mildly reduced, which could indicate difficulties in forepaw targeting. However, their performance in other skilled and unskilled tasks that did not involve R&G remained unaffected, reinforcing the specificity of the injury for R&G and R&G-related movements. Finally, animals that received vehicle injections at vC2-C3 did not show significant impairments, confirming that the observed deficits in the experimental groups were due to the excitotoxic lesions themselves and not to the surgical procedure.

We then focused on the candidate spinal cord segments, vC2 (~ sC3) and vC3 (~ sC4), to further refine the localization of the neuronal network responsible for R&G. At this stage, it remained unclear whether the impairments observed in the vC2-C3 group were primarily due to the effect of kainic acid at vC2 or whether they resulted from the combined impact on both vC2 and vC3. This distinction was critical, as our previous results had already demonstrated that kainic acid injections confined to vC3 alone did not impair forelimb function. To address this, we conducted a new experiment in which kainic acid or vehicle was injected exclusively into vC2. Surprisingly, the results were drastically different from those observed in the vC3 group (Figures 23-24). Rats with excitotoxic lesions at vC2 lost the ability to perform any successful R&G attempts, both from a platform and from the bottom of a grid. This strongly suggests that the neurons responsible for coordinating these movements are located at vC2 (i.e., sC3). Importantly, sensory function and food manipulation remained unaffected, indicating that the observed deficits were specific to R&G and related movements. Notably, the impairments in the vC2 group were even more pronounced than those observed in rats with lesions spanning both vC2 and vC3. This may be due to a more targeted effect of kainic acid, resulting in a higher concentration of neuronal loss within the critical region. Another consideration is that kainic acid injections at vC2 tended to slightly affect not only sC3 but also sC2, which raises the possibility that sC2 might also be involved in this putative spinal network. However, directly targeting sC2 remains a significant technical challenge due to its compromised anatomical accessibility. Finally, although rats from the vC2-C3 group had lesions extending into vC3, the absence of functional deficits in the vC3-only group suggests that interneurons at this segment are not essential for the correct execution of R&G and R&G-related movements. This further reinforces the idea that sC3 plays a pivotal role in the spinal control of forelimb dexterity.

Importantly, the injection of kainic acid not only damaged the interneurons from the spinal cord segment injected but was also accompanied by a reduction in the number of motoneurons preserved at the level of injection (Figure 27). It is important to remind that our objective with the injections of kainic acid was to damage the upstream neuronal network needed for the R&G movement, which would be formed of interneurons, but we aimed to preserve the motoneurons as much as possible. In fact, one of the reasons we chose kainic acid as the excitotoxic compound for our experiments was that it shows preference for interneurons over motoneurons (Urca

& Urca, 1990). Obviously, if the effector neurons responsible for the contraction of a specific muscle are lost, the muscle would not be able to function. So, if the motoneurons that innervate forelimb muscles are eliminated, the R&G movement will not be able to take place. Two considerations must be made with that respect. First, there was a reduction (and not a complete ablation) in the number of motoneurons, and the minimum number of motoneurons needed to correctly perform the R&G movement is unknown, so the preserved motoneurons could be enough to execute the movement. In fact, it is well known that only a subset of all motor units of a given muscle are recruited to obtain enough contraction force for most daily activities. Moreover, it has been reported in a mouse model of ALS, the most frequent form of motoneuron diseases, that motoneuronal loss was evident at timepoints where no behavioural impairments were detectable yet (Mancuso *et al.*, 2011). Second, even if the percentage of preserved motoneurons was not enough, we must consider that the motoneurons that innervate forelimb muscles are located more caudally than vC2 (~ sC3) in the spinal cord (the cervical enlargement expands from sC5-T1 approximately (McKenna *et al.*, 2000)), so we would be affecting neck and not forelimb movements.

Spinal root sectioning confirms sC3 interneurons as key players in R&G control

To further validate our hypothesis, we conducted an additional experiment aimed at ruling out the possibility that the observed behavioural deficits were due to the partial loss of motoneurons and/or sensory feedback, rather than the disruption of an interneuronal network responsible for R&G control. To achieve this, we performed a unilateral surgical section of both the dorsal and ventral roots of the spinal segment sC3, corresponding to the dominant forelimb of each animal. This approach ensured the complete elimination of direct sensory afferences and motor efferences from the affected segment while preserving the integrity of the spinal grey matter and its interneuronal networks. If the animals subjected to this procedure retained their ability to perform R&G and R&G-related tasks, it would strongly indicate that the impairments observed following kainic acid injections were not due to the loss of motoneurons or sensory neurons but rather to the excitotoxic lesioning of interneurons.

Despite the clear rationale behind this experimental approach, its practical implementation proved to be highly challenging. The surgical procedure, particularly the precise sectioning of the ventral roots at such a rostral spinal level, required meticulous execution to avoid unintended damage to surrounding structures. To ensure the reliability of our results, we established rigorous selection criteria: only animals that exhibited no secondary damage during surgery, anatomical dissection, or histological analysis were included in the final functional and histological assessments. As predicted by our hypothesis, animals that underwent successful sectioning of the sC3 roots did not exhibit impairments in R&G tasks, including food pellet retrieval from an elevated platform, from the bottom of a grid, or from different steps of a staircase (Figures 28-29). Their performance in other forelimb functional tests, such as adhesive removal, food manipulation, and overground locomotion, also remained intact. These findings provided strong evidence supporting the presence of a dedicated spinal interneuronal network at sC3 that is essential for manual dexterity.

Nevertheless, one could argue that despite successfully demonstrating that sC3 motoneurons and sensory afferences were not responsible for the deficits observed following kainic acid injections, there remained a minor caveat. Specifically, while kainic acid injections at vC2 (~ sC3) were predominantly localized to sC3, some mild diffusion into the most rostral part of sC4 was observed. This raised the possibility that our root-sectioning experiment, which exclusively targeted sC3, might not have fully validated our biological interpretation. However, it is crucial to highlight that previous experiments had already demonstrated that kainic acid injections limited to vC3 (~ sC4) alone did not result in forelimb dysfunction.

To further strengthen our hypothesis and address this concern, we performed an additional root-sectioning experiment in which we surgically transected both the dorsal and ventral roots of segments sC3 and sC4 in a new group of animals. Similar to the previous root-sectioning experiment, this procedure presented significant technical challenges, and only animals that met strict selection criteria were included in the analysis. In retrospect, performing the root sectioning at the postganglionic rather than preganglionic level may have facilitated the procedure and reduced the number of excluded animals. Notably, even after bilateral root sectioning at both sC3 and sC4, animals retained their ability to execute all skilled and non-skilled forelimb movements with the same proficiency as before the intervention (Figures 26-27).

These results confirm that the neurons within sC3 (and potentially sC4) involved in manual dexterity are neither motoneurons nor sensory neurons, reinforcing our hypothesis that a dedicated interneuronal network exists at this spinal level.

Of note, previous studies have reported motoneuron loss following spinal root sectioning in rodents (Gaja-Capdevila *et al.*, 2021, 2022). However, in our experiment, motoneuron preservation in the affected segments was comparable to control animals (data not shown). It is possible that the discrepancies between our results and those of prior studies stem from differences in the distance between the site of the section and the location of the neuronal somas. Neuronal susceptibility to axotomy-induced cell death is known to depend on the proximity of the injury to the soma, with longer distances generally resulting in reduced neuronal degeneration. The aforementioned studies were conducted in mice, where the distance between the soma and the lesion site is smaller than in rats, which could account for the observed differences. Even if there were an undetected loss of motoneurons in our model, or if surviving motoneurons exhibited morphological alterations, the absence of functional deficits in our animals following root sectioning strongly supports our hypothesis that sC3 interneurons, rather than motoneurons, are crucial for the execution of R&G movements.

Neuronal activation patterns (IEG expression) support sC3 involvement but not only it

After identifying spinal segment sC3 as a key region containing a neuronal network necessary for the correct execution of R&G, we aimed to further investigate the neuronal populations involved. While kainic acid injections were instrumental for our functional mapping study, they did not allow for precise characterization of the specific neuronal subtypes or their localization within spinal laminae, as excitotoxicity leads to neuronal death. To overcome this limitation, we sought to obtain a more refined activation map of cervical spinal cord neurons in intact animals during R&G and locomotor movements, using IEGs as markers of neuronal activity. IEGs are rapidly and transiently activated in response to calcium influx into neurons and are widely used as indicators of neuronal activation (Yap & Greenberg, 2018). Among them, c-Fos was the first to be discovered (Greenberg & Ziff, 1984) and remains the most commonly used. The earliest applications of IEG-based activity

mapping in the spinal cord focused on nociception (Presley *et al.*, 1990), and subsequent studies extended this approach to identifying neurons activated during locomotion (Jasmin *et al.*, 1994; Ahn *et al.*, 2006). More recently, IEGs have been employed to study neuronal activity in other spinal functions, such as micturition (Wiedmann *et al.*, 2021). Based on these precedents, we selected two IEGs, c-Fos and FosB, to investigate the activation pattern of spinal neurons in response to different forelimb tasks. FosB, and particularly its ΔFosB isoform, exhibits cumulative and stable expression following repeated neuronal activation (Hiroi *et al.*, 1998; Nestler, 2015). This makes it an ideal marker for identifying neuronal populations that are recurrently engaged during behavioural training sessions, complementing the more transient activation detected by c-Fos. Thus, if we identified clusters of neurons that were specifically activated in R&G-performing rats but not in other groups, we could infer their involvement in R&G execution and their potential contribution to the underlying neuronal network, even though R&G and locomotion recruit similar forelimb muscles.

To address this question, Long Evans rats were divided into four experimental groups: (1) an "early R&G training" group, perfused at the peak of their learning process; (2) a "late R&G training" group, perfused once their performance had plateaued; (3) a treadmill locomotion group, performing a forelimb task distinct from R&G; and (4) a "no reaching" control group, where rats were exposed to the R&G chamber without performing the task, with food pellets placed on the floor instead. This experimental design allowed us to compare the neuronal activation pattern of cervical spinal cord segments across intact animals performing R&G, locomotion, and baseline conditions without forelimb-specific activity. The division of the R&G groups was based on the assumption that neuronal networks exhibit plasticity throughout learning and that task-specific networks may become more refined as training progresses. We hypothesized that animals in the "early R&G" group, still actively improving their performance, would exhibit a broader, more dispersed activation pattern, whereas animals in the "late R&G" group, having reached a stable proficiency, would show a more spatially restricted pattern. The inflection point between these two learning stages was defined as the first day a rat successfully retrieved ≥ 60 pellets with a success rate of ≥ 40 % from a minimum of 150 attempts. Importantly, the learning curves of both R&G groups were equivalent (Figure 28), ensuring that differences in

neuronal activation were not confounded by variations in learning speed. All animals were perfused 90–120 minutes after their final training session, the time window in which c-Fos expression is expected to peak.

A major challenge in this experiment was the suboptimal tissue preservation in a substantial number of animals, which posed a risk of confounding results. Following discussions with other lab members, it was suspected that buffer degradation during the processing steps may have been responsible. To mitigate this issue, we assessed tissue integrity via NeuN immunostaining, allowing us to identify and exclude poorly preserved samples (Figure 31). Unfortunately, this led to the exclusion of a significant number of animals (22 out of 40). Nonetheless, we proceeded with the remaining samples, quantifying IEG expression rostrocaudally (from sC2 to sT3) and dorsoventrally (across Rexed laminae) within and between experimental groups. Interestingly, no significant differences in c-Fos or FosB expression were observed between left and right hemicords or between preferred and non-preferred paws (Figure 33). This result was expected for the locomotion and "no reaching" groups but was somewhat surprising for R&G-trained animals, given the unilateral nature of the task. Consequently, for subsequent analyses, we averaged IEG counts across both hemicords.

Regarding c-Fos expression, the overall number of immunopositive cells was remarkably low across all spinal cord segments, Rexed laminae, and experimental groups (Figure 34). Although statistically significant differences were found in the caudal cervical enlargement (sC8-T2), which houses motoneurons responsible for skilled forelimb control, the absolute increase in c-Fos⁺ cells in the "late R&G" group was minimal (from ~ 2 to ~ 4 neurons per segment), limiting the biological relevance of these findings.

In contrast, FosB immunostaining revealed a substantially greater number of labelled cells—approximately tenfold higher than c-Fos+ cells (Figure 33)—likely reflecting the accumulation of ΔFosB due to repeated neuronal activation. Consistent with this interpretation, rats in the "late R&G" group exhibited a fourfold increase in FosB⁺ cells throughout the cervical and rostral thoracic spinal cord compared to those in the "early R&G" group. Furthermore, rats in the "early R&G" group exhibited significantly fewer FosB⁺ cells at sC3 and sC7 compared to treadmill-trained animals, despite the latter performing a different forelimb task. Dorsoventrally, approximately 90 % of FosB⁺ cells were confined to

laminae I-IV, consistent with previous reports (Man'kovskaya *et al.*, 2014). Notably, in the "late R&G" group, the number of FosB$^+$ cells was nearly twice as high in rostral cervical segments (sC2-C5) compared to caudal cervical and rostral thoracic segments (sC6-T3). Moreover, while statistical significance was not reached in all comparisons, a trend toward increased FosB expression in rostral segments was observed across experimental groups, suggesting a potential role for these segments in R&G execution across multiple attempts and training sessions. Correlation analyses further revealed that the number of IEG$^+$ cells increased with the number of R&G training sessions and cumulative attempts, suggesting an unexpected expansion—rather than restriction—of the network with training, though further studies will be needed to validate this hypothesis.

Our findings did not fully align with our initial expectations. The low number of c-Fos$^+$ cells could be explained by several, non-mutually exclusive possibilities. First, there may be a high degree of redundancy in the spinal network, with only a small subset of neurons recruited per trial. A similar redundancy has been reported in rodent locomotion, where only ~ 20 % of neurons are consistently reactivated across repeated trials of the same motor task (Pham *et al.*, 2020). Second, neuronal heterogeneity may extend to differences in IEG transcription, meaning that distinct neuronal subtypes preferentially express different IEGs upon activation (Spiegel *et al.*, 2014; Mardinly *et al.*, 2016). For instance, motoneurons (ChAT$^+$ cells) rarely express c-Fos in response to activation (Vizzard, 2000; Wiedmann *et al.*, 2021), suggesting that additional markers such as Npas4 (Lin *et al.*, 2008) or Egr1 (Christy & Nathans, 1989) may provide a more complete picture. Third, ΔFosB has been shown to inhibit c-Fos expression, which could explain why c-Fos expression is elevated following acute activation but suppressed with chronic activity (Corbett *et al.*, 2017).

Considering our kainic acid and root-sectioning experiments, we initially expected to observe a peak of IEG$^+$ cells at sC3. While we found increased FosB expression in rostral cervical segments (including sC3), the distribution was broader than anticipated. However, previous studies offer a coherent explanation. The earliest spinal IEG studies reported that most c-Fos$^+$ cells were activated by sensory feedback rather than direct motor execution (Presley *et al.*, 1990). Moreover, locomotion studies have shown that c-Fos expression is highest in spinal segments controlling limb muscles, rather than in CPG-associated segments (Ahn *et al.*, 2006). Given that we previously demonstrated that sC3 function in R&G is

independent of sensory and motor afferences, it follows logically that c-Fos expression at this level would be limited.

Finally, the challenges faced in this experiment highlight the underutilization of IEG-based activation mapping in the spinal cord, particularly in forelimb skilled movements (Man'kovskaya *et al.*, 2014). The limitations of this approach have likely driven the adoption of alternative techniques, such as calcium imaging in behaving mice (Shekhtmeyster *et al.*, 2023) and phosphorylation-based metabolic markers like pyruvate dehydrogenase (Yang *et al.*, 2024), which may provide complementary insights into spinal circuit function.

Reversible silencing of sC3-to-C7 projecting neurons

Given the promising evidence suggesting that a neuronal network at spinal segment sC3 is essential for the correct execution of forelimb reaching, we sought to further investigate its precise role within the motor control system using a different approach. While excitotoxic lesions helped localize a functionally critical region, they did not reveal whether sC3 directly generates the movement or plays a more modulatory role. To address this, we opted for a reversible silencing strategy, enabling us to transiently inactivate a defined neuronal population without causing cell death or inflammation.

One potential strategy for achieving this was the use of DREADDs, a chemogenetic approach that allows reversible neuronal activation or inhibition via G-protein coupled receptors (GPCRs) that respond selectively to synthetic ligands, typically CNO (Armbruster *et al.*, 2007). DREADD expression can be controlled through viral vectors and targeted to specific neuronal subtypes using appropriate promoters. However, applying this technology to the rat spinal cord presented two major challenges: (1) the methodology was still under development for this region, and (2) no known promoter selectively targeting all interneurons (while excluding motoneurons) was available, making it difficult to restrict the intervention to the desired population. This same limitation also applied to modern optogenetic techniques for spinal cord manipulation (Mondello *et al.*, 2023).

Fortunately, an alternative approach had been developed by the group of Dr. David S. K. Magnuson at the University of Louisville, which allows for reversible silencing of spinal interneurons in rats. Their methodology, originally established in non-human primates (Kinoshita *et al.*, 2012), and later adapted to rats (Pocratsky *et al.*, 2017; Shepard *et al.*, 2021), targets neurons based on their anatomical connectivity rather than genetic specificity. The

approach involves injecting two distinct viral vectors into separate spinal segments: an adenoviral vector integrates into neuronal somas at the first injection site, while a lentiviral vector is retrogradely transported from the second injection site to neurons projecting to that location. Only neurons that receive both vectors express enhanced tetanus neurotoxin under a Dox-sensitive promoter, rendering them selectively silenced in the presence of Dox. The timeline of this intervention requires 3–4 weeks for maximal viral expression, 3–5 days for effective neuronal silencing upon Dox administration, and reversion of silencing a few days after Dox withdrawal (for further methodological details, see Materials and methods).

This technique allowed us to transiently inactivate sC3 interneurons while preserving circuit integrity and avoiding non-specific effects on motoneurons or sensory neurons. We specifically targeted sC3-to-C7 projecting interneurons, as sC7 is a key segment of the cervical enlargement that houses many motoneurons innervating distal forelimb muscles (McKenna *et al.*, 2000). If sC3 contained a circuit critically responsible for executing R&G movements, analogous to the lumbar locomotor CPG, then silencing its descending projections to sC7 should result in motor deficits similar to those observed with excitotoxic lesions.

A notable difference in this experiment was that, unlike our previous studies using Long Evans rats, we performed these procedures in Sprague Dawley rats. This decision was based on the fact that the viral constructs and silencing methodology had been successfully optimized in this strain (Pocratsky *et al.*, 2017; Shepard *et al.*, 2021), whereas there was no precedent for their use in Long Evans rats. Although one study suggested minor differences in R&G kinematics between these strains, it also reported that overall success rates and cortical motor maps remained consistent across them (Whishaw *et al.*, 2003). Before proceeding with silencing, we verified that Sprague Dawley rats exhibited similar R&G learning curves as Long Evans rats, confirming the validity of this model (Figure 38).

Before conducting the silencing experiment, we first characterized the connectivity of sC3 interneurons projecting to sC7. Using the dual-viral tracing approach described above (without silencing), we injected AAV2-CAG-FLEx-GFP at sC3 and HiRet-Lenti-Cre at sC7 to selectively label sC3-to-C7 projecting neurons. This allowed us to quantify the number and distribution of these neurons. Interestingly, the labelled neurons were distributed approximately equally between ipsilateral (50 %) and contralateral (50 %) projections (Figure 37). While no significant dorsoventral differences were observed, ipsilateral projections appeared more spatially restricted, whereas contralateral projections were more

widely distributed. This pattern is reminiscent of the distribution observed in the lumbar locomotor CPG, where sL2 interneurons project to sL5 motoneurons (Pocratsky *et al.*, 2017).

For the silencing experiment, we used the same viral constructs but incorporated the tetanus neurotoxin system to inactivate neurons upon Dox administration. Before surgery, animals were assessed in both R&G and high-speed locomotion tasks to establish baseline performance. Two weeks after viral injections at sC3 and sC7, animals were reassessed to confirm that the surgical procedure itself did not cause deficits. Dox was then introduced into the drinking water, and behavioural assessments were conducted at days 5 and 8, when silencing was expected to be fully effective. Surprisingly, neither R&G performance nor locomotion was affected by the silencing intervention (Figures 40–41). Not only did rats maintain their pre-silencing success rates in skilled reaching, but they also preserved their movement strategies and error types (see Materials and methods for details). Locomotion was similarly unaffected, aligning with the expectation that this circuit is specifically involved in skilled forelimb use.

Histological analyses provided a likely explanation for this unexpected result. GFP labelling revealed that very few neurons were successfully silenced: an order of magnitude lower than the number of interneurons typically implicated in robust locomotor circuits, such as L2-to-L5 connections in the hindlimb locomotor CPG (Pocratsky *et al.*, 2017). Given that the majority of forelimb-controlling motoneurons are located between sC5 and sC8 (McKenna *et al.*, 2000), it is possible that silencing only sC3-to-sC7 projections was insufficient to disrupt R&G. A more effective approach might involve silencing sC3 projections to multiple segments (e.g., sC5–sC8). However, this would require removing the dorsal vertebrae of several consecutive spinal segments, posing significant post-surgical recovery challenges. A potential alternative could be targeting fewer laminectomy sites (e.g., at vC4 and vC6) while injecting viral constructs in a manner that allows diffusion across segments.

Another possible reason for the preserved R&G ability is compensatory plasticity. Previous studies using similar silencing techniques have reported partial recovery of function within 5–6 days of sustained inactivation, likely due to the engagement of alternative circuits or reorganization within the network (Kinoshita *et al.*, 2012; Shepard *et al.*, 2021). In our case, the first behavioural assessment was conducted on day 5 of Dox administration, meaning that compensatory mechanisms could already have been in effect by that time. Future experiments assessing earlier time points (e.g., 2–3 days after silencing initiation) could help determine whether transient deficits occur before compensation stabilizes function.

Finally, our results suggest that sC3 is not functioning as a traditional CPG that directly generates R&G movements. If it were, even partial inactivation of its descending output should have produced measurable deficits. Instead, our findings hint that the C3 network may play a more integrative role, modulating or relaying information rather than executing motor commands. It is also possible that the critical neurons within sC3 influence R&G via projections to supraspinal centres rather than directly controlling forelimb motoneurons. Supporting this idea, past studies have failed to identify sC3-C4 propriospinal neurons as key mediators of R&G through direct projections (Alstermark & Ogawa, 2004; Alstermark *et al.*, 2004). Future studies could explore this by applying the same silencing methodology to sC3 neurons projecting to the brainstem or cerebellum, assessing whether inactivation of ascending pathways disrupts skilled forelimb movements.

Contextualising sC3 in the broader motor control framework

Considering all results together, we propose that segment sC3 functions as a key integrative hub in the spinal control of skilled forelimb movement, rather than as an autonomous pattern generator. This perspective reconciles our findings with the broader literature on motor control across species. The classical view from cat and primate studies assigns the sC3–C4 propriospinal system a pivotal role in relaying and integrating motor commands for reaching. In cats, lesioning the sC3–C4 propriospinal neurons severely disrupts reaching behaviour (Illert *et al.*, 1977), and in macaque monkeys these neurons are involved in both R&G synergies, effectively acting as a bridge between the cortex and the spinal motor neurons (Alstermark *et al.*, 1999). In humans, evidence for analogous propriospinal pathways also exists (e.g. via indirect cortico-reticulospinal connections) (Malmgren & Pierrot-Deseilligny, 1988). Rodents, on the other hand, were thought to execute reaching mainly through direct corticospinal and brainstem (rubrospinal/reticulospinal) pathways, without a significant propriospinal interneuron relay at sC3–C4. Indeed, electrophysiological studies in rats have shown a lack of monosynaptic cortico-motoneuronal connections, implying that cortical signals must engage interneurons or brainstem circuits to reach the motor pools (Alstermark & Ogawa, 2004; Alstermark *et al.*, 2004). Our results bridge this understanding by demonstrating that even in rats, a focal spinal network at sC3 is indispensable for proper reaching. How can these seemingly divergent views

be reconciled? One clue comes from our hypothesis (supported by the silencing outcomes) that the sC3 network may not drive forelimb muscles directly but instead interacts heavily with supraspinal centres. We envision the sC3 interneurons as an integrative node that processes sensory feedback and limb-position information during reaching, and then projects this information to supraspinal structures (such as the brainstem reticular formation or the cerebellum) to adjust or fine-tune the ongoing movement. This would align with known roles of the brainstem in coordinating reach and grasp; for example, the medullary reticulospinal system has been implicated in proximal forelimb control and postural support during reaching. By sending real-time updates or modulatory signals upstream, sC3 interneurons could ensure that higher motor centres are informed of the limb's progress, enabling corrections and smooth execution. Such a mechanism fits the notion of error correction or feedback integration: the spinal cord doesn't just blindly execute commands; it actively shapes the movement by communicating with the brain. Thus, the role of the sC3 circuit in rats may be more about coordinating and relaying information than generating motor patterns de novo. In broader terms, our findings might expand the concept of CPG and modularity in the spinal cord. We suggest that, beyond the well-established locomotor CPG in the lumbar cord, there are task-specific spinal substrates for other complex movements. The cervical spinal cord is not merely a conduit for the brain's commands to the arm; it contains specialized circuitry that can determine success or failure in skilled tasks. This idea is in line with emerging views in motor neuroscience that motor control is distributed across multiple levels of the neuraxis, with spinal circuits handling a surprising amount of preprocessing and integration even for apparently "voluntary" actions (such as reaching to grasp an object). By showing that the integrity of a particular spinal segment is necessary for a distinct behaviour, we provide a clear example of such distributed control. It reminds us that evolution may have endowed mammals with redundant and layered motor systems: the cortex and brainstem initiate and plan movements, but the spinal interneurons ensure those plans are executed smoothly and adapt to immediate feedback. Another intriguing insight from our work is how different spinal networks can operate independently without mutual interference. The sC3 lesion caused a deficit in reaching but did not hamper locomotion, even though both locomotion and reaching use the shoulder and elbow muscles. Conversely, lumbar lesions can disrupt hindlimb stepping but would not affect

(hypothetical) skilled digit movements of the hind paws. This independence suggests that the spinal cord contains multiple parallel modules (or microcircuits), each tuned to the demands of a specific motor task. Our identification of a reaching/grasping-related module at sC3 adds to the catalogue of known spinal modules and invites further investigation into how these modules interact with each other and with higher centres.

Limitations and future perspectives

The work presented in this thesis is not without limitations. Acknowledgedly, several animals had to be excluded from the final analyses due to technical reasons, which reduced the total n in certain experiments. However, our commitment to the principles of the Three Rs (Replacement, Reduction, and Refinement) in animal research is paramount. We strictly adhered to ethical guidelines and procedures aimed at maximizing animal welfare and minimizing suffering. Our experimental design required animals to be handled almost daily for several weeks, followed by an extensive training phase for voluntary behavioural tests in which the animals were freely moving. Post-surgical care was administered daily, and behavioural assessments continued until perfusion. Given the considerable investment of time, effort, emotional involvement, and financial resources in each animal, every exclusion was deeply regretted. The decision to remove an animal from the study was based strictly on objective criteria, such as the presence of unintended damage during surgery or suboptimal tissue preservation, ensuring that erroneous conclusions were not drawn from compromised data. Efforts were made, and will continue to be made, to reduce the number of discarded animals, ideally approaching zero. Fortunately, in the experiments where the number of analysed animals was relatively low (e.g., the root sectioning studies), the results were consistent and displayed minimal variability, lending robustness to the derived conclusions.

Most of the methodological drawbacks have been discussed in previous sections, but one of the most relevant limitations remains the incomplete characterization of the sC3 neuronal network. Our results strongly suggest that a network at sC3 is necessary for the correct execution of R&G movements, possibly by integrating sensory and propriospinal information and relaying it to supraspinal structures such as the brainstem and cerebellum. However, we have not directly demonstrated that this is

the mechanism through which these neurons exert their function; what we have done is provide evidence for what they do not do. The next crucial step is to further define the characteristics of these neurons. Where do they project? What are their afferent inputs? Are they excitatory or inhibitory? What neurotransmitters do they use? Answering these questions requires a combination of advanced anatomical tracing techniques, potentially including transsynaptic viral tracers, and molecular profiling methods, such as immunohistochemistry for neurotransmitter markers or single-cell RNA sequencing. These approaches would allow a deeper understanding of the exact role of sC3 interneurons in R&G.

Another limitation concerns the methodology used to infer neuronal activation patterns. We employed IEG expression, particularly c-Fos and FosB, to visualize task-related activity in the cervical spinal cord. While this approach has been widely used in the field, it has inherent drawbacks, as discussed earlier. The signal from c-Fos was unexpectedly sparse, and its variability made interpretation difficult. This could be due to multiple factors, including neuronal redundancy, differential IEG expression across subtypes, and the known inhibition of c-Fos by ΔFosB. Future studies would benefit from employing in vivo electrophysiology or calcium imaging, both of which offer a more direct and temporally precise readout of neuronal activity during behaviour. Recent technical advances now allow for spinal cord calcium imaging in freely moving mice, which could potentially be adapted to rats or head-fixed paradigms in reaching tasks. If applied successfully, this approach could reveal whether sC3 interneurons are activated at specific moments during reaching (e.g., at movement onset or in response to sensory feedback adjustments), providing a much clearer functional map of the network.

Additionally, while our functional assessments were comprehensive, they could be improved in two key ways. First, kinematic analysis of the reaching and locomotion movements would provide a higher level of detail regarding both functional deficits and compensatory strategies. We lacked the technical expertise to apply such an approach ourselves, so we attempted to bypass this limitation by categorizing error types in R&G and analysing specific movement components, which provided valuable insights. However, in future studies, incorporating motion capture or high-speed video-based joint angle analysis would allow for the detection of subtle changes in movement strategy that might remain masked in endpoint measures. This could

clarify whether R&G deficits reflect slower, less direct, or more variable movements, even if overall success rates remain stable. Second, electrophysiological recordings from forelimb muscles could offer additional insights into how circuit dysfunction translates to motor output. Since electromyography is highly sensitive, it could reveal impairments that behavioural assays alone might miss, further refining our understanding of how sC3 contributes to motor control.

A related limitation is that our silencing experiments did not yield the expected behavioural deficits. This was not evidence against the importance of sC3 interneurons in R&G, but rather a result of technical and anatomical constraints. Post-mortem analysis revealed that only a very small subset of sC3-to-C7 neurons was successfully inactivated, roughly ten times fewer than the number of interneurons implicated in lumbar locomotor circuits (Pocratsky *et al.*, 2017). It is likely that sC3 interneurons influencing R&G do not all project to sC7, but rather to multiple cervical segments or supraspinal regions, meaning that our silencing approach did not capture the full extent of the relevant network. A more comprehensive strategy (targeting sC3 projections to sC5–C8 collectively, for instance) would likely yield more conclusive results. Another consideration is compensatory plasticity, as previous studies using similar silencing techniques have reported functional recovery within a few days of inactivation, due to the engagement of alternative pathways (Kinoshita *et al.*, 2012; Shepard *et al.*, 2021). In our case, behavioural assessments occurred on day 5 of Dox administration, meaning that compensatory mechanisms may have already been in effect. Future experiments should test earlier time points (e.g., day 2–3) to determine if transient deficits emerge before the system adapts. Lastly, it remains possible that sC3 does not act as a "command generator" for R&G but instead serves a more integrative role, processing sensory feedback and relaying it to supraspinal centres such as the brainstem or cerebellum. If this is the case, future work could focus on silencing sC3 projections to these supraspinal regions instead of downstream spinal segments to determine whether disrupting ascending signals impairs skilled forelimb movements.

Of note, we only used female rats. The decision to use only females was based on the absence of published evidence for sex differences in forelimb skilled function. While one study suggested minor postural adjustments may differ between sexes, no significant differences were found in R&G proficiency (Field & Whishaw, 2005). In

SCI research, female rodents are more commonly used due to lower mortality rates from bladder infections in comparison to males. However, it could be argued that this concern does not directly apply to our experimental paradigm, and future studies should include male subjects to verify the generalizability of our findings.

Finally, while our results establish a spinal contribution to skilled R&G, the translational relevance of these findings remains to be fully explored. As pointed out, rodents and primates differ in motor circuit organization, with primates relying more on direct corticospinal projections for fine motor control, while rodents depend on propriospinal and reticulospinal pathways (Alstermark & Isa, 2012; Zaaimi *et al.*, 2012). Nevertheless, spinal circuits contribute to upper limb control in all mammals, including humans, particularly for integrating sensory feedback and coordinating multi-joint movements. If a homologous sC3-like module exists in humans, it could have profound implications for neurorehabilitation strategies. For instance, targeting specific cervical segments with neuromodulation techniques such as transcutaneous spinal stimulation might enhance upper limb function after cervical SCI or stroke. Future collaborative efforts with clinical researchers should aim to investigate the existence of a comparable circuit in the human spinal cord, using functional neuroimaging or post-mortem histological studies.

Despite these limitations, our core finding remains robust: there is a functionally significant population of spinal neurons at sC3 that is necessary for normal R&G. We have systematically ruled out alternative explanations, reinforcing that this network plays a crucial role in forelimb skilled function. Moving forward, additional experiments will further refine our understanding of its precise function and connectivity, paving the way for potential translational applications in motor recovery and rehabilitation.

Concluding remarks

This thesis aimed to unveil the role of the cervical spinal cord in manual dexterity in general and in R&G in particular. We began with two alternative hypotheses, the existence of a localized controlling centre, namely CPG, or the segmental distribution of the different subphases of the movement throughout the spinal cord. Nonetheless, our findings point towards a third explanation. The R&G movement is neither

segmentally subdivided equitably throughout the cervical spinal cord nor there is a CPG responsible of it, as seen in locomotion. Instead, there is a neuronal network at spinal segment sC3 that has proven necessary for the proper execution of R&G and other movements with a relevant R&G-component. Possibly, these neurons would integrate feedback information to be transmitted to supraspinal centres, namely the brainstem, so that the movement can be correctly performed.

Overall, these findings offer important insights into the mechanisms underlying forelimb skilled function and could serve as a basis for the development of therapeutic strategies, such as neuromodulation, in order to improve the recovery of manual dexterity after SCI and other related motor disorders. Considering that the restoration of arm and hand function is the first priority for patients suffering from cervical SCI, even a small improvement would result in a dramatic increase in their quality of life.

VIII. Conclusions

Chapter 1. Identifying a spinal neuronal network controlling reaching and grasping.

- This study provides the first evidence in rodents of a spinal neuronal network critically involved in R&G control, localised within the C3 spinal segment (sC3).
- The loss of function experiments demonstrated that damage to sC3 significantly impaired reaching movements, while more caudal lesions did not induce comparable deficits.
- The impairment observed after sC3 lesions was selective for R&G movements, as other forelimb functions such as locomotion and food manipulation remained largely unaffected.
- The deficits were particularly evident in the reaching phase, rather than grasping or postural adjustments, suggesting that sC3 is crucial for limb advancement towards the target.

Chapter 2. Characterising the identified spinal neuronal network controlling reaching and grasping.

- IEG analysis in intact animals confirmed that sC3 is highly recruited during R&G execution, further supporting its role in movement control.
- The expression of c-Fos and FosB was significantly increased in sC3 neurons of trained R&G animals compared to locomotion or resting conditions.
- The findings suggest that sC3 contains interneurons that coordinate skilled forelimb movement, potentially functioning as an intrinsic spinal module.
- Anatomical tracing experiments confirmed the presence of sC3 neurons projecting to sC7, where motoneurons controlling distal forelimb muscles reside.
- However, reversible silencing of these sC3-to-C7 projecting neurons did not induce significant motor impairments, suggesting either compensation by other pathways or methodological limitations.
- Identifying a key spinal region for reaching control could help refine neuromodulatory therapies (e.g., transcutaneous or epidural stimulation at sC3) for motor recovery in patients with SCI, stroke or neurodegenerative diseases.

IX. References

Ahn, S.N., Guu, J.J., Tobin, A.J., Edgerton, V.R., & Tillakaratne, N.J.K. (2006) Use of c-fos to identify activity-dependent spinal neurons after stepping in intact adult rats. *Spinal Cord*, **44**, 547–559.

Ahuja, C.S., Wilson, J.R., Nori, S., Kotter, M.R.N., Druschel, C., Curt, A., & Fehlings, M.G. (2017) Traumatic spinal cord injury. *Nat. Rev. Dis. Prim.*, **3**, 17018.

Alizadeh, A., Dyck, S.M., & Karimi-Abdolrezaee, S. (2019) Traumatic Spinal Cord Injury: An Overview of Pathophysiology, Models and Acute Injury Mechanisms. *Front. Neurol.*, **10**, 282.

Allred, R.P., Adkins, D.L., Woodlee, M.T., Husbands, L.C., Maldonado, M.A., Kane, J.R., Schallert, T., & Jones, T.A. (2008) The vermicelli handling test: a simple quantitative measure of dexterous forepaw function in rats. *J. Neurosci. Methods*, **170**, 229–244.

Alstermark, B. & Isa, T. (2012) Circuits for skilled reaching and grasping. *Annu. Rev. Neurosci.*, **35**, 559–578.

Alstermark, B., Isa, T., Ohki, Y., & Saito, Y. (1999) Disynaptic pyramidal excitation in forelimb motoneurons mediated via C(3)-C(4) propriospinal neurons in the Macaca fuscata. *J. Neurophysiol.*, **82**, 3580–3585.

Alstermark, B., Isa, T., Pettersson, L.-G., & Sasaki, S. (2007) The C3-C4 propriospinal system in the cat and monkey: a spinal pre-motoneuronal centre for voluntary motor control. *Acta Physiol. (Oxf).*, **189**, 123–140.

Alstermark, B., Lundberg, A., Norrsell, U., & Sybirska, E. (1981) Integration in descending motor pathways controlling the forelimb in the cat. 9. Differential behavioural defects after spinal cord lesions interrupting defined pathways from higher centres to motoneurones. *Exp. brain Res.*, **42**, 299–318.

Alstermark, B., Lundberg, A., & Sasaki, S. (1984) Integration in descending motor pathways controlling the forelimb in the cat. 11. Inhibitory pathways from higher motor centres and forelimb afferents to C3-C4 propriospinal neurones. *Exp. brain Res.*, **56**, 293–307.

Alstermark, B. & Ogawa, J. (2004) In vivo recordings of bulbospinal excitation in adult mouse forelimb motoneurons. *J. Neurophysiol.*, **92**, 1958–1962.

Alstermark, B., Ogawa, J., & Isa, T. (2004) Lack of monosynaptic corticomotoneuronal EPSPs in rats: disynaptic EPSPs mediated via reticulospinal neurons and polysynaptic EPSPs via segmental interneurons. *J. Neurophysiol.*, **91**, 1832–1839.

Alstermark, B. & Pettersson, L.-G. (2014) Skilled reaching and grasping in the rat: lacking effect of corticospinal lesion. *Front. Neurol.*, **5**, 103.

Alstermark, B., Pettersson, L.G., Nishimura, Y., Yoshino-Saito, K., Tsuboi, F., Takahashi, M., & Isa, T. (2011) Motor command for precision grip in the macaque monkey can be mediated by spinal interneurons. *J. Neurophysiol.*, **106**, 122–126.

Alstermark, B. & Sasaki, S. (1985) Integration in descending motor pathways controlling the forelimb in the cat. 13. Corticospinal effects in shoulder, elbow, wrist, and digit motoneurones. *Exp. brain Res.*, **59**, 353–364.

Anderson, K.D., Sharp, K.G., Hofstadter, M., Irvine, K.-A., Murray, M., & Steward, O. (2009) Forelimb locomotor assessment scale (FLAS): novel assessment of forelimb dysfunction after cervical spinal cord injury. *Exp. Neurol.*, **220**, 23–33.

Anjum, A., Yazid, M.D., Fauzi Daud, M., Idris, J., Ng, A.M.H., Selvi Naicker, A., Ismail, O.H.R., Athi Kumar, R.K., & Lokanathan, Y. (2020) Spinal Cord Injury: Pathophysiology, Multimolecular Interactions, and Underlying Recovery Mechanisms.

Int. J. Mol. Sci., **21**.

Armbruster, B.N., Li, X., Pausch, M.H., Herlitze, S., & Roth, B.L. (2007) Evolving the lock to fit the key to create a family of G protein-coupled receptors potently activated by an inert ligand. *Proc. Natl. Acad. Sci. U. S. A.*, **104**, 5163–5168.

Azim, E., Jiang, J., Alstermark, B., & Jessell, T.M. (2014) Skilled reaching relies on a V2a propriospinal internal copy circuit. *Nature*, **508**, 357–363.

Barritt, A.W., Davies, M., Marchand, F., Hartley, R., Grist, J., Yip, P., McMahon, S.B., & Bradbury, E.J. (2006) Chondroitinase ABC promotes sprouting of intact and injured spinal systems after spinal cord injury. *J. Neurosci.*, **26**, 10856–10867.

Battistuzzo, C.R., Rank, M.M., Flynn, J.R., Morgan, D.L., Callister, R., Callister, R.J., & Galea, M.P. (2017) Effects Of treadmill training on hindlimb muscles of spinal cord-injured mice. *Muscle Nerve*, **55**, 232–242.

Baylo-Marín, O., Flores, Á., & García-Alías, G. (2022) Long-term rehabilitation reduces task error variability in cervical spinal cord contused rats. *Exp. Neurol.*, **348**, 113928.

Bear, M.F., Connors, B.W., & Paradiso, M.A. (2007) *Neuroscience: Exploring the Brain*, 3rd ed. edn. Lippincott Williams and Wilkins.

Ben-Ari, Y. & Cossart, R. (2000) Kainate, a double agent that generates seizures: two decades of progress. *Trends Neurosci.*, **23**, 580–587.

Bensimon, G., Lacomblez, L., & Meininger, V. (1994) A controlled trial of riluzole in amyotrophic lateral sclerosis. ALS/Riluzole Study Group. *N. Engl. J. Med.*, **330**, 585–591.

Bernhard, C.G. & Bohm, E. (1954) Cortical representation and functional significance of the corticomotoneuronal system. *Arch. Neurol. Psychiatry*, **72**, 473–502.

Bertelli, J.A. & Mira, J.C. (1993) Behavioral evaluating methods in the objective clinical assessment of motor function after experimental brachial plexus reconstruction in the rat. *J. Neurosci. Methods*, **46**, 203–208.

Bito, H., Deisseroth, K., & Tsien, R.W. (1996) CREB phosphorylation and dephosphorylation: a Ca(2+)- and stimulus duration-dependent switch for hippocampal gene expression. *Cell*, **87**, 1203–1214.

Blackwell, A.A., Köppen, J.R., Whishaw, I.Q., & Wallace, D.G. (2018) String-pulling for food by the rat: Assessment of movement, topography and kinematics of a bilaterally skilled forelimb act. *Learn. Motiv.*, **61**, 63–73.

Bouet, V., Boulouard, M., Toutain, J., Divoux, D., Bernaudin, M., Schumann-Bard, P., & Freret, T. (2009) The adhesive removal test: A sensitive method to assess sensorimotor deficits in mice. *Nat. Protoc.*, **4**, 1560–1564.

Boyden, E.S., Zhang, F., Bamberg, E., Nagel, G., & Deisseroth, K. (2005) Millisecond-timescale, genetically targeted optical control of neural activity. *Nat. Neurosci.*, **8**, 1263–1268.

Brown, R.H. & Al-Chalabi, A. (2017) Amyotrophic Lateral Sclerosis. *N. Engl. J. Med.*, **377**, 162–172.

Capogrosso, M., Wagner, F.B., Gandar, J., Moraud, E.M., Wenger, N., Milekovic, T., Shkorbatova, P., Pavlova, N., Musienko, P., Bezard, E., Bloch, J., & Courtine, G. (2018) Configuration of electrical spinal cord stimulation through real-time processing of gait kinematics. *Nat. Protoc.*, **13**, 2031–2061.

Cazalets, J.R., Borde, M., & Clarac, F. (1995) Localization and organization of the central pattern generator for hindlimb locomotion in newborn rat. *J. Neurosci.*, **15**, 4943–4951.

Christy, B. & Nathans, D. (1989) DNA binding site of the growth factor-inducible protein Zif268. *Proc. Natl. Acad. Sci. U. S. A.*, **86**, 8737–8741.

Clarke, R.W. & Harris, J. (2004) The organization of motor responses to noxious stimuli. *Brain Res. Brain Res. Rev.*, **46**, 163–172.

Corbett, B.F., You, J.C., Zhang, X., Pyfer, M.S., Tosi, U., Iascone, D.M., Petrof, I., Hazra, A., Fu, C.-H., Stephens, G.S., Ashok, A.A., Aschmies, S., Zhao, L., Nestler, E.J., & Chin, J. (2017) ΔFosB Regulates Gene Expression and Cognitive Dysfunction in a Mouse Model of Alzheimer's Disease. *Cell Rep.*, **20**, 344–355.

Corona, J.C. & Tapia, R. (2004) AMPA receptor activation, but not the accumulation of endogenous extracellular glutamate, induces paralysis and motor neuron death in rat spinal cord in vivo. *J. Neurochem.*, **89**, 988–997.

Côté, M.-P., Gandhi, S., Zambrotta, M., & Houlé, J.D. (2014) Exercise modulates chloride homeostasis after spinal cord injury. *J. Neurosci.*, **34**, 8976–8987.

Côté, M.-P., Murray, L.M., & Knikou, M. (2018) Spinal Control of Locomotion: Individual Neurons, Their Circuits and Functions. *Front. Physiol.*, **9**, 784.

Courtine, G. & Sofroniew, M. V (2019) Spinal cord repair: advances in biology and technology. *Nat. Med.*, **25**, 898–908.

D'Amico, J.M., Condliffe, E.G., Martins, K.J.B., Bennett, D.J., & Gorassini, M.A. (2014) Recovery of neuronal and network excitability after spinal cord injury and implications for spasticity. *Front. Integr. Neurosci.*, **8**, 36.

de Leon, R.D., Hodgson, J.A., Roy, R.R., & Edgerton, V.R. (1998) Locomotor capacity attributable to step training versus spontaneous recovery after spinalization in adult cats. *J. Neurophysiol.*, **79**, 1329–1340.

Dharani, K. (2015) Chapter 1 - Functional Anatomy of the Brain. In Dharani, K.B.T.-T.B. of T. (ed), . Academic Press, San Diego, pp. 3–29.

Dietz, V. (2002) Proprioception and locomotor disorders. *Nat. Rev. Neurosci.*, **3**, 781–790.

Doble, A. (1996) The pharmacology and mechanism of action of riluzole. *Neurology*, **47**, S233-41.

Dobson, R. & Giovannoni, G. (2019) Multiple sclerosis - a review. *Eur. J. Neurol.*, **26**, 27–40.

Donoghue, J.P. & Wise, S.P. (1982) The motor cortex of the rat: cytoarchitecture and microstimulation mapping. *J. Comp. Neurol.*, **212**, 76–88.

El-Shamayleh, Y. & Horwitz, G.D. (2019) Primate optogenetics: Progress and prognosis. *Proc. Natl. Acad. Sci. U. S. A.*, **116**, 26195–26203.

Esposito, M.S., Capelli, P., & Arber, S. (2014) Brainstem nucleus MdV mediates skilled forelimb motor tasks. *Nature*, **508**, 351–356.

Ettema, A.M., Zhao, C., An, K.-N., & Amadio, P.C. (2006) Comparative anatomy of the subsynovial connective tissue in the carpal tunnel of the rat, rabbit, dog, baboon, and human. *Hand (N. Y).*, **1**, 78–84.

Faist, M., Mazevet, D., Dietz, V., & Pierrot-Deseilligny, E. (1994) A quantitative assessment of presynaptic inhibition of Ia afferents in spastics. Differences in hemiplegics and

paraplegics. *Brain*, **117 (Pt 6**, 1449–1455.

Fawcett, J.W. & Asher, R.A. (1999) The glial scar and central nervous system repair. *Brain Res. Bull.*, **49**, 377–391.

Ferrucci, M., Lazzeri, G., Flaibani, M., Biagioni, F., Cantini, F., Madonna, M., Bucci, D., Limanaqi, F., Soldani, P., & Fornai, F. (2018) In search for a gold-standard procedure to count motor neurons in the spinal cord. *Histol. Histopathol.*, **33**, 1021–1046.

Field, E.F. & Whishaw, I.Q. (2005) Sexually dimorphic postural adjustments are used in a skilled reaching task in the rat. *Behav. Brain Res.*, **163**, 237–245.

Fink, A.J.P., Croce, K.R., Huang, Z.J., Abbott, L.F., Jessell, T.M., & Azim, E. (2014) Presynaptic inhibition of spinal sensory feedback ensures smooth movement. *Nature*, **509**, 43–48.

Finnerup, N.B. (2017) Neuropathic pain and spasticity: intricate consequences of spinal cord injury. *Spinal Cord*, **55**, 1046–1050.

Flores, Á., López-Santos, D., & García-Alías, G. (2021) When Spinal Neuromodulation Meets Sensorimotor Rehabilitation: Lessons Learned From Animal Models to Regain Manual Dexterity After a Spinal Cord Injury. *Front. Rehabil. Sci.*, **2**, 755963.

Fouad, K., Metz, G.A., Merkler, D., Dietz, V., & Schwab, M.E. (2000) Treadmill training in incomplete spinal cord injured rats. *Behav. Brain Res.*, **115**, 107–113.

Fouad, K. & Tetzlaff, W. (2012) Rehabilitative training and plasticity following spinal cord injury. *Exp. Neurol.*, **235**, 91–99.

Gaja-Capdevila, N., Hernández, N., Yeste, S., Reinoso, R.F., Burgueño, J., Montero, A., Merlos, M., Vela, J.M., Herrando-Grabulosa, M., & Navarro, X. (2022) EST79232 and EST79376, Two Novel Sigma-1 Receptor Ligands, Exert Neuroprotection on Models of Motoneuron Degeneration. *Int. J. Mol. Sci.*, **23**.

Gaja-Capdevila, N., Hernández, N., Zamanillo, D., Vela, J.M., Merlos, M., Navarro, X., & Herrando-Grabulosa, M. (2021) Neuroprotective Effects of Sigma 1 Receptor Ligands on Motoneuron Death after Spinal Root Injury in Mice. *Int. J. Mol. Sci.*, **22**.

García-Alías, G., Barkhuysen, S., Buckle, M., & Fawcett, J.W. (2009) Chondroitinase ABC treatment opens a window of opportunity for task-specific rehabilitation. *Nat. Neurosci.*, **12**, 1145–1151.

García-Alías, G., Truong, K., Shah, P.K., Roy, R.R., & Edgerton, V.R. (2015) Plasticity of subcortical pathways promote recovery of skilled hand function in rats after corticospinal and rubrospinal tract injuries. *Exp. Neurol.*, **266**, 112–119.

Gensel, J.C., Tovar, C.A., Hamers, F.P.T., Deibert, R.J., Beattie, M.S., & Bresnahan, J.C. (2006) Behavioral and histological characterization of unilateral cervical spinal cord contusion injury in rats. *J. Neurotrauma*, **23**, 36–54.

Georgopoulos, A.P., Kalaska, J.F., Caminiti, R., & Massey, J.T. (1982) On the relations between the direction of two-dimensional arm movements and cell discharge in primate motor cortex. *J. Neurosci.*, **2**, 1527–1537.

Gharios, M., Stenimahitis, V., El-Hajj, V.G., Mahdi, O.A., Fletcher-Sandersjöö, A., Jabbour, P., Andersson, M., Hultling, C., Elmi-Terander, A., & Edström, E. (2024) Spontaneous spinal cord infarction: a systematic review. *BMJ Neurol. open*, **6**, e000754.

Gómez-Pinilla, F., Ying, Z., Roy, R.R., Molteni, R., & Edgerton, V.R. (2002) Voluntary exercise induces a BDNF-mediated mechanism that promotes neuroplasticity. *J.*

Neurophysiol., **88**, 2187–2195.

Gould, S.J. (1991) Exaptation: A Crucial Tool for an Evolutionary Psychology. *J. Soc. Issues*, **47**, 43–65.

Greenberg, M.E. & Ziff, E.B. (1984) Stimulation of 3T3 cells induces transcription of the c-fos proto-oncogene. *Nature*, **311**, 433–438.

Grillner, S. (1981) Control of Locomotion in Bipeds, Tetrapods, and Fish. In *Comprehensive Physiology*. pp. 1179–1236.

Grillner, S. (2006) Biological pattern generation: the cellular and computational logic of networks in motion. *Neuron*, **52**, 751–766.

Hamers, F.P., Lankhorst, A.J., van Laar, T.J., Veldhuis, W.B., & Gispen, W.H. (2001) Automated quantitative gait analysis during overground locomotion in the rat: its application to spinal cord contusion and transection injuries. *J. Neurotrauma*, **18**, 187–201.

Harkema, S., Angeli, C., & Gerasimenko, Y. (2022) Historical development and contemporary use of neuromodulation in human spinal cord injury. *Curr. Opin. Neurol.*, **35**, 536–543.

Harkema, S., Gerasimenko, Y., Hodes, J., Burdick, J., Angeli, C., Chen, Y., Ferreira, C., Willhite, A., Rejc, E., Grossman, R.G., & Edgerton, V.R. (2011) Effect of epidural stimulation of the lumbosacral spinal cord on voluntary movement, standing, and assisted stepping after motor complete paraplegia: a case study. *Lancet (London, England)*, **377**, 1938–1947.

Hays, S.A., Khodaparast, N., Sloan, A.M., Hulsey, D.R., Pantoja, M., Ruiz, A.D., Kilgard, M.P., & Rennaker, R.L. (2013) The isometric pull task: a novel automated method for quantifying forelimb force generation in rats. *J. Neurosci. Methods*, **212**, 329–337.

Hiroi, N., Marek, G.J., Brown, J.R., Ye, H., Saudou, F., Vaidya, V.A., Duman, R.S., Greenberg, M.E., & Nestler, E.J. (1998) Essential role of the fosB gene in molecular, cellular, and behavioral actions of chronic electroconvulsive seizures. *J. Neurosci.*, **18**, 6952–6962.

Hoerbelt, P. & Heifets, B.D. (2018) Chapter Sixteen - Native System and Cultured Cell Electrophysiology for Investigating Anesthetic Mechanisms. In Eckenhoff, R.G. & Dmochowski, I.J.B.T.-M. in E. (eds), *Chemical and Biochemical Approaches for the Study of Anesthetic Function, Part A*. Academic Press, pp. 301–338.

Holmes, D. (2017) Repairing the neural highway. *Nature*, **552**, S50–S51.

Holt, C.E. & Schuman, E.M. (2013) The central dogma decentralized: new perspectives on RNA function and local translation in neurons. *Neuron*, **80**, 648–657.

Illert, M., Lundberg, A., & Tanaka, R. (1977) Integration in descending motor pathways controlling the forelimb in the cat. 3. Convergence on propriospinal neurones transmitting disynaptic excitation from the corticospinal tract and other descending tracts. *Exp. brain Res.*, **29**, 323–346.

Irvine, K.-A., Ferguson, A.R., Mitchell, K.D., Beattie, S.B., Beattie, M.S., & Bresnahan, J.C. (2010) A novel method for assessing proximal and distal forelimb function in the rat: the Irvine, Beatties and Bresnahan (IBB) forelimb scale. *J. Vis. Exp.*,.

Irvine, K.A., Ferguson, A.R., Mitchell, K.D., Beattie, S.B., Lin, A., Stuck, E.D., Huie, J.R., Nielson, J.L., Talbott, J.F., Inoue, T., Beattie, M.S., & Bresnahan, J.C. (2014) The Irvine, Beatties, and Bresnahan (IBB) forelimb recovery scale: An assessment of reliability and

validity. *Front. Neurol.*, **5 JUL**, 1–19.

Isa, T. (2019) Dexterous Hand Movements and Their Recovery After Central Nervous System Injury. *Annu. Rev. Neurosci.*, **42**, 315–335.

Iwaniuk, A.N. & Whishaw, I.Q. (2000) On the origin of skilled forelimb movements. *Trends Neurosci.*, **23**, 372–376.

Jankowska, E. (1992) Interneuronal relay in spinal pathways from proprioceptors. *Prog. Neurobiol.*, **38**, 335–378.

Jankowska, E. & Edgley, S.A. (2006) How can corticospinal tract neurons contribute to ipsilateral movements? A question with implications for recovery of motor functions. *Neuroscientist*, **12**, 67–79.

Jasmin, L., Gogas, K.R., Ahlgren, S.C., Levine, J.D., & Basbaum, A.I. (1994) Walking evokes a distinctive pattern of Fos-like immunoreactivity in the caudal brainstem and spinal cord of the rat. *Neuroscience*, **58**, 275–286.

Jordan, L.M. & Sławińska, U. (2014) The Brain and Spinal Cord Networks Controlling Locomotion. In *Neuronal Networks in Brain Function, CNS Disorders, and Therapeutics*. Elsevier, pp. 215–233.

Kanagal, S.G. & Muir, G.D. (2009) Task-dependent compensation after pyramidal tract and dorsolateral spinal lesions in rats. *Exp. Neurol.*, **216**, 193–206.

Karl, J.M. & Whishaw, I.Q. (2011) Rodent Skilled Reaching for Modeling Pathological Conditions of the Human Motor System. pp. 87–107.

Karl, J.M. & Whishaw, I.Q. (2013) Different evolutionary origins for the reach and the grasp: an explanation for dual visuomotor channels in primate parietofrontal cortex. *Front. Neurol.*, **4**, 208.

Kiehn, O. (2006) Locomotor circuits in the mammalian spinal cord. *Annu. Rev. Neurosci.*, **29**, 279–306.

Kiehn, O. (2016) Decoding the organization of spinal circuits that control locomotion. *Nat. Rev. Neurosci.*, **17**, 224–238.

Kinoshita, M., Matsui, R., Kato, S., Hasegawa, T., Kasahara, H., Isa, K., Watakabe, A., Yamamori, T., Nishimura, Y., Alstermark, B., Watanabe, D., Kobayashi, K., & Isa, T. (2012) Genetic dissection of the circuit for hand dexterity in primates. *Nature*, **487**, 235–238.

Kjell, J. & Olson, L. (2016) Rat models of spinal cord injury: from pathology to potential therapies. *Dis. Model. Mech.*, **9**, 1125–1137.

Krakauer, J.W., Carmichael, S.T., Corbett, D., & Wittenberg, G.F. (2012) Getting neurorehabilitation right: what can be learned from animal models? *Neurorehabil. Neural Repair*, **26**, 923–931.

Krisa, L., Runyen, M., & Detloff, M.R. (2018) Translational Challenges of Rat Models of Upper Extremity Dysfunction After Spinal Cord Injury. *Top. Spinal Cord Inj. Rehabil.*, **24**, 195–205.

Kuypers, H.G.J.M. (1981) Anatomy of the Descending Pathways. In *Comprehensive Physiology*. Wiley, pp. 597–666.

Kuzhandaivel, A., Nistri, A., & Mladinic, M. (2010) Kainate-mediated excitotoxicity induces neuronal death in the rat spinal cord in vitro via a PARP-1 dependent cell death

pathway (Parthanatos). *Cell. Mol. Neurobiol.*, **30**, 1001–1012.

Kwon, M., Altin, M., Duenas, H., & Alev, L. (2014) The role of descending inhibitory pathways on chronic pain modulation and clinical implications. *Pain Pract.*, **14**, 656–667.

Lakes, E.H. & Allen, K.D. (2016) Gait analysis methods for rodent models of arthritic disorders: reviews and recommendations. *Osteoarthr. Cartil.*, **24**, 1837–1849.

Lane, M.A. (2011) Spinal respiratory motoneurons and interneurons. *Respir. Physiol. Neurobiol.*, **179**, 3–13.

Lawrence, D.G. & Kuypers, H.G. (1968) The functional organization of the motor system in the monkey. I. The effects of bilateral pyramidal lesions. *Brain*, **91**, 1–14.

Lemon, R.N. (2008) Descending pathways in motor control. *Annu. Rev. Neurosci.*, **31**, 195–218.

Lerma, J. (1997) Kainate reveals its targets. *Neuron*, **19**, 1155–1158.

Liddell, E.G.T. & Sherrington, C.S. (1925) Recruitment and some other features of reflex inhibition. *Proc. R. Soc. London. Ser. B, Contain. Pap. a Biol. Character*, **97**, 488–518.

Lima, R., Monteiro, A., Salgado, A.J., Monteiro, S., & Silva, N.A. (2022) Pathophysiology and Therapeutic Approaches for Spinal Cord Injury. *Int. J. Mol. Sci.*, **23**.

Lin, Y., Bloodgood, B.L., Hauser, J.L., Lapan, A.D., Koon, A.C., Kim, T.-K., Hu, L.S., Malik, A.N., & Greenberg, M.E. (2008) Activity-dependent regulation of inhibitory synapse development by Npas4. *Nature*, **455**, 1198–1204.

Liu, D., Xu, G.Y., Pan, E., & McAdoo, D.J. (1999) Neurotoxicity of glutamate at the concentration released upon spinal cord injury. *Neuroscience*, **93**, 1383–1389.

Lyford, G.L., Yamagata, K., Kaufmann, W.E., Barnes, C.A., Sanders, L.K., Copeland, N.G., Gilbert, D.J., Jenkins, N.A., Lanahan, A.A., & Worley, P.F. (1995) Arc, a growth factor and activity-regulated gene, encodes a novel cytoskeleton-associated protein that is enriched in neuronal dendrites. *Neuron*, **14**, 433–445.

Magnuson, D.S., Trinder, T.C., Zhang, Y.P., Burke, D., Morassutti, D.J., & Shields, C.B. (1999) Comparing deficits following excitotoxic and contusion injuries in the thoracic and lumbar spinal cord of the adult rat. *Exp. Neurol.*, **156**, 191–204.

Magnuson, D.S.K., Lovett, R., Coffee, C., Gray, R., Han, Y., Zhang, Y.P., & Burke, D.A. (2005) Functional consequences of lumbar spinal cord contusion injuries in the adult rat. *J. Neurotrauma*, **22**, 529–543.

Maier, I.C., Baumann, K., Thallmair, M., Weinmann, O., Scholl, J., & Schwab, M.E. (2008) Constraint-induced movement therapy in the adult rat after unilateral corticospinal tract injury. *J. Neurosci.*, **28**, 9386–9403.

Malmgren, K. & Pierrot-Deseilligny, E. (1988) Evidence for non-monosynaptic Ia excitation of human wrist flexor motoneurones, possibly via propriospinal neurones. *J. Physiol.*, **405**, 747–764.

Man'kovskaya, Y.P., Maisky, V.A., Vlasenko, O. V, & Maznychenko, A. V (2014) 7-Nitroindazole enhances c-Fos expression in spinal neurons in rats realizing operant movements. *Acta Histochem.*, **116**, 1427–1433.

Mancuso, R., Santos-Nogueira, E., Osta, R., & Navarro, X. (2011) Electrophysiological analysis of a murine model of motoneuron disease. *Clin. Neurophysiol.*, **122**, 1660–1670.

Manzanares, G., Brito-da-Silva, G., & Gandra, P.G. (2018) Voluntary wheel running: patterns and physiological effects in mice. *Brazilian J. Med. Biol. Res. = Rev. Bras. Pesqui. medicas e Biol.*, **52**, e7830.

Mardinly, A.R., Spiegel, I., Patrizi, A., Centofante, E., Bazinet, J.E., Tzeng, C.P., Mandel-Brehm, C., Harmin, D.A., Adesnik, H., Fagiolini, M., & Greenberg, M.E. (2016) Sensory experience regulates cortical inhibition by inducing IGF1 in VIP neurons. *Nature*, **531**, 371–375.

Martin, S.S., Aday, A.W., Almarzooq, Z.I., Anderson, C.A.M., Arora, P., Avery, C.L., Baker-Smith, C.M., Barone Gibbs, B., Beaton, A.Z., Boehme, A.K., Commodore-Mensah, Y., Currie, M.E., Elkind, M.S. V, Evenson, K.R., Generoso, G., Heard, D.G., Hiremath, S., Johansen, M.C., Kalani, R., Kazi, D.S., Ko, D., Liu, J., Magnani, J.W., Michos, E.D., Mussolino, M.E., Navaneethan, S.D., Parikh, N.I., Perman, S.M., Poudel, R., Rezk-Hanna, M., Roth, G.A., Shah, N.S., St-Onge, M.-P., Thacker, E.L., Tsao, C.W., Urbut, S.M., Van Spall, H.G.C., Voeks, J.H., Wang, N.-Y., Wong, N.D., Wong, S.S., Yaffe, K., Palaniappan, L.P., & American Heart Association Council on Epidemiology and Prevention Statistics Committee and Stroke Statistics Subcommittee (2024) 2024 Heart Disease and Stroke Statistics: A Report of US and Global Data From the American Heart Association. *Circulation*, **149**, e347–e913.

Martinez, M., Brezun, J.-M., Bonnier, L., & Xerri, C. (2009) A new rating scale for open-field evaluation of behavioral recovery after cervical spinal cord injury in rats. *J. Neurotrauma*, **26**, 1043–1053.

Mathis, A., Mamidanna, P., Cury, K.M., Abe, T., Murthy, V.N., Mathis, M.W., & Bethge, M. (2018) DeepLabCut: markerless pose estimation of user-defined body parts with deep learning. *Nat. Neurosci.*, **21**, 1281–1289.

Matute, C., Alberdi, E., Domercq, M., Sánchez-Gómez, M.-V., Pérez-Samartín, A., Rodríguez-Antigüedad, A., & Pérez-Cerdá, F. (2007) Excitotoxic damage to white matter. *J. Anat.*, **210**, 693–702.

Mazzone, G.L., Margaryan, G., Kuzhandaivel, A., Nasrabady, S.E., Mladinic, M., & Nistri, A. (2010) Kainate-induced delayed onset of excitotoxicity with functional loss unrelated to the extent of neuronal damage in the in vitro spinal cord. *Neuroscience*, **168**, 451–462.

McKenna, J.E., Prusky, G.T., & Whishaw, I.Q. (2000) Cervical motoneuron topography reflects the proximodistal organization of muscles and movements of the rat forelimb: a retrograde carbocyanine dye analysis. *J. Comp. Neurol.*, **419**, 286–296.

McKenna, J.E. & Whishaw, I.Q. (1999) Complete compensation in skilled reaching success with associated impairments in limb synergies, after dorsal column lesion in the rat. *J. Neurosci.*, **19**, 1885–1894.

Mendell, L.M. & Henneman, E. (1971) Terminals of single Ia fibers: location, density, and distribution within a pool of 300 homonymous motoneurons. *J. Neurophysiol.*, **34**, 171–187.

Metz, G.A. & Whishaw, I.Q. (2000) Skilled reaching an action pattern: stability in rat (Rattus norvegicus) grasping movements as a function of changing food pellet size. *Behav. Brain Res.*, **116**, 111–122.

Metz, G.A. & Whishaw, I.Q. (2002) Cortical and subcortical lesions impair skilled walking in the ladder rung walking test: a new task to evaluate fore- and hindlimb stepping, placing, and co-ordination. *J. Neurosci. Methods*, **115**, 169–179.

Molteni, R., Zheng, J.-Q., Ying, Z., Gómez-Pinilla, F., & Twiss, J.L. (2004) Voluntary exercise increases axonal regeneration from sensory neurons. *Proc. Natl. Acad. Sci. U. S. A.*,

101, 8473–8478.

Mondello, S.E., Pedigo, B.D., Sunshine, M.D., Fischedick, A.E., Horner, P.J., & Moritz, C.T. (2021) A micro-LED implant and technique for optogenetic stimulation of the rat spinal cord. *Exp. Neurol.*, **335**, 113480.

Mondello, S.E., Sunshine, M.D., Fischedick, A.E., Dreyer, S.J., Horwitz, G.D., Anikeeva, P., Horner, P.J., & Moritz, C.T. (2018) Optogenetic surface stimulation of the rat cervical spinal cord. *J. Neurophysiol.*, **120**, 795–811.

Mondello, S.E., Young, L., Dang, V., Fischedick, A.E., Tolley, N.M., Wang, T., Bravo, M.A., Lee, D., Tucker, B., Knoernschild, M., Pedigo, B.D., Horner, P.J., & Moritz, C.T. (2023) Optogenetic spinal stimulation promotes new axonal growth and skilled forelimb recovery in rats with sub-chronic cervical spinal cord injury. *J. Neural Eng.*, **20**.

Montoya, C.P., Campbell-Hope, L.J., Pemberton, K.D., & Dunnett, S.B. (1991) The "staircase test": a measure of independent forelimb reaching and grasping abilities in rats. *J. Neurosci. Methods*, **36**, 219–228.

Morris, R., Tosolini, A.P., Goldstein, J.D., & Whishaw, I.Q. (2011) Impaired arpeggio movement in skilled reaching by rubrospinal tract lesions in the rat: a behavioral/anatomical fractionation. *J. Neurotrauma*, **28**, 2439–2451.

Murray, M. (2015) General Overview of Spinal Anatomy and Physiology Organization. In *Encyclopedia of Computational Neuroscience*. Springer New York, New York, NY, pp. 1272–1284.

Nakae, A., Nakai, K., Yano, K., Hosokawa, K., Shibata, M., & Mashimo, T. (2011) The animal model of spinal cord injury as an experimental pain model. *J. Biomed. Biotechnol.*, **2011**, 939023.

Navarro, X. & Udina, E. (2009) Neurofisiología de la espasticidad. In *Evaluación Clínica y Tratamiento de La Espasticidad*. Editorial Médica Panamericana, pp. 1–15.

Neafsey, E.J., Bold, E.L., Haas, G., Hurley-Gius, K.M., Quirk, G., Sievert, C.F., & Terreberry, R.R. (1986) The organization of the rat motor cortex: a microstimulation mapping study. *Brain Res.*, **396**, 77–96.

Nees, T.A., Finnerup, N.B., Blesch, A., & Weidner, N. (2017) Neuropathic pain after spinal cord injury: the impact of sensorimotor activity. *Pain*, **158**, 371–376.

Nees, T.A., Tappe-Theodor, A., Sliwinski, C., Motsch, M., Rupp, R., Kuner, R., Weidner, N., & Blesch, A. (2016) Early-onset treadmill training reduces mechanical allodynia and modulates calcitonin gene-related peptide fiber density in lamina III/IV in a mouse model of spinal cord contusion injury. *Pain*, **157**, 687–697.

Nestler, E.J. (2015) ΔFosB: a transcriptional regulator of stress and antidepressant responses. *Eur. J. Pharmacol.*, **753**, 66–72.

Nica, I., Deprez, M., Nuttin, B., & Aerts, J.-M. (2017) Automated Assessment of Endpoint and Kinematic Features of Skilled Reaching in Rats. *Front. Behav. Neurosci.*, **11**, 255.

Nishida, F., Zanuzzi, C.N., Martínez, A., Barbeito, C.G., & Portiansky, E.L. (2015) Functional and histopathological changes induced by intraparenchymal injection of kainic acid in the rat cervical spinal cord. *Neurotoxicology*, **49**, 68–78.

Nithianantharajah, J. & Hannan, A.J. (2006) Enriched environments, experience-dependent plasticity and disorders of the nervous system. *Nat. Rev. Neurosci.*, **7**, 697–709.

Olney, J.W., Rhee, V., & Ho, O.L. (1974) Kainic acid: a powerful neurotoxic analogue of

glutamate. *Brain Res.*, **77**, 507–512.

Oyinbo, C.A. (2011) Secondary injury mechanisms in traumatic spinal cord injury: a nugget of this multiply cascade. *Acta Neurobiol. Exp. (Wars).*, **71**, 281–299.

Paschon, V., Correia, F.F., Morena, B.C., da Silva, V.A., Dos Santos, G.B., da Silva, M.C.C., Cristante, A.F., Willerth, S.M., Perrin, F.E., & Kihara, A.H. (2020) CRISPR, Prime Editing, Optogenetics, and DREADDs: New Therapeutic Approaches Provided by Emerging Technologies in the Treatment of Spinal Cord Injury. *Mol. Neurobiol.*, **57**, 2085–2100.

Penfield, W. & Rasmussen, T. (1950) *The Cerebral Cortex of Man: A Clinical Study of Localization of Function*. MacMillan Publishing Co.

Pham, B.N., Luo, J., Anand, H., Kola, O., Salcedo, P., Nguyen, C., Gaunt, S., Zhong, H., Garfinkel, A., Tillakaratne, N., & Edgerton, V.R. (2020) Redundancy and multifunctionality among spinal locomotor networks. *J. Neurophysiol.*, **124**, 1469–1479.

Pisharodi, M. & Nauta, H.J. (1985) An animal model for neuron-specific spinal cord lesions by the microinjection of N-methylaspartate, kainic acid, and quisqualic acid. *Appl. Neurophysiol.*, **48**, 226–233.

Pocratsky, A., Pocratsky, A., Whittemore, S.R., & Magnsuon, D.S.K. (2018) Intraspinal injections to double-infect L2 spinal interneurons that project to L5 in the adult rat. *Protoc. Exch.*,.

Pocratsky, A.M., Burke, D.A., Morehouse, J.R., Beare, J.E., Riegler, A.S., Tsoulfas, P., States, G.J.R., Whittemore, S.R., & Magnuson, D.S.K. (2017) Reversible silencing of lumbar spinal interneurons unmasks a task-specific network for securing hindlimb alternation. *Nat. Commun.*, **8**, 1963.

Pocratsky, A.M., Shepard, C.T., Morehouse, J.R., Burke, D.A., Riegler, A.S., Hardin, J.T., Beare, J.E., Hainline, C., States, G.J., Brown, B.L., Whittemore, S.R., & Magnuson, D.S. (2020) Long ascending propriospinal neurons provide flexible, context-specific control of interlimb coordination. *Elife*, **9**.

Presley, R.W., Menétrey, D., Levine, J.D., & Basbaum, A.I. (1990) Systemic morphine suppresses noxious stimulus-evoked Fos protein-like immunoreactivity in the rat spinal cord. *J. Neurosci.*, **10**, 323–335.

Regan, R.F. (1996) The vulnerability of spinal cord neurons to excitotoxic injury: comparison with cortical neurons. *Neurosci. Lett.*, **213**, 9–12.

Rexed, B. (1952) The cytoarchitectonic organization of the spinal cord in the cat. *J. Comp. Neurol.*, **96**, 414–495.

Romi, F. & Naess, H. (2016) Spinal Cord Infarction in Clinical Neurology: A Review of Characteristics and Long-Term Prognosis in Comparison to Cerebral Infarction. *Eur. Neurol.*, **76**, 95–98.

Rossignol, S., Dubuc, R., & Gossard, J.-P. (2006) Dynamic sensorimotor interactions in locomotion. *Physiol. Rev.*, **86**, 89–154.

Rossignol, S. & Frigon, A. (2011) Recovery of locomotion after spinal cord injury: some facts and mechanisms. *Annu. Rev. Neurosci.*, **34**, 413–440.

Ruder, L., Schina, R., Kanodia, H., Valencia-Garcia, S., Pivetta, C., & Arber, S. (2021) A functional map for diverse forelimb actions within brainstem circuitry. *Nature*, **590**, 445–450.

Sacrey, L.-A.R., Alaverdashvili, M., & Whishaw, I.Q. (2009) Similar hand shaping in reaching-for-food (skilled reaching) in rats and humans provides evidence of homology in release, collection, and manipulation movements. *Behav. Brain Res.*, **204**, 153–161.

Saleeba, C., Dempsey, B., Le, S., Goodchild, A., & McMullan, S. (2019) A Student's Guide to Neural Circuit Tracing. *Front. Neurosci.*, **13**, 897.

Sasaki, S., Isa, T., Pettersson, L.-G., Alstermark, B., Naito, K., Yoshimura, K., Seki, K., & Ohki, Y. (2004) Dexterous finger movements in primate without monosynaptic corticomotoneuronal excitation. *J. Neurophysiol.*, **92**, 3142–3147.

Schallert, T., Fleming, S.M., Leasure, J.L., Tillerson, J.L., & Bland, S.T. (2000) CNS plasticity and assessment of forelimb sensorimotor outcome in unilateral rat models of stroke, cortical ablation, parkinsonism and spinal cord injury. *Neuropharmacology*, **39**, 777–787.

Schallert, T., Upchurch, M., Lobaugh, N., Farrar, S.B., Spirduso, W.W., Gilliam, P., Vaughn, D., & Wilcox, R.E. (1982) Tactile extinction: distinguishing between sensorimotor and motor asymmetries in rats with unilateral nigrostriatal damage. *Pharmacol. Biochem. Behav.*, **16**, 455–462.

Sharp, K.G., Duarte, J.E., Gebrekristos, B., Perez, S., Steward, O., & Reinkensmeyer, D.J. (2016) Robotic Rehabilitator of the Rodent Upper Extremity: A System and Method for Assessing and Training Forelimb Force Production after Neurological Injury. *J. Neurotrauma*, **33**, 460–467.

Shekhtmeyster, P., Carey, E.M., Duarte, D., Ngo, A., Gao, G., Nelson, N.A., Clark, C.L., & Nimmerjahn, A. (2023) Multiplex translaminar imaging in the spinal cord of behaving mice. *Nat. Commun.*, **14**, 1427.

Sheng, M. & Greenberg, M.E. (1990) The regulation and function of c-fos and other immediate early genes in the nervous system. *Neuron*, **4**, 477–485.

Sheng, M., Thompson, M.A., & Greenberg, M.E. (1991) CREB: a Ca(2+)-regulated transcription factor phosphorylated by calmodulin-dependent kinases. *Science*, **252**, 1427–1430.

Shepard, C.T., Pocratsky, A.M., Brown, B.L., Van Rijswijck, M.A., Zalla, R.M., Burke, D.A., Morehouse, J.R., Riegler, A.S., Whittemore, S.R., & Magnuson, D.S. (2021) Silencing long ascending propriospinal neurons after spinal cord injury improves hindlimb stepping in the adult rat. *Elife*, **10**.

Sherrington, C.S. (1910) Flexion-reflex of the limb, crossed extension-reflex, and reflex stepping and standing. *J. Physiol.*, **40**, 28–121.

Silva, N.A., Sousa, N., Reis, R.L., & Salgado, A.J. (2014) From basics to clinical: a comprehensive review on spinal cord injury. *Prog. Neurobiol.*, **114**, 25–57.

Silver, J. & Miller, J.H. (2004) Regeneration beyond the glial scar. *Nat. Rev. Neurosci.*, **5**, 146–156.

Soblosky, J.S., Colgin, L.L., Chorney-Lane, D., Davidson, J.F., & Carey, M.E. (1997) Ladder beam and camera video recording system for evaluating forelimb and hindlimb deficits after sensorimotor cortex injury in rats. *J. Neurosci. Methods*, **78**, 75–83.

Sofroniew, M. V (2009) Molecular dissection of reactive astrogliosis and glial scar formation. *Trends Neurosci.*, **32**, 638–647.

Spiegel, I., Mardinly, A.R., Gabel, H.W., Bazinet, J.E., Couch, C.H., Tzeng, C.P., Harmin, D.A., & Greenberg, M.E. (2014) Npas4 regulates excitatory-inhibitory balance within

neural circuits through cell-type-specific gene programs. *Cell*, **157**, 1216–1229.

Sukhorukova, E., Kirik, O., Zelenkova, N., & Korzhevskii, D. (2015) Neuronal nuclear antigen NeuN as an indicator of the nervous tissue preservation and suitability for immunocytochemical study. *Med. Acad. J.*, **15**, 63–67.

Sun, H., Kawahara, Y., Ito, K., Kanazawa, I., & Kwak, S. (2006) Slow and selective death of spinal motor neurons in vivo by intrathecal infusion of kainic acid: implications for AMPA receptor-mediated excitotoxicity in ALS. *J. Neurochem.*, **98**, 782–791.

Takahashi, Y. & Nakajima, Y. (1996) Dermatomes in the rat limbs as determined by antidromic stimulation of sensory C-fibers in spinal nerves. *Pain*, **67**, 197–202.

Takei, T. & Seki, K. (2010) Spinal interneurons facilitate coactivation of hand muscles during a precision grip task in monkeys. *J. Neurosci.*, **30**, 17041–17050.

Thomas, G.M. & Huganir, R.L. (2004) MAPK cascade signalling and synaptic plasticity. *Nat. Rev. Neurosci.*, **5**, 173–183.

Tölle, T.R., Berthele, A., Zieglgänsberger, W., Seeburg, P.H., & Wisden, W. (1993) The differential expression of 16 NMDA and non-NMDA receptor subunits in the rat spinal cord and in periaqueductal gray. *J. Neurosci.*, **13**, 5009–5028.

Torres-Espín, A., Beaudry, E., Fenrich, K., & Fouad, K. (2018) Rehabilitative Training in Animal Models of Spinal Cord Injury. *J. Neurotrauma*, **35**, 1970–1985.

Tosolini, A.P. & Morris, R. (2012) Spatial characterization of the motor neuron columns supplying the rat forelimb. *Neuroscience*, **200**, 19–30.

Ueno, M., Nakamura, Y., Li, J., Gu, Z., Niehaus, J., Maezawa, M., Crone, S.A., Goulding, M., Baccei, M.L., & Yoshida, Y. (2018) Corticospinal Circuits from the Sensory and Motor Cortices Differentially Regulate Skilled Movements through Distinct Spinal Interneurons. *Cell Rep.*, **23**, 1286-1300.e7.

Urca, G. & Urca, R. (1990) Neurotoxic effects of excitatory amino acids in the mouse spinal cord: quisqualate and kainate but not N-methyl-D-aspartate induce permanent neural damage. *Brain Res.*, **529**, 7–15.

van Praag, H., Kempermann, G., & Gage, F.H. (2000) Neural consequences of environmental enrichment. *Nat. Rev. Neurosci.*, **1**, 191–198.

Verma, R., Virdi, J.K., Singh, N., & Jaggi, A.S. (2019) Animals models of spinal cord contusion injury. *Korean J. Pain*, **32**, 12–21.

Vizzard, M.A. (2000) Increased expression of spinal cord Fos protein induced by bladder stimulation after spinal cord injury. *Am. J. Physiol. Regul. Integr. Comp. Physiol.*, **279**, R295-305.

Watson, C., Paxinos, G., & Kayalioglu, G. (2009) *The Spinal Cord*. Elsevier.

Wayman, G.A., Lee, Y.-S., Tokumitsu, H., Silva, A.J., & Soderling, T.R. (2008) Calmodulin-kinases: modulators of neuronal development and plasticity. *Neuron*, **59**, 914–931.

Werner, W. (1993) Neurons in the primate superior colliculus are active before and during arm movements to visual targets. *Eur. J. Neurosci.*, **5**, 335–340.

West, A.E., Chen, W.G., Dalva, M.B., Dolmetsch, R.E., Kornhauser, J.M., Shaywitz, A.J., Takasu, M.A., Tao, X., & Greenberg, M.E. (2001) Calcium regulation of neuronal gene expression. *Proc. Natl. Acad. Sci. U. S. A.*, **98**, 11024–11031.

West, A.E. & Greenberg, M.E. (2011) Neuronal activity-regulated gene transcription in synapse development and cognitive function. *Cold Spring Harb. Perspect. Biol.*, **3**.

Whishaw, I.Q., Gorny, B., Foroud, A., & Kleim, J.A. (2003) Long-Evans and Sprague-Dawley rats have similar skilled reaching success and limb representations in motor cortex but different movements: some cautionary insights into the selection of rat strains for neurobiological motor research. *Behav. Brain Res.*, **145**, 221–232.

Whishaw, I.Q., O'Connor, W.T., & Dunnett, S.B. (1986) The contributions of motor cortex, nigrostriatal dopamine and caudate-putamen to skilled forelimb use in the rat. *Brain*, **109 (Pt 5**, 805–843.

Whishaw, I.Q. & Pellis, S.M. (1990) The structure of skilled forelimb reaching in the rat: a proximally driven movement with a single distal rotatory component. *Behav. Brain Res.*, **41**, 49–59.

Whishaw, I.Q., Pellis, S.M., & Gorny, B.P. (1992) Skilled reaching in rats and humans: evidence for parallel development or homology. *Behav. Brain Res.*, **47**, 59–70.

Whishaw, I.Q., Travis, S.G., Koppe, S.W., Sacrey, L.A., Gholamrezaei, G., & Gorny, B. (2010) Hand shaping in the rat: Conserved release and collection vs. flexible manipulation in overground walking, ladder rung walking, cylinder exploration, and skilled reaching. *Behav. Brain Res.*, **206**, 21–31.

Whishaw, I.Q., Whishaw, P., & Gorny, B. (2008) The structure of skilled forelimb reaching in the rat: A movement rating scale. *J. Vis. Exp.*, 1–2.

Wiedmann, N.M., Wong, A.W., Keast, J.R., & Osborne, P.B. (2021) Sex differences in c-Fos and EGR-1/Zif268 activity maps of rat sacral spinal cord following cystometry-induced micturition. *J. Comp. Neurol.*, **529**, 311–326.

Wijesekera, L.C. & Leigh, P.N. (2009) Amyotrophic lateral sclerosis. *Orphanet J. Rare Dis.*, **4**, 3.

Witts, E.C., Zagoraiou, L., & Miles, G.B. (2014) Anatomy and function of cholinergic C bouton inputs to motor neurons. *J. Anat.*, **224**, 52–60.

Wouterlood, F.G. (2015) A Survey of Current Neuroanatomical Tracing Techniques. In Arenkiel, B.R. (ed), *Neural Tracing Methods: Tracing Neurons and Their Connections*. Springer New York, New York, NY, pp. 1–49.

Xing, J., Ginty, D.D., & Greenberg, M.E. (1996) Coupling of the RAS-MAPK pathway to gene activation by RSK2, a growth factor-regulated CREB kinase. *Science*, **273**, 959–963.

Yang, D., Wang, Y., Qi, T., Zhang, X., Shen, L., Ma, J., Pang, Z., Lal, N.K., McClatchy, D.B., Seradj, S.H., Leung, V.H., Wang, K., Xie, Y., Polli, F.S., Maximov, A., Gonzalez, O.C., de Lecea, L., Cline, H.T., Augustine, V., Yates, J.R., & Ye, L. (2024) Phosphorylation of pyruvate dehydrogenase inversely associates with neuronal activity. *Neuron*, **112**, 959-971.e8.

Yap, E.-L. & Greenberg, M.E. (2018) Activity-Regulated Transcription: Bridging the Gap between Neural Activity and Behavior. *Neuron*, **100**, 330–348.

Yezierski, P.R., Liu, S., Ruenes, L.G., Kajander, J.K., & Brewer, L.K. (1998) Excitotoxic spinal cord injury: behavioral and morphological characteristics of a central pain model. *Pain*, **75**, 141–155.

Yizhar, O., Fenno, L.E., Davidson, T.J., Mogri, M., & Deisseroth, K. (2011) Optogenetics in neural systems. *Neuron*, **71**, 9–34.

Zaaimi, B., Edgley, S.A., Soteropoulos, D.S., & Baker, S.N. (2012) Changes in descending motor pathway connectivity after corticospinal tract lesion in macaque monkey. *Brain*, **135**, 2277–2289.

Zanuzzi, C.N., Nishida, F., Sisti, M.S., Barbeito, C.G., & Portiansky, E.L. (2019) Reactivity of microglia and astrocytes after an excitotoxic injury induced by kainic acid in the rat spinal cord. *Tissue Cell*, **56**, 31–40.

Zehr, E.P. & Duysens, J. (2004) Regulation of arm and leg movement during human locomotion. *Neuroscientist*, **10**, 347–361.

Zholudeva, L. V, Abraira, V.E., Satkunendrarajah, K., McDevitt, T.C., Goulding, M.D., Magnuson, D.S.K., & Lane, M.A. (2021) Spinal Interneurons as Gatekeepers to Neuroplasticity after Injury or Disease. *J. Neurosci.*, **41**, 845–854.

Zholudeva, L. V, Qiang, L., Marchenko, V., Dougherty, K.J., Sakiyama-Elbert, S.E., & Lane, M.A. (2018) The Neuroplastic and Therapeutic Potential of Spinal Interneurons in the Injured Spinal Cord. *Trends Neurosci.*, **41**, 625–639.

Zhong, H., Zhu, C., Minegishi, Y., Richter, F., Zdunowski, S., Roy, R.R., Vissel, B., Gad, P., Gerasimenko, Y., Chesselet, M.-F., & Edgerton, V.R. (2019) Epidural Spinal Cord Stimulation Improves Motor Function in Rats With Chemically Induced Parkinsonism. *Neurorehabil. Neural Repair*, **33**, 1029–1039.

Zhou, X., He, X., & Ren, Y. (2014) Function of microglia and macrophages in secondary damage after spinal cord injury. *Neural Regen. Res.*, **9**, 1787–1795.